https://dspace.org/

Geology and spatial distribution of uranium mineralisation in the SK anomaly area, Rossing area, Namibia

Abraham, Irene M

2010-07-09T11:35:36Z
http://hdl.handle.net/10539/8283

Downloaded from a DSpace repository. https://dspace.org/

GEOLOGY AND SPATIAL DISTRIBUTION OF URANIUM MINERALISATION IN THE SK ANOMALY AREA, RÖSSING AREA, NAMIBIA

By

Irene M Abraham

A dissertation submitted to the Faculty of Science, University of the Witwatersrand, Johannesburg, in partial fulfilment of the requirements for the degree of Master of Science

University of the Witwatersrand, Johannesburg

2009

Declaration

I declare that this thesis is my own, unaided work. It is being submitted for degree of Master of Science in the University of the Witwatersrand, Johannesburg. It is not been submitted before for any degree or examination in any other University.

I while employed by Rössing Uranium Mine, Namibia, have obtained most of the information used in this dissertation.

Signature of candidate

day of 2009

Dedicated To My Late Parents

David Abraham

And

Claudia Abraham

ACKNOWLEDGEMENTS

First and foremost my utmost thanks to the Rössing Uranium Mine Management, especially Mr Bernard Morwe for sponsoring my studies in geology (MSc by research, part time) at the University of the Witwatersrand, Johannesburg.

Secondly, I would like to thank the project supervisor Professor Judith Kinnaird, for her endless patience, supervision, and determination to make this project a success.

ABSTRACT

The nature, geology and spatial distribution of uranium minerals in the SK anomaly area, Rössing Uranium Mine, Namibia, is investigated to perceive if the mineralogy is favourable for uranium extraction using sulphuric acid plant. In addition to the SK anomaly area, the Rössing Uranium Mine area has two other uranium-rich areas, the SH and SJ anomalies. At present only the SJ anomaly area is being mined due to its favourable mineralogy of 55% uraninite, 40% secondary minerals and 5% betafite. The SK anomaly is made up of about 32 sub-anomalies, of which SK4 is part off.

Geological mapping, radiation survey analyses, petrographic analyses, 3-D modelling, SEM, QEMSCAN, uranium budget and geochemical analyses have been carried out with the aim to understand the area's geology, outline the high priority exploration targets within the SK anomaly, spatial distribution, and proportions of the primary, secondary and refractory uranium bearing minerals in the SK area.

Of the different six leucogranites observed by Nex (1997) in the Goanikontes area; only four types (B to E) are found in the SK area. Betafite is associated with type D leucogranite, although traces are present in type E leucogranite.

Betafite ($(U,Ca)(Ti,Ta,Nb)_3O_9$) is a Ti-rich member of the pyrochlore group and does not readily release uranium with acid, even in an oxidized state. Currently betafite cannot be leached at atmospheric pressure with sulphuric leach. Due to its high abundance in SH area, if SK area has high betafite, Rössing Uranium Mine has to come with another approach to leach the uranium out of betafite.

The SJ area contains sheeted leucogranites emplaced into the Rössing Formation calc-silicates and the meta-pelitic sediments of the Khan Formation. The same geological setting is also observed in the SK area. The Rössing and Khan lithological units seem to increase in thickness from the SJ to the SK area. The bedding/foliation relationship and the relative ages of the lithological units indicate that the SK area is an anticline; while the SK4 area is a syncline.

In the SK anticline, where the marble unit tripled in thickness from the SJ pit, there is 65% betafite, 8% uraninite and 27% secondary uranium bearing minerals. The SK4 area is a minor syncline within the major SK anticline area; has 5% betafite, 64% uraninite and 31% secondary uranium bearing minerals. This study concludes that there is a structural and

lithological control on betafite formation in the SK anticline and SK4 areas.

If the current acid plant is used to process material from the SK anticline area, recoveries will be low as most of the uranium is hosted in betafite form. In fact only U-silicates and uraninite will be leached successfully. Considering the fact that the SH area also has a high betafite content, Rössing Uranium Mine may have to find ways to leach the uranium from betafite, to make SH and SK areas feasible for mining.

CHAPTER1
INTRODUCTION

1.1. Preamble……..……..…….8
1.2. Brief History……..…….....8
1.3. Purpose of the Study……..…….....10

CHAPTER 2
GENERAL GEOLOGY OF THE DAMARA OROGENIC BELT

2.1. Introduction to the Geology of the Damara Orogen…….....….…….…....13
2.2. General Geology of the Central Zone.…….....….…….……15
2.2.1. Introduction to the Geology of the Central Zone…….....…...…..…..……..15
2.2.2. Regional Structural Evolution of the Central Zone…….....…..…..…..……17
2.2.3. Metamorphism of the Central Zone…….…..……..…20
2.2.4. Granites in the Central Zone…….....……..…..……..…20
2.3. Uranium Mineralisation in the Central Zone…….....……..…..…....…22

CHAPTER 3
LOCAL RÖSSING GEOLOGY

3.1. Country Rocks……...……..…….…..24
3.1.1. Etusis Formation……..…….…...24
3.1.2. Khan Formation……..…….....25
3.1.3. Rössing Formation……..…….……26
3.2. Structural Evolution of the Rössing Area……..….....…26
3.3. Granite Intrusion……...….....28
3.4. Metamorphism……..…….....29
3.5. Uranium Mineralisation in the Rössing Area……....…....…29
3.6. Proportion of Uranium Minerals……..…..…30

CHAPTER 4
SK AREA

4.1. Introduction……....…...……..31
4.2. Methodology……...……...……. 32
4.3. Stratigraphy of the SK Area…….....…….…33
4.3.1. Khan Formation……..…...……... 34
4.3.2. Rössing Formation……..……...……....37
4.4. Sheeted Leucogranites in the SK Area……..…..…...…....38
4.5. Bedding and Foliation in the SK Area……..……...…..…40
4.6. SK4 Sub-Anomaly……..……..…...40
4.7. SK3 Sub-Anomaly……..……...…..44
4.8. Radiation Survey……..……..……..46
4.8.1. Contouring of Scintillation Data using Surfer®……..……..…..…...46
4.9. Three Dimensional (3D) Geological Model of the SK Area. ……..…...…48
4.10. Discussion and Conclusion on the SK Area……..…...…..49

CHAPTER 5
SAMPLE COLLECTION AND PETROGRAPHY OF THE SHEETED LEUCOGRANITES

5.1. Introduction……..……...50
5.2. Sampling Rationale……...…..…50
5.3. Methodology……..…...…...53

5.4. Petrological Variation of Leucogranites……..…....…54
5.5. Petrography of the Leucogranites…….…..…...…..56
5.5.1. Modal Classification of SK Area Thin Sections…….…..…56
5.6. Discussion…….....…61

CHAPTER 6
GEOCHEMISTRY OF THE SK AREA LEUCOGRANITE SAMPLES

6.1. Introduction…….....…....62
6.2. Sample Preparation…….…….……....62
6.3. Geochemical Results…….…….....63
6.3.1. Geochemical Classification of the Sheeted Leucogranites…….…….....65
6.3.2. Trace-Element Geochemical Classification of the Sheeted Leucogranites in the SK Area….....67
6.3.2.1. Nb, Ti and U…….....…....69
6.3.2.2. U, Th, Zr, Ce and Y……...……..…..…70
6.5. Discussion……..……..…....75

CHAPTER 7
EVALUTATION OF THE DEPORTMENT OF URANIUM IN THE RÖSSING AREA

7.1. Introduction……..…..…….....…..76
7.1.1. Uraninite…….….....…...76
7.1.2. Betafite. …….….....…...77
7.1.3. Secondary Uranium Minerals…….....…..78
7.1.4. Additional Minerals……..……..……78
7.2. Theoretical Calculation of Betafite Abundance……..……....…..79
7.2.1. Results…….…….….....79
7.2.2. Comparison of Theoretical Betafite Calculation between SK, SH and SJ Areas…….……..….80
7.2.3. Summary……..…..…....81
7.3. Scanning Electron Microprobe……..…...…...82
7.3.1. Sample Preparation…….……..…..…83
7.3.2. Results…….……...…85
7.3.3. Discussion on the SEM Data…….……....…..88
7.4. QEMSCAN…….…….....…...89
7.4.1. Methodology…….……..……...89
7.4.2. Results…….……....…...90
7.4.3. Discussion on the QEMSCAN Data……..…….....92
7.5. Betafite and Uranium Variation with Depth……..…....93
7.5.1. Results…….….....94
7.5.2. Discussion on the Comparison of U-mineral Proportions with Depth……..…....94
7.6. Discussion…….....94

CHAPTER 8
DISCUSSION AND CONCLUSIONS

Discussions…….…..……..…96
Conclusions……..……..…...…98
References……..……..…100

LIST OF FIGURES

Figure 1.1: The location of Rössing Uranium Mine.
Figure 1.2: The location of the three main anomalies; SJ, SH and SK.
Figure 2.1: The sinistral movement of the Congo and Kalahari Craton during the late Precambrian early Palaeozoic, resulting in the formation of the Damara belt.
Figure 2.2: Map of the tectono-stratigraphic zones of the Damara Orogen.
Figure 2.3: Rössing Uranium Mine is located in the south Central Zone between the Okahandja and Omaruru Lineament.
Figure 3.1: Local Rössing geology.
Figure 3.2: Highlights of the structural features in the Rössing area.
Figure 4.1: The SK anomaly is situated north of the Khan River. At least 32 sub-anomalies form part of the SK overall anomaly.
Figure 4.2: Banded gneiss showing layers 2-10 mm thick.
Figure 4.3: Partial melts of quartz and feldspar in banded gneiss.
Figure 4.4: Boundinaged amphibolite veins within the Khan Formation (banded gneiss), with partial melting in boudin necks.
Figure 4.5: Banded gneiss xenolith in leucogranite sheet.
Figure 4.6: Sharp contact between granite and banded gneiss.
Figure 4.7: En-echelon quartz veins within banded gneiss, indicating a dextral sense of movement.
Figure 4.8: Equal angle stereographic projection of the SK country rock bedding.
Figure 4.9: Equal angle stereographic projection of the SK foliation. .
Figure 4.10: Detailed geology of the SK4 sub-anomaly.
Figure 4.11: Equal angle stereographic projection of the SK4 country rock bedding.
Figure 4.12: The geology of the SK4 area prior to granite intrusion.
Figure 4.13: Leucogranite intruded along a fault zone.
Figure 4.14: SK3 drill section 250E.
Figure 4.15: Summary of the granite behaviour in SK3 drill sections showing the en-echelon nature of the leucogranites.
Figure 4.16: Image map of the SK scintillation counts, indicating the most favourable exploration target area.
Figure 4.17: The pre-intrusion 3D macro model of the SK area, looking towards the northeast.
Figure 5.1: SK diamond drillholes logs from the 2007 drilling programme.
Figure 5.2: QAP diagrams showing the modal minerals of the different sheeted leucogranites.
Figure 5.3: SK1AB under cross polars - Coarse-grained quartz, showing undulose extinction and crystal boundary dissolution.
Figure 5.4: SK2EA in plane polarised light - Graphic quartz-feldspar texture, showing irregular crystal boundaries.
Figure 5.5: SK2EA under crossed polars - Film perthites representing the feldspars in the graphic quartz-feldspar texture, shown in Figure 5.4.
Figure 5.6: SK1B in plane polarised light - Betafite crystal surrounded by a rim of haematite and radial cracks within the quartz grain.
Figure 5.7: S3 under crossed polars- Subhedral to euhedral plagioclase grains some altered to sericite and quartz grains showing undulose extinction.
Figure: 6.1: Geochemical plot of the SK surface leucogranites on a diagram of Streckeisen and Le Maitre (1976) ANOR = (100 x An/ (Or + An)) versus Q' = (Q/ (Q + Or + Ab + An)) diagram. Figure: 6.2: Streckeisen and Le Maitre (1976) ANOR-Q' diagram of leucogranite samples from cores in the SK anticline and SK4 syncline.
Figure 6.3: Alkali-silica diagram showing the composition of the granitoid rocks in the SK, SJ, and SH areas.

Figure 6.4: Plot of Al_2O_3/ (Na_2O + K_2O+ CaO) against SiO_2, showing the aluminium saturation of the SK, SH and SJ samples in the Rössing area. The A/CNK ratio varies little with range of SiO_2 content.
Figure 6.5: Granitoid discrimination diagram (Log Rb against Log (Y+Nb)) after Pearce *et al*. (1984.
Figure 6.6: A plot of U and Th (ppm) versus SiO_2 and K_2O (wt %), for the different leucogranite types from the SK, SJ and SH area showing a poor correlation.
Figure 6.7: A plot of Nb (ppm) versus U (ppm), showing a clear increase in Nb as U increases, a good indication that betafite may be present in the SK area.
Figure 6.8: A plot of Nb+Ti (ppm) versus U (ppm), showing a clear increase in Nb as U increases, again this gives a good indication that betafite may be present in the SK area.
Figure 6.9: A plot of log Th (ppm) against log U (ppm), showing a dominant Th: U ratio of slightly below 1:1.
Figure 6.10: Log U versus Log Zr showing a poor relationship for the SK samples.
Figure 6.11: Log Th versus Log Zr showing a poor relationship for the SK surface samples, an unsystematic positive trend within the SK4 core samples and a systematic positive for the SK core samples.
Figure 6.12: Log U versus Log Ce showing a poor relationship for the SK samples.
Figure 6.13: Log Th versus Log Ce showing a poor relationship for the SK surface samples.
Figure 6.14: Log U versus Log Y showing a poor relationship for the SK surface samples, an unsystematic positive trend within the SK4 core samples and a systematic positive trend for the SK core samples.
Figure 6.15: Log Th versus Log Y showing a poor relationship for the SK surface samples and systematic positive trend within the SK4 and SK core samples.
Figure 7.1: SEM element maps from sample SK2E.
Figure 7.2: SEM element mapping from sample SK9.
Figure 7.3: S Heavy minerals proportions for the SK area as determined by the SEM technique.
Figure 7.4: Pie chart of the major and minor uranium-bearing minerals from surface samples in the SK, as determined by the SEM technique.
Figure 7.5: The main uranium-bearing minerals in the Rössing area (SJ pit) are uraninite, u-silicates and betafite.
Figure 7.6: U-deportment summary from the SK and SK4 samples.
Figure 7.7: Comparison of the abundance of uraninite, U-silicates and betafite at different size fractions.
Figure 7.8: The main uranium-bearing minerals in the Rössing Area (SJ pit) are uraninite, U-silicates and betafite.
Figure 7.9: The main uranium-bearing minerals in the Rössing Area (SJ pit) are uraninite, U-silicates and betafite. This pie chart shows the proportions of these minerals in the SK4 syncline, as indicated by the QEMSCAN.

LIST OF TABLES

Table 2.1: Stratigraphic column of the Central Zone in the Damaran Orogenic Belt (Jacob *et al*., 1986).
Table 2.2: Deformation events in the Rössing area.
Table 2.3: Ages and field characteristics of the three main granite groups of the Central Zones.
Table 4.1: Example of the true thickness of various lithologies using apparent thickness of a surface- exposed rock or diamond drilling intersected depth.
Table 4.2: Comparison of the lithological thicknesses of the SJ and SK stratigraphy.
Table 5.1: List of the surface samples taken from the SK area showing the sample coordinates, sample numbers and sampled depths.
Table 5.2: List of samples taken from the SK 2007 diamond drillholes.
Table 5.3: List of samples taken from the SK4 historic diamond drillholes.
Table 5.4: Classification of leucogranites in the Central Zone of the Damara Orogen Belt, with their associated average radiation counts per second (Nex *et al*., 2001).
Table 5.5: Leucogranite description and classification of the surface samples from the SK area.
Table 5.6: Petrographic description of the samples taken from the SK4 diamond drillholes.
Table 6.1: Comparison of the major-element in the SK (22 surface samples), SH (11 surface samples) and SJ (43 core samples and 36 surface samples) areas.
Table 6.2: Comparison of the trace-element in the in the SK (22 surface samples), SH (11 surface samples) and SJ (43 core samples and 36 surface samples) areas.
Table 7.1: Subgroups and species of the pyrochlore group (from Hogarth, 1989).
Table 7.2: Theoretical calculation of the betafite in the SK area showing the almost complete loss of uranium due to a calculated U occurrence in betafite.
Table 7.3: Theoretical calculation of the betafite in the SH area (data from Herd (1996) and Freemantle (2006) showing the almost complete loss of uranium due to a calculated U occurrence in betafite.
Table 7.4: Theoretical calculation of the betafite in the SJ area (data from Herd (1996) and Freemantle (2006), showing varying potential loss of uranium due to betafite occurrence.
Table 7.5: Known and theoretical betafite values in the SJ, SH and SK areas.
Table 7.6: SK heavy minerals together with their proportions and diameters as determined by the SEM technique.
Table 7.7: Mineralogy of the heavy minerals from the SK area, together with their proportions, based on wavelength dispersive microprobe compositional data.

CHAPTER 1

INTRODUCTION

1.1. Preamble

Rössing Uranium Mine, which is located in the Namib Desert (Figure 1.1), is one of the world's principal uranium producers. It has about 6% of the world's known resources, and accounts for 7.5% of world production. Rössing's uranium output, currently accounts for an estimated US$115 million of Namibia's annual export earnings. The Rössing area has attracted geological researchers for the last 30 years because it is currently the only producer of primary uranium ore from granitic rocks.

Rössing Uranium Mine, a subsidiary of Rio Tinto Company, is mining the SJ ore body, which is the largest uranium open pit mine in the world. The current exploration and expansion programme at Rössing Uranium Mine is focused on two additional anomaly areas close to the current SJ pit, the SH area to the southwest and the SK area to the northeast of the Rössing open pit and southwest of the Rössing dome (Figure 1.2). The exploration and expansion programme aims to understand the geology and uranium distribution patterns as part of feasibility studies on the SK and SH anomalies. The SK area forms the focus of this thesis.

The SK anomaly is located in the Rössing area of the Damara Orogenic Belt in Namibia. Topographically, the Rössing area is at an elevation of about 575 m above sea level (Basson and Greenway, 2004). The area has a desert climate, dry and at times dusty, with rather large variations in temperature (4.5-40°C) and humidity (5%-80%). The SK area occupies an area of about 1x2 km^2 some 65 km inland from the coastal town of Swakopmund (Figures 1.1 and 1.2).

1.2. Brief History

The Rössing deposit has been known since 1910, when Dr E. Reuning discovered radioactive minerals in the area. In 1956, limited prospecting on the SJ radioactive anomaly was undertaken by the Anglo American Prospecting Company (Basson and Greenway, 2004). The upswing in the uranium market in the 1970s, led to extensive uranium exploration in Namibia. The Geological Survey conducted several airborne radiometric surveys during this period and several uranium deposits were discovered in the Central Zone of the Damara Orogen, mainly in the western portion

between the Omaruru and Okahandja Lineaments (Basson and Greenway, 2004). These are grouped into three basic types: (1) those that occur in/and associated with plutonic rocks, (2) pedogenic occurrences and (3) sedimentary occurrences. The uranium in the Rössing area is either in, or associated with, plutonic rocks (Basson and Greenway, 2004).

Figure 1.1: The location of Rössing Uranium Mine in the Namib Desert, Erongo Region, Namibia, (Rössing Internal Report, 050505, 2005).

Airborne surveys identified several uraniferous anomalies within the Rössing mining grant. The principal areas, SH, SK and SJ, are characterised by sheeted leucogranites which intruded the Khan and Rössing Formations. In the SK area the sheeted leucogranites are intruded into an anticline, while in the SH area they are intruded into a synform, although the major structure is also an anticline.

The SK area is being evaluated as a potential open pit mine of similar dimensions to the SJ pit. Previous evaluations tried to establish small underground resources on the richer radiometric sub-anomalies such as the SK4 and SK3 (Scott and Northam, 2005) but were unsuccessful.

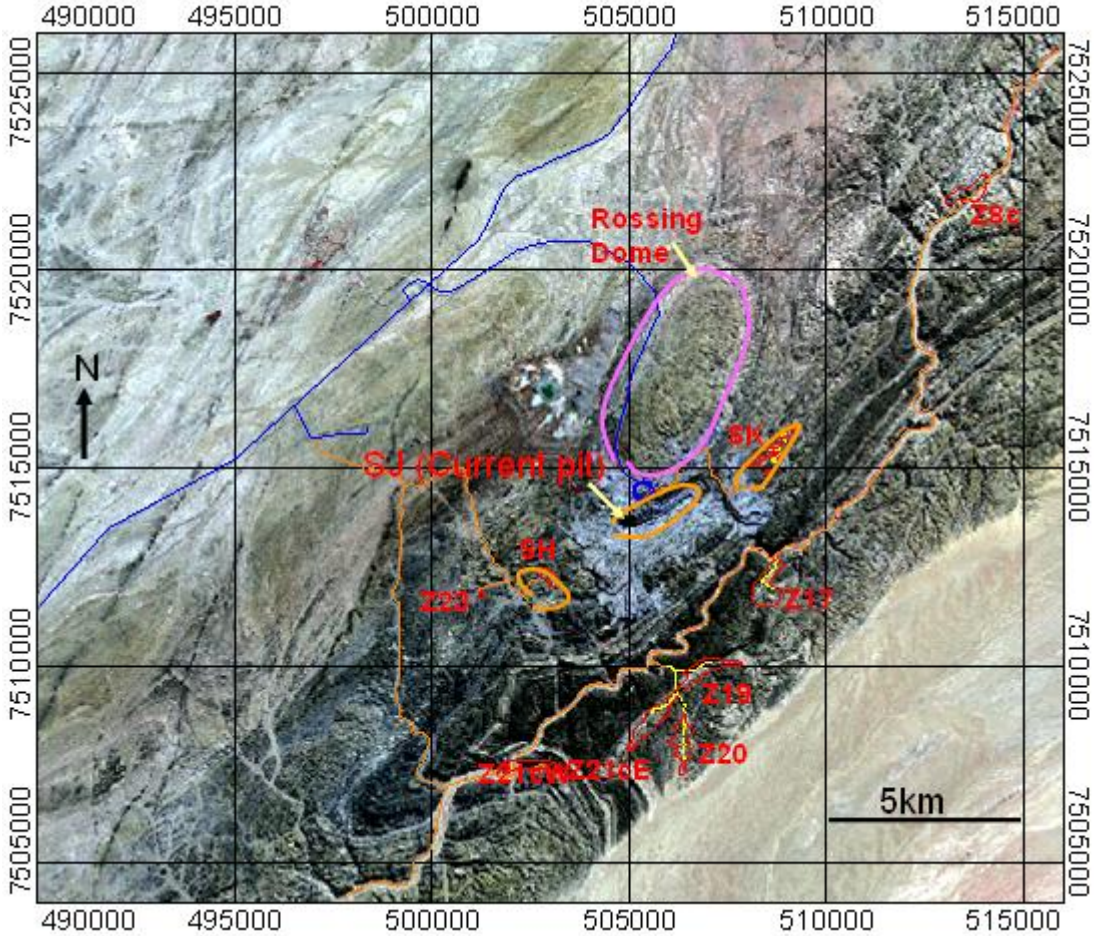

Figure 1.2: The location of the three main anomalies; SJ, SH and SK anomalies within the Rössing area, in relation to the Rössing Dome, Central Zone, Damara Orogenic Belt (Scott and Northam, 2005).

1.3. Purpose of the Study

The increase in uranium prices in recent years has put pressure on Rössing Uranium Mine to increase production and, consequently, to expand the lifespan of the mine. As part of this expansion programme, there has been a re-assessment of the adjacent anomalies such as the SK and SH areas. In spite of the fact that the SH and SK anomalies have been known since the discovery of the SJ orebody in the 1970's, there is currently little understanding of the geology and mineralisation distribution of these areas, especially that of the SK area. The SK area has therefore been targeted for this project for the following reasons:

1. A mineralogical study has never been carried out on the granites of the SK area.
2. There has previously been no thorough systematic sampling across many of the individual sub-anomalies of the SK area.
3. Previous detailed drilling was restricted to the small area of the SK4 anomaly. The subsurface geometry and overall grade of the SK area is still unknown.
4. Although it has been suggested that the mineralogy in the SK area is similar to that in the SJ main open pit (Murphy, 1996), this requires further detailed investigation.

The principal aim of this project is to investigate the local geology and the spatial distribution of primary and secondary mineralisation and the variation in composition of the primary uranium-bearing minerals in the SK area, taking into account the country rock lithologies, structural controls on leucogranite sheet emplacement and evaluating whether any textural, petrographic and hydrothermal alteration can be related to variations in proportions of primary and secondary uranium minerals (U-silicates). The study also aims to produce a 3D model of the SK area.

The initial objectives of the project were to undertake geological mapping and map verification of the SK area, to construct a 3D geological model, to compile a surface map of scintillation data and to collect surface samples and material from diamond drillholes for analysis. Secondly, detailed petrographic, geochemical and mineralogical analyses were undertaken on these samples in order to test and compare the variations of the granites within the SK area and to assess the spatial distribution of the uranium minerals. The SK geochemical and mineralogical results were compared with similar data for the SJ and SH areas, in order to compare and contrast geochemical and mineralogical variations between the three areas, a factor that is vital to both the metallurgist and geologist for any future development.

If the geochemical and mineralogical data of SK area is found to be similar to that of the SJ current pit, then the SK area could be mined concurrently with the SJ area, using the sulphuric acid leach plant. If the study indicates that the mineralogy of the SK area is similar to the SH area, where the dominant primary uranium mineral at surface is refractory betafite, then the mining of the SK area needs to be delayed because the current extraction process does not extract the uranium from betafite ore successfully. To date, all the uranium hosted in betafite ends up at the tailings dam.

The geological mapping/map verification was undertaken to outline the overall structural geology and to understand the relationship between the lithologies. The 3D model was created from the mapping information to provide a three dimensional view of the SK area. The 3D macro model has never been attempted before, thus the model created during this study will provide the basis of the 3D model, which will be modified and improved as more information is acquired (mainly by drilling) by the mine.

CHAPTER 2

GENERAL GEOLOGY OF THE DAMARA OROGENIC BELT

2.1. Introduction to the Geology of the Damara Orogen

The Damara Orogen belongs to the late Precambrian, early Palaeozoic (650 Ma to 460 Ma), Pan African Mobile Belt, which transects the African continent. The Damara Orogen was formed during collision between the Kalahari and Congo Cratons (Coward, 1983). Major deformation, metamorphism and intrusive events have taken place throughout the history of the Orogen and there is an indication of oblique subduction of the Kalahari Craton under the Congo Craton (Coward, 1983). Compression during collision resulted in contemporaneous transpressive shortening and lateral extension and escape of structures to the southwest as indicated in Figure 2.1 (Oliver, 1994).

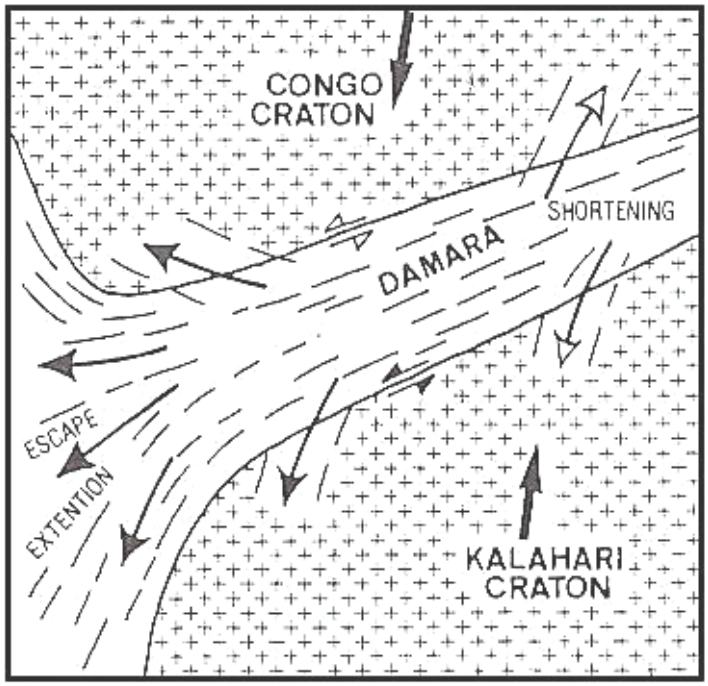

Figure 2.1: The sinistral movement of the Congo and Kalahari Craton during the late Precambrian early Palaeozoic, resulting in the formation of the Damara belt (after Oliver, 1994).

The Damara Orogen consists of two main sectors, the north-trending Coastal Branch, and the NE-trending Intercontinental Branch, which extends from Namibia into Botswana and Zimbabwe. The 400 km-wide Intercontinental Branch between the Congo and Kalahari Cratons is divided into four

major northeast-trending tectono-stratigraphic domains stretching from northeast to southwest, as indicated in Figure 2.2 (Miller, 1983a and b).

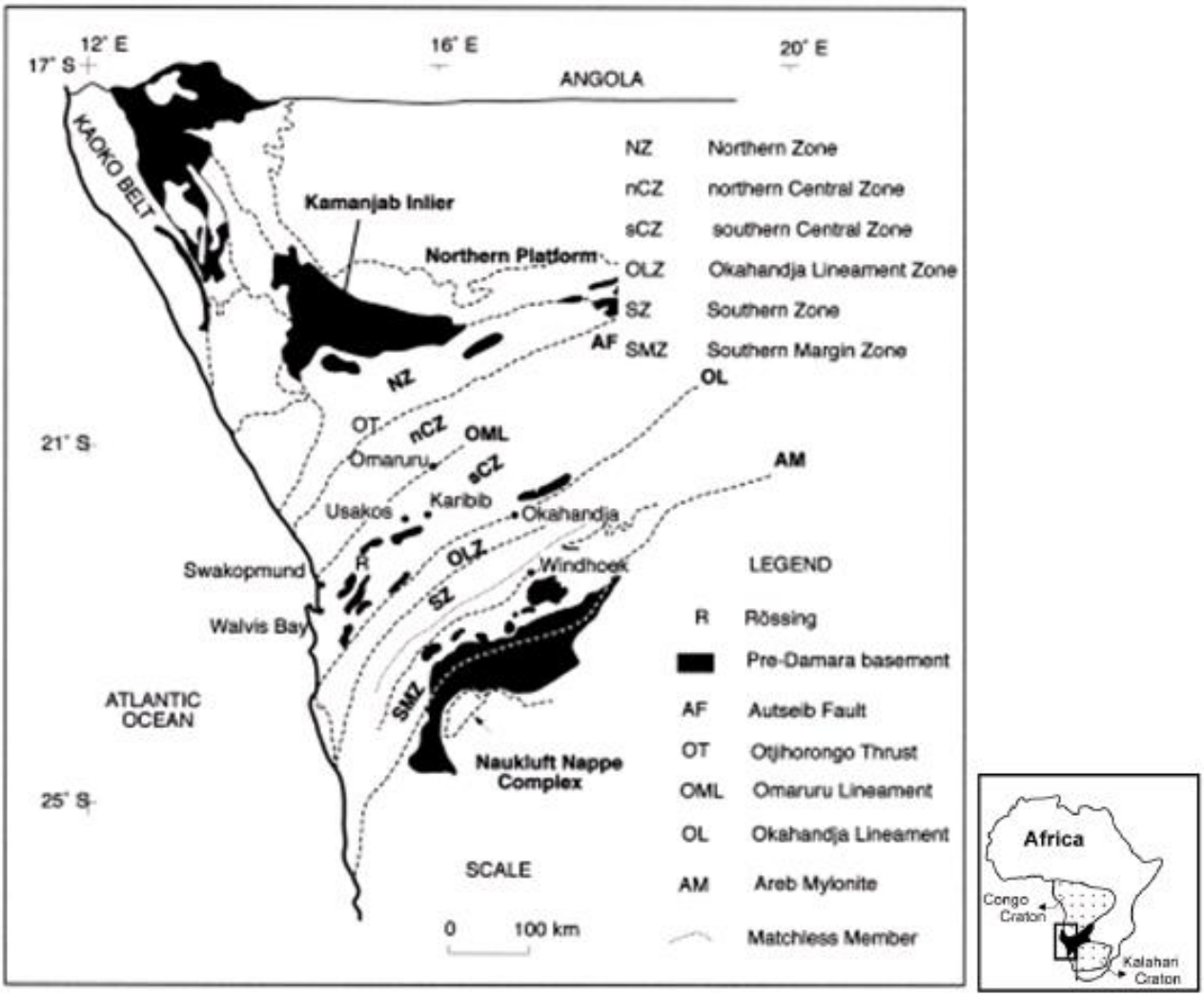

Figure 2.2: Map of the tectono-stratigraphic zones of the Damara Orogen in Namibia; showing the major faults and lineaments that separate the zones. Inset shows the location of the Damara Orogenic Belt in relation to Africa and the bounding cratons (Miller, 1983a and b).

The main structural domains in the Intercontinental Branch of the Damara Orogenic Belt recognised by Martin and Porada (1977) were: (1) the Northern Platform, consisting of a thick sequence of Otavi Group carbonates; (2) the northern Central Zone, consisting of folded and northward-thrusted rift volcanic and sedimentary rocks and related intrusive bodies; (3) the southern Central Zone, within which the Rössing ore body is located, (4) the Okahandja Lineament Zone, which separates the dominant dome-and-basin pattern of the Central Zone from the linear structures to the south (5) the southern Zone, comprising SE-thrusted accretion prism sequences (Corner, 1983); and (6) the

southern Margin Zone. The zone boundaries are formed by major linear structures, such as faults or lineaments with major aeromagnetic expression (Corner, 1983).

2.2. General Geology of the Central Zone

2.2.1. Introduction to the Geology of the Central Zone

The Central Zone is bounded by the Otjihorongo Thrust in the north and the Okahandja Lineament in the south (Figure 2.3), whilst the Omaruru Lineament divides the Central Zone into a northern Central Zone and a southern Central Zone (Figure 2.2). The northern and southern Central Zones are distinguished by lithofacies differences, the presence of basement inliers in the southern Central Zone, and most importantly, the occurrences of abundant granite plutons, which are characteristic of the southern Central Zone (Miller, 1983b). Between 660 and 460 Ma the Central Zone was extensively deformed and metamorphosed to amphibolite-granulite facies during polyphase deformation (Anderson and Nash, 1997). Nex *et al*. (2001a) also noted that the Central Zone experienced low-pressure, high-temperature metamorphism at the facies indicated by Anderson and Nash (1997). In the southern Central Zone, more than 300 granite plutons were intruded. These include pre-tectonic, syn-tectonic and post-tectonic granites.

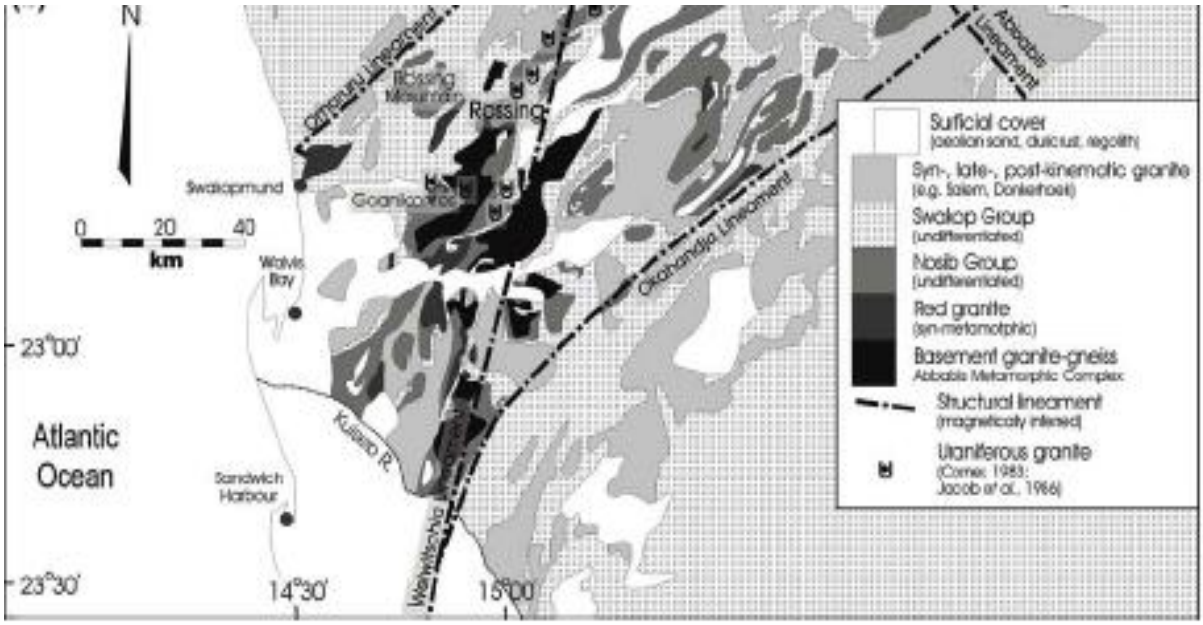

Figure 2.3: Rössing Uranium Mine is located in the Southern Central Zone between the Okahandja and Omaruru Lineament (Basson and Greenway, 2004).

A generalised stratigraphy of the Central Zone is shown in Table 2.1, (Jacob *et al*., 1986). The Abbabis basement complex is dominated by ortho- and paragneiss with minor schists, quartzites, marbles, amphibolites and calc-silicates. New age dating by Longridge et al (2008) shows consistent ages of ~2000 Ma for Abbabis lithologies. Such dates are in agreement with those of Jacob et al (1978).

Table 2.1: Stratigraphic column of the Central Zone in the Damaran Orogenic Belt (Jacob *et al*. (1986).

Group	Subgroup	Formation	Max thickness	Lithology
Swakop	Khomas	Kuiseb	>3000	Pelitic and semi-pelitic schist and gneiss, migmatite, calc-silicate, quartzite. Tinkas member: Pelitic and semi-pelitic schist, calc-silicate, marble, para-amphibolite.
		Karibib	1000	Marble, calc-silicate, pelitic and semi-pelitic schist and gneiss, biotite amphibolite schist, quartz schist, migmatite.
		Chuos	700	Diamictite, calc-silicate, pebbly schist, quartzite, ferruginous quartzite, migmatite.
	Discordance			
	Ugab	Rössing	200	Marble, pelitic schist and gneiss, biotite-hornblende schist, migmatite, calc-silicate, quartzite, metaconglomerate.
	Discordance			
Nosib		Khan	1100	Migmatite, banded and mottled quartzofeldspathic clinopyroxene-amphibole gneiss, hornblende-biotite schist, biotite schist and gneiss, migmatite, pyroxene-garnet gneiss, amphibolite, quartzite, metaconglomerate.
		Etusis	3000	Quartzite, metaconglomerate, pelitic and semi-pelitic schist and gneiss, migmatite, quartzofeldspathic clinopyroxene-amphibole gneiss, calc-silicate rock, metarhyolite.
Major unconformity				
Abbabis Complex				Gneissic granite, augen gneiss, quartzofeldspathic gneiss, pelitic schist and gneiss, migmatite, quartzite, marble, calc-silicate, amphibolite.

The basal Etusis Formation lies unconformably on the Abbabis metamorphic basement complex. In the Rössing area the Etusis Formation consists predominantly of metaquartzite with minor biotite schist. Elsewhere in the Orogen, rift related acid volcanics close to the base of the Damaran succession have been dated at 746±2 by Hoffman et al (1996) and 752±7 by de Kock et al (2000). The Khan Formation consists of pyroxene-garnet amphibole gneiss with a distinctive marker horizon of dark biotite-amphibole schist commonly at the top of the Khan Formations. The Rössing Formation, which overlies the Khan Formation, consists of metaquartzite, metapelitic gneiss and marble.

The succeeding Khomas subgroup lithologies are not exposed in the environs of the Rossing Mine although they are well exposed in the Khan River to the south of the mine lease. The Chuos diamictite is correlated with the worldwide Sturtian glacial event by Hoffman (2005) which constrains the age for the Chuos at around 710 Ma. Thus sedimentation of the Damaran lithologies in the Rössing area occurred between ~750 and 710 Ma.

2.2.2. Regional Structural Evolution of the Central Zone

The metasedimentary cover, together with the basement rocks, was subject to polyphase deformation during the Damara orogeny resulting from the collision of the Kalahari and Congo cratons. A north-east trending structural grain dominates the Central Zone of the Damara Orogen with a prominent elongate dome and basin pattern. An overview of regional deformation events in the Southern Central Zone is summarised in Table 2.2. The major NNE-oriented Welwitschia (F4) lineament in the central Damara Orogen, shown in Figure 2.3, was initially recognised by Corner (1983) and Jacob *et al*. (1986) from the pre-existing regional aeromagnetic data. The regional interpretation suggests that this major lineament is a series of en-echelon sinistral strike slip faults associated with late (post-F3) evolution of the Damara Orogen.

Planar bedding and pyritic quartzite bands are preserved in the marbles of the Rössing Formation, especially in the Rössing area. Original sedimentary layering (S0) is preserved in the form of bedding and cross-bedding within the Khan and Etusis formations in the Goanikontes area (Nex, 1997) and cross-bedding that is highlighted by a concentration of iron oxides along fore-sets can be seen in Etusis quartzites on the edge of the Rössing Dome, close to the mine gate.

Table 2.2: Deformation events in the Rössing area. From Basson and Greenway 2004, after Smith (1965), Sawyer (1978), Martin (1983), Coward (1980), Buhn and Stannistreet (1992), Anderson and Nash (1997) and Nex *et al*. (2001a, b).

Deformation event	**Deformation event Major fold trend**	**Rössing Formation**	**Khan Formation**	**Etusis Formation**
Original layering		Planar bedding in marbles and pyritic bands	Not evident in Rössing area	Relict heavy mineral layering in orthoquartzites S1 and S2 migmatitic banding
D1	F1: unknown	S1 and S2 laminar foliation in pelites	S1 and S2 migmatitic banding to the west of the Rössing Dome	
D2	F2: NW (?)			
D3	F3: NE	S1and S2 transposed into subparallelism with S3; flow folding in marbles	S3 schistosity superimposed on migmatitic banding	Non-systematic brittle–ductile deformation of migmatitic banding
D4	(F4): NNE Rössing Dome axis orientation and Welwitschia Trend.	Small, isolated folds with axial planar foliation (S4) Inferred NNE-trending left lateral shears cross-cutting and re-orienting NE-trending F3 folds (shears later intruded by Karoo dolerites)	Inferred NNE-trending left-lateral shears crosscutting and re-orienting NE-trending F3 folds	Not discernible

Major deformation events took place at about 650 m. y., (D_1), 610 m. y. (D_2) and 530 m. y. ago (D_3) (Oliver, 1995). There is a high strain zone between Abbabis granite gneiss domes and Damaran cover, interpreted as a mid-crustal detachment following the collision of Kalahari and Congo Cratons at about 550 Ma. (Oliver, 1995).

D1 produced an intense S- to SSE-verging series of recumbent isoclinal folds with associated ductile shear zones. The folds have wavelengths and amplitudes on the order of 100s of metres and are interpreted as second-order features on a large recumbent fold nappe (Longridge et al., 2008). D_1 produced a widespread gneissosity with rare isoclinal intrafolial folds preserved that pre-date magmatism and metamorphism in the Orogen (Longridge et al., 2008). Evidence for D1 was not noted in the Rössing environs.

D_2 resulted in upright, northeast-trending open to tight folds with wavelengths and amplitudes ranging from the m-scale to the km-scale, generally verging to the SE but varying from south to east according to Longridge et al (2008). Again evidence for this phase of deformation is not clear in the Rössing mine area although Buhn & Stannistreet (1992) suggested that the polyphase deformation of

the metasedimentary cover and basement rocks during D2 resulted in prominent gneissosity which was deformed by later events.

D3 is characterised by gentle, large wavelength and amplitude folds (metres to tens of metres), with shallow dipping axial planes that dip to the N or NE (Longridge et al., 2008). Evidence for this phase of deformation dominates the structural fabric of the Rössing mine area area with highly ductile flow folding in the marbles of the Rössing Formation (Basson and Greenway, 2004).

D4 deformation is characterised by the ductile-brittle transition and NNE Welwitschia trend sinistral strike-slip zones (Basson and Greenway, 2004). The NNE-trending axis of the Rossing Dome is ascribed to rotation of the NE-trending F3 axis during D4 (Basson and Greenway, 2004).

The Central Zone is characterised by abundant Damaran country rock domes. Doming is commonly ascribed to D3 deformation, although the actual mechanisms of dome formation are controversial (Kisters *et al*., 2004). The domes have been attributed to regional scale fold interference by Smith (1961), while Ramsberg (1972) has stated that the folds are caused by the buoyant rise of granitic (basement) diapirs into the meta-sedimentary cover rocks, and Coward (1980) has postulated that the domes are sheath folds within shear zones. Smith (1961), Jacob *et al*. (1983) and Kroner (1984) suggested that the domes tend to be elongated in the NE-SW direction. The domes are often asymmetric with the NE-facing sides dipping moderately to the NE whilst the SW facing sides are either steeply dipping to the SW, vertical or overturned so that they also dip moderately or steeply to the NE. The domes have been intruded by granites; mainly by a non-foliated pegmatitic alkali leucogranite which intrudes as sheets following the stratigraphy as sills and dykes (Oliver, 1995). Kisters *et al*. (2004) highlighted the presence of two orthogonal structural domains within the southern Central Zone. The regional dome structures (Karibib and Usakos domes), together with the Mon Repos thrust zone, a regional scale emergent thrust, form part of a deeply eroded foreland NW vergent fold and thrust belt. Kisters *et al*. (2004), further stated that the granitoids that intruded the Mon Repos thrust zone constrain the time of thrust and dome formation to between 550 and 540 Ma. This period corresponds with the collision between the Kalahari and Congo Cratons (Kisters *et al*. (2004).

2.2.3. Metamorphism of the Central Zone

Hartmann *et al*. (1983) indicated that in the Central Zone there was an increase in metamorphic grade from east to west reaching high-grade conditions with local partial melting near the Atlantic coast. These high-temperature conditions led to the formation of garnet-cordierite-(spinel)-bearing migmatites and to incipient melting of fertile metasediments (Jung *et al*., 1998). There is a suspected metamorphic gap between basement and Damara cover and Oliver (1994) concludes that the contact is an extensional detachment.

In the Goanikontes area, Nex (1997) identified two phases of metamorphism based on mineral geothermometry. M1 regional metamorphism based on early garnet-cordierite indicated 718±35°C for cores and 610°C for rims at a pressure of 5-6 kbars, which is consistent with Masberg *et al*., (1992), Buhn *et al*., (1994,1995) and Jung *et al*., 1998. Garnet and monazite geochronometry suggests M1 metamorphism occurred between 530-523 Ma (Goscombe et al., 2004)

A higher temperature M2 granulite facies event overprinted the D3 extensional fabric and was probably caused by voluminous magmatism in the area extending from Otjosonu towards Swakopmund ((Masberg *et al*., 1992; Nex, 1997, 2001). Spinel symplectites with co-existing quartz and cordierite indicate temperatures in excess of 770°C at <3 kbar (Nex, 1997). These were associated with high T decompression and growth of unoriented sillimanite which overprints earlier fabrics. Masberg *et al*. (1992) also indicated the presence of low-pressure granulite-facies conditions, with microscopic evidence of mesoperthitic string–perthites and antiperthites in feldspars and oriented exsolution of rutile needles in quartz.

M1 occurred at about the time of D_1 and perhaps M2 occurred from D_3 onwards (after Miller, 1983a and b).

2.2.4. Granites in the Central Zone

The Central Zone of the Damara Orogen is noted for voluminous granitic intrusions which crop out over an area of at least 75 000 km^2. There are more than 300 intrusions, of these, 96% are granitic with 4% minor calc-alkaline gabbroic to granodioritic rocks (Miller, 1983). The granitoid intrusions vary in size from the Donkerhuk granite (5 000km^2) to numerous small stocks (10's kms. Miller,

1983 and swarms of late-stage sheeted leucogranites only a few meters in thickness (Haack *et al.*, 1982).

Table 2.3: Field characteristics and age dates for the main granite groups of the Central Zones.

Granite Type	**Age**	**Field Characteristics**
Sheeted leucogranites	509 ± 1 Ma U–Pb monazite, isotope dilution. Briqueu et al., 1980.	Subdivided into six distinct types based on detailed fieldwork by Nex (1997), see Table 5.4 for a detailed description. All the sheeted leucogranites (SLGs) show clear sharp contacts with their host rocks frequently cross-cutting the main gneissosity although some are intruded parallel to this regional foliation. Mineralogically, all SLGs consist of quartz, alkali-feldspar and plagioclase in varying proportions ranging from tonalite to alkali-feldspar granite. (Nex et al., 2001b)
Grey granite	517 ± 7 Ma (U–Pb monazite. 520.4 ± 4.2 - 519.1 ± 4.2 Ma. Shrimp zircon Longridge *et al.*, (2008)	Homogeneous, fine to medium grained. Forms irregular plugs (<50 m^2) or sheets within the high strain zones 1–4 m in width. Variable foliation, where present this is defined by prominent biotite. Cross-cuts red granite (Nex et al., 2001b).
Syn-tectonic red syenogranites	534 ± 7 Ma U–Pb, zircon, isotope dilution. Briqueu et al., 1980.	Homogenous, fine to medium grained. Forms irregular plugs or sheets within the high strain zones at Goanikontes 1-30 m in width. Foliation defined by biotite and opaque oxides. Xenoliths and enclaves generally absent (Nex et al., 2001b)
Salem granite	549±11 Ma U-Pb zircon LAM-ICP-MS. Johnson et al, 2006	Syn-tectonic granite suite. Typically porphyritic (Miller 1983)
Red granite gneiss	2093 ± 51 Ma. SHRIMP U-Pb zircon. Kröner *et al.*, (1991)	Abbabis basement red granitic gneiss

Marlow (1981) subdivided these granites of the Central Zone into (1) early biotite-rich Red granite, (2) Salem-type porphyritic granite, (3) leucogranite and (4) late alaskites. Brandt (1987) also recognised Red granite as the oldest intrusive type followed by Salem-type. However, Brandt then distinguished post tectonic red and grey homogeneous granites followed by alaskites. Nex (1997) concurred with the classification of Brandt (1987) for the granites of the Goanikontes area (Table 2.3) although no Salem-type granites were noted in the Swakop River. Jung (2005) suggested three types: (1) The S-type syn-orogenic granites (530 to 520 Ma) which are garnet- and cordierite-bearing, (2) post-orogenic granites (490 Ma) which are hornblende- and titanite-bearing, and (3) post-orogenic leucogranites (480 Ma) which are garnet bearing. Longridge *et al*., (2008) following the classification scheme of Brandt (1987) and Nex (1997), recognised several different grey granite facies with an early dark grey phase, an intermediate medium-grey phase and a late leucocratic phase. Longridge *et al*. (2008) indicated, based on U-Pb SHRIMP zircon age dating, that there is no significant age difference between the oldest grey granites (520.4 ± 4.2 Ma) and the youngest granite phases (519.1 ± 4.2 Ma) (Table 2.3).

Six sheeted leucogranite types were recognised at Goanikontes on the basis of structural setting, field characteristics, colour, mineralogy and major- and trace-element geochemistry (Nex *et al*., 2001a and b). These were termed types A-F with A representing the earliest sheets and F the latest. An increase in alkali feldspar abundance is associated with an increase in the primary uranium mineralisation for types C, D and E granite (Nex *et al*., 2001a). The garnetiferous B-type leucogranite sheets which were emplaced during peak metamorphism yielded an age of about 520.3 ± 4.6 Ma, whilst U-Pb SHRIMP monazite dating gives a slightly younger age of 514.1 ± 3.1 Ma (Table 2.3).

Miller (1983a and b) regarded the granites as local products of in situ melting of the local basement rocks. Oliver (1994) interpreted the structures of the Khan River area and suggested that the basement cover contacts are represented by generally subhorizontal, partly mylonitic high strain zones, locally developed as ductile extensional shear zones that promoted intrusion of granite. Oliver (1995) regarded granite magma generation as a consequence of orogenic extension following the collision between the Congo and Kalahari Cratons. Tack and Bowden (1999) provided field evidence suggesting successive generations of Damaran post-collisional granitoids at around 550 Ma. These include medium-grained syeno-monzogranites and younger pegmatitic leucogranites invading the Damaran cover sequence and the pre-Damaran basement. The source of the granites in the Central Zone is still under discussion, with the main focus being migmatisation, partial melting and melt segregation. The post-orogenic S-type leucogranites have an isotopic signature which suggests additional input from mid-Proterozoic volcaniclastics sources (Jung, 2005).

2.3. Uranium Mineralisation in the Central Zone

Namibia constitutes a uraniferous province with known uranium enrichment occurring in basement granite gneiss, in Damaran metasedimentary rocks and intrusives, in Karoo sediments and carnotite-rich calcrete and in siliciclastic-hosted surficial deposits which developed in the Tertiary (Kinnaird et al, 2009).

Uranium mineralisation within the Central Zone was noted in the early 1920s in the vicinity of Rössing Mountain (Jacob, 1974b). Further prospecting and exploration ultimately resulted in the discovery of the Rössing uranium deposit. Other primary alaskite-hosted anomalies in the southern Central Zone are currently under exploration and evaluation at Valencia, the Ida Dome, and Goanikontes (Mouillac *et al*., 1986; Nex & Kinnaird, 1995; Nex, 1997; Nex *et al.*, 2001b). Early workers noted that uranium mineralisation appears to be confined to late undeformed alaskitic

intrusions (Jacob, 1974b). Nex *et al.*, (2001b) showed that sheeted leucogranites can be divided into six different types based on field characteristics of colour, grain-size, structural setting and mineralogy (Nex and Kinnaird 1995; Nex 1997). Of these six types of alaskite (A-F), three are barren of U mineralisation and were pre-D_3 while post D_3 alaskites are more prospective for uranium. Although this classification is based on the Goanikontes area, some 30 km to the southwest, this scheme can be applied to the Rössing area (Basson and Greenway, 2004).

Granites in the Rössing Uranium Mine SJ area are dominated by sheeted leucogranites that intruded into weak zones such as faults and shear zones and preferentially at the Khan/Rössing Formation contact. At Valencia the main mineralised body is formed by a series of coalesced leucogranite sheets intruded into a local disharmonic kink fold to the east of a major anticlinorium (Freemantle, 2006, Kinnaird et al., 2009). Around the Ida Dome, uranium-bearing sheeted leucogranites have intruded preferentially along the east and southeast sides of the Dome approximately at the Khan-Rössing Formation contact although thinner sheets also intrude the Rossing marbles. In Garnet Valley and the Holland's Dome to the southeast of Ida Dome, these sheets have locally coalesced into small plutons. The Ida Dome leucogranites pre-date those of Rössing SJ area, according to Marlow, (1983) based on an Rb-Sr age of 542±33 Ma. In the Goanikontes area, a pre-Damara basement in the east, is separated from a lower to middle Damaran succession folded around a northeast plunging anticlinal structure to the west by a high strain zone of attenuated Damara lithologies (Nex, 1977). Uraniferous sheeted leucogranites preferentially intruded this high-strain zone

Uranium in the Rössing, Valencia, Ida and Goanikontes areas, is hosted in primary uraninite and betafite (a pyrochlore-group) within late-stage leucogranites. Secondary uranium minerals such as β-uranophane and uranophane occur as replacements of the primary minerals in the granites, or as films and coatings along fractures in both the granites and country rocks (Nex and Kinnaird, 2005) although metatorbernite, metahaweeite, carnotite, thorogummite and gummite have been noted (von Backström, 1970).

In addition to the leucogranite-hosted uranium mineralisation, post Damaran re-mobilisation of uranium occurred during the Mesozoic while surficial uranium was concentrated in fluvial deposits in paleochannels of ancient rivers that flowed westwards from the Great Escarpment across the Namib Desert probably since early to mid Tertiary (Kinnaird *et al*., 2009).

CHAPTER 3

LOCAL RÖSSING GEOLOGY

3.1. Country Rocks

The country rocks of the Rössing area consist mainly of deformed Khan and Rössing Formations, with minor Etusis quartzite (Table 3.1.). The leucogranite sheets of the SJ, SH and SK areas are preferentially located within the Khan and Rössing Formations, or at the boundary between them (Figure 3.1).

Table 3.1: The stratigraphy of the SJ area. From Nash (1971).

Group	Formation	Unit	Thickness (metres)	Lithology
Swakop	Rössing	Quartzite	< 100	Medium-grained quartzite, gritty near base
		Upper cordierite gneiss	40-50	Diopside-biotite(-scapolite) gneiss with thin inter-bedded quartz grit and marble near base; grading upwards into cordierite-biotite gneiss
		Upper marble	50-70	Serpentine marble and diopside-quartz marble with inter-bedded biotite-diopside granofels and cordierite-biotite gneiss. Conglomerate-grit at base.
		Lower cordierite gneiss	30-40	Migmatised cordierite-biotite-sillimanite gneiss, locally garnet-bearing, grading into biotite-diopside granofels and pelitic schist.
		Lower Marble	20-50	Serpentine marble and subordinate graphite marble, with irregular intercalations of biotite-diopside granofels and pelitic schist
Nosib	Khan	Para-amphibolite and conglomerate	10-20	
		Upper basic gneiss	70-120	Amphiobole-biootite schist containing local pebble bands
		Pyx-gnt gneiss	0-120	Strongly migmatised amphibole and pyroxene gneiss
		Orthoamphibolite		
		Pyx-gnt gneiss		
		Lower basic gneiss	70-150	Migmatised pyroxene-garnet gneiss; local concordant bodies of hornblende-oligoclase orthoamphibolite
				Strongly banded, partially migmatised pyroxene-amphibole gneisses
	Etusis	Psammitic gneiss	> 300	Strongly migmatised quartzofeldspathic gneisses with numerous biotite foliae.

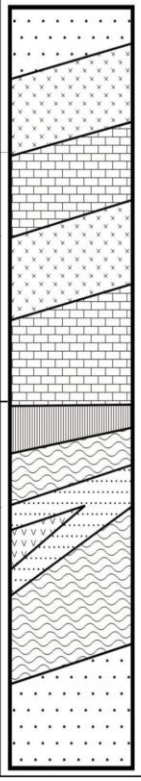

3.1.1. Etusis Formation

In the Rössing area, psammites of the Etusis Formation (Nosib Group) form the core of the Rössing Dome. The Etusis Formation consist of quartzites and meta-arkoses which have a pale pink coloration

and exhibit cross bedding on a small scale (100-200mm), with foresets highlighted by concentrations of Fe-Ti oxide minerals. The psammites gradationally pass into Khan Formation with an increase in biotite and cordierite (Nex, 1997).

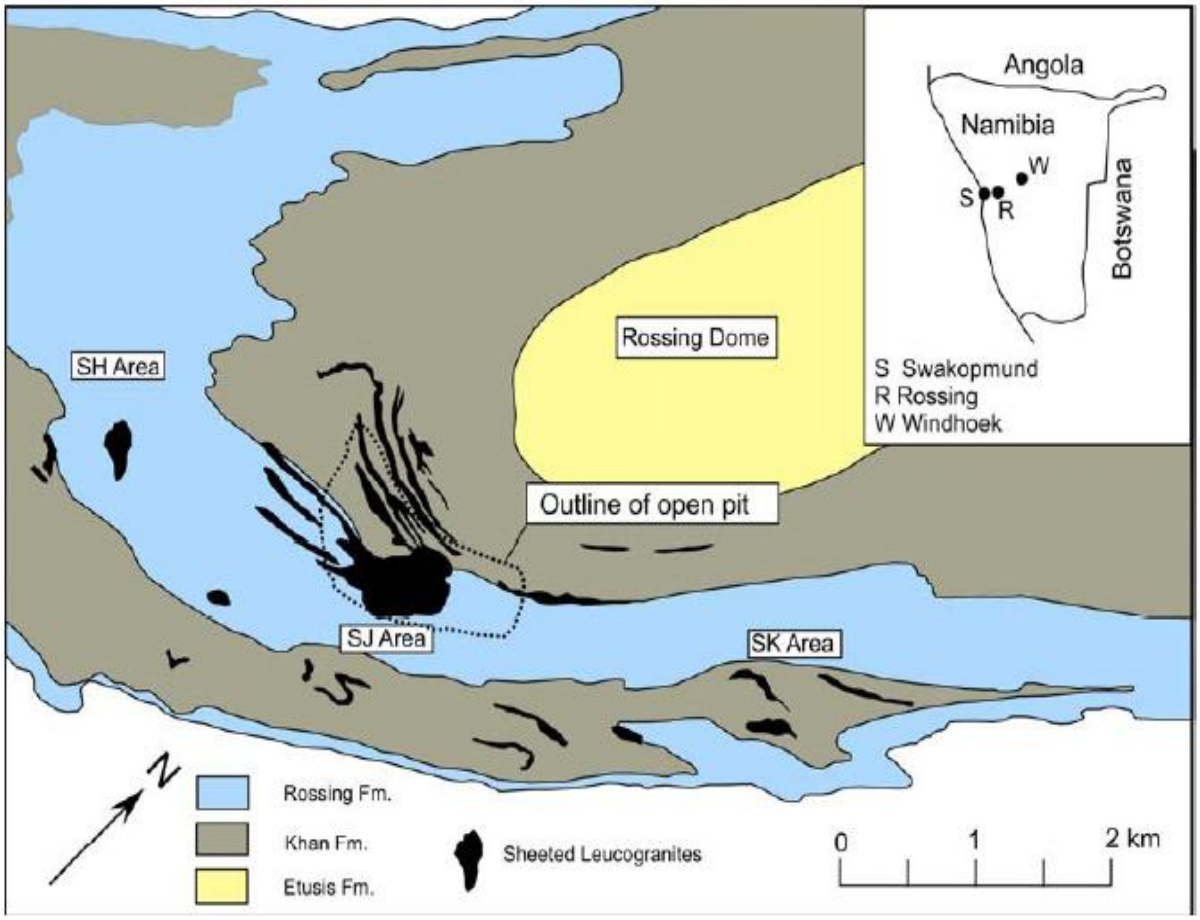

Figure 3.1: Local Rössing geology showing the main anomalies (SH, SJ and SK) after Smith (1961).

3.1.2. Khan Formation

The Khan Formation (Nosib Group) comprises locally banded migmatitic amphibole–clinopyroxene gneisses. Towards the top of the Khan Formation, there is an increase in amphibole content in place of pyroxene, terminating in a thin unit of amphibole–biotite schist with minor, discontinuous pebble horizons (Nash, 1971).

The lower and upper basic gneisses of Nash (1971), shown in Table 3.1, are termed the lower and upper banded pyroxene hornblende gneisses on the Rössing Uranium Mine lease. The banded

appearance is caused by the orientation of the migmatitic leucosomes parallel to the foliation (Nash, 1971).

Between the lower and upper banded gneisses is a pyroxene-garnet gneiss unit which shows metamorphic banding in the area east of the deposit, but has a massive and mottled appearance to the west (Rössing Internal report, 050505, 2005). This unit carries discontinuous massive bodies and lenses of amphibolites that are exposed in the NW section of the SJ open pit.

3.1.3. Rössing Formation

The Rössing Formation is paraconformably and disconformably overlying the Khan Formation (Table 3.1) although in the Rössing area there appears to be a gradual transition between the two Formations. In the vicinity of the Rössing Uranium Mine, the Rössing Formation is subdivided into a lower serpentinitic marble, a meta-pelitic gneiss and an upper siliceous and serpentinitic metacarbonate unit interbedded with granofelsic/schistose layers and is succeeded by meta-pelitic gneiss subunits (Basson and Greenway, 2004). A typical Khan/Rössing contact succession can be observed in the SJ pit, where the Khan Formation is separated from the Rössing Formation by the biotite amphibole schist that bisects the pit.

3.2. Structural Evolution of the Rössing Area

Original sedimentary layering (S0) is preserved in the form of bedding and cross bedding within the Etusis and Rössing Formations. Planar bedding and pyritic quartzite bands are preserved in the marbles of the Rössing Formation.

S1 and S2 migmatitic banding, particularly in areas to the west of the Rössing Dome, are preserved within the Khan and Etusis Formations, while S1 and S2 occur as foliations in Rössing Formation meta-pelites. D3 deformation produced highly ductile flow-folding in the marbles of the Rössing Formation. An S3 gneissosity to schistosity, as observed in the Rössing Dome and the Rössing deposit, almost pervasively replaced migmatitic S1 and S2 banding. The Etusis Formation shows non-systematic brittle–ductile deformation of S1/S2 migmatitic banding (Anderson and Nash, 1997).

Jacob and Kerber (1997) noted the persistent F3 deformation in the area to the SW of Rössing. Jointing, which formed during late D3, has a NW–SE trend. There is a discordance of approximately 25° between the regional trends of F3 folds (042°) and the long axis of the Rössing Dome (017°). Basson and Greenway (2004) stated that the difference in orientation between the folds and the dome is due to dome rotation during F3 to F4. They noted the left-lateral shear to the east of the dome that translates locally into a thrust in the area just SSE of the Dome.

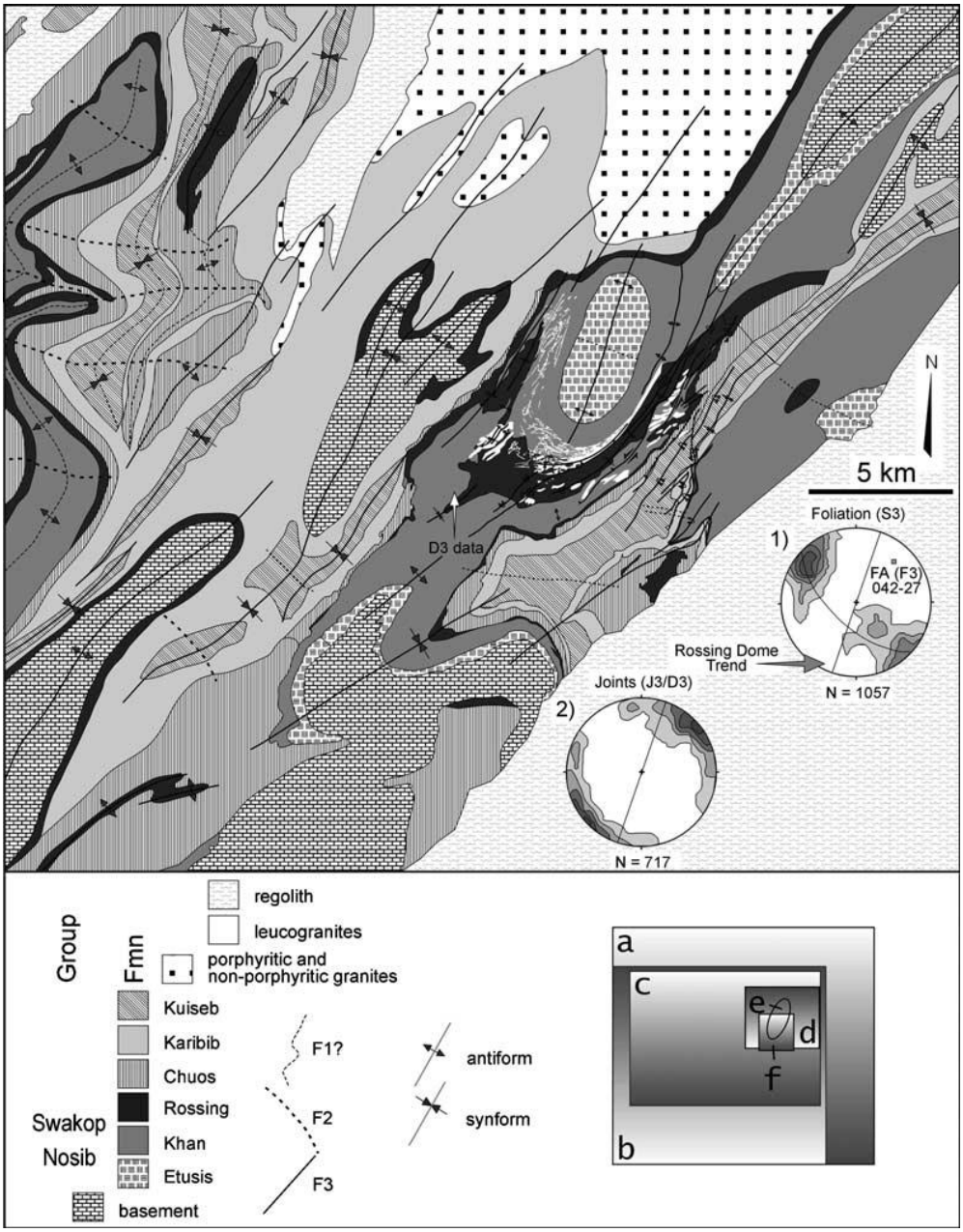

Figure 3.2: Highlights of the structural features in the Rössing area, showing that there is a discordance of approximately 25° between the regional trends of F3 folds and the long axis of the Rössing Dome (Anderson and Nash, 1997).

Anderson and Nash (1997) concluded that polyphase folding, terminating in F3, was followed by the development of a post-D3 to D4 Welwitschia Lineament, sinistral strike-slip zones and the NNE orientation of the Rössing Dome axis.

Most uraniferous alaskites in the Rössing area are located near the major F4 NNE trending lineament, and locally folds are also parallel to this structure. Anderson and Nash (1997) support a post-folding shear event, characterised by NNE oriented sinistral wrench faulting and ENE oriented SE vergent thrusting. Nex (1997) stated that unmineralised leucogranites are pre-D3; whereas the mineralised ones are post D3.

The development of anticlinoria and synclinoria (Figure 3.2) in the Rössing area was caused by constrictional tectonic events which possibly included doming, following the model of Oliver (1995). The pervasive F3 folding or constrictional deformation produced an average fold plunge of 042/27 (Jacob and Kerber, 1997).

3.3. Granite Intrusion

The sheeted leucogranites, locally termed alaskites at the Rössing Uranium Mine, vary in thickness from centimetres to metres and are intruded parallel and sub-parallel to banding mainly in the SK (anticline) and SJ (syncline) areas. Within the SH anticline of the SH area, the leucogranite constitutes a plug flanked by sheets on the margins. These leucogranites of the Rössing area are similar in terms of age, colour, and texture and emplacement history to the leucogranites of the Goanikontes area, 30 km west of Rössing Uranium Mine (Basson and Greenway, 2004).

According to the recommendations of the Terminological Commission of the Petrographic Committee of the USSR (1969), the term alaskite is used to describe granitoid rocks in which quartz constitutes 20-60% of the felsic minerals and in which the ratio of alkali feldspar to total feldspar is greater than 90%. Nex (1997) has supported the above definition, and has determined an alaskite as a leucocratic variety of alkali feldspar granite consisting almost entirely of quartz and alkali feldspar. The term alaskite therefore is now very much regarded as a term synonymous with leucocratic alkali feldspar granite of the QAPF field.

Nex *et al*. (2001b) suggested that the sheeted leucogranites span a compositional range from granodiorite, through monzo- and syenogranites to alkali feldspar granite; it is therefore incorrect to refer to them all as alaskites. However, since it is generally the alkali feldspar granites that are uranium enriched, the term alaskite remains a useful field description.

3.4. Metamorphism

Contact metamorphic effects are evident in metasedimentary rocks bordering the granite bodies, particularly where the granites have intruded the marbles of the Rössing Formation. Skarn bodies, ranging in size from a few centimetres to several metres are widespread in the Rössing area, the majority being composed of coarse aggregates of pale green clinopyroxene, brown calcic garnet up to several centimetres in size (Nash, 1971) and varying amounts of scapolite, magnetite, sphene and other accessories. High temperature regional metamorphism is evident with the development of garnet, cordierite and unoriented sillimanite within Etusis psammites.

3.5. Uranium Mineralisation in the Rössing Area

Although uranium minerals were known from the area since the 1920's (Smith, 1965), the first description in the area was presented by von Backström and Jacob (1978) and later, more detail was provided by Berning *et al*. (1976). The Rössing area hosts both primary and secondary uranium minerals. Primary uranium minerals are hosted in granites, while secondary uranium minerals can be found in both granites and country rock.

The main primary uranium minerals found in the Rössing area are uraninite (UO_2) and betafite $(Ca,Na,U)_2(Ti,Ta,Nb)_2O_6(O,OH)$, although other primary minerals (davidite and rössingite) can also be found in trace amounts. Beta-uranophane ($Ca(UO_2)_2[SiO_3(OH)]_2.5H_2O$) is the dominant secondary uranium mineral, although other secondary uranium minerals such as the uranophane ($Ca((UO_2)_2[SiO_3(OH)]_2.5H_2O$), boltwoodite $(K,Na)[UO_2)(SiO_3OH)](H_2O)_{1.5})$, thorogummite $((Th,U)(SiO_4)_{1-x}(OH)_{4x})$, haiweeeite $((Ca(UO_2)_2(Si_5O_{12}(OH)_2]4.5H_2O)$ and metahaiweeite $(Ca(UO_2)_2(Si_6O_{15}(OH)_2].nH_2O)$ also occur in small amounts (Nex and Kinnaird, 2005). The ratio of primary to secondary minerals is roughly 1:1 in the SJ area (Nex and Kinnaird, 2005), but might vary in the SK area.

Duarte (2006) stated that most of the above mentioned primary uranium minerals are attached to, or locked into feldspar, quartz, Ti-oxides, mica, titanite and Fe-oxides. Secondary U-minerals are not confined to leucogranites like the primary U-minerals but can be found in leucogranites, country rocks, lithological contacts, fault and joints. Economic mineralisation in the SJ (current main pit) occurs in country rocks and leucogranites in two merging arcs around the southern tip of the Rössing Dome and extending towards the shear zone to the east (Basson and Greenway, 2004).

3.6. Proportion of Uranium Minerals

The current acid leach in the processing plant has 90% efficiency of removal of the U^{4+} from uraninite and the U^{6+} from betauranophane and other secondary minerals. However, uranium from refractory betafite is lost in the current processing. Betafite forms only around 5% of the uranium mineral population is the SJ open pit whereas it is the dominant uranium phase at surface in the SH area (Nex and Kinnaird, 2005). Little is known of the uranium deportment in the anomalies of the SK area and hence formed the basis for the research of this thesis in this area.

CHAPTER 4

SK AREA

4.1. Introduction

The SK area is characterised by a major anticline with a core of Khan Formation and flanks of Rössing lithologies. Evidence for the anticline are the bedding/cleavage relationship further discussed in this chapter and the SK lithologies which young outward. The trend of the SK anticline is about 038°; Jacob and Kerber (1997) stated that persistent F3 regional folding deformation has an average orientation of about 042°.

The SK area comprises a series of uranium anomalies (Murphy, 1996) that have been delineated using radiometric data. These include areas such as SK2, SK4, SK9, SK12 etc that are shown on Figure 4.1. The individually numbered anomalies are further subdivided (by the addition of an alphabetic suffix) resulting in 32 anomalies within the SK area. Not all the SK anomalies are currently exposed; some anomalies such as SK14, SK15, SK16 and SK17 have been covered with waste material.

Previous geological work carried out in the SK area focussed on the high-grade sub-anomalies. This work included geological mapping and detailed ground radiometric surveys of the individual sub-anomalies. Little attention was paid to the feasibility of the SK area as one large, low-grade deposit. This study considered the SK area as one single anomaly and produced a detailed geological map, using the available Rio Tinto historic maps. Rio Tinto's data was derived from Louw (1977, 1979).

A detailed field map is shown in Appendix 1. The field map contains both the lithological and structural information of the SK area. An initial 3D geological macro-model was established prior to drilling. In this chapter, an interpreted pre-intrusion country rock surface map (presented in Appendix 2), was used to produce a 3D geological model.

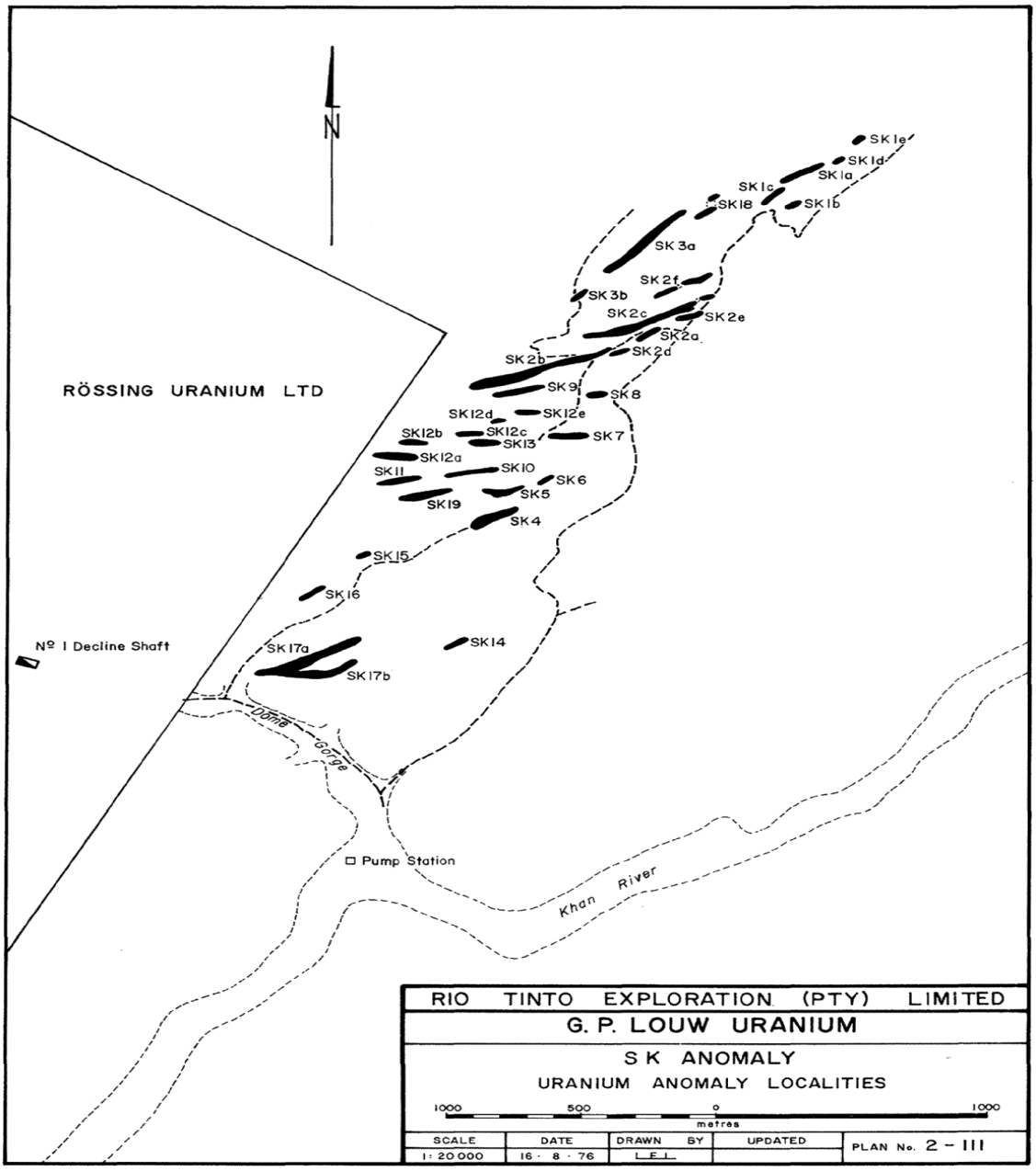

Figure 4.1: The SK anomaly is situated north of the Khan River. At least 32 sub-anomalies form part of the SK overall anomaly. (Rössing Internal report, 050505, 2005).

4.2. Methodology

Small scale maps containing both the lithological and structural information, were selected from historic data available in Rossing Uranium records and synthesised into one map with a LO coordinate system. In order to do this, old maps with a geo-reserve local mine coordinate system needed to be converted back to the LO system in the AutoCAD system. These maps were then geo-

referenced to the correct field positions as a basis for fieldwork. Verification of the geo-referenced was undertaken in the field. Ground-truthing of the constructed map included checking the correct identification of the lithologies, correct mapping of lithological contacts and structural features were checked and supplementary data gathered. Where necessary, subsequent field mapping was completed in order to infill areas where the available maps lacked data, so as to compile a complete up-to-date map of the whole of the SK area. Once this completed map had incorporated all the original historic data and infill mapping, the data were digitised using the AutoCAD program. Lithologies shown on the various maps were merged to produce an overall SK area geological map.

The ground truth verification of the compilation was important as it provided an overall understanding of the area in terms of geology, stratigraphy and structural analyses and formed the basis of the construction of a 3D model for the SK area. The 3D model was produced using Minesite program. Minesite is a geological and mine planning computer program, that helps with the creation of 2D sections and 3D model of areas.

4.3. Stratigraphy of the SK Area

The stratigraphy of the SK area is similar to the SH and SJ areas. The three areas are all characterised by Khan and Rössing Formations. Calculations of the true thickness of lithologies in the SK area were obtained using surface mapping data or diamond drillhole information for non-outcropping rocks (Table 4.1). This data was compared to that for the SJ area (Table 4.2).

Table 4.1: Example of the true thickness of various lithologies using apparent thickness of a surface- exposed rock or diamond drilling intersected depth.

Rock type	**Bedding/hole dip in degrees**	**Apparent thickness**	**True thickness using sin of dip**	**True thickness (m)**
Lower cordierite gneiss	50	15 to 50	Sin50 x 15 to 50	11 to 38
Lower marble	70	70 to 150	Sin70 x 70 to 150	66 to 141
Amphibole-biotite schist	65	30 to 125	Sin65 x 30 to 125	27 to 138
Upper banded gneiss	80	100 to 250	Sin80 x 100 to 250	98 to 246
Mottled gneiss	60	>245	Sin60 x >245	>212
Lower banded gneiss	60	Undefined	Undefined	Undefined

4.3.1. Khan Formation

The upper banded gneiss and amphibole-biotite schist form the Khan Formation in the SK area and it is within these two lithologies that most of the leucogranite sheets are hosted.

Table 4.2: Comparison of the lithological thicknesses of the SJ and SK stratigraphy. Most lithologies increased in thickness from SJ to SK, except for the lower cordierite gneiss, which seems to decrease in thickness. Note the Mottled Gneiss thickness is only known from core in the SK area and the lower Banded Gneiss is not found

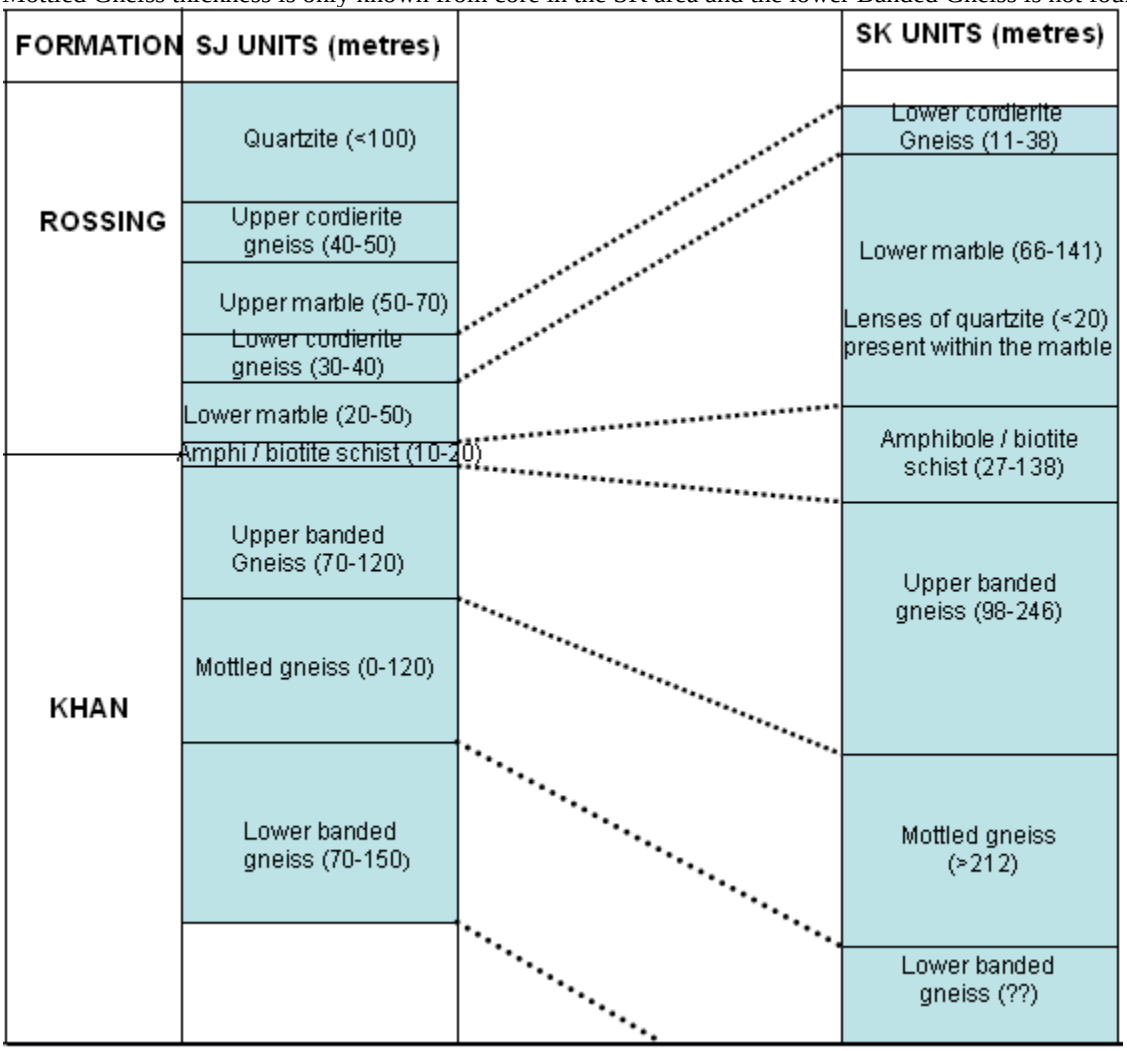

Lower Banded Gneiss

The lower Banded Gneiss was neither observed during surface mapping, nor during core logging. Stratigraphically, the lower banded gneiss is older than the Mottled Gneiss and probably occurs at depth within the SK area.

Mottled Gneiss

The Mottled Gneiss is continuous from the SJ pit area to the SK area although it does not outcrop in the SK area. The presence of this lithology and its thickness of >212 m were determined from core logging. Mottled Gneiss occurs between the upper and lower Banded Gneiss but logging the lower and upper contacts of the Mottled Gneiss in core was not straightforward, due mainly to overlap between banded and mottled textures. The mottled texture is a result of migmatic segregations. The rock forming components are quartz, plagioclase and hornblende.

Upper Banded Gneiss

The upper banded gneiss, which varies from 98 to 246 m in thickness, is the most prominent rock type exposed in the SK area. The 2-10 mm thick banding (Figure 4.2) comprises alternating dark layers composed of clinopyroxene, biotite and hornblende with minor iron oxides and beta-uranophane and light bands comprising plagioclase, quartz and K-feldspar. The banding is most pronounced away from the granite contacts. In close proximity to leucogranites, dark minerals such as biotite and hornblende increase at the expense of the lighter coloured minerals. The rock also exhibits small migmatite lenses indicative of localised partial melting (Figure 4.3). There are about 30cm thick amphibolite veins within the upper banded gneiss, with partial melting in boudin necks (Figure 4.4).

Figure 4.2: Banded gneiss showing layers 2-10 mm thick comprising alternating dark minerals (clinopyroxene, biotite and hornblende with minor iron oxides and beta-uranophane) and light coloured minerals (plagioclase, quartz and K-feldspar). Small migmatite lenses are indicative of localised partial melting in the area.

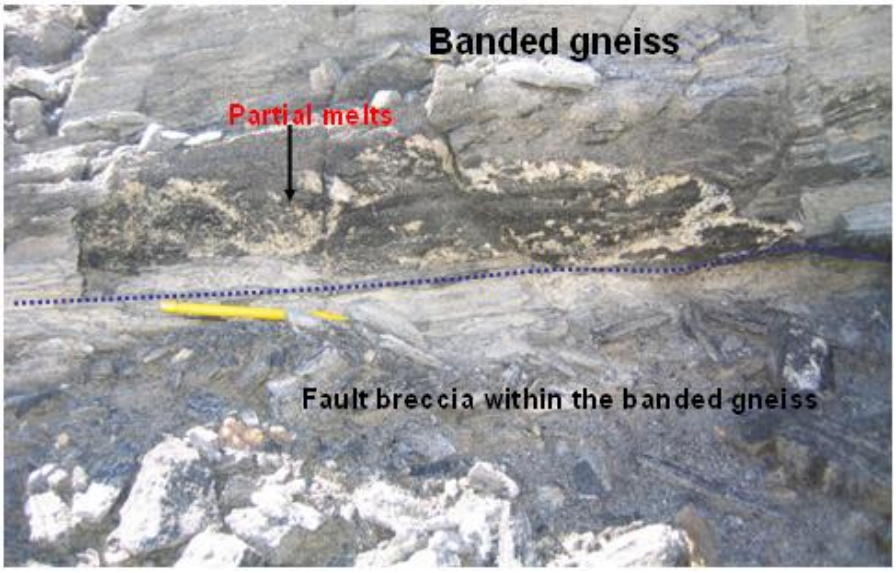

Figure 4.3: Partial melts of quartz and feldspar in banded gneiss, above a fault breccia. Photograph taken east of the SK12e sub-anomaly.

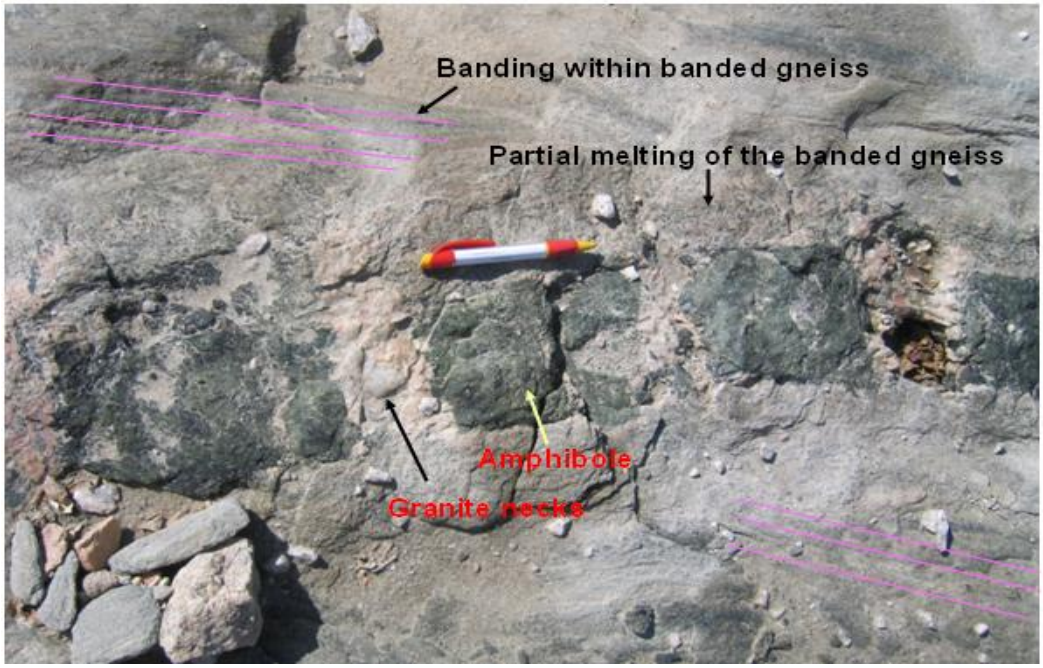

Figure 4.4: Boundinaged amphibolite veins within the Khan Formation (banded gneiss), with partial melting in boudin necks. Photograph taken 2 m south of the SK2B sub-anomaly.

Amphibole-Biotite Schist

The amphibole-biotite schist is continuous from the SJ pit area into the SK area and forms the uppermost lithology of the Khan Formation. The amphibole-biotite schist ranges between 27 to 138 m in thickness. The major rock forming components are K-feldspar, plagioclase, hornblende, quartz and biotite.

4.3.2. Rössing Formation

The stratigraphy of the Rössing Formation in the SK area consists of intercalated beds of marble, cordierite gneiss and quartzite. The marbles are generally medium to coarse-grained but vary from place to place from dirty brown serpentine and graphite-rich, to pure clean, white marble.

Lower Marble

The Lower Marble covers a large area in the northwest parts of the SK area and beyond. The lower marble is 66 to 141 m thick. It has a greyish overall colour but with greenish, white and light-grey patches when diopside, serpentinised forsterite or other calc-silicate are developed. The coarse-grained marble contains mica and serpentine that imparts a banded appearance.

Quartzite lenses

Quartzites mainly occur interbedded with marbles in the southern part of the SK area, around the SK4. The quartzites, which are about 20 m thick, range from pyritic- to micaceous-bearing. The pyritic-rich quartzite is orange brownish in colour, generally fine-grained equigranular and homogeneous in texture. The main minerals observed in the field and during core logging are quartz, feldspar and pyrite. The micaceous quartzite is dark-grey, medium-grained and equigranular in texture. The major minerals are quartz, feldspar and biotite. The relative age of the quartzite in relation to the Lower Marble is not clear.

Biotite Schist

Biotite schist is locally found around the SK4 area within the Lower Marble unit, close to the amphibole biotite schist. The major minerals in the biotite schist are biotite and quartz. This rock type was not observed in the core and the relative age in relation to the marble and amphibole schist is not clear.

Lower Cordierite Gneiss

The lower Cordierite Gneiss crops out in the south of SK area, near the SK4 sub-anomaly. It ranges in thickness from 11 to 38 m. This medium to coarse-grained, gneissic textured rock contains distinctive grains of cordierite with biotite, feldspar, quartz and garnet.

The data compiled in Table 4.2 shows that the stratigraphy thickens eastwards from the SJ pit towards the SK area. Further, the SJ stratigraphy includes additional younger units such as the Upper Marble and upper Cordierite Gneiss that are not present in the SK area. In the SJ area, quartzite lies above the upper Cordierite Gneiss, while in the SK area quartzite is observed as thin beds within the Lower marbles.

4.4. Sheeted Leucogranites in the SK Area

The sheeted leucogranites of the SK area are preferentially intruded into upper Banded Gneiss at the core of the anticline, with a minor focus at the boundary between the Khan and Rössing Formations. The leucogranite sheets are roughly parallel to each other and have a dextral en-echelon shape across the anticline (Appendix 1). The leucogranites crosscut bedding and foliation in the area. The sheeted leucogranite pinch and swell as seen on the SK area geological map and commonly host xenoliths of country rock (Figure 4.5). The possible pre-intrusion geology interpretation of the SK area is shown in Appendix 2.

Contacts between leucogranite sheets and country rocks are sharp and clear (Figure 4.6). Where the leucogranites intrude the Banded Gneiss, a 2 to 5 cm contact metamorphic aureole is observed within the gneiss. The contact aureole is expressed by grain coarsening and an increase of biotite and hornblende towards the intrusion.

Quartz veins and pods occur within the granites at the contact with the country rock, or as infill in the joints of the Banded Gneiss. Most of the quartz veins are milky in colour, with minor smoky veins. These were the result of late magmatic processes rather than metamorphism. En-echelon quartz veins within Banded Gneiss indicate a dextral sense of movement (Figure 4.7).

Figure 4.5: Banded Gneiss xenolith in leucogranite sheet. Photograph taken from the SK9 sub-anomaly.

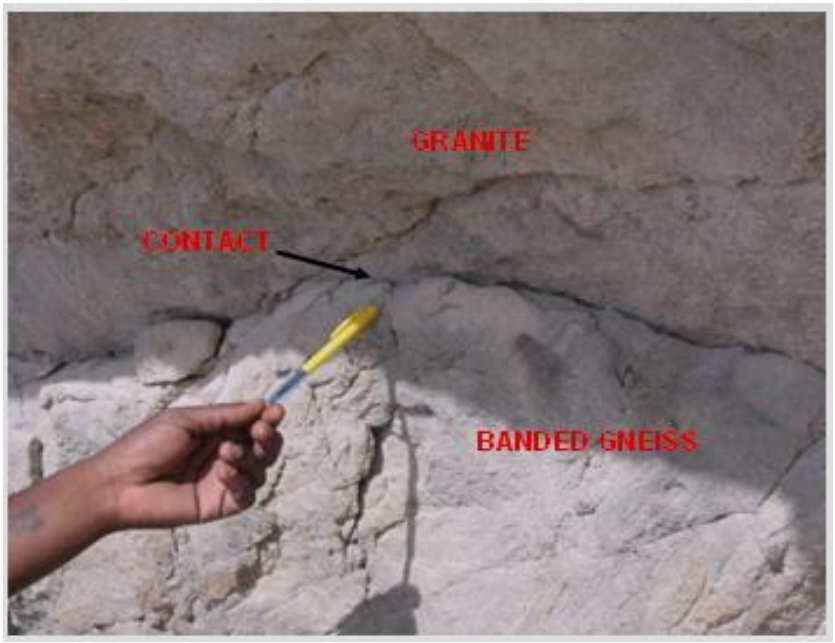

Figure 4.6: Sharp contact between granite and banded gneiss. Photograph taken north of the SK9 sub-anomaly.

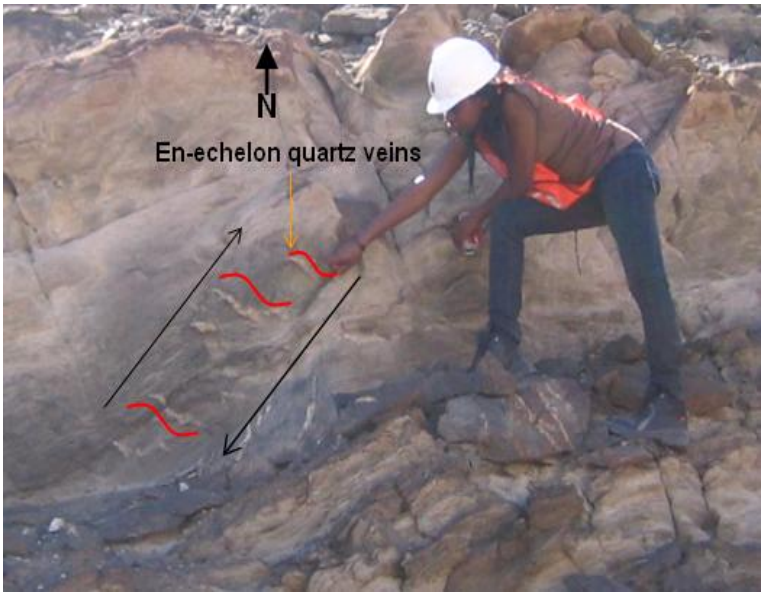

Figure 4.7: En-echelon quartz veins within banded gneiss, indicating a dextral sense of movement.

4.5. Bedding and Foliation in the SK Area

The bedding in the Banded Gneiss, Amphibole-Biotite Schist and Lower Marble provides two sets of data (240/68°NW) and (041/61°SE), representing limb A and B respectively (Figure 4.8). Foliation in the SK area is distinctive and penetrative, especially in the Khan Formation. A mean foliation of 223/75°NW is dominant in the area, as indicated in Figure 4.9. There are data that do not fit the overall foliation pattern, maybe because of displacement of minor faults, measurements taken from outcrops that may not have been in situ or another second set of foliation. The bedding/foliation relationship in the SK area indicates the presence of an anticline which is supported by the presence of older rocks (e.g. banded gneiss) in the core and younger rocks (lower marble) on the outside of the anticline. The fold is plunging at 22°NW.

4.6. SK4 Sub-Anomaly

The SK4 sub-anomaly is located at the SW end of the SK area. A detailed geological map of Louw (1979) was verified in the field and modified where appropriate (Figure 4.10). The SK4 map has been digitised in AutoCAD so that it can be kept in electronic format and exported to additional software programs (e.g. minesight). The SK4 area is characterised by a syncline with Banded Gneiss and Amphibole-Biotite Schist of the older Khan Formation on the flanks and then successively younger

Rössing Formation with lower Cordierite Schist at the fold hinge. Bedding in relation to the dominant SK foliation confirms the presence of the syncline (Figure 4.11).

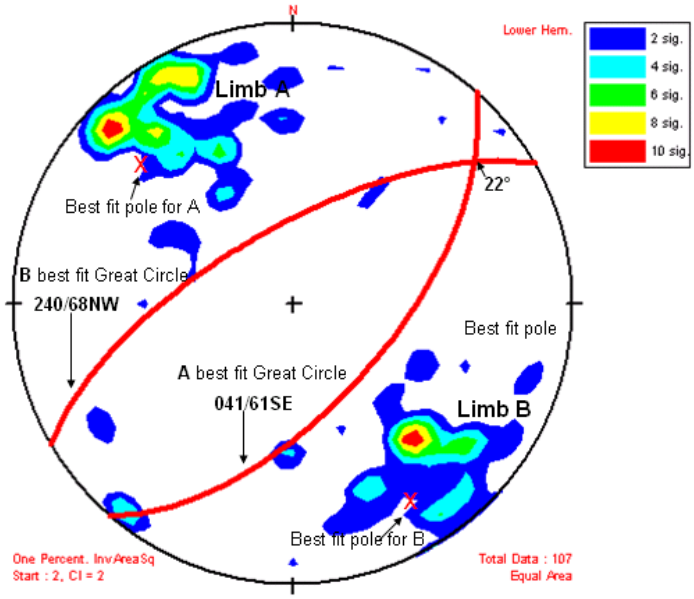

Figure 4.8: Equal angle stereographic projection of the SK country rock bedding representing two data sets (A (240/68NW) and B (041/61SE)). Each data set has its own best fit orientation. The two great circles show a plunge of 22° to the NE. STEREOSTAT analyzer tool was used to calculate average orientations.

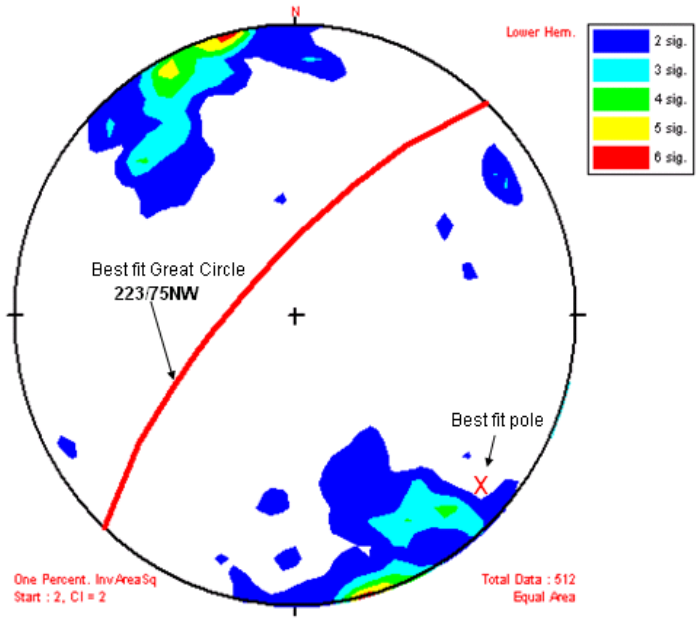

Figure 4.9: Equal angle stereographic projection of the SK foliation. The X represents the best fit pole and the red line represents the best fit great circle. Best fit orientation is 223/75NW. The blue represents a low concentration of the total poles, while red is the high concentration. STEREOSTAT analyzer tool was used to calculate average orientations.

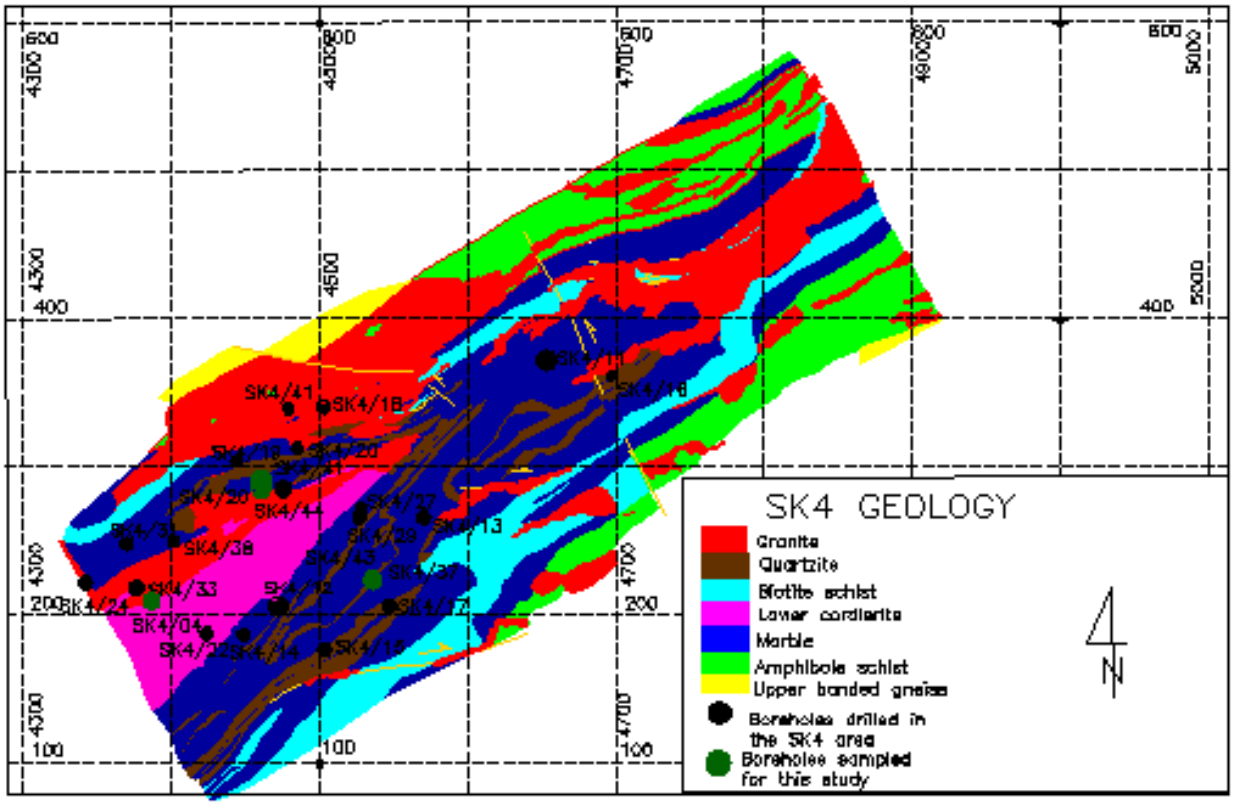

Figure 4.10: Detailed geology of the SK4 sub-anomaly verified in the field, modified and digitised in AutoCAD (after Louw, 1979). The black dots represent boreholes in the SK4, while green dots represent boreholes that have been sampled for this study. Coordinates are Rössing Uranium Mine local grid (Georeserve coordinates).

.

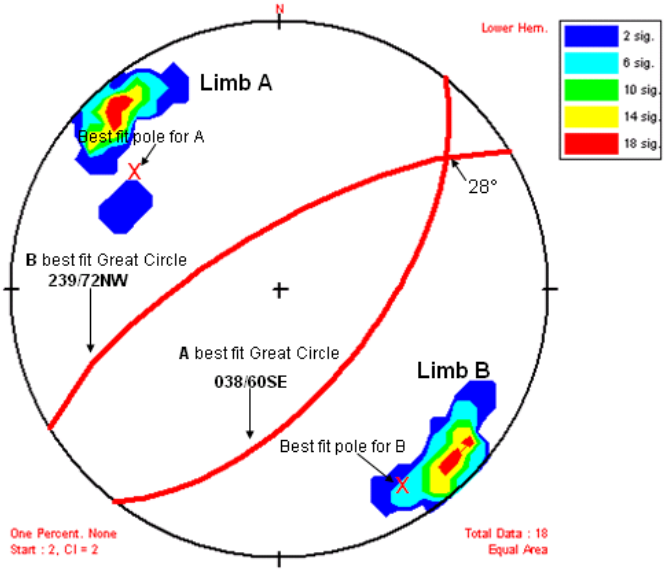

Figure 4.11: Equal angle stereographic projection of the SK4 country rock bedding representing two data sets (A (038/60SE) and B (239/72NW). The two data set planes indicate a plunge of 28° to the NE. A STEREOSTAT analyzer tool was used to calculate average orientations.

Uranium mineralisation occurs along the southern edge of an irregular granite body. Primary mineralisation is confined to the granite, while some secondary uranium mineralisation extends out into the country rocks. The mineralogy is quoted as 45% uraninite, 55% secondary uranium minerals (U-silicates), with 5% refractory minerals such as betafite and pyrochlore, with recoveries averaging 90% (Rössing Internal Report, 050505, 2005).

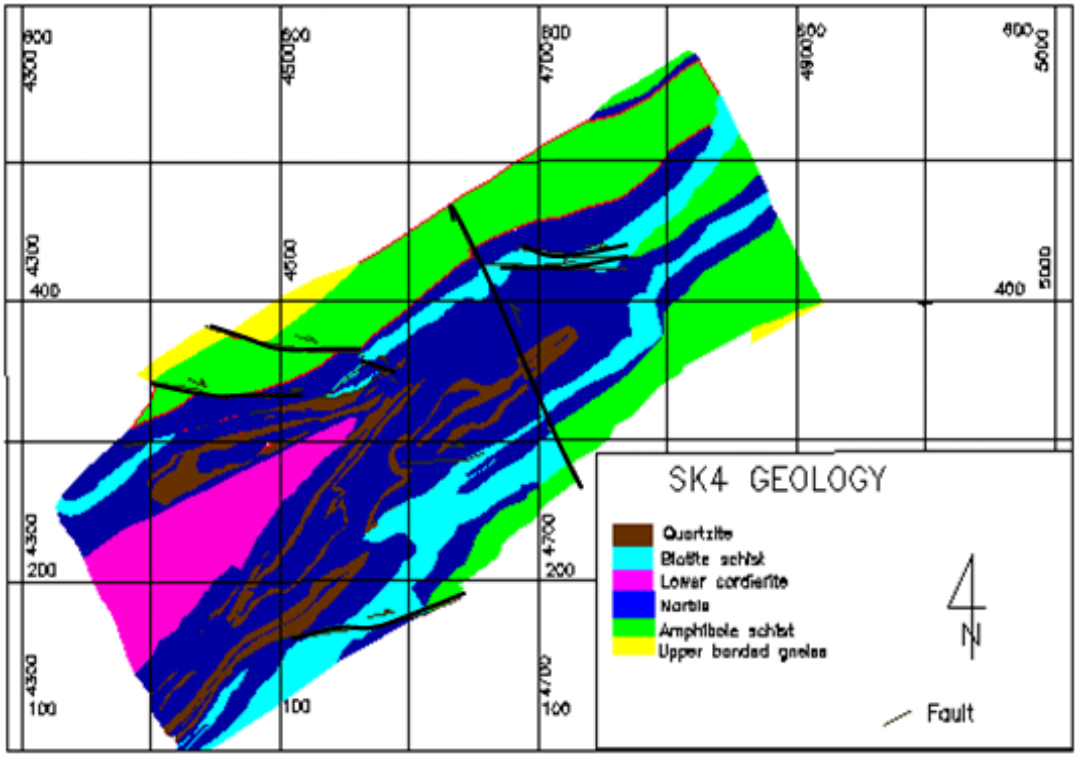

Figure 4.12: The geology of the SK4 area prior to granite intrusion showing the cordierite gneiss in the core and the amphibole-biotite schist on the flanks and faults structures displacing the country rocks. Coordinates are Rössing Uranium Mine local grid (Georeserve coordinates).

In order to understand the geology of the area, it is important to visualise the geology prior to the intrusion of the leucogranites. Figure 4.12, shows a pre-intrusion geological map of the SK4 area. The leucogranites have been removed, and the country rock extrapolated. Displacement in the country rocks and shift in orientation of bedding were considered as an indication of fault zones through which the leucogranite sheets may have preferentially intruded (Figure 4.13).

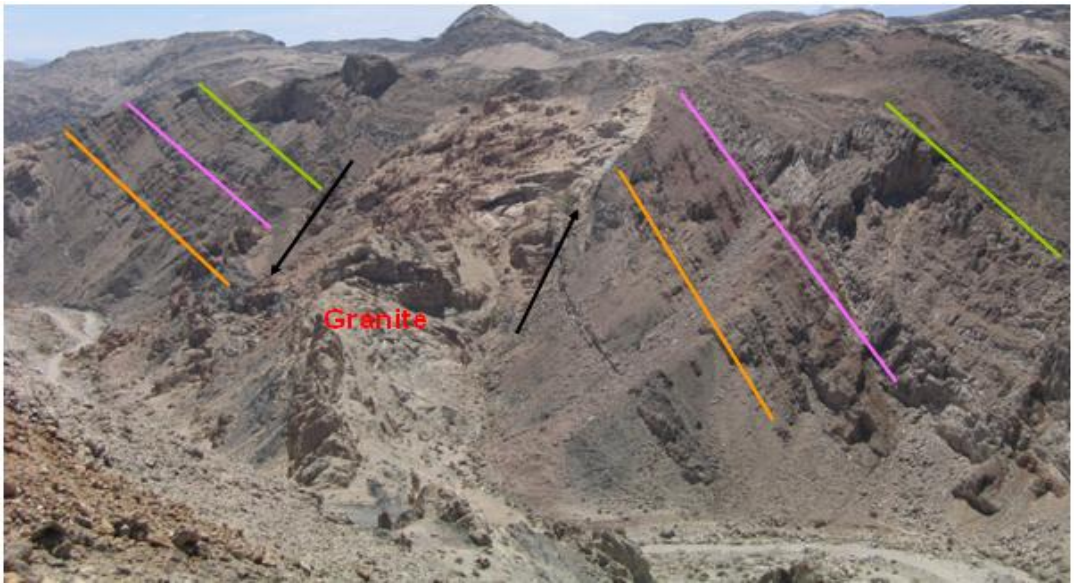

Figure 4.13: Leucogranite intruded along a fault zone. The displacement of the country rocks on either side of the intrusion is highlighted by the coloured lines. Looking southeast of the SK4 sub-anomaly.

4.7. SK3 Sub-Anomaly

The SK3 anomaly was also mapped in detail and extensively drilled by Louw (1979). A section interpretation of the geology using the historical diamond drillholes information is shown in Figure 4.14. Figures 4.14 and 4.15 indicate that the en-echelon and swelling-pinching nature is not only observed along strike in plan view, but also with depth. The en-echelon nature of the leucogranites makes it difficult to model using surface information, because of the changing dips.

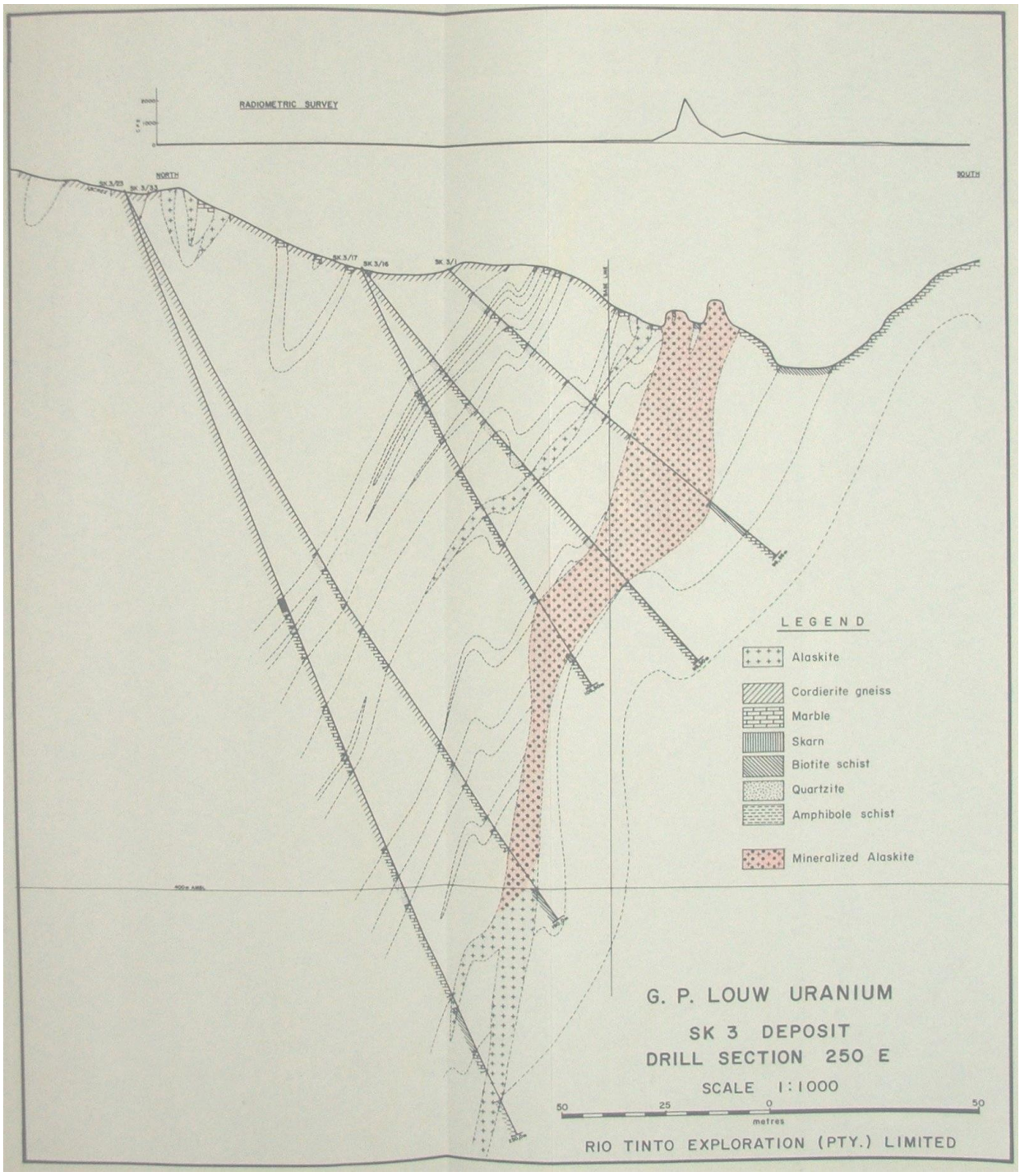

Figure 4.14: SK3 drill section 250E showing the mineralised leucogranite and associated country rocks (Louw, 1979).

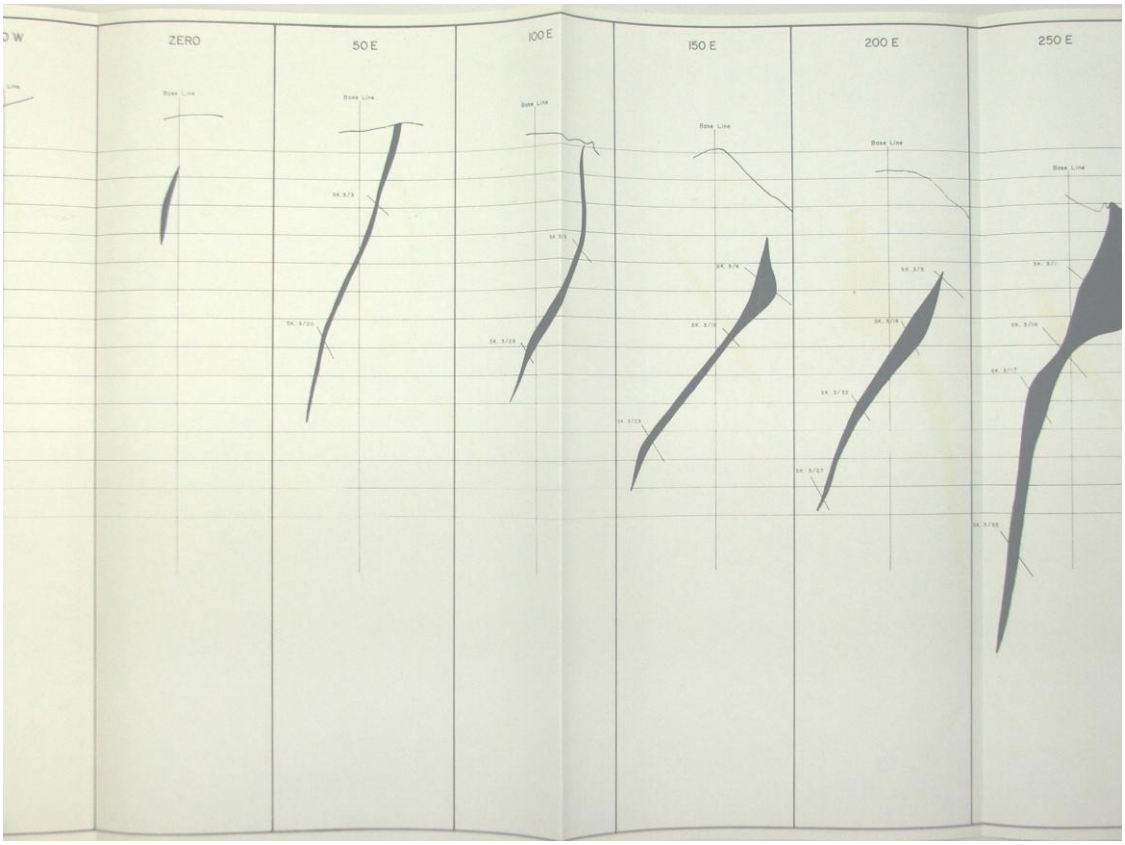

Figure 4.15: Summary of the granite behaviour in SK3 drill sections (Louw, 1979) showing the en-echelon nature of the leucogranites.

4.8. Radiometric Survey

A detailed historical ground radiometric, survey previously undertaken in the SK area, was verified in the field prior to incorporation into the present study. This project embarked on a random ground radiation survey on few exact positions in the field in order to verify the historic data. Although high counts coincided in both historic and current surveys, the actual values differed as historic radiation survey were much higher compared to the survey carried out during this study. The radiation survey methodology is presented in Appendix 3, section A and it is also concluded that the historic data can be integrated into the current data if the latter are multiplied by a factor of 2.2427.

4.8.1. Contouring of Radiometric Data using Surfer®

The historic radiometric data for the SK area was plotted on maps which had been kept in the Rössing Uranium Mine's geology strong room. The data was plotted on a 30m x 90m grid and XY coordinates of this historic radiometric were not recorded so it was difficult to locate individual points in the field.

The original radiometric map was scanned, and imported into an AutoCAD program and georeferenced. The 1400 scintillation points on the map were digitised in AutoCAD, and then entered into a Microsoft Excel spreadsheet alongside their coordinates. The Excel spreadsheet will be used for future reference and verification (Appendix 3, section B).

As part of this study, the historic radiometric data was contoured in Surfer®, at an interval of 100 counts per second (cps). The contouring helps in delineating the most favourable exploration target within the SK anomaly, which is the area where exploration geologists would be expected to focus their drilling. The contoured data is summarised in Figure 4.16, which indicates the main exploration target zone within the SK area, while delineating areas that have the highest radiation counts, such as the SK4 area.

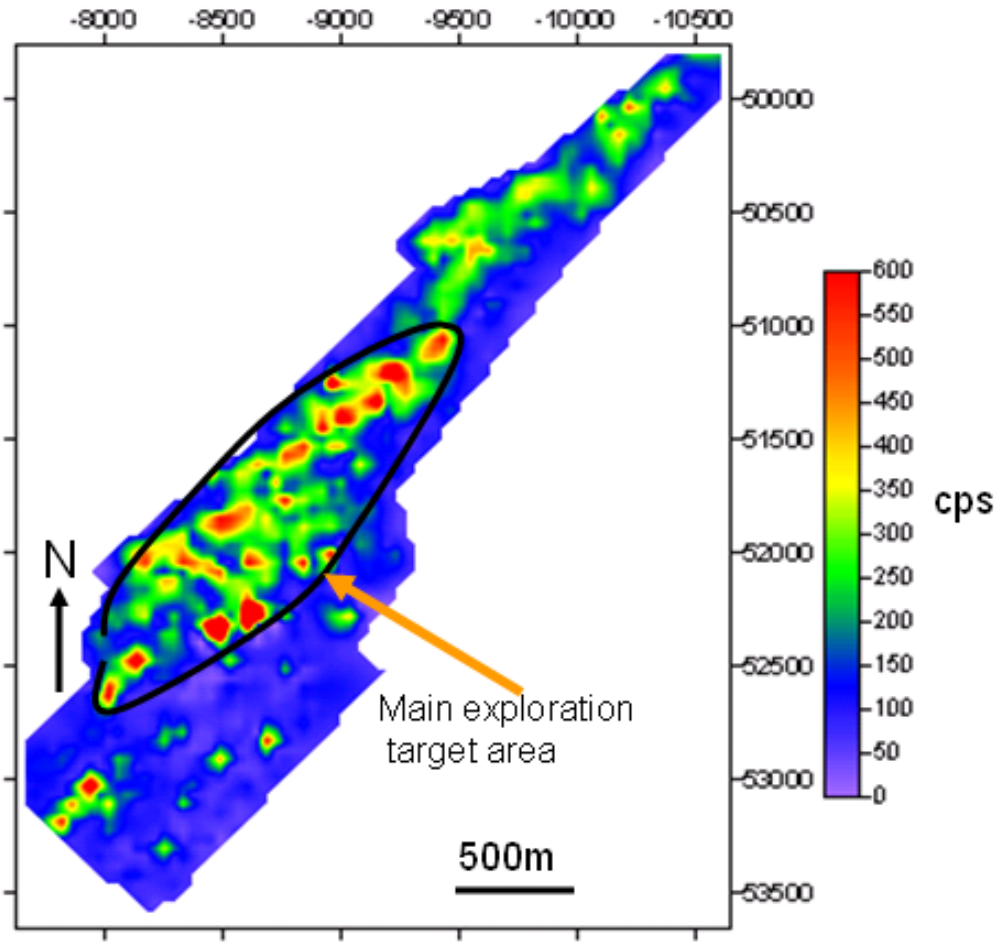

Figure 4.16: Contoured map of the SK radiometric data, indicating the most favourable exploration target area. Areas shown in red have the highest radiation readings. Coordinates are Rössing Uranium Mine local grid (LO coordinates).

4.9. Three Dimensional (3D) Geological Model of the SK Area

To produce a three dimensional macro-structure model of the SK area, the geology needed to be simplified. The model was based on information from surface mapping information due to the lack of borehole data at the time. Historical borehole data was too shallow (about 150 m) and in most cases, too localised to be used. Due to limited information, bedding and lithological contact information was used to produce 2D sections, which were subsequently joined to produce a 3D model in a Minesight® program.

All intrusions were removed to indicate the nature of the geology before the granites intruded the country rocks. The presence of xenoliths in the leucogranite sheets made it easier to extrapolate the original geology when the granites were removed. The pre-intrusion map was used to produce the 3D structure model of the SK area (Appendix 2). Displacement in the country rocks and shift in bedding orientation was considered as an indication of a fault zone and leucogranite sheets may have preferentially intruded along faults zones.

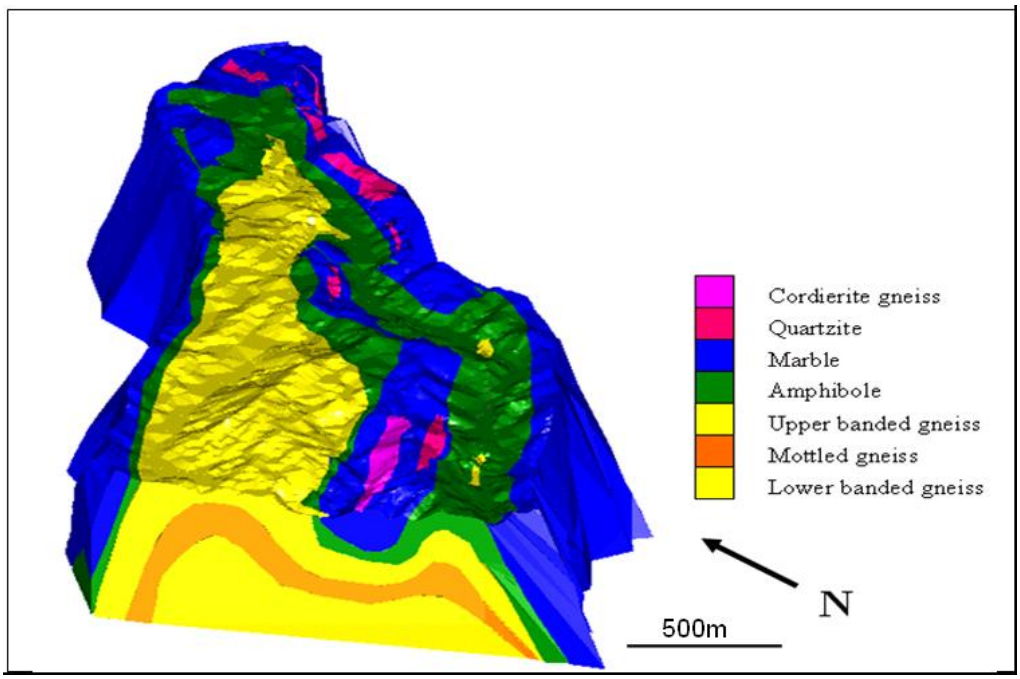

Figure 4.17: The pre-intrusion 3D macro model of the SK area, looking towards the northeast. Prepared based on surface geology and a few SK4 drillholes (biotite schist cannot be seen at this scale).

The country rock map was produced in the AutoCAD program and exported into Minesight. In Minesight, a (N-S) 100 m distance grid set was created and strings dipping at the same angle as the

bedding were designed to lead the polyline designs. The sectional polylines designs examined the geology from the surface map, and this was led by the bedding dip information. On each section, different polylines representing different rock types were produced. Once each section had been outlined, the surfaces/solids were assigned to each polyline set. This produced solids for each polyline set. The top portion of the anticlinal structure has been clipped using surface topography in Minesight.

The three-dimensional macro model shows an overall anticlinal structure with minor parasitic folds as indicated in Figure 4.17.

4.10. Discussion and Conclusion on the SK Area

The stratigraphy thickens from the SJ area eastwards towards the SK area. The lower Rössing Marble, which forms the cap rock of the SK area, has a thickness that increases from 20-50 m in the SJ area, to 66-141 m in the SK area. The thickening of the stratigraphy may be explained by structural controls, such as parasitic folds. The SK may have thicker lithological units, because it is on the flanks of the dome rather than at the nose of the dome.

The SK area may have been affected by dextral shearing; as suggested by en-echelon structures of the leucogranites, quartz veins and the pseudo-concordant behaviour of the leucogranites towards the Rössing Formation. Oliver (1994) described the regional movement of the Congo and Kalahari Craton during the late Precambrian early Palaeozoic as sinistral, whereas in the SK area a local dextral movement took place.

Zones with high scintillometer counts (cps) are particularly associated with leucogranites predominantly hosted by the Banded Gneiss. The two highest uraniferous zones at surface are from the SK4 sub-anomaly. Contouring results have highlighted the best exploration target zone and indicate that the SK area must be viewed as one big anomaly rather than as a series of different sub-anomalies. Initial drilling should commence in the high count target area and spread outwards to the low-grade areas. Although Louw (1979) of the Rio Tinto Exploration group contoured the SK sub-anomalies as individual targets, it will not be economically feasible to mine sub-anomalies as individual targets because some of the sub-anomalies may be less than ten metres apart. In addition, metasedimentary country rocks between the primary uranium-rich granites may also host secondary uranium minerals.

CHAPTER 5

SAMPLE COLLECTION AND PETROGRAPHY OF THE SHEETED LEUCOGRANITES

5.1. Introduction

Having established the regional geology and distribution of high uranium-enriched zones, a programme of sampling was undertaken on the SK4 historic drillholes as this is the area where mine expansion will begin. Surface sampling was supplemented with material from recent drillholes. Surface sampling gives an overview of the textural, geochemical and mineralogical variations, which can be compared with data from depth. This is important as any variation in mineralogy, geochemistry or mineralisation with increasing depth may have important implications for any future mining programme.

5.2. Sampling Rationale

The SK area is made up of 32 sub-anomalies for example; the SK4 anomaly (100 m by 15 m) is one of the SK area sub-anomalies. The entire SK area is an anticline, with an exception of the SK4 area, which is a syncline. During this study, the part of the SK area that does not include the SK4 is referred to as the SK anticlinal area. Herd (1996) noted that geological structure (e.g. whether an anticline or syncline) plays a major role in the betafite formation, during this study the SK anticlinal area was treated and sampled separately from the SK4 (syncline) area, to confirm if the difference in fold geometry contributed to the formation of betafite.

Twenty-one surface samples were collected (Table 5.1), of which seventeen granites represent known sub-anomalies, four were chosen for mineralogical and textural variations. The reasons for sampling surface granite outcrops were to obtain an overall representation of all major and trace-elements distribution in the surface leucogranites and to compare this data with that derived from leucogranite samples collected from core. Care was taken to ensure that the samples collected were fresh and representative of the granite as a whole.

Six diamond drillholes were drilled in the SK area in 2007, the survey coordinates of the drillholes are in Table 5.2 and their geology given in Figure 5.1. These cores intersect mottled gneiss, which is not exposed on the surface, and overall the stratigraphy is similar to that of SJ area. From the six

drillholes, drilled from the 2007 drilling programme, three drillholes were selected for chemical and mineralogical analysis (SK07D005, SK07D041 and SK07D048). Ten half core samples were collected for XRF and QEMSCAN analysis.

Table 5.1: List of the surface granite samples from the SK area, showing the co-ordinates for each sample site and U values obtained by XRF analysis.

Sample Number	Eastings	Northings	U (ppm)
K1	-9519.16	50624.92	33
S1	-8373.25	52037.32	9
S2	-8240.03	52100.1	299
S3	-8239.01	52128.52	97
S10	-8206.8	52166.08	18
SK1A	-97774.1	50405.05	9
SK1B	-9824.63	50596.8	65
SK1D	-9919.05	50415.28	11
SK1E	-9965.92	50343.581	36
SK2A	-9240.93	51369.691	71
SK2B	-8735.48	51548.693	92
SK2D	-9086.92	51465.382	147
SK2E	-9311.95	51289.603	48
SK4	-8539.7	52305.56	57
SK5A	-8762.48	52026.693	13
SK5B	-8762.48	52049.69	10
SK8	-9055.15	51621.104	42
SK9	-8685.6	51624.579	379
SK12A	-8217.54	51983.67	250
SK12D	-8661.11	51887.75	151
SK12E	-8748.5	51748.88	253

Table 5.2: List of granite core samples from the SK 2007 diamond drillholes, showing the co-ordinates for each core and depth at which samples were taken.

.

Hole ID	Eastings	Northings	Sample Number	Sample depth (m)
SK07D005	-8689.28	52184.71	N10062	45.18-46.65
			N10158	178.32-179.81
			N10187	220.34-221.25
			N10290	363.65-365.06
SK07D041	-8649.27	52247.55	N9944	31.28-33
			N9947	35.73-37.17
			N9982	82.86-84.34
SK07D012	-8404.48	52094.65	N10343	60.85-62.18
			N10357	79.40-80.85
			N10456	216.73-218.21

Historic core material from the SK4 drilled in 1977 was re-sampled for mineralogical test-work, to confirm the historic data on the proportion of the various uranium minerals and to confirm the grades that were obtained more than ten years ago.

Five historic diamond drillholes (SK4/4, SK4/20, SK4/37, SK4/41 and SK4/43) from the SK4 area were selected due to their high uranium grades (Table 5.3). SK4/4 and SK4/43 have been sampled at different depths from the surface, in order to detect any change in mineralogical proportions with depth. SK4/20, SK4/37, and SK4/41 have been sampled along strike rather than depth, to ensure that the spatial distribution of the minerals is also determined. The SK4 historic holes were very short, the longest core being about 150 m deep.

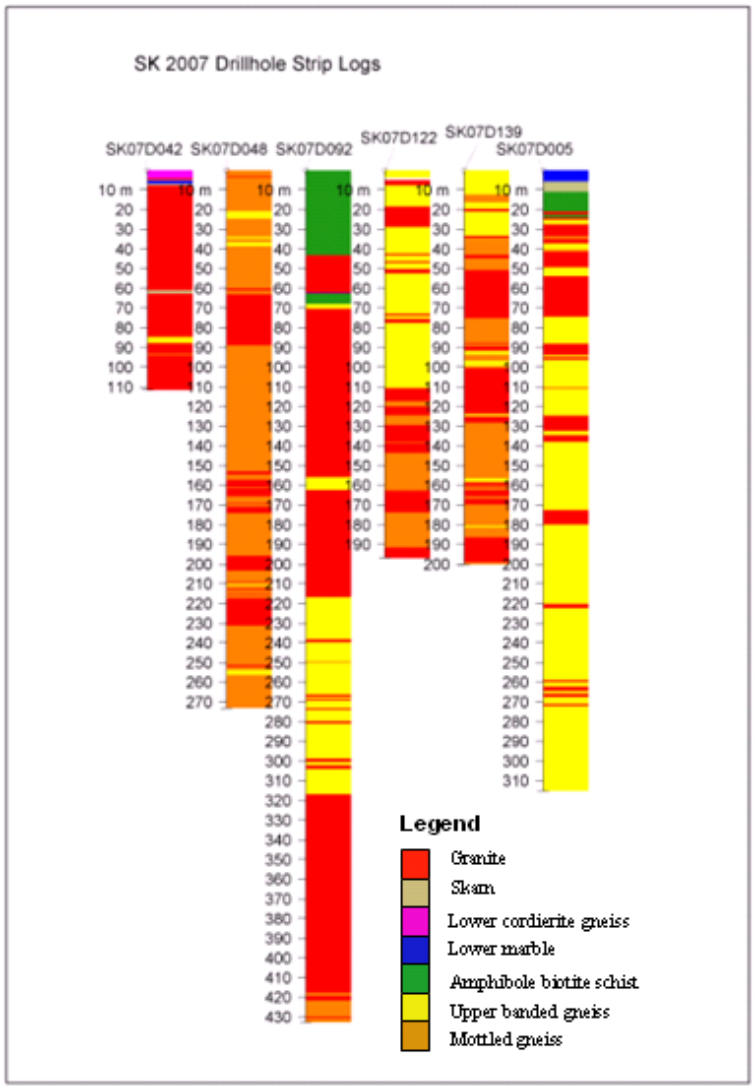

Figure 5.1: SK diamond drillholes logs from the 2007 drilling programme showing lower banded gneiss and mottled gneiss which do not crop out on surface.

Table 5.3: List of samples taken from the SK4 historic diamond drillholes. Information obtained from the log and sampling sheets, stored in the Rössing Strong Room.

Sample Number	Eastings	Northings	Depth	U (ppm)	Rock Type
SK4/20 25I	-8602.56	52238.31	47-49	273	Granite
SK4/4 20I	-8567.87	52325.46	36.40-38.40	1499	Granite with biotite schist xenoliths
SK4/41 21-22I	-8591.45	52218	38.7-42.7	189	Granite
SK4/4 22I	-8567.87	52325.46	40.40-42.40	662	Granite
SK4/37 8I	-8640.11	52200.1	12.2-13.9	803	Granite with biotite schist xenoliths
SK4/43 13I	-8689.78	52238.51	21.5-23.5	192	Granite
SK4/43 18I	-8689.78	52238.51	31.5-33.5	247	Granite

5.3. Methodology

The surface and core samples were split and macroscopically described in detail. Two to three thin sections were cut from each of the surface samples and a total of 30 thin sections were prepared. Thin sections were selected to represent a range of colours and textures from fine- medium- and coarsely crystalline, whilst pegmatitic samples were excluded, because they are poorly mineralised.

Nex *et al.* (2001b) divided the leucogranites of the Goanikontes area into six distinct types based on field characteristics and structural setting, backed by geochemical data and fluid extraction analyses (Table 5.4). Detailed petrological descriptions of the SK area leucogranites followed that of Nex *et al.* (2001b).

Table 5.4: Classification of leucogranites in the Central Zone of the Damara Orogen Belt, with their associated average radiation counts per second (Nex *et al*, 2001)

TYPE	COLOUR	TEXTURE	MINERALOGY	DEFORMATION EVENT	Counts per second (CPS)
A	Pale pink	Pale pink, irregular, folded, fine-medium grain size, homogeneous	Dominantly white feldspar	Pre-D4	< 20
B	Dominantly white	White, fine-pegmatitic, frequently boundinaged, occasionally folded, +/-garnet , biotite, tourmaline	Garnetiferous, with tourmaline and biotite as infrequent accessory minerals	Pre-D4	< 20
C	White to pale pink	Pale pink-cream, medium-pegmatitic, two-feldspars, interstitial clear quartz	Two feldspar, accessory magnetite, ilmenite and tourmaline	Pre-D4	10-20
D	White	White, irregular and anastomosing, medium-coarse grain size, granular texture, smoky quartz	White feldspar, smoky quartz, betauranophane occasional betafite and apatite	D4	100-350
E	Red to pink, very variable colour with oxidation haloes	Pink, variable colour and grain size, contain oxidation haloes, occasionally boudinaged	Consist entirely of smoky quartz and pink feldspar.	D4	30-300
F	Red	Red, tabular, coarse-pegmatitic, milky quartz	Pink, coarse perthitic feldspar, milky quartz, accessory biotite, magnetite and ilmenite	D4	<20

5.4. Petrological Variation of Leucogranites

The leucogranite samples taken from the SK area (Table 5.5 and 5.6) show significant variations in grain size, colour, mineralogy, texture and uranium content. The textural variation ranges from fine, fine/medium, medium and medium to coarsely crystalline and in colour from white or pale pink to pink. Mineralogically, the granites are comprised of assemblages of quartz, feldspar and minor biotite. The colour of the quartz ranges from clear and glassy, through slightly smoky or smoky, to dark and almost black. The feldspars range from white, cream, pale pink to red/pink. From Table 5.5 it can be concluded that fine-grained textured facies are generally low in grade compared to medium and coarser textures. The smokier the quartz, the higher the scintillation counts but there is no relationship between feldspar colour and scintillation counts. For each leucogranite sample a suggested type based on the classification scheme of Nex *et al.* (2001) is suggested. The type A is sparse in the SK area and Type F was not found.

Table 5.5: Leucogranite description and classification of the surface samples from the SK area. The possible leucogranite type refers to the classification scheme of Nex *et al.* (2001) as shown in Table 5.4. There is a low confidence level of correlation with the Nex *et al.* (2001) classification system for SK9, SK8, SK1D and SK2A.

Sample No	Colour	Quartz	Feldspar	Texture	Radiation	Add. Features	Possible leucogranite type
SK4	White	Slightly smoky	White	Medium/coarse	High		D
S2	Pale pink	Smoky	Pink/white	Medium/granular	High	Two feldspar	E
SK12A	White/cream	Dark smoky	White/cream	Fine/medium	High		E
SK12E	White	Dark smoky	Pale pink	Fine/granular	High	Magnetic	E
S1	White	Dark smoky	Pink	Fine/medium	High		E
SK2B	Pale pink/White	Slightly smoky	White	Fine/medium	Moderate	Slightly magnetic	E
S10	White	Slightly smoky	White	Fine/medium	Low	Biotite	B
SK9	White	Smoky	White	Medium/coarse	High	Magnetic	D/C
SK5A	White	Glassy	White	Fine	Low		B
SK2D	White	Slightly smoky	White	Medium	Moderate		B
SK8	White	Slightly smoky	White	Variable	Moderate	Magnetic	D
SK12D	White/pale pink	Slightly smoky	White	Fine/medium	Moderate	Magnetic	C
K1	Red/pink	Dark smoky	Red/pink	Medium/granular	Moderate		E
SK1E	White	Dark smoky	White	Fine/medium	Moderate	Magnetic	C
SK1A	White	Slightly smoky	White	Medium	Moderate		C
SK2E	Pale pink	Glassy/smoky	Pale pink	Fine/medium	Moderate		A/C
S3	White/pale pink	Slightly smoky	White/pink	Fine/medium	Moderate		E
SK1B	Pale pink	Dark smoky	Pale pink	Fine/medium	Moderate	Slightly magnetic	E
SK5B	White	Glassy	White	Variable	Low		A
SK1D	White	Slightly smoky	White	Medium	Moderate		C
SK2A	White/coarse	Slightly smoky	White	Medium/coarse	Moderate	Slightly magnetic	C

Table 5.6: Petrographic description of samples from SK4 diamond drillholes.

Sample Number	Rock description
SK4/20 25I	White to pale, medium-grained granite, with smoky quartz.
SK4/4 20I	Biotite schist with a few granite lenses. Major minerals in the homogenous black schist are biotite, quartz and beta-uranophane.
SK4/4I 21-22I	Homogenous equigranular pale pink granite, with localised graphic texture. Main rock forming minerals are feldspar and quartz.
SK4/4 22I	White, coarse pegmatite. Dominant minerals are feldspar, quartz, biotite and beta-uranophane.
SK4/37 8I	Medium- to coarse-grained, dark-grey biotite schist, with melt leucosomes. Main minerals are feldspar, smoky quartz, biotite and beta-uranophane.
SK4/43 13I	Equigranular, saccharoidal homogeneous white granite, with feldspar and quartz as major rock forming minerals.
SK4/43 18I	Equigranular medium-grained pale pink granite, with dark smoky quartz.

5.5. Petrography of the Leucogranites

5.5.1. Modal Classification of SK Area Thin Sections

The modal mineralogy of the leucogranite samples was determined in order to provide each granite type with a name based on the modal classification scheme of Streckeisen (Figure 5.2). The nomenclature derived from this technique can be compared with the names assigned by the variety of geochemical classification diagrams. A point count of 30 thin sections from the SK area was completed; this includes instances where the rock sample had two or three thin sections. Samples with more than one thin section were averaged, and altogether 16 different samples have been analysed. Alkali feldspars are dominant, followed by quartz, plagioclase feldspar and biotite. The petrographic description of all surface leucogranite samples is presented in Appendix 4, Table 1.

A total of 6000 points were counted, 200 per thin section (Appendix 4, Table 2). The following minerals were counted: quartz, plagioclase, microcline, orthoclase, biotite and accessory minerals. Based on modal mineralogy, the SK area leucogranite samples range from tonalite through to alkali feldspar granite (Figure 5.2). These covered the Type B-E of Nex *et al.* (2001).

Type B

For type B samples, one plots in the field of alkali feldspar granite and one in the granodiorite field (Figure 5.2). They comprise perthite, quartz and minor microcline and oligoclase. Perthites are generally subhedral and coarse-grained. Lamellar and film perthites are dominant and are slightly altered to sericite. Quartz is dominantly coarse-grained, although an exception of fine-grained well-rounded quartz is present in section SK1AB. Undulose extinction and boundary dissolution are common (Figure 5.3). Oligoclase is common in section SK1A, ranging from An20-An30. Thin-sections SK5BC and SK1AB, contain graphic quartz-feldspar intergrowths. Biotite is also common in Type B leucogranites. It forms ragged euhedral laths. Other accessory minerals include hematite and zircon. Hematite may have been weathered from ilmenite and/or magnetite. Zircon occurs as single grains mainly between quartz and feldspar crystals. Apatite and monazite are rare and occur as euhedral crystals, generally interstitial to quartz and feldspar.

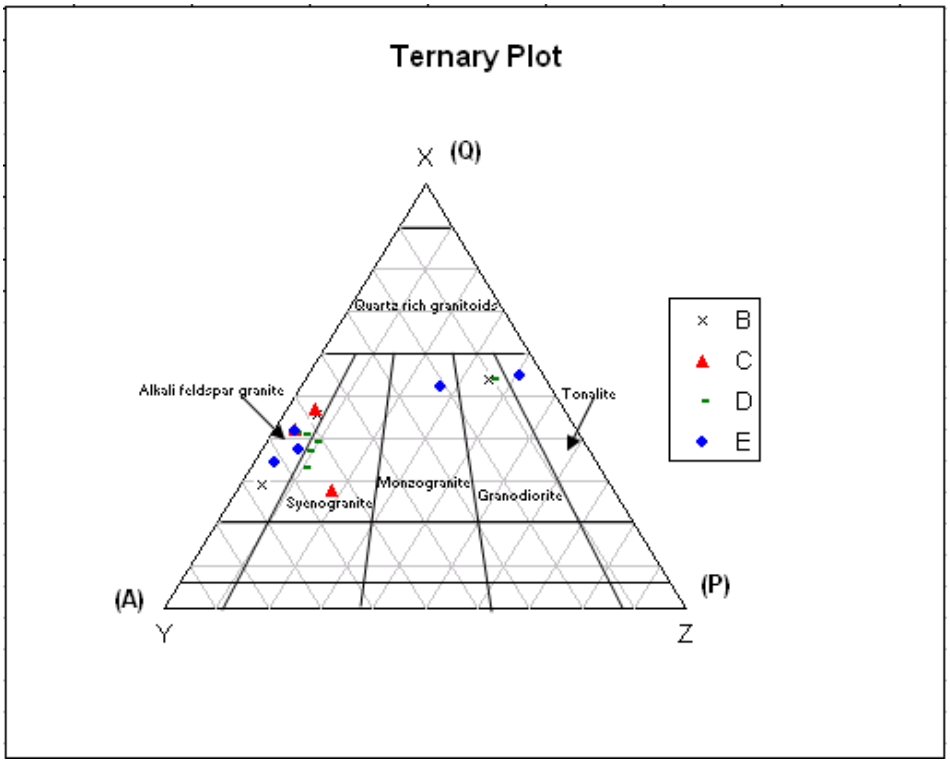

Figure 5.2: QAP diagram showing the modal minerals of the different sheeted leucogranites. The composition of the leucogranites varies from alkali feldspar to tonalite.

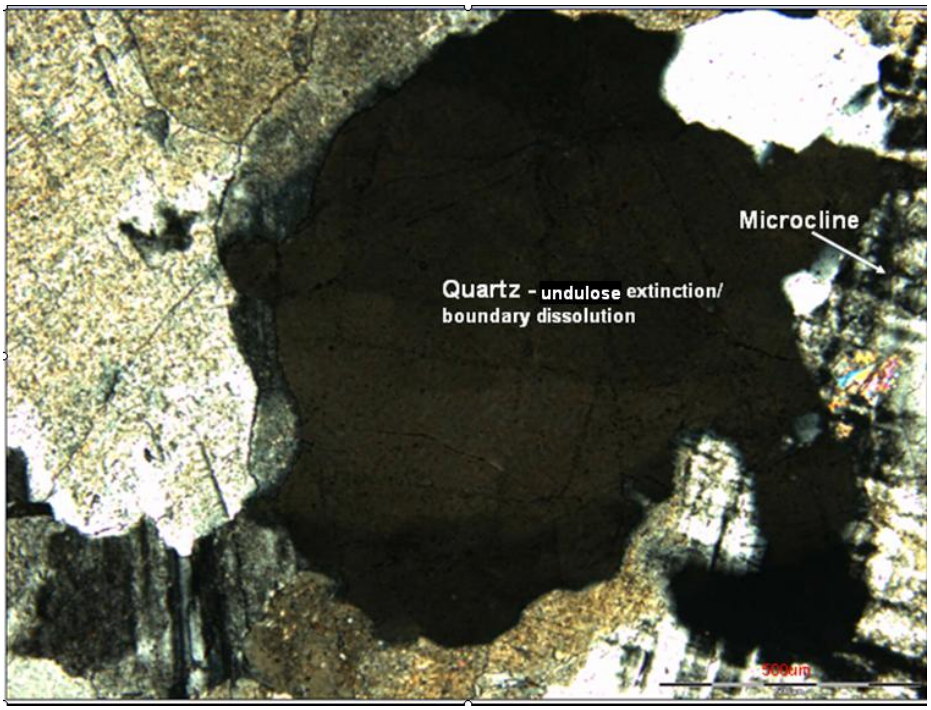

Figure 5.3: SK1AB Type B leucogranite under cross polars - Coarse-grained quartz, showing undulose extinction and crystal boundary dissolution.

Type C

Granite samples that correlate with Type C of Nex *et al.* (2001), range in composition from alkali feldspar granite to syenogranites (Figure 5.2). They comprise quartz, perthite, microcline, and plagioclase in varying proportions. Quartz varies from fine to coarse-grained, although fine-grain sizes are more dominant. The fine-grained quartz grains are well rounded, locally forming beaded chains or otherwise enclosed in large feldspar grains, whereas coarse quartz grains form a composite texture in section SK2E. Graphic quartz-feldspar intergrowths (Figure 5.4) are present in SK2E.

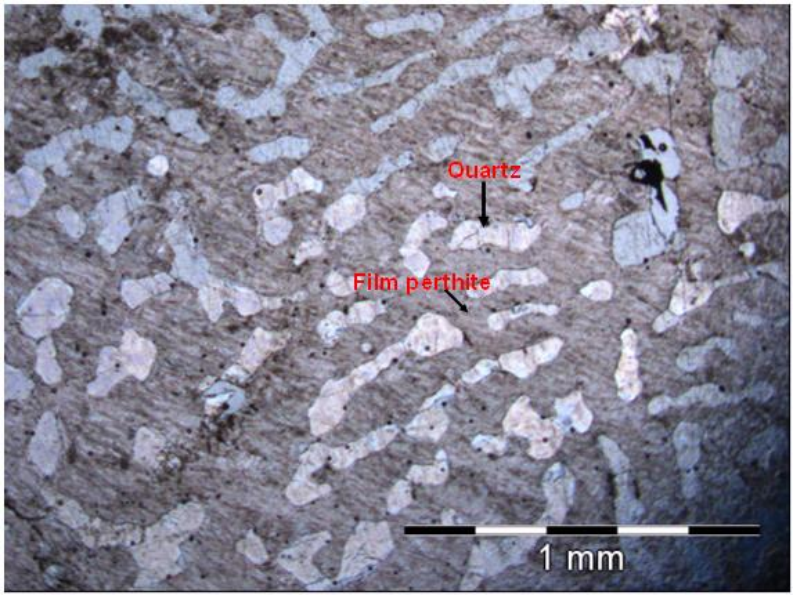

Figure 5.4: SK2EA showing graphic quartz-feldspar with irregular crystal boundaries (PPL).

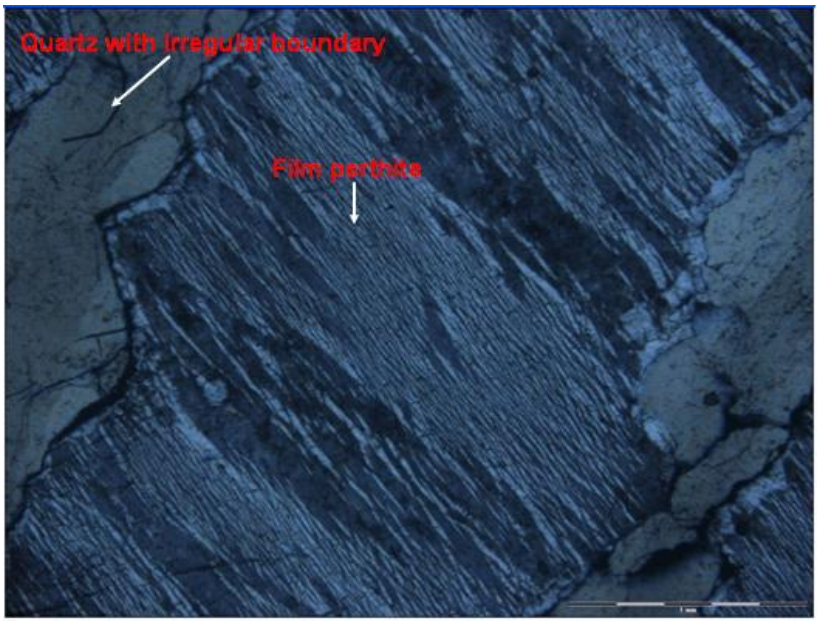

Figure 5.5: A high magnification image between two quartz grains in Figure 5.4 showing film perthites in SK2EA under crossed polars,

Minor undulose extinction is also present. Perthites are dominantly film or lamellar textured, locally with patch perthite (Figure 5.5). Most microcline grains are coarse-grained and heavily sericitised. The anhedral plagioclase is generally oligoclase in composition (An18-An25) and is less sericitised than the microcline. Minor accessory hematite and magnetite occur and traces of euhedral zircon.

Type D

Type D leucogranite samples plot at the border between the alkali feldspar and syenogranite fields, while one sample plots as a monzogranite (Figure 5.2). Essentially, they are comprised of quartz, perthite and plagioclase. Quartz is very common, with two population groups: one group forms fine-, well rounded crystals that form as beaded chains or scattered crystals. When scattered it is mainly enclosed in feldspars. The other type occurs as coarse-grained, anhedral clusters. The plagioclase is of oligoclase composition varying from An10 to An23. Plagioclase is mainly subhedral, with varying degrees of sericitisation. The dominant alkali feldspar is patch perthite and lamellar perthite, although film perthite is also present in small amounts. Biotite is also common; it occurs as ragged veins or at grain boundaries and in places is chloritised. The accessory minerals in the type D leucogranites are: pyrochlore, magnetite, hematite, zircon, topaz and monazite. Zircon occurs as isolated crystals interstitial to quartz and feldspar. Euhedral betafite is common, appearing as dodecahedral crystals with hematite rims surrounded by radial cracks in quartz (Figure 5.6). Topaz in a subhedral form is fairly common. Traces of euhedral monazite occur interstitial to quartz and feldspar.

Type E

Compositionally, most of the Type E leucogranites plot in the alkali feldspar granite field; although there is one sample that plots in the monzogranite field and another that plots as a tonalite (Figure 5.2). Quartz is very common and exists in two populations: Group 1 is fine-grained, well rounded and forms beaded chains. Group 2 has course-grained quartz, with undulose extinction and composite textures. Plagioclase is subhedral to euhedral in shape (Figure 5.7), and of oligoclase composition (An20-An24). Perthites are mainly lamellar or patch perthite, which have been highly altered to sericite. Ragged or skeletal biotite is extensively altered to chlorite. Accessory minerals are mainly pyrochlore group minerals, apatite, zircon and hematite. Pyrochlore group minerals (probably betafite) are surrounded by radiating cracks, filled with hematite. Apatite and monazite are rare and occur in a euhedral form, mainly interstitial to quartz and feldspar. Zircon occurs as single crystals, which are also interstitial between quartz and feldspar. Hematite may represent altered ilmenite and/or magnetite.

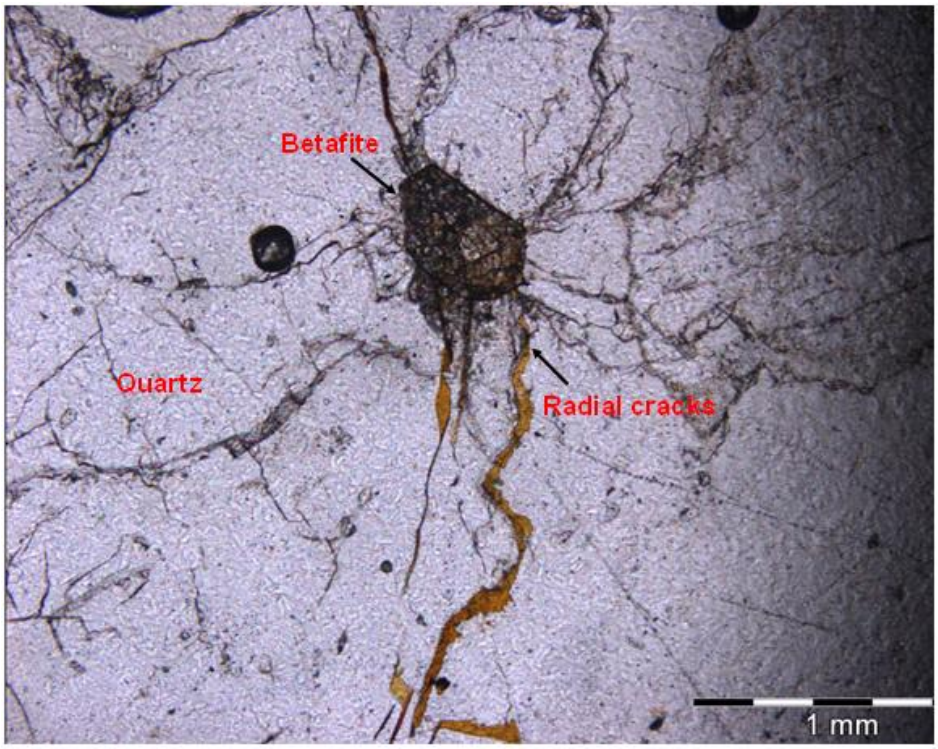

Figure 5.6: SK1B in plane polarised light - Betafite crystal surrounded by a rim of haematite and radial cracks within the quartz grain.

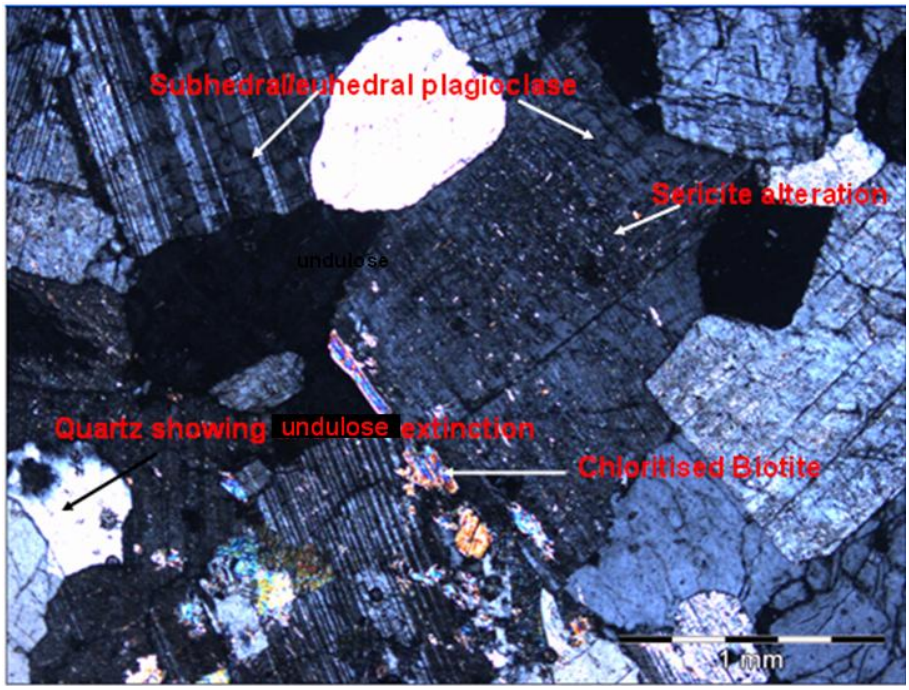

Figure 5.7: S3 under crossed polars- Subhedral to euhedral plagioclase grains some altered to sericite and quartz grains showing undulose extinction.

5.6. Discussion

Nex *et al*. (1997), observed six different leucogranite sheets in the Goanikontes area. Of the six leucogranites, only four are observed in the SK area (B, C, D and E). Nex *et al*. (2001) also found that there was a range of leucogranite compositions from tonalite to alkali feldspar granite. Further, they showed that samples with high scintillometer counts tended to plot within, or close to the alkali feldspar granite field. For the SK area, leucogranites also plot in the compositional range from tonalite to alkali feldspar granite with those with high scintillometer counts also plotting within, or close to the alkali feldspar granite field. Scintillometer counts are low in Type B, moderate in C and high in Type D and E. A pyrochlore group mineral, which is probably betafite, occurs mainly in Type D leucogranite, although trace amounts can be observed in Type E leucogranites.

Chapter 4 and 5 concentrated at the characteristics of the lithologies found in the SK area. In chapter 6, detailed geochemical descriptions of leucogranites are presented and discussed.

CHAPTER 6

GEOCHEMISTRY OF THE SK AREA LEUCOGRANITE SAMPLES

6.1. Introduction

The textural range of the sheeted leucogranites as observed by Nex *et al*. (1997) in the Goanikontes area has also been noted in the SK area. The leucogranites not only vary from fine-grained to pegmatitic but these textural variations can sometimes be observed within a single alaskite sheet. Major-element whole-rock analyses have been undertaken to provide a geochemical nomenclature for these textural variants based on composition, and to compare this with the classification from the modal analysis obtained from petrographic studies. Such compositional data can then be compared with data from alaskites in the SH and SJ areas and with historical data. In addition to evaluating whether different textural types have distinctive chemical signatures, trace-element data will enable comparisons between uranium-rich and uranium-poor variants to be made. All XRF data provided below, were produced by the XRF section, at the University of the Witswatersrand, Johannesburg.

6.2. Sample Preparation

The 22 surface samples, 10 SK area core samples from recent drilling and 6 SK4 historic core sample described in Chapter 5 have been analysed by XRF. The samples were crushed in an Osborn-Massco jaw crusher to a size of 3 to 4 cm. Each crushed sample was divided into two: one sample for whole-rock XRF analysis, the other for heavy mineral analysis.

Large crushed samples were mechanically split into two equal homogeneous sizes using the Jones splitter. The splitter consists of many chutes alternately inclined in opposite directions. The original sample was poured in the top, and the split halves were collected in rectangular pans on the sides of the splitter and put into new sample bags to avoid contamination. Acetone was used to clean equipment between samples.

The geochemical samples were milled to a very fine powder using a rotary swing mill, in order to ensure accurate geochemical results. Bulky powders were reduced in size using a method of coning and halving, in which a large milled sample was placed on a piece of flat clean paper and folded into a cone form. The sample cone was split into two halves by a 30 cm ruler and every time the division was made; one half was removed, while the other was kept for the next splitting. This method was

repeated until the right amount of rock powder was attained for the preparation of pellets and fused beads.

Approximately 6 grams of powder from each sample was placed into aluminium pellet cups and this was used to prepare pellets for trace-element analyses with the XRF analyses. To avoid contamination, all the tools used in this process were cleaned with acetone between each sample preparation. The following trace-elements were analysed: As, Ba, Ce, Co, Cr, Cu, Ga, La, Ni, Nb, Pb, Rb, Sc, Sr, Th, U, V, Y, Zn and Zr.

About 10 grams of each sample were placed in a new separate sample bag and sent for major-element analyses. The following major-elements were analysed: SiO_2, TiO_2, Al_2O_3, Fe_2O_3, MnO, MgO, CaO, Na_2O, K_2O and P_2O_5.

6.3. Geochemical Results

Standards used for calibration of PW1400 XRFS for silicate analysis and analytical precision for major-element analysis, at the University of the Witwatersrand, Johannesburg, are shown in Appendix 5, section A. The XRF analytical data for SK surface samples is presented in Appendix 5, section B; SK core samples in Appendix 5, section B, while XRF analyses for SK4 are in Appendix 5, section C.

The range of major-element chemistry is presented in Table 6.1, while the range of trace-elements is in Table 6.2. There is a limited range of silica content, which varies from 59.99-77.08%, alumina from 11.46-17.1%. For the alkalis, potash is dominant: Na_2O varies from 2.28-5.85% and the range of K_2O is from 1.07-8.94%. The SK area leucogranites are characterised by variable high field strength cations Ba, Pb, Rb and Sr and large ion lithophile cations: Ce, La, Nb, Sc, Th, U, Y and Zr. They have low Co, Cu, Zn and V (Table 6.2), whereas Ni values are surprisingly high for granitic rocks varying up to 700 ppm. It is assumed that this has been derived from the country rock schists.

Table 6.1: Comparison of the major-element in the SK (22 surface samples), SH (11 surface samples) and SJ (43 core samples and 36 surface samples) areas.

AREA	MAJOR-ELEMENT	SiO_2%	TiO_2%	Al_2O_3%	Fe_2O_3%	MnO%	MgO%	CaO%	Na_2O%	K_2O%	P_2O_5%
SK	Mean	72.81	0.13	13.89	0.69	0.02	0.15	0.94	4.38	5.10	0.08
	Minimum	59.99	0.06	11.46	0.18	0.01	0	2.26	2.28	1.07	0.00
	Maximum	77.08	0.87	17.19	5.12	0.05	2.26	6.43	5.85	8.94	0.78
SH	Mean	82.30	0.09	12.12	0.20	0.01	0.12	0.36	3.89	5.10	0.05
	Minimum	71.54	0.01	11.31	0.14	0.01	0.06	0.28	3.79	4.31	0.01
	Maximum	79.38	0.14	15.52	0.31	0.02	0.20	0.74	5.60	6.15	0.29
SJ	Mean	76.77	0.12	12.29	0.75	0.02	0.24	1.20	3.58	4.89	0.07
	Minimum	62.88	0.02	5.42	0.02	0.00	0.00	0.13	0.25	0.47	0.00
	Maximum	88.42	1.03	18.49	6.98	0.21	1.93	11.61	8.90	7.96	0.92

Table 6.2: Comparison of the trace-element abundances for the SK area (22 surface samples), SH area (11 surface samples) and SJ area (43 core samples and 36 surface samples) areas.

AREA	Trace element	Rb (ppm)	Sr (ppm)	Y (ppm)	Nb (ppm)	Cu (ppm)	Zn (ppm)	V (ppm)	Cr (ppm)	Ba (ppm)	Pb (ppm)	Ga (ppm)	La (ppm)	Ce (ppm)	Sc (ppm)	Th (ppm)	As (ppm)	U (ppm)
SK	Mean	382.4	82.05	25.52	74.1	6.05	6.67	5.9	31.7	145.4	19.67	22.5	21.38	23.4	1.14	42.76	0	100
	Minimum	333	18	7	<3	<6	4	<12	<12	33	<9	<10	19	15	<10	<12	<12	<9
	Maximum	975	216	108	503	27	18	77	123	359	42	28	86	96	24	207	<12	379
SJ	Mean	12.34	2.73	1.37	6.37	4.46	0.23	0.97	91.35	198.11	0.53	18.53	19.42	43.84	0.30	2.62	0.15	4.80
	Minimum	19	4	5	1	5	0	1	65	23	5	5	1	5	1	2	<12	3
	Maximum	728	422	245	223	103	124	425	302	762	186	31	158	257	<10	224	<12	2561
SH	Mean	376.18	52	15.55	80.55		2.45	12.09	227		25.36	26	5.64			39.09		232.64
	Minimum	299	38	8	3		1	6	200		6	24	1			2		10
	Maximum	455	66	27	333		10	25	249		47	31	19			96		700

6.3.1. Geochemical Classification of the Sheeted Leucogranites

The geochemical data were used to calculate a CIPW (Cross, Iddings, Pirrson and Washington) norm using a calculation table adapted from Johanssen (1931). Because of the chemical similarity between granite and rhyolite, the Fe composition of the whole rock was estimated to have similar Fe_2O_3: FeO ratios to those of a rhyolitic magma. The CIPW norm data for the surface samples was plotted in the Streckeisen and Le Maitre (1976) diagram (Figure 6.1), while CIPW norm data for core samples are shown in Figure 6.2. The surface samples have been plotted on the basis of their leucogranite types because they have been fully described in hand specimen and thin section and have been confidently classified according to their types. Core samples from the overall SK anticline have been plotted and compared with SK4 syncline core.

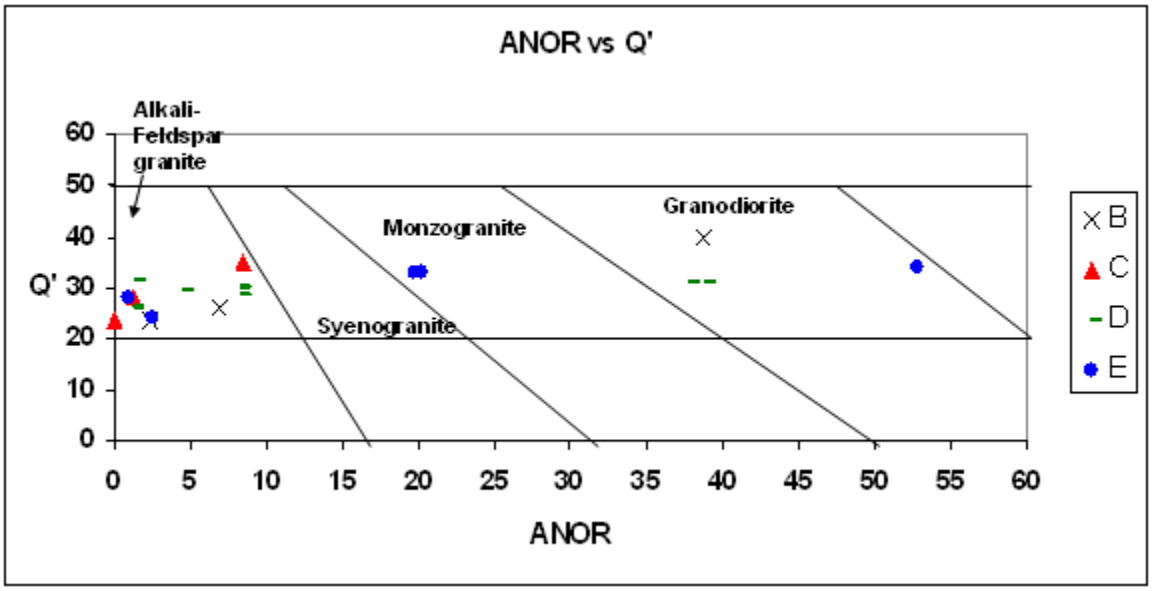

Figure: 6.1: Geochemical plot of the SK surface leucogranites on a diagram of Streckeisen and Le Maitre (1976) ANOR = (100 x An/ (Or + An)) versus Q' = (Q/ (Q + Or + Ab + An)). All Type C leucogranites samples plot in the alkali feldspar field, Types B and D plot in the alkali feldspar granite and granodiorite fields, while Type E samples plot in the alkali feldspar granite, monzogranite and granodiorite fields.

In the ANOR = (100xAn / (Or+An)) versus Q' = (Q / (Q+Or+Ab+An)) diagram of Figure 6.1, the Type C leucogranites plot in the alkali feldspar granite field. The Type B and D leucogranites plot in the alkali feldspar granite and granodiorite fields. The Type E leucogranites plot in the alkali feldspar granite, monzogranite and granodiorite fields.

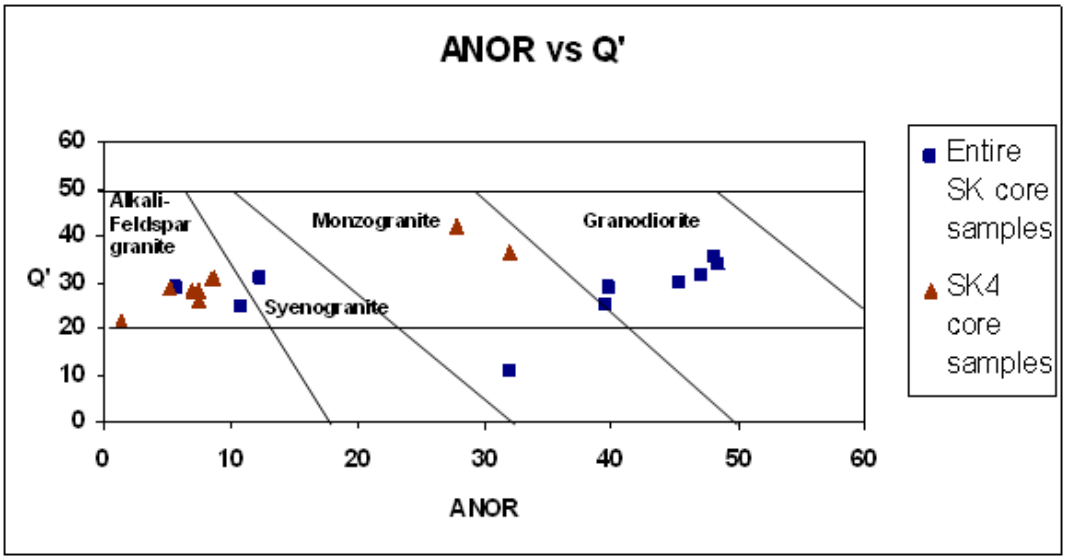

Figure: 6.2: Streckeisen and Le Maitre (1976) ANOR-Q' diagram of leucogranite samples from cores in the SK anticline and SK4 syncline. The SK anticline leucogranite samples plot from alkali feldspar granite, through syenogranite, and monzogranite to granodiorite. The SK4 leucogranite samples mainly plot in the alkali feldspar granite field, although there are two samples that plot as monzogranites.

In Figure 6.2, the SK area core leucogranite samples range from alkali feldspar granite, syenogranite and monzogranite to granodiorite. The SK4 leucogranite samples mainly plot in the alkali feldspar granite field, although there are two samples, which plot as monzogranites.

In addition, the leucogranites from the SK area are also plotted on a SiO_2 vs. Na_2O + K_2O wt% diagram (Figure 6.3) for granitoid classification purposes. The compositional range obtained from the total alkalis versus silica plot mainly plot in the granite field with few samples plotting in the granodiorite and syenite fields and indicates a similar compositional range to that derived from the ANOR versus Q' diagrams.

Using the major-element chemistry, the leucogranites of the SK area plot as peraluminous on the A/CNK vs. Si diagram (Figure 6.4), which shows the degree of Al saturation in each sample, although three samples fall in the metaluminous category. The A/CNK ratio varies little with a range of SiO_2 content.

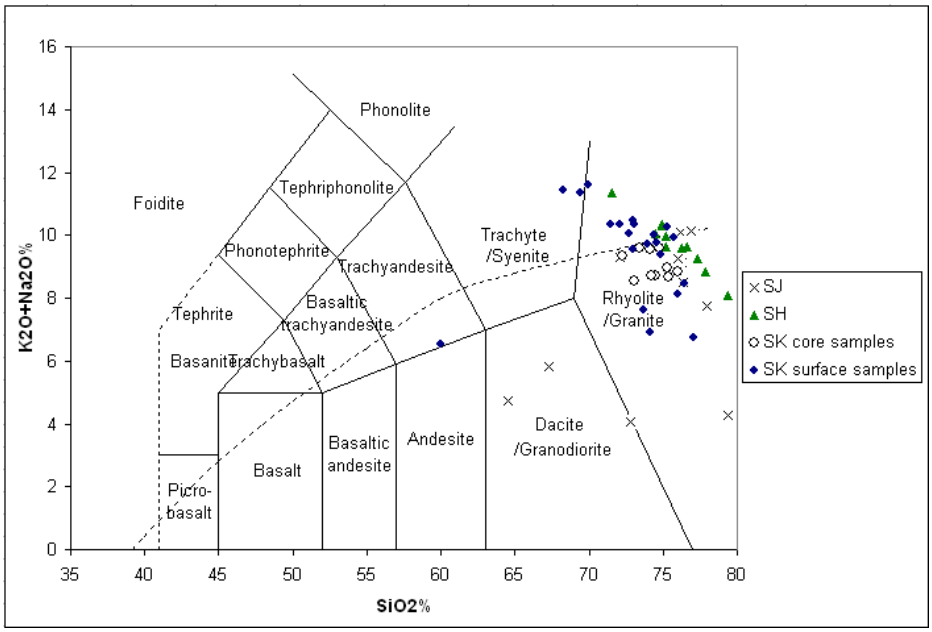

Figure 6.3: Alkali-silica diagram showing the composition of the granitoid rocks in the SK, SJ, and SH areas. The dotted line subdivides the alkaline rocks above and the subalkaline rocks below. SH and SJ data provided by the University of the Witswatersrand, Johannesburg.

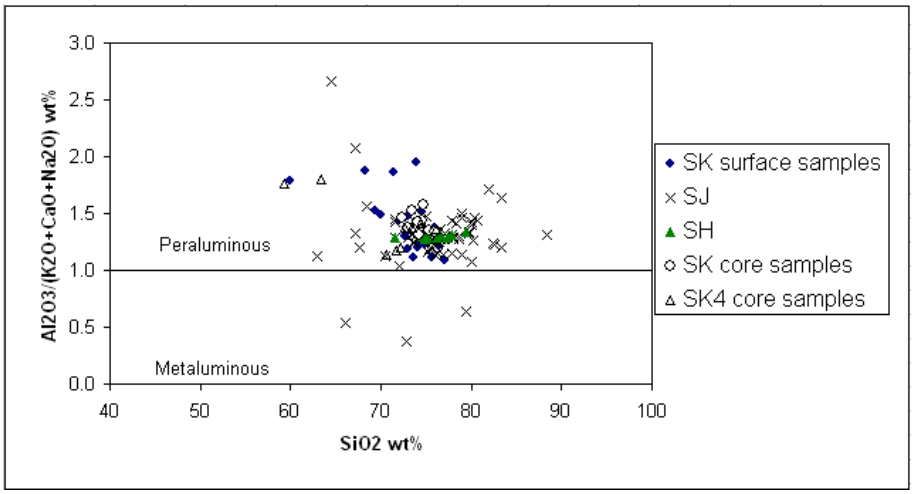

Figure 6.4: Plot of SiO_2 against Al_2O_3/ (Na_2O + K_2O+ CaO), showing the aluminium saturation of the SK, SH and SJ samples in the Rössing area. The A/CNK ratio varies little with range of SiO_2 content. SH and SJ data provided by the University of the Witswatersrand, Johannesburg.

6.3.2. Trace-Element Geochemical Classification of the Sheeted Leucogranites in the SK Area

Pearce *et al*. (1984) used trace-elements such as Nb vs.Y, Ta vs.Yb, Rb vs. (Y+Nb), and Rb vs. (Yb+Ta) to differentiate between granites and to geochemically distinguish their tectonic settings. In Figure 6.5 the granitoid discrimination diagram of Rb vs. (Y+Nb) used by Pearce *et al*. (1984) to indicate tectonic setting for granitoid emplacement shows that most SK data fall in the syn-collision field, with a few plotting in the 'within plate' field and VAG field.

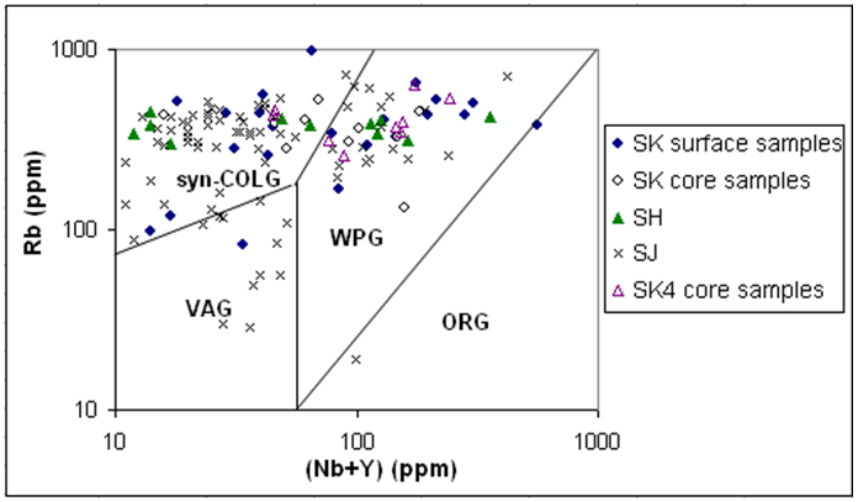

Figure 6.5: The granitoid discrimination diagram of (Y+Nb) vs. Rb used by Pearce *et al*. (1984) to indicate tectonic setting for granitoid emplacement shows that most SK data fall in the syn-collision field, with a few plotting in the 'within plate' field and a few occur in the VAG field. SH and SJ data provided by the University of the Witswatersrand, Johannesburg.

The SK area leucogranite samples plot randomly on a U + Th versus SiO_2+K_2O diagram (Figure 6.6), suggesting that an increase in U and Th concentrations does not correlate with increasing SiO_2 and K_2O values. U and Th enrichment in the SK area leucogranites may therefore not be due to straightforward fractionation.

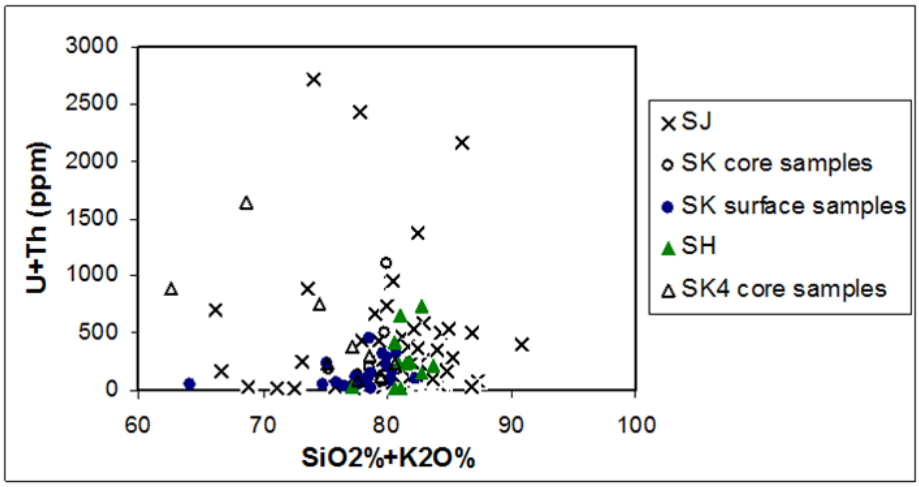

Figure 6.6: A plot of SiO_2 and K_2O (wt %) versus U and Th (ppm), for the different leucogranite types from the SK, SJ and SH area shows a poor correlation. SH and SJ data provided by the University of the Witswatersrand, Johannesburg.

6.3.2.1. Nb, Ti and U

Betafite, $(Ca,Na,U)_2(Ti,Ta,Nb)_2O_6(O,OH)$, is the predominant primary U phase in the SH area. Various trace element plots are evaluated to investigate the potential of betafite occurrence in the SK area. Betafite occurrence is undesirable for pit expansion as the current metallurgical process does not extract the uranium from betafite. Since betafite is a U, Nb and Ti mineral, the behaviour of Nb versus U is important (Figure 6.7) and is presumed to show a positive trend. However, Nb may also occur in pyrochlore, biotite, magnetite, ilmenite and cordierite, so the behaviour of U versus Nb+Ti has been used as being a better indicator of potential betafite presence.

The SH samples have been used as reference to determine the betafite zone in Figure 6.7 and 6.8. In Figure 6.7 there is a clear correlation of U and Nb for the majority of SK area surface and core samples, which suggest that a significant proportion of uranium may be incorporated in betafite. The SK4 core samples plots outside the betafite zone. Figure 6.8, shows a similar trend to that observed in Figure 6.7.

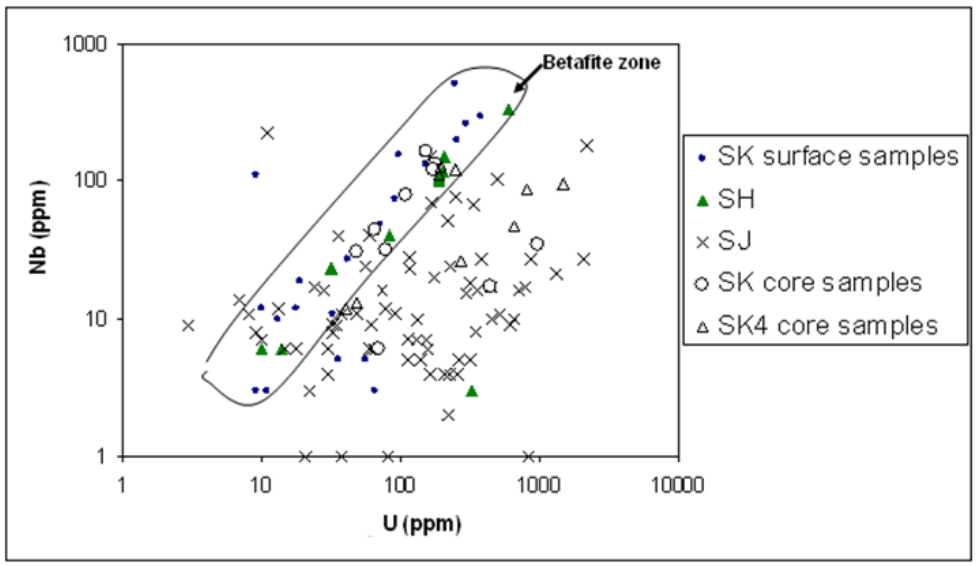

Figure 6.7: A plot of U (ppm) versus Nb (ppm), showing a clear increase in Nb as U increases, a good indication that betafite may be present in the SK area. The ellipse 'betafite zone' is chosen on the basis of SH samples that are high in betafite content. SH and SJ data provided by the University of the Witswatersrand, Johannesburg.

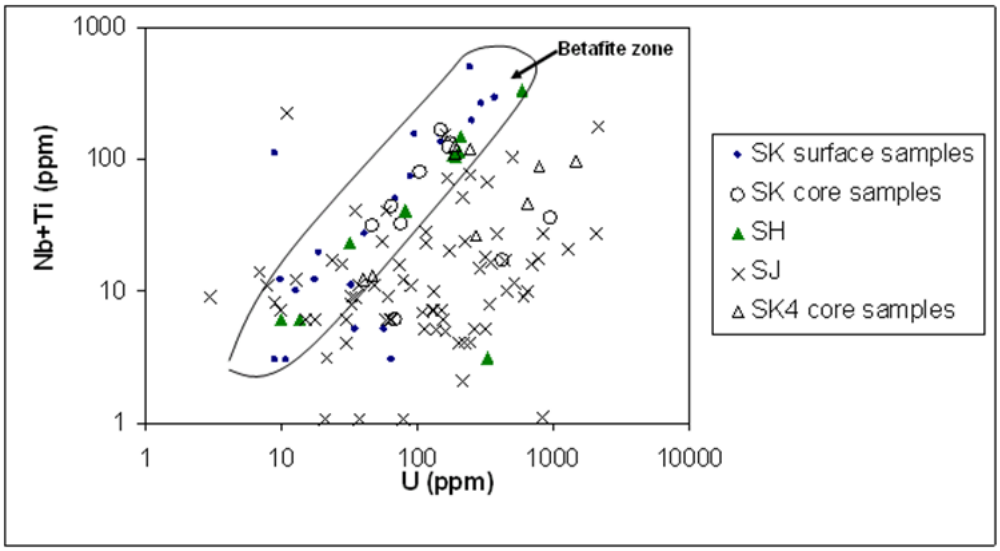

Figure 6.8: A plot of U (ppm) versus Nb+Ti (ppm), showing a clear increase in Nb as U increases, again this gives a good indication that betafite may be present in the SK area. SH and SJ data provided by the University of the Witswatersrand, Johannesburg.

In addition to betafite, the leucogranites also host minor to trace accessory amounts of other Nb, Ti and/or U bearing minerals that are also locally abundant. The most common of these minerals is ilmenorutile ($Fe_X(Nb, Ta)2X4Ti1_{-X}O_2$) that is also usually present as tiny, elongated crystals that are located along grain boundaries between the quartz and alkali feldspars. Other minerals that may also be present in small amounts include Nb-rutile and polycrase ($(U, Y, REE)(Ti, Nb, Ta)_2 O_6$). These minerals are subordinate to betafite in abundance, but it is important to recognise their presence because not all of the Nb and Ti reported in the assays are necessarily present in betafite (Reynolds, 2006).

6.3.2.2. U, Th, Zr, Ce and Y

U and Th may occur in uranium and thorium minerals respectively, or may substitute into other minerals such as zircon, monazite and xenotime. A series of trace elements plots have been investigated to determine potential hosts for Th and U.

SK area samples generally show a Th: U ratio between 0.4 to 1, with a few samples plotting between 1 and 10. There is a general correlation between Th and U concentrations as shown in Figure 6.9, although the Th: U ratio is lower than the typical crustal ratio of Rollinson (1993) which is 4 to 1.

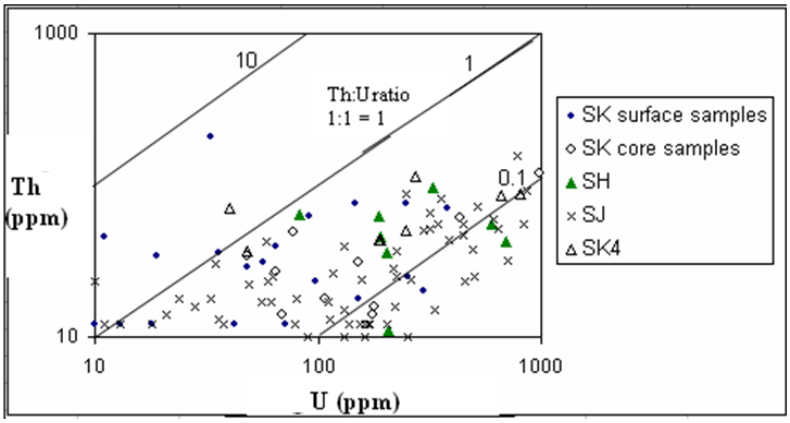

Figure 6.9: A plot of U (ppm) against Th (ppm), showing a dominant Th: U ratio below 1:1. Note that some SK samples indicate a Th: U ratio above the 1:1 line. SH and SJ data provided by the University of the Witswatersrand, Johannesburg.

U, Th and Zr

U versus Zr, and Th versus Zr, are used to investigate whether U and/or Th is linked to zircon ($ZrSiO_4$) occurrence. The relationship between Zr and U is discussed by Hiemstra and Beukes (1969), who indicated that U is common in zircon because uraninite forms nuclei for the growth of zircon crystals in the Rössing area. Additionally, U may also substitute for Zr due to the similar ionic charge. However, the data in Figure 6.10 there is a poor correlation between U and Zr and it would therefore appear that zircon is not a significant host of the uranium.

In Figure 6.11, Th versus Zr for the SK area surface samples is scattered, but the SK area and SK4 core samples seem to indicate a positive correlation. Thus Th concentration may be controlled by zircon at depth.

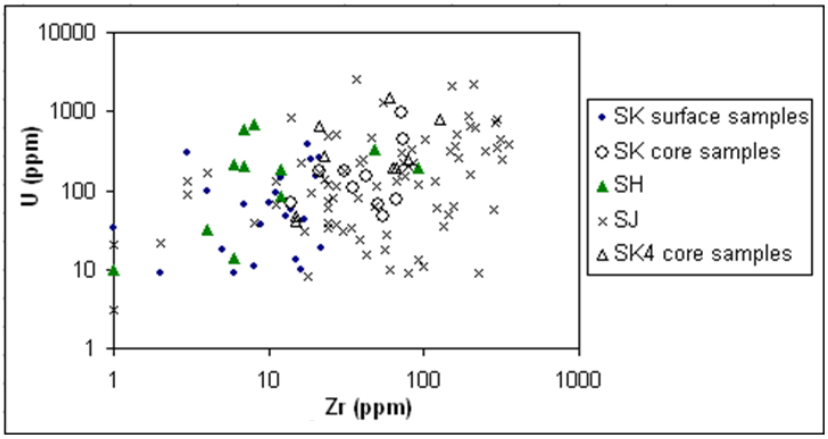

Figure 6.10: Zr ppm versus U ppm showing a poor relationship for the SK samples. SH and SJ data provided by the University of the Witswatersrand, Johannesburg.

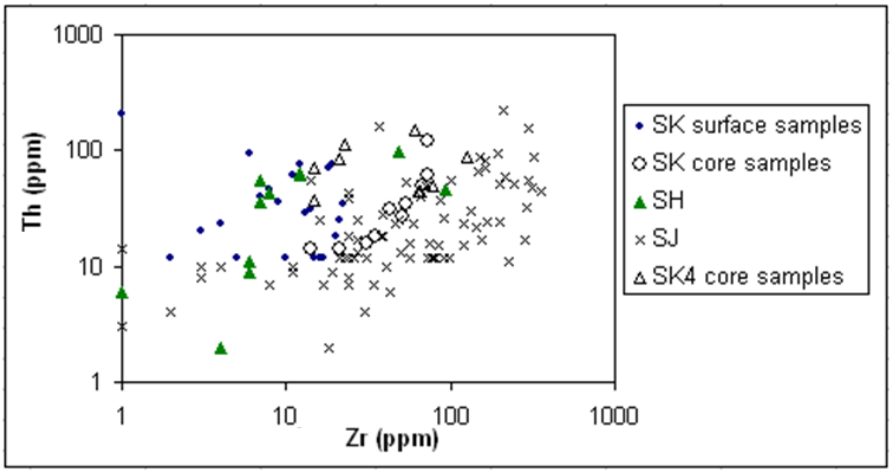

Figure 6.11: Zr versus Th showing a poor relationship for the SK surface samples, an unsystematic positive trend within the SK4 core samples and a systematic positive for the SK core samples. SH and SJ data provided by the University of the Witswatersrand, Johannesburg.

U, Th and Ce

U versus Ce and Th versus Ce, investigate whether U and/or Th is governed by monazite occurrence. Monazite ((Ce, La, Nd, Th) PO_4), is essentially a Ce phosphate mineral, although La and to a lesser extent Th may substitute into the structure.

Figure 6.12 and Figure 6.13; indicate that both SK area surface and core samples do not show any correlation between U and Ce or Th and Ce, respectively. This observation may suggest that monazite does not control U and Th distribution in the SK area.

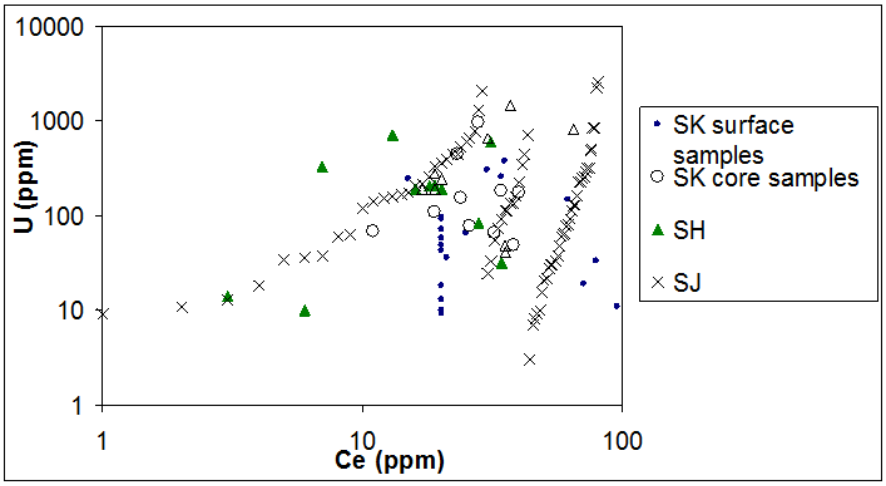

Figure 6.12: Ce versus U showing a poor relationship for the SK samples. SH and SJ data provided by the University of the Witswatersrand, Johannesburg.

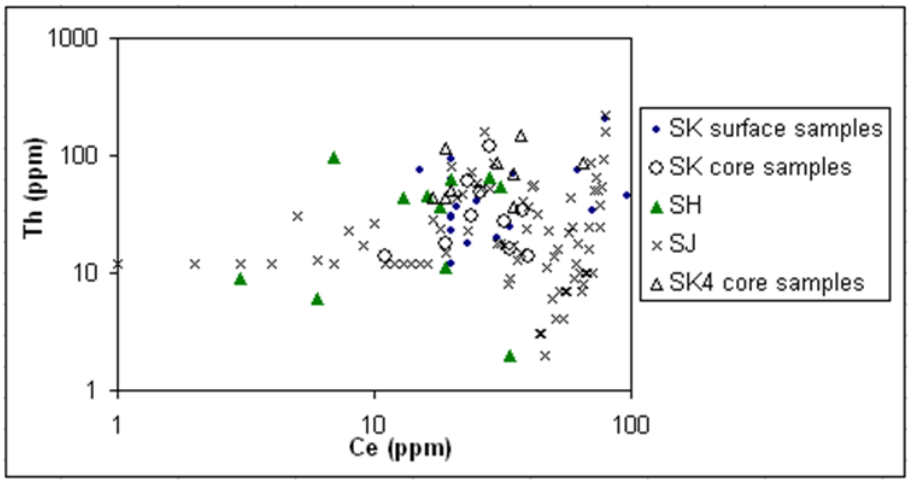

Figure 6.13: Ce versus Th showing a poor relationship for the SK surface samples. SH and SJ data provided by the University of the Witswatersrand, Johannesburg.

U, Th and Y

Y is important element in the formation of xenotime (YPO_4). Figure 6.14 shows a poor correlation between U versus Y and Th versus Y, for SK area surface samples. SK area and SK4 core samples on the other hand, indicate a non-systematic positive correlation between U versus Y and Th versus Y (Figure 6.15). The above observations may suggest that, U and Th are controlled by xenotime at depth. At surface the effect maybe hidden by the effects of weathering.

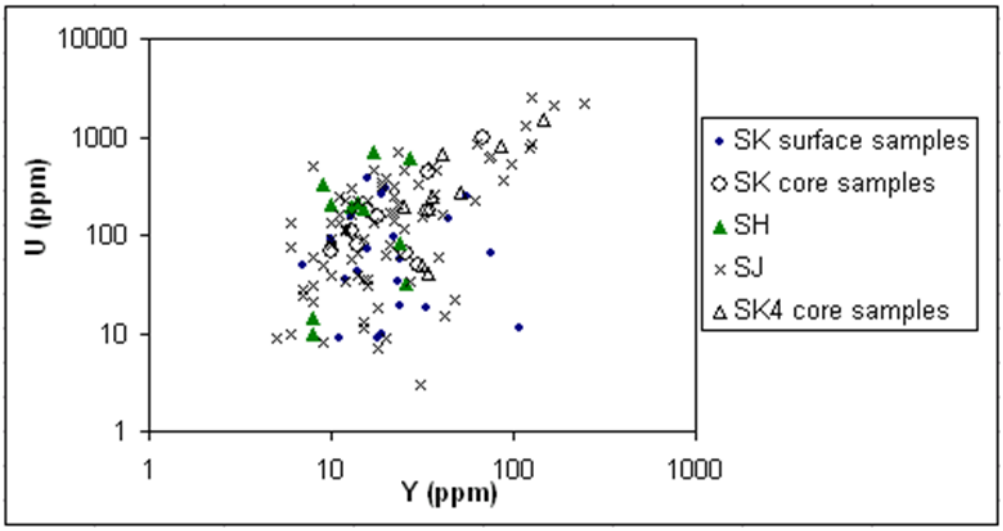

Figure 6.14: Y versus U showing a poor relationship for the SK surface samples, an unsystematic positive trend within the SK4 core samples and a systematic positive trend for the SK core samples. SH and SJ data provided by the University of the Witswatersrand, Johannesburg.

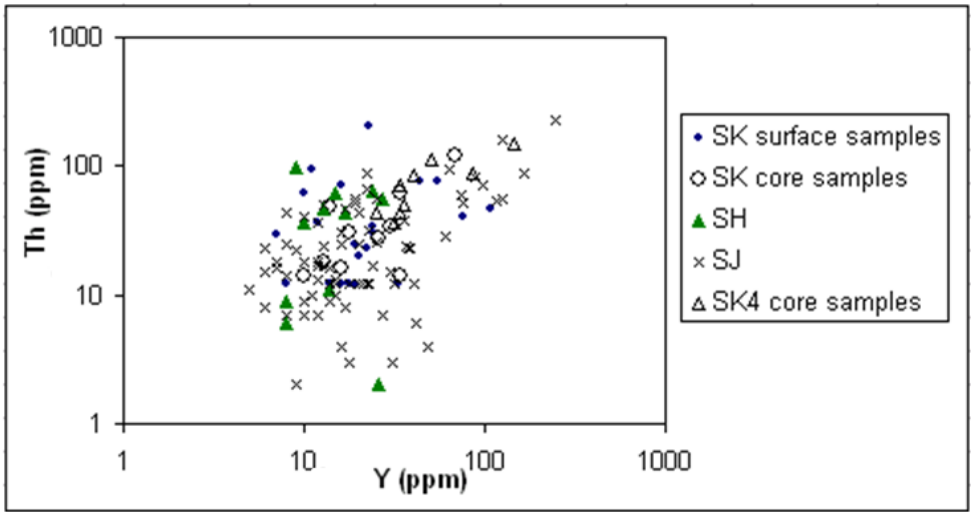

Figure 6.15: Y versus Th showing a poor relationship for the SK surface samples and systematic positive trend within the SK4 and SK core samples. SH and SJ data provided by the University of the Witswatersrand, Johannesburg.

6.4. Discussion

The SJ and SH leucogranites show a wide compositionally range from granite, through syenite to granodiorite fields on the alkali-silica diagram although they all plot in the peraluminous field in the Al_2O_3/ (Na_2O + K_2O+ CaO) against SiO_2 classification system. In geochemical classification schemes, the leucogranites from the SK area are generally peraluminous and also range in composition from alkali feldspar granite, through syenogranite and monzogranite to granodiorite. The SK4 leucogranite samples mainly plot in the alkali feldspar granite field, although there are two samples, which plot as monzogranites. Type B, C and D leucogranites plot predominantly in the alkali feldspar granite field while Type E shows a compositional range from alkali feldspar granite, monzogranite to granodiorite, so there is no clear correlation between whole-rock composition and U abundance.

The trace element classification schemes for tectonic setting of granitoid emplacement employed by Pearce *et al*. (1984) show a complete range for the data of the Rössing area, with many of the SK samples plotting in the syn-collision field. Since Type D and E sheets are generally regarded as post D3, it would seem unreasonable to regard them as syn-collisional which cast considerable doubt as to the validity of such schemes for valid interpretation of the tectonic setting.

The SK area samples generally show a Th: U ratio between 0.4 to 1, with a few samples plotting between 1 and 10. The Th: U ratio is lower than the typical crustal ratio of Rollinson (1993). The fact that Th is less than U in most samples has positive implications. Although both Th and U are toxic; Th is more deleterious to health than U, because thorium emits high energy particles that are more penetrating than those emitted by U (Uranium conference, 2007). For this reason, it is beneficial for the U concentration to be higher than the Th concentration in a potential ore deposit. Areas with high Th and U produce the radioactive gases thoron and radon. Thoron and radon are natural health hazards that need to be dealt with when mining uranium. The World Nuclear Association estimates an average Th: U ratio of 4, based on lead isotope studies, in contrast, the ratio of Th: U ratio in the samples from the Rössing area ranges from 0.04 to 1, although there are a few samples mainly from the SK area that plot over the ratio of 1 but below ratio of 10 so Th may still be a concern in the SK area, due to the samples higher Th:U ratios.

U and Th can substitute in other minerals such as zircon, monazite and xenotime. This study indicates that zircon may influence the Th concentration but not U concentration. Even though monazite seems to be controlling the U in the SJ area, this is not the case in the entire SK area. Xenotime partially governs the U and Th concentrations in the SK area.

The correlation between Nb versus U and Nb+Ti versus U for the SK area suggests the presence of betafite except in the SK4 samples, which are similar to samples from the SJ open pit. Since it is known that U-rich SH samples are betafite-bearing and that SJ samples are uraninite-bearing and betafite-poor, the plots appear to provide a good indicator of potential betafite occurrence.

CHAPTER 7

EVALUTATION OF THE DEPORTMENT OF URANIUM IN THE RÖSSING AREA

7.1. Introduction

The sheeted leucogranites in the Rössing area host primary uranium minerals. Uranium may be remobilised into secondary minerals, which coat mineral grains and infill cracks and joints in the granites and percolate out into surrounding country rocks, especially the amphibole-biotite schist. Primary uranium minerals recorded in the Rössing area include uraninite (UO_2) and betafite (Ca, Na, U)$_2$ (Ti,Ta,Nb$_2$O$_6$(O,OH) (Nex and Kinnaird, 2005) although other primary minerals (davidite and rössingite) can also be found in trace amounts (Nex and Kinnaird, 2005). In addition, uranium may be hosted in zircon, monazite and/or pyrochlore.

Betafite may contain a significant uranium content, which according to Herd (1996) may be up to 30%. Uranium in betafite is not released from the pyrochlore structure during mineral processing; using the acid leach plant currently used at Rössing Uranium Mine (Nex and Kinnaird, 2005). The major aim of this dissertation is to determine the relative abundance and distribution of betafite in the SK area and if possible to understand the controls on its occurrence.

7.1.1. Uraninite

The black cubic uraninite is not visible in hand specimen. Duarte (2006) stated that species classified as uraninite, sometimes contains traces of other elements such as Pb or Ti-Ca. Uraninite may also be metamict and exhibit a range of alteration features (Reynolds, 2006). The bulk of the occurrence is as free grains or a nucleus enclosed in other minerals such as zircon, feldspars and quartz, generally close to the crystal boundaries of these minerals (Reynolds, 2006). The uraninite is often euhedral and this, along with the uraninite association with zircon, indicates early crystallisation. Uraninite is found in varying proportions around the Rössing area. For the SJ pit, uraninite constitutes about 55% of all the uranium minerals while in the betafite-dominated SH area, it forms around 2.5% of the uranium population (Nex and Kinnaird, 2005)

7.1.2. Betafite

Betafite is a Ti-rich pyrochlore group mineral. Nex *et al*. (2003) stated that betafite occurs as small octahedral to subrounded, isolated, dodecahedral crystals or clusters of crystals up to 2 cm in size, although commonly of 1-3 mm diameter in the Goanikontes area. Typically, betafite is greenish brown or yellowish brown in colour, although it shows a range from yellowish- or greenish-brown through grey to progressively darker colours, such as reddish brown or almost black body colour. The proportions of U, Ti, Nb, and Ta vary between betafite grains giving rise to the variety of colours (Herd, 1996).

Betafite/pyrochlore is found dominantly in the medium-grained microcline-perthite facies of the leucogranites, often within quartz or at the contact between quartz and feldspar grains (Nex, 1997). The presence of betafite is characterised by dark smoky quartz and a distinctive halo of radial cracks around the mineral. The quartz and feldspar in immediate contact with the betafite are often fractured due to expansion during metamictisation, and this zone is permeated with red or yellow staining (Figure 5.6) caused by the presence of various secondary uranium-, iron- and titanium-bearing minerals (Nex *et al*., 2003).

Crystals of the pyrochlore end member were mainly found in samples from the SJ pit (Herd, 1996). These occur as isolated honey-coloured crystals in a medium-grained, white leucogranite interbanded with amphibolite (Herd, 1996). Betafite increases from 5% in the SJ pit to 94% in the SH area (Herd and Kinnaird, 1999).

The pyrochlore group minerals are classified in three subgroups (pyrochlore, betafite and microlite) according to atomic proportions of B atoms while subgroup species are classified according to A-site atoms as shown in Table 7.1 (Hogarth, 1989). Pyrochlore group minerals have a group cell-formula of A_{16} - $xB_{16}O_{48}$ $(O, OH, F)_8$ – y. zH_2O where x and y are vacant sites in the unit cell, z indicates variable degrees of hydration and x, y, and z are non-rational (Hogarth, 1989). A-site atoms which occupy the cubic sites are dominated by Ca, U and REE's but may include As, Ba, Bi, Cs, K, Mg, Mn, Na, Pb, Sb, Sn, Sr, Th, and Y (Nex *et al*., 2003). The B atoms fill the octahedral site in the structure are dominated by Nb, Ti and Ta with lesser Zr and W (Nex *et al*., 2003).

Table 7.1: Subgroups and species of the pyrochlore group. From Hogarth (1989).

Subgroups defined by *B* atoms i.e. Nb, Ta, Ti			PYROCHLORE sub-group Nb+Ta >2Ti Nb >Ti	MICROLITE sub-group Nb+Ta >2Ti Ta ≥Nb	BETAFITE sub-group 2Ti ≥Nb+Ta
Species defined by *A*-atoms K, Sn, Ba REE, Pb Bi, U	Na+Ca but no other *A*-atoms > 20% total *A*-atoms		pyrochlore	microlite	calciobetafite
	One or more *A*-atoms other than Na or Ca, > 20% total *A*-atoms Species named by most abundant *A*-atom, other than Na or Ca	K	kalipyrochlore		
		Cs		cestibtantite	
		Sn		stannomicrolite	
		Ba	bariopyrochlore	bariomicrolite	
		REE*	yttropyrochlore ceriopyrochlore		yttrobetafite
		Pb	plumbopyrochlore	plumbomicrolite	plumbobetafite
		Bi		bismutomicrolite	
		U	uranopyrochlore	uranmicrolite	betafite
*REE = Y + (lanthanides), and for the purposes of species definition, REE counts as one *A*-atom yttro = Y + (Gd →Lu), cerio = La →Eu.					

7.1.3. Secondary Uranium Minerals

Secondary uranium minerals are all U silicates. According to Berning (1986) in the Rössing area, the dominant secondary uranium mineral is beta-uranophane ($Ca(UO_2)_2[SiO_3(OH)]_2 5H_2O$) which formed from the alteration of uraninite. Nex and Kinnaird (2004) have recorded minor uranophane ($Ca((UO_2)_2[SiO_3(OH)]_2.5H_2O$), boltwoodite ($(K,Na)[UO_2)(SiO_3OH)](H_2O)_{1.5}$), thorogummite ($((Th,U)(SiO_4)_{1-x}\ (OH)_{4x}$), haiweeeite ($((Ca(UO_2)_2(Si_5O_{12}(OH)_2]4.5H_2O$) and metahaiweeite ($(Ca(UO_2)_2(Si_6O_{15}(OH)_2].nH_2O$).

The secondary minerals are not confined to the leucogranites but are present within cracks and joints of the surrounding meta-sediments especially in the amphibole biotite schist (Herd and Kinnaird, 1999). In situ alteration of primary uranium minerals is also common. Secondary uranium minerals account for 40% of the uranium mineral proportion in the SJ area and 13.5% of the SH area (Herd and Kinnaird, 1999). No mineral proportions are known for the SK area, except for the SK4 sub-anomaly (Rössing Internal Report, 050505, 2005).

7.1.4. Additional Minerals

In addition to uraninite, betafite and secondary uranium minerals, uranium has been reported in a wide range of accessory minerals, such as:

- thorianite (ThO_2), found in minor amounts widely distributed throughout the sample suite, but it is of very low abundance (Reynolds, 2006).

- davidite [$Fe_x(Nb, Ta)_{2x}$ $4Ti_{1-X}O_2$], usually present as tiny, elongated crystals that are located along grain boundaries between the quartz and alkali feldspar gangue minerals (Reynolds, 2006). These crystals rarely exceed 50 μm in length and are generally very much smaller. They occur both as isolated phases and in association with betafite with which they may also be intergrown (Reynolds, 2006).
- Nb-rutile (Nb-$TiO_{2)}$ and polycrase [(U, Y, REE) (Ti, Nb, Ta)$_2O_6$], have been reported in trace amounts by Reynolds (2006).
- coffinite ($U(SiO_4)_{0.9}(OH)_{0.4}$), Th-U-Y-Silicate and monazite sometimes containing U have been identified by Duarte (2006).
- zircon, sphene and apatite have been noted as hosts to uranium by Nex *et al*. (2003).
- rössingite, metatorbernite and gummite occurrence have been identified by Hiemstra and Beukes (1969).

7.2. Theoretical Calculation of Betafite Abundance

Following previous work done by Herd (1996), on the NW prong of the SJ pit, it was found that it was possible to determine the worst case scenario for uranium loss in betafite during processing to the tailings. This calculation used the niobium content of the rock and assigned it all to betafite, although it was recognised that some Nb occurs in other minerals such ilmenite.

XRF analyses yielded values for Nb and U in ppm. The calculation assigned the entire Nb to betafite and then assumed that betafite contained 30% uranium which would be lost to extraction, since according to Herd (1996), on average betafite contain 30% uranium and 20% niobium. All samples with less than 30 ppm U_3O_8 and 20 ppm Nb_2O_5 were discounted as they are lower than the cut-off grade, and at low values of Nb and U the calculation gives spurious results. A conversion factor of U to U_3O_8 of 1.18 was used.

7.2.1. Results

The theoretical betafite calculations for the SK, SH and SJ areas are presented in Tables 7.2, 7.3 and 7.4 respectively. Because of the recent acquisition of new data which is continuously being added to the database, the geochemical analyses for the SH and SJ were also recalculated during this study to compare with previous results.

Tables 7.2 to 7.4 indicate how much uranium is potentially lost in each specific area. According to the calculations in Table 7.2, for the SK area all of the U_3O_8 would be lost to the tailings dam in the form

of betafite. As the calculations indicate a >100% loss of U, there is an over supply of Nb in the SK area and that there must be additional host mineral for the Nb.

Table 7.2: Theoretical calculation of the betafite in the SK area.

SK AREA							
SAMPLE NO	Nb (ppm)	Nb2O5 (wt%)	U (ppm)	U3O8 (wt%)	Betafite in ore (g/t)	U3O8 in betafite (g/t)	% U3O8 in loss
S2	263.00	376.09	299.00	352.82	1880.45	564.70	160.05
S3	156.00	223.08	97.00	114.46	1115.40	334.95	292.64
SK2A	49.00	70.07	71.00	83.78	350.35	105.21	125.58
SK2B	75.00	107.25	92.00	108.56	536.25	161.04	148.34
SK2D	155.00	221.65	147.00	173.46	1108.25	332.81	191.86
SK2E	33.00	47.19	48.00	56.64	235.95	70.86	125.10
SK8	27.00	38.61	42.00	49.56	193.05	57.97	116.98
SK9	290.00	414.70	379.00	447.22	2073.50	622.67	139.23
SK12A	503.00	719.29	250.00	295.00	3596.45	1080.02	366.11
SK12D	133.00	190.19	151.00	178.18	950.95	285.57	160.27
SK12E	196.00	280.28	253.00	298.54	1401.40	420.84	140.97
							178.83

Table 7.3: Theoretical calculation of the betafite in the SH area (data from Herd (1996) and Freemantle (2006) showing the almost complete loss of uranium due to a calculated U occurrence in betafite.

SH AREA							
SAMPLE NO	Nb (ppm)	Nb2O5 (wt%)	U (ppm)	U3O8 (wt%)	Betafite in ore (g/t)	U3O8 in betafite (g/t)	% U3O8 in loss
SH15	23.00	32.89	32.00	37.76	164.45	49.38	130.78
SH3	40.00	57.20	83.00	97.94	286.00	85.89	87.69
SH4	107.00	153.01	187.00	220.66	765.05	229.74	104.12
SH20	102.00	145.86	190.00	224.20	729.30	219.01	97.68
SH8	116.00	165.88	203.00	239.54	829.40	249.07	103.98
SH14	150.00	214.50	209.00	246.62	1072.50	322.07	130.59
SH1	333.00	476.19	602.00	710.36	2380.95	715.00	100.65
							107.93

7.2.2. Comparison of Theoretical Betafite Calculation between SK, SH and SJ Areas

According to Tables 7.2 to 7.4, the SK area has the highest percentage of U_3O_8 hosted within betafite with concomitant potential loss of uranium during potential processing. The SH area is known to have a high betafite content (Herd, 1996), whilst the SJ area has been shown to have a low betafite content (Herd, 1996). These findings have been confirmed with the findings in Table 7.3 and 7.4, respectively. This has been supported by previous studies (Kinnaird, pers. comm.). However, it is accepted that the betafite theoretical calculation is an over-estimation of the presence of betafite, and is therefore a worst-case scenario. Table 7.5 compares the known betafite percentage for the SH and SJ areas and compares this to the theoretical calculation.

Table 7.4: Theoretical calculation of uranium loss due to betafite in the SJ area (data from Herd (1996) and Freemantle (2006).

SJ AREA							
SAMPLE NO	Nb (ppm)	Nb2O5 (wt%)	U (ppm)	U3O8 (wt%)	Betafite in ore (g/t)	U3O8 in betafite (g/t)	% U3O8 in loss
RD126-249.9	41.00	58.63	36.00	42.48	293.15	88.03	207.23
R2800E2Z-26988	40.00	57.20	60.00	70.80	286.00	85.89	121.31
RD110-256	23.00	32.89	117.00	138.06	164.45	49.38	35.77
R2800E2Z-26952	71.00	101.53	168.00	198.24	507.65	152.45	76.90
RD218-27	20.00	28.60	171.00	201.78	143.00	42.94	21.28
R2800E2Z-26911	51.00	72.93	219.00	258.42	364.65	109.50	42.37
RD218-28.5A	67.00	95.81	334.00	394.12	479.05	143.86	36.50
1561597.2-104.75	16.00	22.88	358.00	422.44	114.40	34.35	8.13
RD187-198	27.00	38.61	385.00	454.30	193.05	57.97	12.76
RD186-322.5	17.00	24.31	449.00	529.82	121.55	36.50	6.89
1561597.2-106.05	17.00	24.31	785.00	926.30	121.55	36.50	3.94
R2800E2-58.3	21.00	30.03	1315.00	1551.70	150.15	45.09	2.91
R2800E2-56.90A	27.00	38.61	2076.00	2449.68	193.05	57.97	2.37
RD207-31.50	24.00	34.32	56.00	66.08	171.60	51.53	77.98
RD110-326.10	16.00	22.88	74.00	87.32	114.40	34.35	39.34
RD187-247.50	24.00	34.32	225.00	265.50	171.60	51.53	19.41
RD125-329.20	17.00	24.31	448.00	528.64	121.55	36.50	6.90
RD125-378.00	16.00	22.88	707.00	834.26	114.40	34.35	4.12
SJ90-8	16.00	22.88	28.00	33.04	114.40	34.35	103.98
SJ90-34	28.00	40.04	116.00	136.88	200.20	60.12	43.92
SJ90-2	152.00	217.36	163.00	192.34	1086.80	326.37	169.68
SJ90-9	77.00	110.11	247.00	291.46	550.55	165.33	56.72
SJ90-5	15.00	21.45	296.00	349.28	107.25	32.21	9.22
SJ90-7	18.00	25.74	317.00	374.06	128.70	38.65	10.33
SJ90-4	105.00	150.15	503.00	593.54	750.75	225.45	37.98
SJ90-24A	27.00	38.61	860.00	1014.80	193.05	57.97	5.71
SJ90-24B	178.00	254.54	2207.00	2604.26	1272.70	382.19	14.68
							23.43

Table 7.5: Calculated theoretical betafite values compared with known abundances in the SJ, SH and SK areas.

Area	SJ	SH	SK
Known betafite %	5	84	N/A
Theoretical Values %	23	108	179
Over-estimation %	18	24	???

7.2.3. Summary

A betafite theoretical calculation method provides an indication of how much uranium might be lost to the tailings in the form of betafite in the SK area. During the theoretical calculations, the total Nb content was assumed to have been derived from betafite, which resulted in an overestimation of the uranium loss.

From the theoretical calculations, it is implied that the SK area seems to have more betafite than the SH and SJ areas. In order to make an actual assessment of the proportion of betafite, heavy mineral concentrates were prepared for study using a scanning electron microscope (SEM).

7.3. Scanning Electron Microprobe (SEM)

SEM data provided in this section were obtained and analysed at the University of Johannesburg, by the student.

In order to make a quantitative assessment of the proportion of uranium minerals in a heavy mineral population, Nex and Kinnaird (2005) used the SEM (X-ray) technique. The technique maps the elements in the mineral images and assigns a name. For betafite, the key elements are Nb, Ti and U; uraninite needs to have U only, while secondary uranium minerals need to indicate the presence of U and Si. Furthermore, the addition of elements such as Ce, Fe and Zr to the SEM presented an opportunity to identify and obtain proportions of minerals such as monazite, davidite and zircon.

The samples used for the SEM section are the SK area surface samples, because the core samples were not ready at the time of study. The sampling rationale is discussed in Chapter 5, Table 5.1.

A number of different heavy minerals were tentatively identified based on the semi-quantitative SEM analyses. These included niobokuleskite ($ZrNbSiO_4$), rutile (TiO_2), betafite ($(Ca, Na, U)_2(Ti,Ta,Nb_2O_6(O,OH))$), titanite ($CaTiSiO_5$), Fe-oxide, ilmenite ($FeTiO_3$), U-silicate, pyrochlore $(Na,Ca)_2Nb_2O_6(OH,F)$ and K-vuoriyarvite ($(K,Na)_2(Nb,Ti)_2Si_4O_{12}(O,OH)_2 \cdot 4(H_2O)$). Selected grains of these minerals that were potentially identified using the SEM were re-analysed using mineral chemistry spectra, with the aim of confirming the identification of minerals suggested by the SEM element mapping. The probe measured Fe by energy dispersion; other elements were determined by wavelength dispersion. The oxygen content has been calculated by stochiometry, assuming Al is present as Al_2O_3, Si as SiO_2, etc.

In the past, attention was mainly given to the minerals associated or containing uranium. During this study, additional heavy minerals have been considered for the following reasons:

1. An evaluation of all the heavy minerals gives a much better overall idea on the range of accessory minerals in individual leucogranites.
2. Knowledge of the variability in the types of heavy minerals between the different ore bodies or within one orebody will contribute towards a better understanding of the effect those minerals will have in the plant during processing.
3. Currently, the plant only considers specific rock types as having negative effects to the plant, while the effects of individual heavy minerals has not been considered.

7.3.1. Sample Preparation

Granite samples were lightly crushed in order to obtain material with the grain size +90-125 µm.. Bromoform ($CHBr_3$) with a density of 2.9 ρ was used to separate out the heavy minerals from the silicates. The thoroughly dried powdered sample of granite was placed into a funnel with bromoform and carefully mixed. Minerals with densities above 2.9 ρ sank, while light minerals with densities below 2.9 ρ floated. The heavy minerals that settled at the bottom of the funnel were carefully drawn off and caught on filter paper, where they were washed with acetone to remove remnant traces of bromoform.

The heavy mineral concentrates were mounted on polished blocks and examined using an electron microprobe. Twenty polished blocks, 2.5 cm thick, were prepared at the SGS Lakefield Laboratory. The number of heavy minerals on each block varied from 200 to 400 grains.

The polished block samples were coated with a ~20 nm layer of carbon before being placed in the specimen chamber. The aim of the carbon coating is to prevent the development of negative charges around the sample when bombarded with electrons. Carbon coating is less dense than most elements analysed and thus had a minimal effect on the analysis.

When the electron beam is fired on the sample surface, electrons are emitted with different energies and wavelengths. Elements such as Ta, Zr, Th, U and Ce were analysed for wavelength dispersion spectroscopy, while Si, Ti, Fe and Nb were analysed by energy dispersion spectroscopy. The rainbow of colours used in each image is computer-generated to highlight element abundances. The smallest grains automatically detected with this technique measure approximately 5µm in diameter. Figure 7.1 and 7.2 shows element mapping images from samples SK2E and SK9, respectively.

Figure 7.1 comprises 11 grains containing uranium, niobium and titanium, which is probably betafite rather than K-vuoriyarvite together with a few secondary uranium minerals. Figure 7.2 has five minerals containing uranium, niobium and titanium, which are probably all betafite.

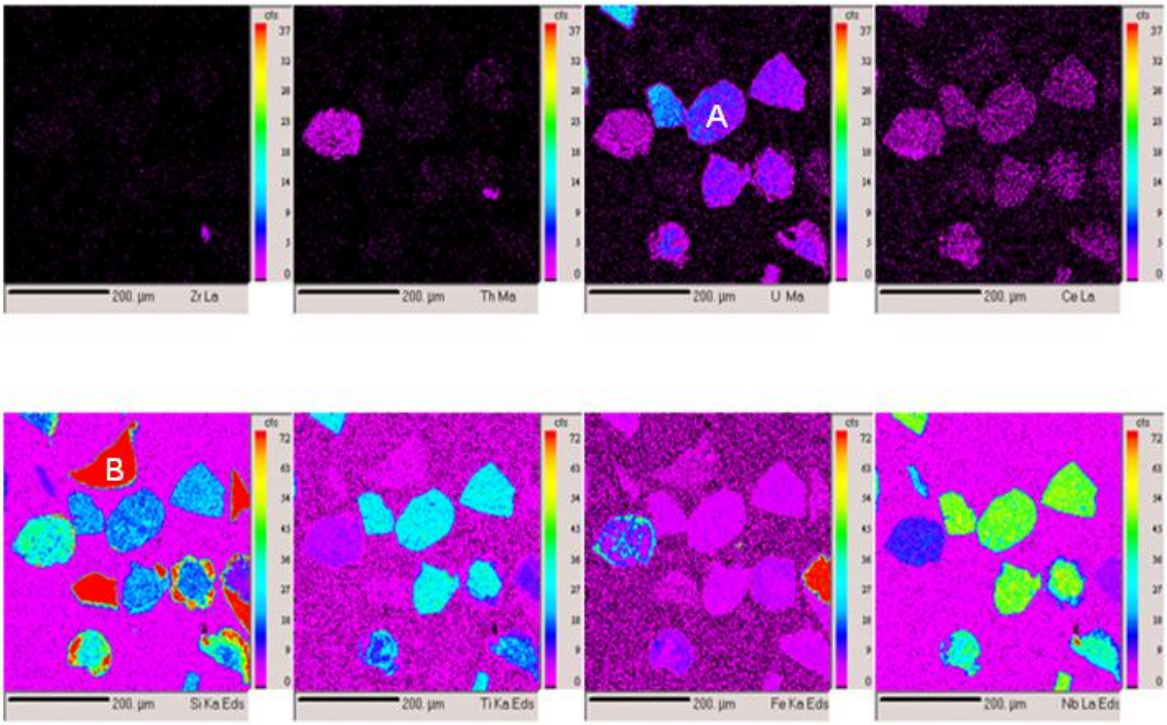

Figure 7.1: SEM element maps from sample SK2E. Element maps in the top row from left to right are: Zr, Th, U and Ce. Element maps in the bottom row from left to right are: Si, Ti, Fe and Nb. Most minerals in this sample belong to either A or B type minerals. A-type minerals contain U, Si, Ti and Nb; which can either be betafite or K-vuoriyarvite. B-type minerals contain Si only, which suggests it may be quartz.

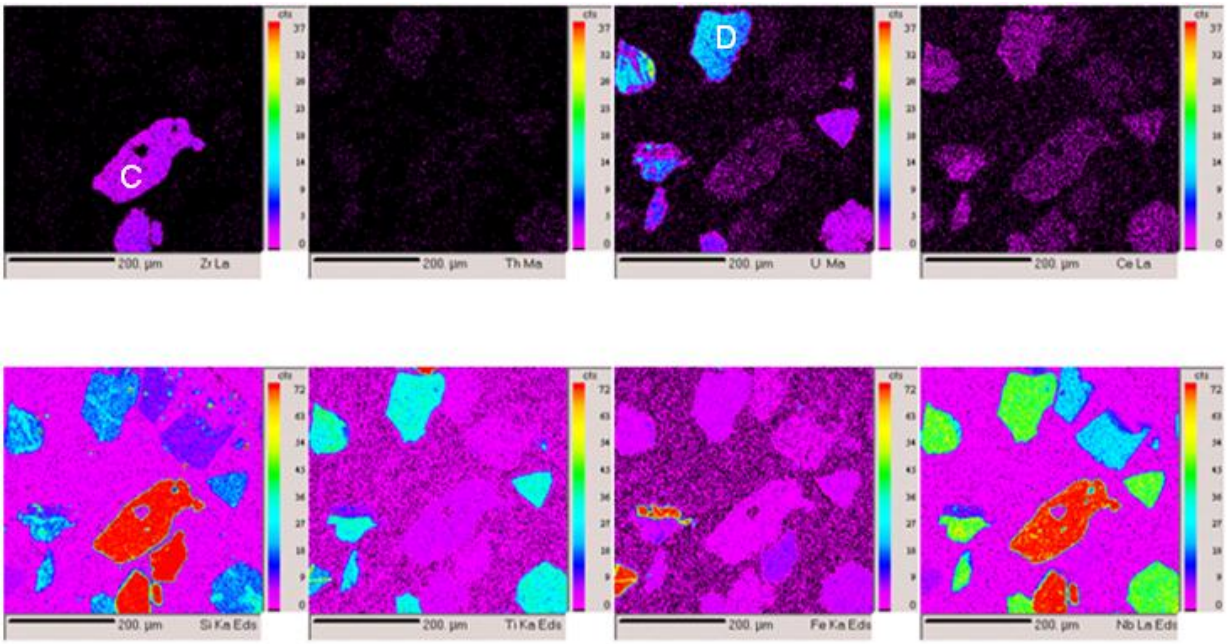

Figure 7.2: SEM element mapping from sample SK9. Element maps in the top row from left to right are: Zr, Th, U and Ce. Element maps in the bottom row from left to right are: Si, Ti, Fe and Nb. Two groups of samples (C and D) are indicated, sample C contains Zr, Si and Nb which; may be zircon or niobokuleskite. D-type mineral contains U, Si, Ti and Nb, which maybe betafite or K-vuoriyarvite.

7.3.2. Results

A total of 2327 minerals grains have been counted. Appendix 6 shows all the elements in each mineral, the diameter and the possible mineral name. The proportion of the minerals is given with respect to the total diameter of the minerals. All heavy minerals found in the SK area are listed in Table 7.6 together with their individual sizes and proportions. The raw element mapping information data is on the Rössing Uranium geology server. Figure 7.3 suggests that K-vuoriyarvite (a Nb Ti silicate) and pyrochlore are the most abundant phases of the heavy mineral assemblage at 24.7% and 24.2% respectively.

The mineral chemistry spectra confirmed the SEM identification of betafite, ilmenite, U-thorite, rutile, titanite, U-titanite and 50% of the Fe-oxide was reassessed as betafite. Niobokuleskite was reassessed as zircon, 50% of the Fe-oxide was identified as betafite, 25% of the pyrochlore was reassigned to betafite and all the K-vuoriyarvite changed to betafite. Table 7.7 presents proportions of heavy minerals, after the mineral chemistry spectra results were considered.

SEM element maps indicate that uraninite in the SK samples occurs as tiny euhedral cubic crystals with an average diameter of 22.50 µm. Uraninite is about 0.40% of the total uranium minerals and about 0.50% of the main three uranium minerals. Uraninite grains are either found liberated or enclosed in zircon. Element maps indicate that betafite occurs as subhedral to euhedral crystals with an average diameter of 81.75 µm and occupies about 59.5% of the total uranium mineral population and 65.5% of the main three uranium minerals (Figure 7.4 and 7.5). Betafite minerals are liberated and easily identifiable due to their larger sizes. Uranium silicates have an average mineral diameter of 514.76µm and form 31% of the total uranium mineral population and 26.55% of the main uranium minerals (betafite, uranium silicates and uraninite). Most of the secondary uranium silicates are found as nodules attached to other uranium minerals, or surrounding other uranium minerals such as betafite, davidite and uraninite, although liberated grains are also present.

Table 7.6: SK heavy minerals together with their proportions and diameters as determined by the SEM technique.

Minerals	Composition	Total diameter	Mineral proportion	No. of grains	Diameter/grain
Ce-Allanite	(Ce,Ca,Y)2(Al,Fe)3(SiO4)3(OH)	50	0.03	1	50.00
U-Titanite	$CaTiSiO_5$	125	0.08	2	62.50
Thorutile	$(Th,U,Ca)Ti_2(O,OH)_6$	160	0.10	1	160.00
Ce-Cebaite	$Ba_3Ce_2(CO_3)_5F_2$	170	0.10	3	56.67
Monazite	$(Ce, La, Nd, Th) PO_4$	300	0.18	2	150.00
Ce-Aeschynite	$(Ce,Ca,Fe)(Ti,Nb)_2(O,OH)_6$	320	0.19	6	53.33
Ce-Niobo-Aeschynite	$(Ce,Ca)(Nb,Ti)_2(O,OH)_6$	406	0.24	6	67.67
Uraninite	UO_2	450	0.27	20	22.50
Ce-Khristovite	$(Ca,REE)(Ce,REE)(Mg,Fe,Cr,Ti,V,Al)Mn,Al(SiO4)(Si_2O_7)(OH)(F,O)$	750	0.45	7	107.14
Thorite	$NbNa_3Ca_3(Ce,La)(Si_2O_7)_2OF_3$	775	0.47	9	86.11
Ce-Nacareniobsite	$NbNa_3Ca_3(Ce,La)(Si_2O_7)_2OF_3$	865	0.52	14	61.79
Ce-Dollaseite	$CaCeMg_2AlSi_3O_{11}(OH,F)_2$	1010	0.61	11	91.82
Uranothorite	$UThSiO_4$	1730	1.04	18	96.11
Fe-silicate	$Fe\text{-}SiO_5$	2175	1.31	37	58.78
Davidite	$La,Ce,Ca)(Y,U)(Ti,Fe)_{20}O_{38}$	2255	1.36	24	93.96
U-Silicate	$U\text{-}SiO_2$	4375	2.63	62	70.56
Niobokuleskite		5035	3.03	72	69.93
Rutile	TiO_2	5875	3.54	73	80.48
Betafite	$(Ca, Na, U)_2(Ti,Ta,Nb_2O_6(O,OH)$	6540	3.94	80	81.75
Titanite	$CaTiSiO_5$	6670	4.01	71	93.94
Fe oxide/hydroxide	FeO/OH	7730	4.65	116	66.64
Ilmenite	$FeTiO_3$	9515	5.73	140	67.96
Silicates	SiO_2	27540	16.58	603	45.67
Pyrochlore	$(Na,Ca)_2Nb_2O_6(OH,F)$	40265	24.23	468	86.04
K-Vuoriyarvite	$(K,Na)_2(Nb,Ti)_2Si_4O_{12}(O,OH)_2\cdot 4(H_2O)$	41059	24.71	458	89.65
Total		166145	100.00	2304	

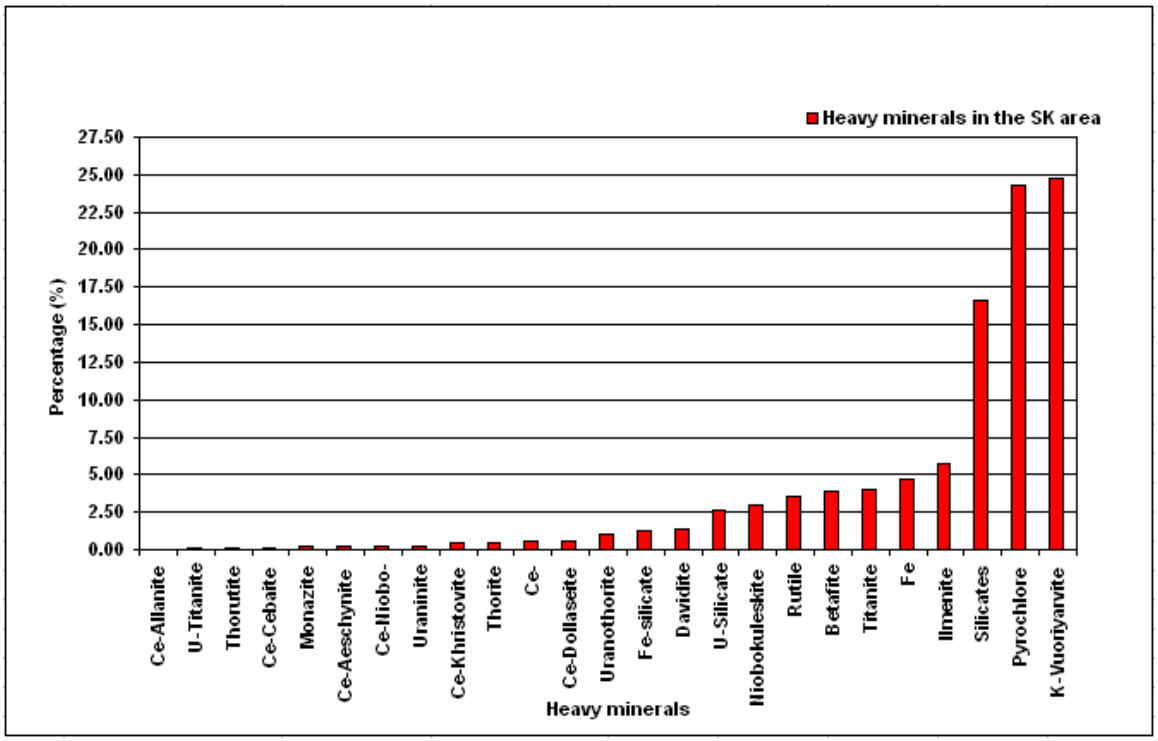

Figure 7.3: S Heavy minerals proportions for the SK area as determined by the SEM technique.

Table 7.7: Mineralogy of the heavy minerals from the SK area, together with their proportions, based on wavelength dispersive microprobe compositional data.

Minerals	Composition	Mineral proportion
Ce-Allanite	(Ce,Ca,Y)2(Al,Fe)3(SiO4)3(OH)	0.03
U-Titanite	$CaTiSiO_5$	0.08
Thorutite	$(Th,U,Ca)Ti_2(O,OH)_6$	0.1
Ce-Cebaite	$Ba_3Ce_2(CO_3)_5F_2$	0.1
Monazite	$(Ce, La, Nd, Th) PO_4$	0.18
Ce-Aeschynite	$(Ce,Ca,Fe)(Ti,Nb)_2(O,OH)_6$	0.19
Ce-Niobo-Aeschynite	$(Ce,Ca)(Nb,Ti)_2(O,OH)_6$	0.24
Uraninite	UO_2	0.27
Ce-Khristovite	(Ca,REE)(Ce,REE)(Mg,Fe,Cr,Ti,V,Al)Mn,Al(SiO4)(Si_2O_7)(OH)(F,O)	0.45
Thorite	$NbNa_3Ca_3(Ce,La)(Si_2O_7)_2OF_3$	0.47
Ce-Nacareniobsite	$NbNa_3Ca_3(Ce,La)(Si_2O_7)_2OF_3$	0.52
Ce-Dollaseite	$CaCeMg_2AlSi_3O_{11}(OH,F)_2$	0.61
Uranothorite	$UThSiO_4$	1.04
Fe-silicate	$Fe\text{-}SiO_5$	1.31
Davidite	$La,Ce,Ca)(Y,U)(Ti,Fe)_{20}O_{38}$	1.36
Fe oxide/hydroxide	FeO/OH	2.33
Zircon	$ZrSiO_4$	3.03
Rutile	TiO_2	3.54
Titanite	$CaTiSiO_5$	4.01
Ilmenite	$FeTiO_3$	5.73
Apatite	$Ca_5(PO_4)_3(OH,F,Cl)$	18.18
U-Silicate	$U\text{-}SiO_2$	19.21
Betafite	$(Ca, Na, U)_2(Ti,Ta,Nb)_2O_6(O,OH)$	37.03
Total		100

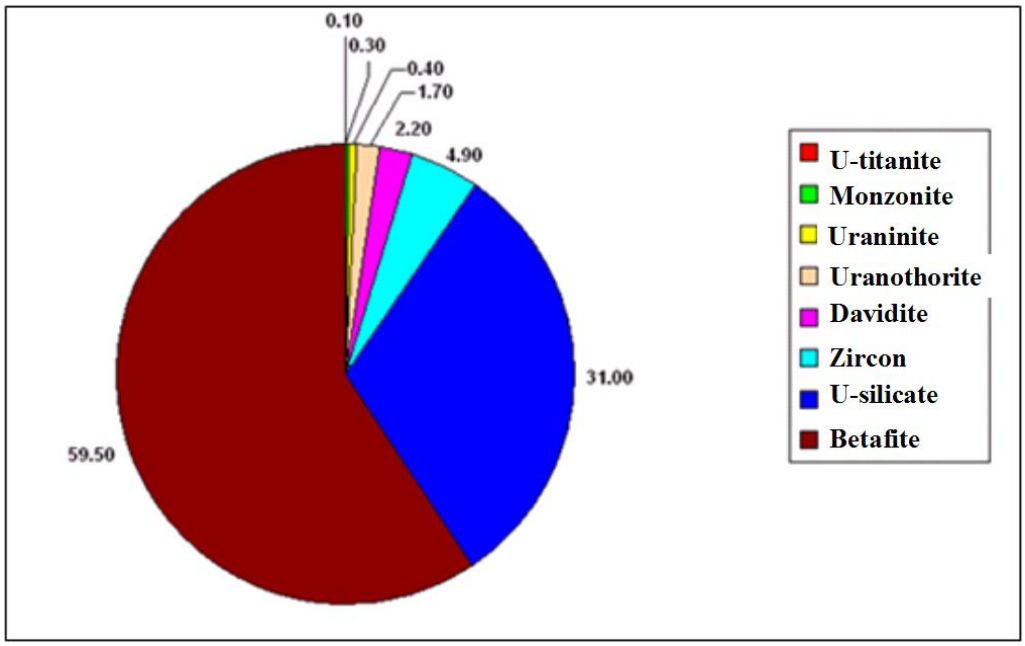

Figure 7.4: Pie chart of the major and minor uranium-bearing minerals from surface samples in the SK, as determined by the SEM technique.

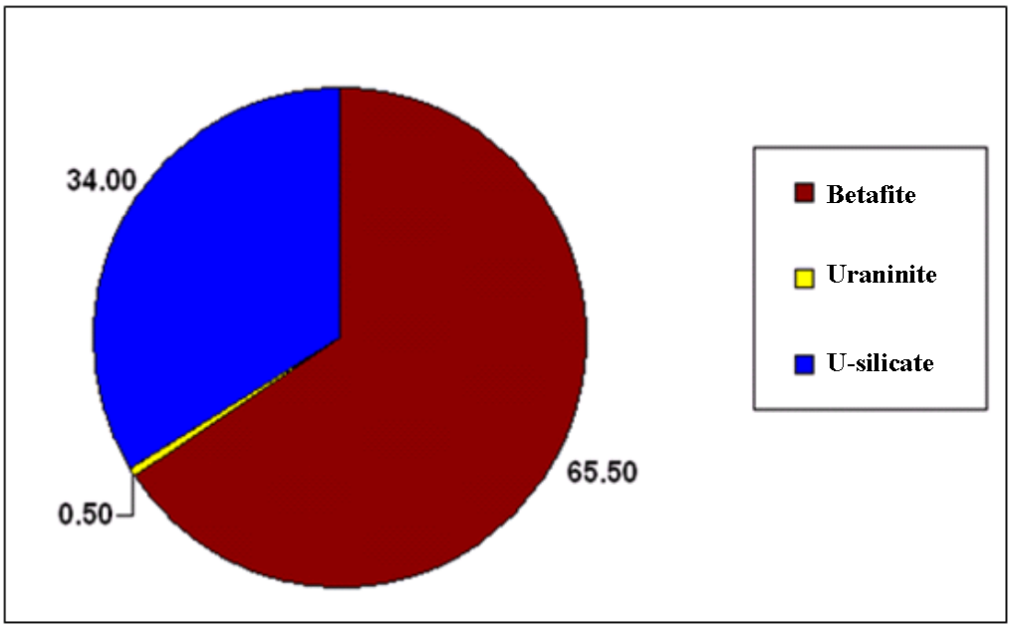

Figure 7.5: Proportion of betafite, uraninite and U-silicates in the SK area, as determined by SEM.

7.3.3. Discussion on the SEM Data

Overlapping peaks during element mapping of the EDX spectrum can result in uncertainty of SEM results, but confidence can be regained by the determination of precise compositional data by using mineral spectra. Apart from confirming the mineral identification obtained from the

SEM, the spectra also indicate other elements that may be present in the phase, as substitutes or inclusions in a mineral.

SEM results have indicated that the SK area has 65.5% betafite, 34% U-silicates and 0.5% uraninite. In order to produce a more reliable quantification of the mineral proportions than those determined by the SEM technique, QEMSCAN analysis of selected heavy mineral concentrates has been undertaken so that the results of the two techniques can be compared.

The samples used for the SEM technique are the SK area surface samples and not the SK area core samples or SK4 core samples as these were not available at the time of study. The SK area surface samples have been sampled from most the SK sub-anomalies (Figure 4.2), to give a representative proportion of the total SK area uranium mineral ratio.

7.4. QEMSCAN

QEMSCAN is a process mineralogical instrument consisting of a scanning electron microscope, equipped with four light element energy dispersive X-ray detectors, a microanalyser and an electronic processing unit (www.met.sgs.com/met_qemscan_services). QEMSCAN can acquire and process vast amounts of chemical, textural and compositional data on liberated grains. The mineral analysis system combines features found in other analytic instruments such as a Scanning Electron Microscope (SEM) and Electron Probe Micro Analyser (EPMA) (www.wikipedia.org/wiki/QEMSCAN). QEMSCAN is the latest, high technology electron-beam analytical scanning electron microscope. As with the SEM technique described in section 7.3, QEMSCAN is able to undertake element mapping. The aim of the investigation was to determine the mode of occurrence and liberation characteristics of the U-bearing mineral grains occurring in each size fraction. The QEMSCAN raw data is presented in Appendix 7 as provided by the SGS Lakesfield Laboratory, Johannesburg.

7.4.1. Methodology

The SK4 anomaly (100 m by 15m) is one of the SK area sub-anomalies. The entire SK area is an anticline, with an exception of the SK4 area, which is a syncline. During this study the overall SK area was treated and sampled separately from the SK4 area, to confirm if the structural setting is likely to be a contributing factor in the formation of betafite.

From the samples listed in Table 5.2 and 5.3 in chapter 5, six samples have been selected for QEMSCAN analysis. Samples SK4/4-22I, SK4/4-20I and SK4/43-18I are from the SK4 historic drilling while N10062, N9947 and N10456 are from the 2007 drilling. Even though N9947 is from the 2007 drilling, it comes from a hole drilled near the SK4 syncline and not from the SK anticline. For each sample, two size fraction were selected (<150>90 µm and <90 µm), which brings the total samples taken for QEMSCAN analysis to twelve. The larger size fraction (<150>90 µm) grains have been dominantly used by previous researchers. The finer <90 µm size fraction was used to investigate whether any uraninite and/or U-silicates are concentrated in the finer size fraction which would indicate that the coarser grain fraction is unrepresentative of the U population as a whole.

7.4.2. Results

Figure 7.6, shows a summary of the uranium deportment from the combined <150>90µm and <90µm size fractions for each of the six samples. QEMSCAN results indicate that the SK4 samples have low betafite content with varying uraninite and U-silicate proportions. In contrast, the samples from the SK anticline (N10062 and N10456) in Figure 7.6 have >60% betafite, 27-29% uraninite and 5-10% of U-silicates. QEMSCAN particle map of samples SK4/4 22I from the SK4 syncline and N10456 from the SK anticline are provided in Appendix 8. The particle maps correspond with the uranium mineral percentages obtained the QEMSCAN.

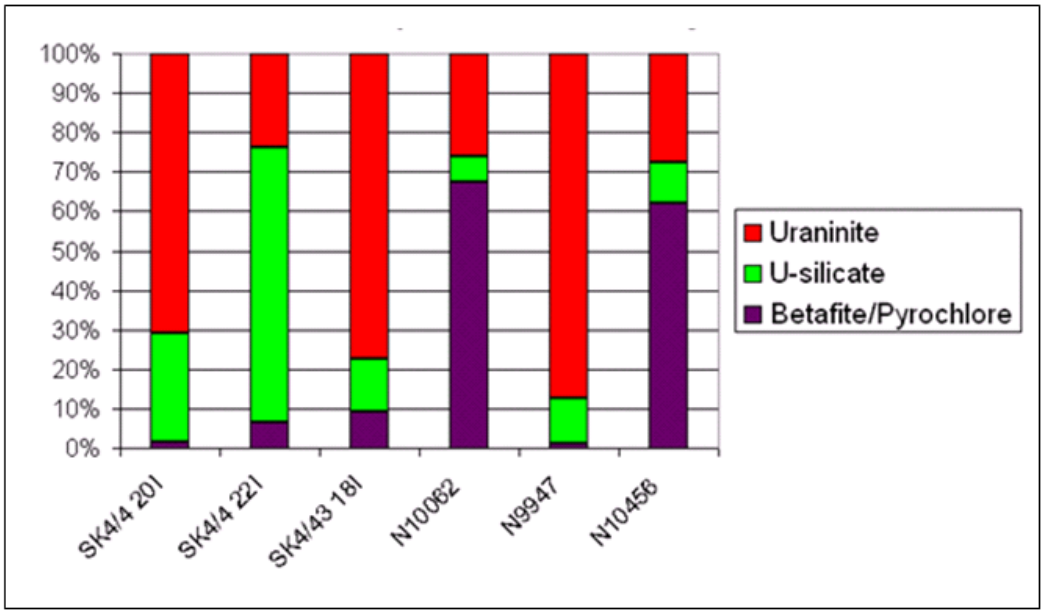

Figure 7.6: U-deportment summary from the SK anticline and SK4 syncline samples.

A comparison of the QEMSCAN analyses from the two different size fractions (-150+90 μm and -90 μm) have been plotted in Figure 7.7. The finer fraction is characterised by a higher proportion of uraninite, U-silicate and betafite/pyrochlore compared with than the larger <150>90 μm size fraction. In the coarser fraction, uraninite has been underestimated by 56%, U-silicates by 30% and betafite by 10% in comparison to the finer fraction.

For the SK anticline core samples, the uranium mineral population comprises 65% betafite, 27% uraninite and 8% secondary uranium minerals (Figure 7.8). The mineralogical proportions of U minerals of the SK4 are 5% betafite, 64% uraninite and 31% secondary uranium minerals (Figure 7.9). Scheelite, molybdenite, galena, Fe-sulphides and calcite/dolomite have been identified by the QEMSCAN as minerals associated with the U phases. The SJ area is a syncline; currently being mined because of its uranium grades and favourable mineralogy of 5% betafite, 45% uraninite, 55% secondary uranium minerals. The SH area is an anticline with favourable uranium grades but adverse mineralogy of 84% betafite and 6% uraninite and secondary mineralisation. In terms of structural comparison, much of the SK area is characterised by an anticline and seem to have high (65%) betafite content. The SK4 area on the other hand, is a syncline and has low (5%) betafite abundance.

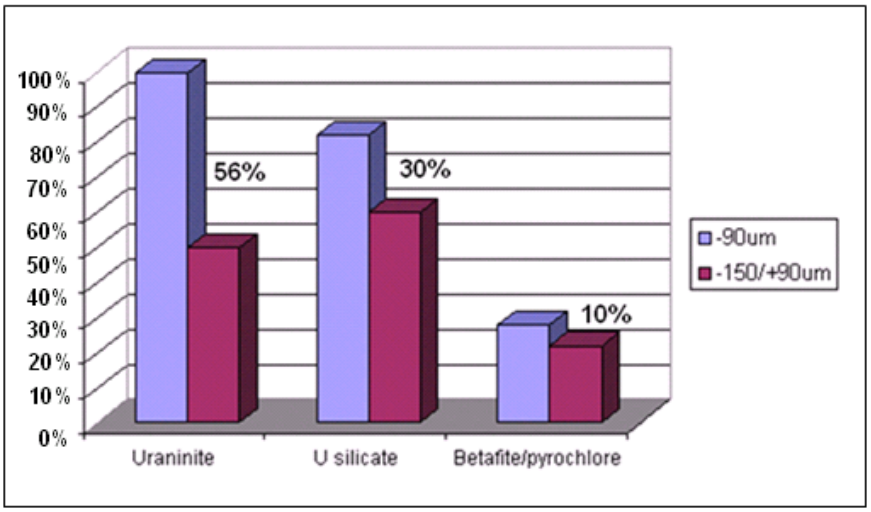

Figure 7.7: Comparison of the abundance of uraninite, U-silicates and betafite at different size fractions. The 56%, 30% and 10% indicates the abundance percentages difference between -90 μm and -150/+90 μm size fractions, with respect to uraninite, U-silicates and betafite. The data used above are a composite of all the twelve samples submitted for QEMSCAN.

7.4.3. Discussion on the QEMSCAN Data

The QEMSCAN results indicate that the SK area is characterised by variable proportions of uranium minerals. For the SK anticline there is a higher proportion of betafite, compared with the SK4 area. The mineralogy in the SK4 area is quoted as 45% uraninite, 55% secondary uranium minerals and 5% betafite/pyrochlore, with recoveries averaging 90% (Rössing Internal Report, 050505, 2005). The previously quoted betafite abundance corresponds with the results derived from the QEMSCAN data, although the proportions of uraninite and secondary uranium minerals differ slightly. The stratigraphy of the SK anticline and the SK4 syncline are similar and there is no difference between the two areas in terms of lithological variation. The significant difference between the two areas therefore is the geometry of the folds and the mineralogical variation is related to the anticlinal and synclinal structures.

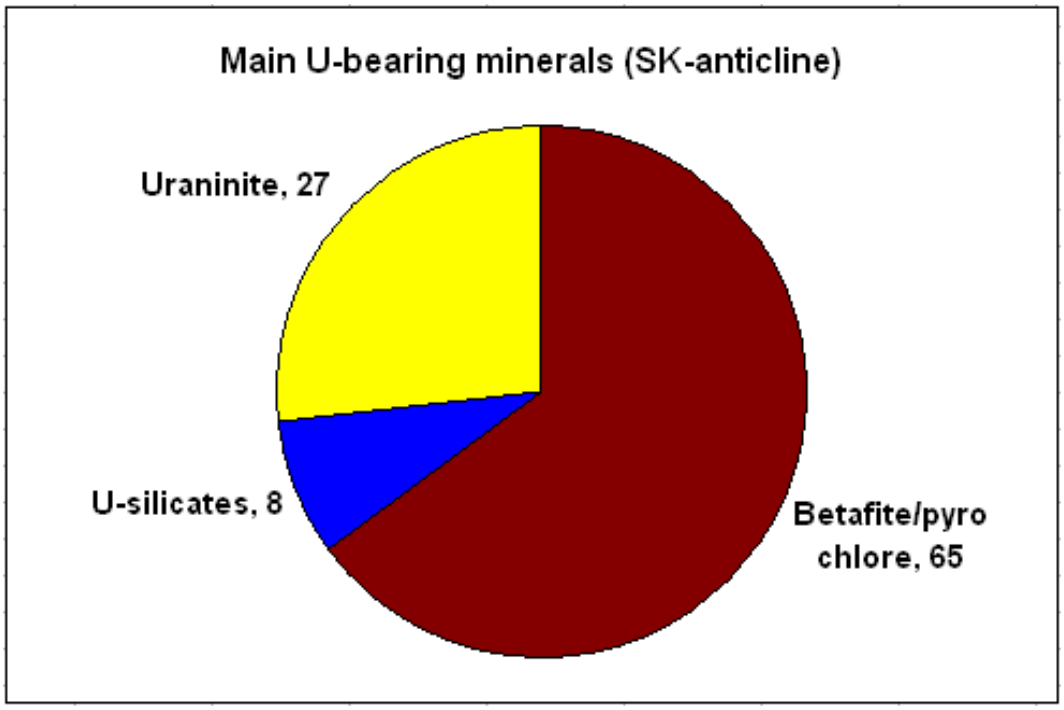

Figure 7.8: The proportion of betafite, uraninite and U-silicates in the SK anticline, determined by QEMSCAN. The results are based on four SK core samples N10062 (-150+90 µm), N10062 (-90 µm), N10456 (-150+90 µm) and N10456 (-90 µm).

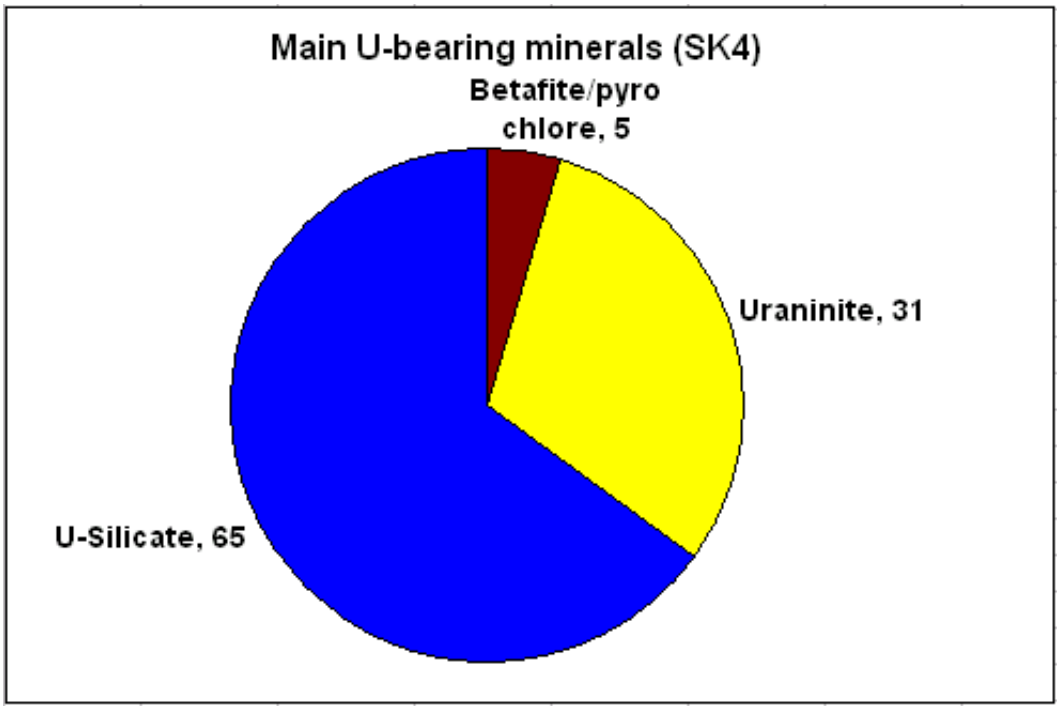

Figure 7.9: The proportions of betafite, uraninite and U-silicates in the SK4 syncline, as indicated by the QEMSCAN, based on eight SK4 core samples (SK4/4 20I (-150+90 μm), SK4/4 20I (-90 μm), SK4/4 22I (-150+90 μm), SK4/4 22I (-90 μm), SK4/43 18I (-150+90 μm), SK4/43 18I (-90 μm) N9947 (-150+90 μm) and N9947 (-90 μm).

The smaller the average sizes of the mineral grains, the higher the underestimation when using the <150>90μm size fractions. To avoid such an underestimation when using QEMSCAN, it would be better to work with the -90μm size fraction. This finding is not only important during mineral analysis studies, but also important to the processing plant. If the plant is not grinding the feed to the correct and profitable size, smaller minerals such as uraninite might end up at the tailings dumps.

7.5. Betafite and Uranium Variation with Depth

It is important to investigate the variation in uraninite and betafite abundance with depth before mining commences in the SK area and before a metallurgical processing plant is designed. If the fold geometry and the marble cap to the leucogranite in the SK area exert a control on betafite formation, then it would be anticipated that betafite should decrease with depth. According to Herd (1996) marble prevents CO_2-rich fluids from escaping due to its ductile nature and the formation of betafite is promoted in an alkaline environment. The marble has tripled in thickness from the SJ area to the SK area although the thickness of the cordierite gneiss, a potential source

of Ti, Ta and Nb, has generally decreased from the SJ area. This study did not test the geochermical formation of betafite, but assumptions were made that the hypothesis provided by Herd (1996) is correct.

It is not clear from the data presented so far whether there is a variation in the uranium mineral proportions with depth. This can be evaluated by a comparison between the SEM and QEMSCAN data. The data used for comparisons in this section are strictly from the SK area surface samples and SK area core samples. SK4 core samples have not been involved as they represent a small portion of the entire SK area.

7.5.1. Results

SEM versus QEMSCAN Comparisons

Results from the SEM technique for surface samples indicate that betafite forms 65.5% of the uranium budget, while core samples taken from depth indicate 65% betafite with a QEMSCAN technique. According to the SEM data, surface sample have a higher proportion of secondary uranium minerals in contrast to core samples, while uraninite is low in surface samples compared with core samples.

7.5.2. Discussion on the Comparison of U-mineral Proportions with Depth

Although it was anticipated that the abundance of betafite might decrease with depth, due to the increase in distance from the marble cap, this has not been proven during this study. The surface samples indicate a similar amount of betafite to the core samples. It maybe that the depth of <400 m is too shallow to see the effect of depth on betafite or perhaps the marble does not control betafite occurrence.

7.6. Discussion

It is important to investigate the variation in the uranium minerals (betafite, uraninite and secondary uranium minerals) abundance with regard to spatial distribution and with regard to depth before mining commence in the SK area and before a metallurgical processing plant is designed.

A betafite theoretical calculation method based on a whole-rock geochemical analysis provides a quick and inexpensive indication that betafite in the SK anticlinal area is much higher than the SJ area. SEM results have supported the theoretical method as the SK area has been found to have 65.5% betafite, 34% U-silicates and 0.5% uraninite. A more reliable quantification of the mineral proportions, the QEMSCAN technique indicates 65% betafite, 27% uraninite and 8% U-silicates for the SK anticlinal area, and 5% betafite, 64% uraninite and 31% U-silicate for the SK4 syncline.

It is clear when comparing the SJ, SK and SH areas, that anticinal areas (SH and SK) have a higher betafite content, while the synclinal areas (SJ and SK4) have a low betafite content. Thus the fold geometry does seem to exert a significant role in the formation of betafite in the area. The anticlinal structures to some extent traps the fluids allowing it time to scavenge all the elements needed for betafite formation. Herd (1996), concluded that the anticlinal marble that forms the cap rock prevents CO_2 rich fluids from escaping due to its ductile nature and the formation of betafite is promoted in an alkaline environment.

If the fold geometry and the marble cap to the leucogranite in the SK area exerts a control on betafite formation, then it would be anticipated that, betafite should decrease with depth. The marble has tripled in thickness from the SJ area to the SK area although the thickness of the cordierite gneiss, a potential source of Ti, Ta and Nb, has generally decreased from the SJ area. Results from the SEM technique for surface samples indicate that betafite forms 65.5% of the uranium budget, while core samples taken from depth indicate 65% betafite with a QEMSCAN technique. So there appears to be no variation with depth. It maybe that the depth of <400 m is too shallow to see the effect of depth on betafite crystallisation.

CHAPTER 8

DISCUSSION AND CONCLUSIONS

The SK area is being evaluated as a potential open pit mine as part of the expansion of the Rössing operations. The principal aim of this project was to investigate the local geology and the spatial distribution of primary and secondary uranium-bearing minerals in the SK area, taking into account the country rock lithologies and structural controls on leucogranite sheet emplacement.

The SK area is characterised by a major anticline with a core of Khan Formation and flanks of Rössing lithologies. Evidence for the anticline are the bedding/cleavage relationship and the outward younging lithologies from core to limb. A minor syncline occurs in the SK4 area with banded gneiss and amphibole-biotite schist of the Khan Formation on the flanks and then successively younger Rössing Formation with cordierite schist at the fold hinge. A 3D model of these structures has been created which shows that the SK area is an anticline structurally similar to the SH area and the SK4 area is a syncline structurally similar to the SJ area.

The SK area comprises a series of uranium anomalies that had been delineated previously using scintillometer data. These anomalies are related to the leucogranites, particularly those that are hosted by the banded gneiss. Contouring of the historical data has highlighted the best exploration target, which occurs in the northwestern part of the SK area. However, it is important not just to identify the areas with good uranium grade but also to know the amount of uranium hosted in betafite, which would be lost using the Rössing Uranium Mine current processing techniques.

The leucogranite sheets in the SK area are roughly sub-parallel to each other and have a dextral en-echelon shape across the anticline and more linear outcrop on the flanks of the anticline. The leucogranites vary in grain size, colour, mineralogy, texture and uranium content and in composition. Nex *et al*. (1997), observed six different leucogranite sheets in the Goanikontes area. Of the six leucogranites, only four are observed in the SK area (B, C, D and E).

Modal mineralogy indicates that the leucogranites range in compositions from tonalite to alkali feldspar granite and samples that have high scintillometer counts tend to plot within, or close to the alkali feldspar granite field. However, in geochemical classification schemes, the peraluminous leucogranites from the SK area range in composition from alkali feldspar granite,

syenogranite and monzogranite to granodiorite. The granite category differs from that assigned in the modal classification scheme.

The trace element classification schemes for tectonic setting of granitoid emplacement employed by Pearce *et al*. (1984) show a complete range of tectonic settings for the data of the Rössing area, although most of the SK samples fall in the syn-collision field. Since Type D and E sheets are generally regarded as post D3, it would seem unreasonable to regard them as syn-collisional and thus casting considerable doubt as to the validity of such schemes for valid interpretation of the tectonic setting.

Betafite occurs mainly in Type D leucogranite, although trace amounts have been also observed in Type E leucogranites. Scintillometer counts are low in Type B, moderate in C and high in Type D and E. Leucogranites in the SK area indicate a compositional range from tonalite to alkali feldspar granite.

Previous work suggested that there are several controls that promote the formation of betafite rather than uraninite (Herd, 1996). This includes a structural and lithological control such that where marble forms the cap of a leucogranite intruded into an anticline, CO_2 is retained and the potential for betafite crystallisation is enhanced in the intruding leucogranite. In the SH area where leucogranite sheets have coalesced in a marble-capped anticline, betafite forms 84% of the uranium mineral population. For the SK anticline, where the marble unit tripled in thickness from the SJ pit there is 65% betafite, 8% uraninite and 27% secondary uranium bearing minerals. The SK4 area which is a minor syncline within the major SK area anticline has 5% betafite, 64% uraninite and 31% secondary uranium bearing minerals. Historically, the mineralogy of the SK4 area is quoted as 55% secondary uranium minerals, 45% uraninite and 5% betafite/pyrochlore, with recoveries averaging 90% (Rössing Internal Report, 050505, 2005). The betafite content corresponds with the value obtained during this study. This study concludes that there is a structural control on betafite formation in the SK anticline and SK4 areas.

If a marble cap to an anticline provides favourable sites for betafite crystallisation in leucogranite in an alkaline environment, betafite abundance with depth was expected to decrease with depth, within the SK anticline. This was not proven, as there is similar betafite abundance in both the surface samples and core samples. It may be that there depth variation has no effect on betafite

formation or that the depth variation of <400 m is insufficient to have a noticeable affect on betafite content. The favourable grades in the SK area seem to extend to 400 m depth.

The northwestern part of the SK area seems to have favourable uranium enrichment. This portion includes part of the SK anticline and the entire SK4 area. Here, the uranium mineralogy is more favourable than in the SK anticline with only 5% of the uranium budget hosted in betafite in contrast to 65% betafite in the SK anticline. If any expansion is to take place in the SK area, it should start with in the SK4 area, and only proceed to the SK anticline once the processing plant has been adjusted to extract uranium from betafite.

If the current acid plant is used to process material from the SK anticline area, recoveries will be low as most of the uranium is hosted in betafite form. In fact only U-silicates and uraninite will be leached successfully. Considering the fact that the SH area also has a high betafite content, Rössing Uranium Mine may have to find ways to leach the uranium from betafite, to make SH and SK areas feasible for mining.

SK area samples on the Th versus U plot, indicates a dominant Th: U ratio between 0.4 to 1, with localised samples plotting between the ratio of 1 and 8. Comparing to the SH and SJ pit, SK samples seem to be higher in thorium as they plot more closely to the ratio of 1 and between 1 and 8. Th is more toxic than U, because thorium emits high energy particles that are more penetrating than those emitted by U (Uranium conference, 2007). For this reason, it is important for the U concentration to be higher than the Th concentration in a potential ore deposit, such as the SK area. The World Nuclear Association estimates an average Th: U ratio of 4, based on lead isotope studies. The apparent increased Th: U ratio in SK samples should be investigated further, with about 100 samples.

Conclusions

This study has added to previous knowledge and interpretations for the SK area. Specific results of importance are:

- That leucogranites of the SK area are of four types (B, C, D and E) that correspond with those described for the Goanikontes area by Nex (Nex *et al.*, 2001) although there is an absence of types A and F.

- That betafite is the dominant U-bearing phase in the SK area except for the SK4 syncline which is dominated by uraninite and secondary U-minerals.
- That betafite abundance does not decline with depth.
- That there will be significant uranium loss during processing SK material because of the abundance of betafite.
- That using a finer grain size fraction of the granites over-estimates the abundance of uranium minerals compared to a coarser fraction.
- That fold geometry may play a major role in betafite formation, in the SK area after comparing the fold geometry and betafite content of areas such as: SJ, SH, SK anticline area and SK4.
- That the SK area should be regarded as one large anomaly rather than evaluated as an entity with lots of sub-anomalies. Determination of uranium mineral proportions and evaluation of Th: U ratios for the SK area.

References

Anderson, H. and Nash, C. (1997). Integrated lithostructural mapping of the Rössing area, Namibia, utilising remotely sensed data. *World Geoscience Corporation Limited,* pp. 1-5.

Basson, I. J. and Greenway, G. (2003). Rössing Uranium Mine: Genesis during late tectonism of the central zone of the Damara Orogen, Namibia, pp. 1-15.

Basson, I.J. and Greenway, G. (2004). The Rössing Uranium Deposit: A product of late-kinematic location of uraniferous granites in the Central Zone of the Damara Orogen, Namibia. *Journal of African Earth Sciences,* **38**, pp. 413–435.

Berning, J., Cooke, R., Hiemstra, S A. and Hoffman, U. (1976). The Rössing Uranium Deposit, South West Africa. *Economic Geology,* **71**, pp. 351 - 368.

Berning, J. (1986). The Rössing uranium deposit, South West Africa / Namibia, In: Anhaeusser, S. Johannesburg, ed., *Mineral Deposits of Southern Africa*. Geological Society of South Africa, **2**, pp. 1819-1832.

Briqueu, L., Lancelot, J.R., Valois, J.P. and Walgenwitz, F. (1980). Geochronologie U–Pb et genese d'un type de mineralisation uranifere: les alaskite de Goanikontes (Namibia) et leur encaissant. *Bulletin Centrale De Recherche Exploration Production, Elf Aquitaine,* **4**, pp. 759–811.

Buhn, B. and Stannistreet, I.G. (1992). A correlation of structural patterns and lithostratigraphy at Otjosondo with the Damara Sequence of the southern Central Zone, Namibia. *Communications of the Geological Survey of Namibia,* **7,** pp. 15–19.

Corner, B. (1983). An interpretation of the aeromagnetic data covering the western portion of the Damara Orogen in South West Africa/ Namibia. In: Miller, R.McG. (ed.), Evolution of the Damara Orogen of South West Africa. Namibia*: Geological Society of South Africa, Special Publication,* **11**, pp. 339–354.

Coward, M.P. (1980). Pan-African gneiss domes, diapirs and sheath folds. In: Coward. M.P. (ed.), Diapirism and gravity tectonics: report of a Tectonics Studies Group conference held at Leeds University, March 1980. *Special Publication of the Journal of Structural Geology,* **3,** pp. 89–95.

Coward, M.P. (1983). The tectonic history of the Damara Belt, pp. 409-421. In: Miller, R. McG. (ed.), Evolution of the Damara Orogen of South West Africa/Namibia: *Geological Society of South Africa, Special Publication,* **11,** pp. 515.

Duarte, V. H. (2006). Mineralogical characterisation of a Rössing Uranium ore milled to 60 % passing 75 µm. Mintek, Unpublished report, pp. 3-8.

Freemantle, G. (2006). Investigation of the Accessory Minerals Assemblages of Sheeted Leucogranites from the Rössing Uranium Mine, Namibia. School of Geosciences, University of the Witwatersrand Johannesburg. Honours Thesis (Unpublished report).

Haack, U., Hoefs, J. and Gohn, E. (1982). Constraints on the origin of Damaran granites by Rb/Sr and delta 18 O data. *Contributions to Mineralogy and Petrology,* **79**, pp. 279-289.

Hartmann, O., Hoffer, E and Haack, U (1983). Regional metamorphism in the Damara Orogen: interaction of crustal motion and heat transfer. *Geological Society South Africa, Special Publication,* **11**, pp. 233-241.

Herd, D.A. (1996). Geochemistry and mineralisation of alaskite in selected areas of the Rössing Uranium Mine, Namibia. M.Sc. dissertation (unpublished), University of St. Andrews, Scotland, pp. 10-100.

Herd, D.A. and Kinnaird, J.A. (1999). Betafite and pyrochlore – mineralogy and chemistry of samples in the Rössing area, Namibia (unpublished), pp. 1-13.

Hiemestra, S.A. and Beukes G.J. (1969). A Petrological Study of Forty Rock Specimens from Rössing, South West Africa. *Confidential Research Report for Rössing Uranium Ltd,* pp. 85.

Hogarth, D.D. (1989). Pyrochlore, apatite and amphibole: distinctive minerals in carbonatite. *In:* Bell, K. (ed.), *Carbonatites, Genesis and Evolution.* Unwin Hyman, London, pp. 105-148.

Jacob, R.E., Snowden, P.A. and Bunting, F.J.L. (1983). Geology and structural development of the Tumas basement dome and its cover rocks, 157-172. In: Miller, R. McG, (ed.), Evolution of the Damara Orogen of South West Africa/Namibia: *Geological Society of South Africa, Special Publication,* **11,** pp. 515.

Jacob, R.E, Corner, B. and Brynard, H.J. (1986). The regional geological and structural setting of the uraniferous granitic provinces of southern Africa. In: Anhaeussser, C.R. and Maske, S. (ed.), Mineral deposits of southern Africa: *Geological Society of South Africa,* **2,** pp. 2335.

Jacob, R.E. and Kerber, P. (1997). Geology of the area around the main tailings dam, Rössing Uranium Mine (unpublished), Rhodes University, pp. 28.

Johannsen, A. (1931). A Descriptive Petrography of the Igneous Rocks. *University of Chicago Press, Chicago*, **1,** pp. 88-92.

Jung, S., Mezger, K., Masberg, P., Hoffer, E and Hoernes, S. (1998). Petrology of an intrusion-related high-grade migmatite – implications for partial melting of metasedimentary rocks and leucosome-forming processes, **16**, pp. 425-445.

Jung, S. (2005). Isotope equilibrium/disequilibrium in granites, metasedimentary rocks and migmatites (Damara Orogen, Namibia) a consequence of polymetamorphism and melting. *Science Direct*, **84**, pp. 168-184.

Kisters, A.F.M., Jordaan, L.S., and Neumaier, K. (2004). Thrust-related dome structures in the Karibib district and the origin of orthogonal fabric domains in the south Central Zone of the Pan-African Damara belt, Namibia. *Precambrian Research,* **133,** pp.283-303.

Kroner, A. (1984). Dome structures and basement reactivation in the Pan-African Damaran belt of Namibia. In: Kroner, A., Greiling, R. (ed.), *Precambrian Tectonics Illustrated. Schweizerbarth, Stuttgart,* pp. 191–206.

Longridge, L., Gibson, R. L., Kinnaird J. A. and Armstrong R. A. (2008). Timing of deformation and granite emplacement in the Central Zone of the Damara Orogen, Namibia. School of Geosciences, University of the Witwatersrand Johannesburg (Unpublished report).

Louw, G.P. (1977). Rössing Uranium, Geology Strong Room Documentations (Maps).

Louw, G.P. (1979). Rössing Uranium, Geology Strong Room Documentations (Maps).

Marlow, A.G. (1983). Geology and Rb-Sr geochronology of mineralised and radioactive granites and alaskites, Namibia. *In:* Miller, R. McG., ed., *Evolution of the Damara Orogen of South West Africa/Namibia*. Geological Society of South Africa, Special Publication **11**, pp. 289-515.

Martin, H. (1983). Overview of the geosynclinal, structural and metamorphic development of the intracontinental branch of the Damara Orogen. In: Martin, H. and Eder, F.W. (ed.), Intracontinental Fold Belts. Springer, Berlin, pp. 473–502.

Martin, H. and Porada, H. (1977). The intracratonic branch of the Damaran Orogen in Namibia. Discussion of geodynamic models. *Precambrian Research,* **5**, pp. 311–338.

Masberg, H.P., Hoffer, E and Hoernes, S (1992). Microfabrics indicating granulite-facies metamorphism in the low-pressure central Damara Orogen, Namibia. *Precambrian Research,* **55**, pp. 243-257.

Miller, R. McG. (1983a). The Okahandja Lineament, a fundamental tectonic boundary in the Damara Orogen of South West Africa/Namibia. *Transactions of the Geological Society of South Africa,* **82**, pp. 349–361.

Miller, R. McG. (1983b). The Pan-African Damara Orogen of South West Africa/Namibia. *In:* Miller, R. McG. (ed.), *Evolution of the Damara Orogen of South West Africa/Namibia.* Geological Society of South Africa, Special Publications, **11**, pp. 431–515.

Murphy, R.L. (1996). Radiometric anomalies surrounding the open pit within the mining grant.

Nash, C.R. (1971). Metamorphic petrology of the SJ area, Swakopmund District, South West Africa. *Bulletin of the Precambrian Research Unit, University of Cape Town,* **9**, pp. 77.

Nex, P.A.M. (1997). Tectono-metamorphic setting and evolution of granitic sheets in the Goanikontes area, Namibia. Ph.D. Thesis (Unpublished), National University of Ireland.

Nex, P.A.M., Oliver, G.J.H. and Kinnaird, J.A. (2001b). Spinel-bearing assemblages and P–T–t evolution of the Central Zone of the Damara Orogen, Namibia. *Journal of African Earth Sciences,* **32**, pp. 471–489.

Nex, P.A.M., Kinnaird, J.A. and Oliver, G.J.H. (2001a). Petrology, geochemistry and mineralisation of post-collisional magmatism around Goanikontes, southern Central Zone, Damara Orogen, *Namibia. Journal of African Earth Sciences*, **33**, pp. 481–502.

Nex, P.A.M., Kinnaird J.A., Herd D. A. (2003). The occurrence, mineralogy and chemistry of betafite and pyrochlore from sheeted leucogranites of the Rössing area, Namibia: implications for the composition of Ceramics for radioactive waste disposal. *Economic Geology Research Institute, School of Geosciences University of the Witwatersrand***, 374**, pp.1-24.

Nex, P.A.M and Kinnaird, J.A. (2005). An investigation of the proportions of betafite, urnainite and secondary uranium minerals in SJ pit samples (Unpublished), pp.1-35.

Oliver, G.J.H. (1994). Mid-crustal detachment and domes in the central zone of the Damaran Orogen, Namibia. *Journal of African Earth Sciences***, 19,** pp. 331-344.

Oliver, G.J.H. (1995). The Central Zone of the Damara Orogen, Namibia as a deep metamorphic core complex. *Communications of the Geological Survey of Namibia*, **10**, pp. 33–41.

Pearce, J.A., Harris, N.B. and Malpas, J. (1984). Trace element discrimination diagrams for tectonic interpretation of granitic rocks. *Journal of Petrology*, **25**, pp. 956-983.

Ramsberg, H. (1972). Theoretical models of density stratification and diapirism in the Earth. *Journal of Geophysical Research*, **77,** pp. 877–889.

Reynolds, I. (2006). A mineralogical characteristic of betafite bearing samples from the mine area. Rio Tinto Technichal Services (Unpublished), pp. 6-25.

Rollinson, H. (1993). *Using geochemical data:evaluation, presentation, intrpretation*. p. 61-63.

Rössing Internal report, 050505, (2005). Summary of the SK Anomalies, pp. 1-7.

Saunders A.D. and Tarney J. (1984). Geochermichal characteristics of basaltic volcanism within back – arc basins. In: Kokelaar B.P. and Howells M.F., (ed.), *Marginal basin geology*, Spec. Publ. Geol. Soc. London, **16** , pp. 59-76.

Sawyer, E.W. (1978). Damaran structural and metamorphic geology of an area southeast of Walvis Bay, S.W. Africa/Namibia. M.Sc. Thesis (Unpublished), University of Cape Town, pp. 12-45.

Scott, B. and Northam, G. (2005). Rössing near mine project (unpublished), pp. 4-30.

Smith, D.A.M. (1961). *The Geology of the Area Around the Khan and Swakop Rivers in South West Africa.* PhD thesis, University of the Witwatersrand, pp. 11-15.

Smith, D.A.M. (1965). The geology of the area around the Khan and Swakop rivers in South West Africa. Memoirs of the Geological Survey of South Africa (South West Africa Series), **33**, pp. 200-301.

Streckeisen, A. and Le Maitre, R.W. (1979). A chemical approximation to the modal QAPF classification of the igneous rocks. *Neues Jahrbuch fur Mineralogie Abhandlung,* **136**, pp. 169–206.

Tack, L. and Bowden, P. (1999). Post-collisional granite magmatism in the central Damaran (Pan-African). *African Earth Sciences,* **28**, pp. 653-674.

Uranium cornference, 2007.

Von Backström, J.W. and Jacob, R.E. (1978). Uranium in South Africa and South West Africa. *Philosophical Transactions of the Royal Society of America*, **291**, pp. 307–319.

www.met.sgs.com/met_qemscan_services

www.wikipedia.org/wiki/QEMSCAN

APPENDIX 1
Geological map of the SK area ***(see attached A3 maps)***

APPENDIX 2
Interpreted pre-intrusion geological map of the SK area ***(see attached A3 maps)***

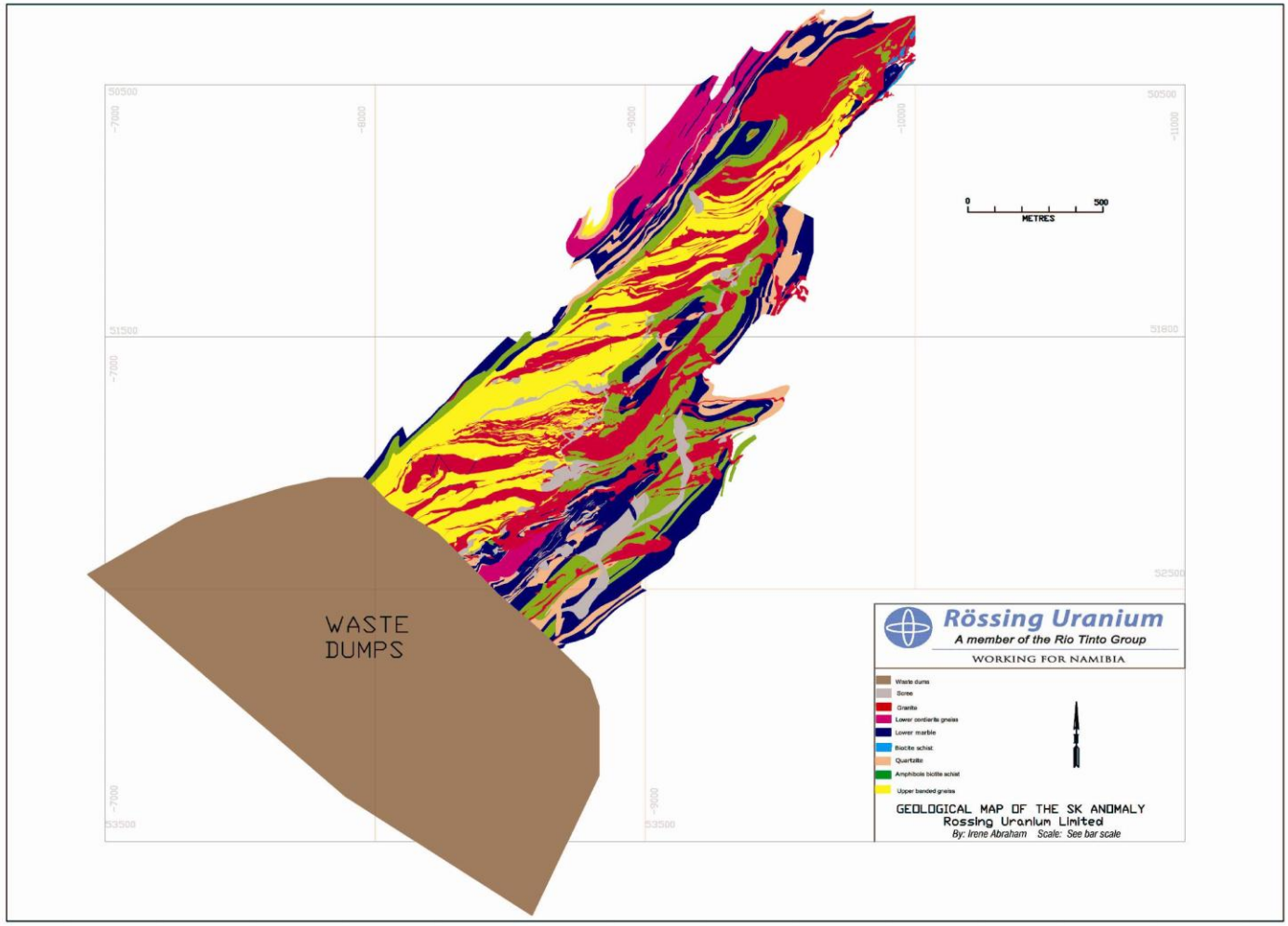
WASTE
DUMPS
0
500
METRES
Rössing Uranium
A member of the Rio Tinto Group
WORKING FOR NAMIBIA
Waste dums
Scree
Granite
Lower cordierite gneiss
Lower marble
Biotite schist
Quartzite
Amphibole biotite schist
Upper banded gneiss
GEOLOGICAL MAP OF THE SK ANOMALY
Rossing Uranium Limited
By: Irene Abraham Scale: See bar scale

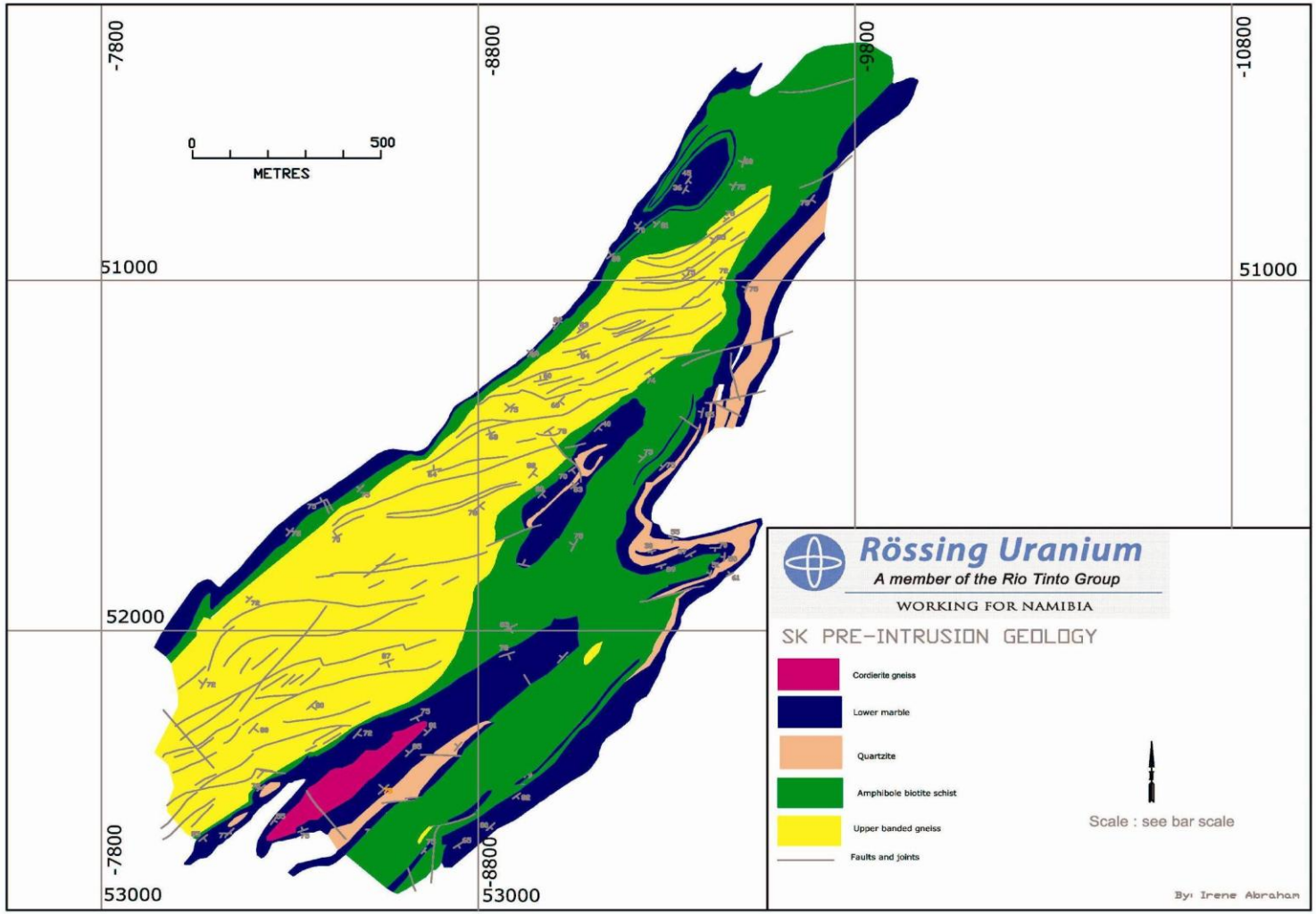
-7800
-8800
-9800
-10800
0
500
METRES
51000
51000
52000
-7800
-8800
53000
53000
Rössing Uranium
A member of the Rio Tinto Group
WORKING FOR NAMIBIA
SK PRE-INTRUSION GEOLOGY
Cordierite gneiss
Lower marble
Quartzite
Amphibole biotite schist
Upper banded gneiss
Faults and joints
Scale : see bar scale
By: Irene Abrahan

APPENDX 3
Section A
RADIATION DISTRIBUTION SURVEYS

Introduction

Whilst scintillometer surveys can be useful in generating exploration targets, the instrument does not distinguish between the radiations emitted by potassium, uranium and thorium. The scintillation counts can be affected by environmental effects such as the amount of attenuating material between the radioactive source and the scintillation detector, the distance from the radiation source, changing temperatures and pressures, soil moisture, precipitation, dust particles in the air and topographic effects.

A random scintillation counter survey has been carried out; the calibration of the scintillation counter that is currently used at Rössing differs from the calibration of the instrument that was used in the past. This is noted from the difference in counts per second measured at exactly the same positions as were measured in the past. The instrumentation department at Rössing mine calibrated the current scintillation counter.

The difference between the historic and current counts per second at a specific point may be due to:

1) Difference in the calibration factors of the two instruments.
2) There may have been changes in the weather. Low air temperature and pressure can cause poor counts per second, as radon gas is normally low during these weather conditions.
3) Height at which the instrument was held. The scintillation counter data can be affected by the height of the person holding the instrument. To make sure that the height did not affect the current data, one field assistant was always used for this job.

The aim of a random scintillation survey was to verify the historic scintillation data and to test if the data that is currently being obtained with the scintillation counter does correlate to what was found in the past. The data was found to correlate in the sense that where high readings were observed, the current survey also picked up high readings. However, the values were different. To solve the difference in data problem a linear and percentile relationship was calculated.

The linear relationship was calculated because it plots the historic data versus current data and gives the linear relationship between the two data. To obtain the percentile relationship, the raw historic and current data were plotted in excel and the data was converted to historic and

current percentile data, which were then plotted against each other to give a linear plot. The percentile plot was used because it smoothes the data and arranges them according to their percentiles, for example the second percentile plot of the historic data will be plotted against the second percentile plot of the current data. This method also classifies the data according to their conveying factors as shown in Table A3.1. The relationship between historic and current scintillation data will be used to convert old historic data to current data and visa versa.

Table A3.1: Historic and current scintillation counter data collected in the SK area.

Area	Historic Data	Current Data	Percentile	Historic Data	Current Data	Factor
SK	320	733	0.00	200.000	441.000	2.205
SK	240	486	0.050	210.000	450.000	2.143
SK	300	666	0.100	210.000	450.000	2.143
SK	340	550	0.150	240.000	484.000	2.017
SK	210	450	0.200	300.000	486.000	1.620
SK	460	850	0.250	300.000	532.000	1.773
SK	460	860	0.300	320.000	550.000	1.719
SK	600	1400	0.350	320.000	550.000	1.719
SK	200	484	0.400	340.000	600.000	1.765
SK	720	1953	0.450	340.000	666.000	1.959
SK	460	683	0.500	400.000	683.000	1.708
SK	340	550	0.550	420.000	733.000	1.745
SK	210	450	0.600	460.000	850.000	1.848
SK	300	532	0.650	460.000	860.000	1.870
SK	620	1651	0.700	460.000	1100.000	2.391
SK	320	441	0.750	500.000	1106.000	2.212
SK	600	1599	0.800	500.000	1316.000	2.632
SK	420	1316	0.850	600.000	1400.000	2.333
SK	500	1106	0.900	600.000	1599.000	2.665
SK	500	1100	0.950	620.000	1651.000	2.663
SK	400	600	1.000	720.000	1953.000	2.713

Results

Normal XY graph of the scintillation data

The normal XY scintillation data graph (Figure A3.1) plots the x (historic radiation count per second) against the y (current radiation count per second). This graph plots the data as they appear in the input columns and does not smoothen anything.

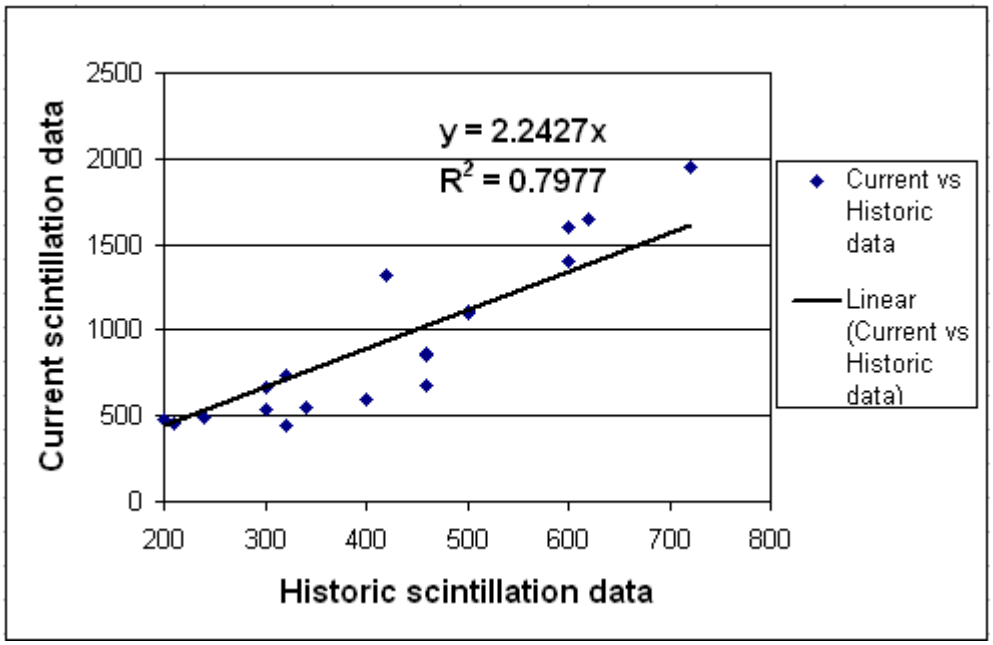

Figure A3.1: Linear relationship between the current and historic scintillation data.

Table 1 and Figure 1; point out that most of the current scintillation values fall in the range of 500 and 2000 cps. Figure 1 also shows the linear trend between the two data sets (current data and historic data). The relationship between the current data and historic data is y= 2.2427x, where y is the current radiation count per second and x is the historic radiation count per second and a level of confidence of 79 %.

Percentile plot of the scintillation data

The plot between historic and current data is similar to the plot described in Figure 2. The only difference is the blue line, which represents percentile historic versus percentile current data. The best fit line is deduced from the red dots which represents the historic versus current scintillation data.

The percentile plots (Figure A3.2) are used in research to filter data and arrange them according to their percentiles e.g. the first percentile data in the historic data will be arranged against the first percentile data in the current data. A 200 cps (x) in the normal xy graph is plotted against 484 cps (y). In the percentile plot, the 200 cps (x) is plotted against the 441 cps (y). The application of percentile plots not only smoothen the data, but it also provides conversion factors that are applied to each percentile historic data to obtain the corresponding percentile current data. The factors are shown alongside each percentile group in Table A3.1.

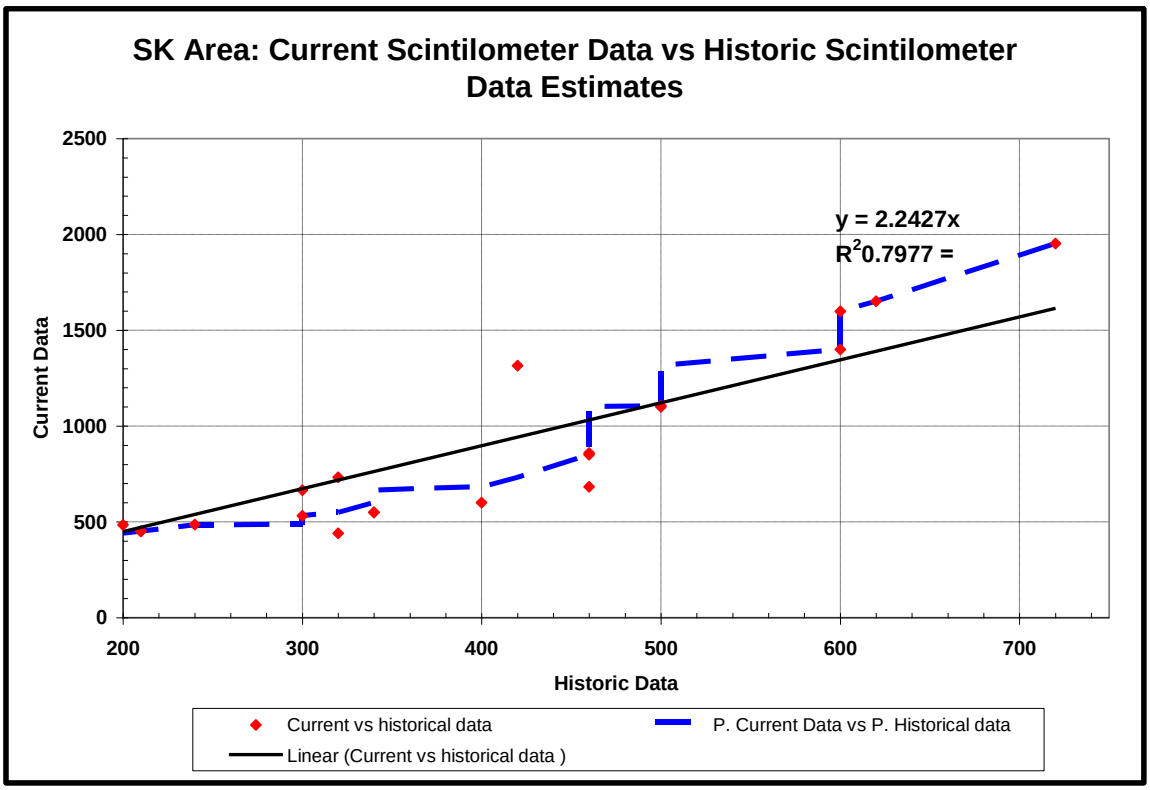

Figure A3.2: A plot of the current data versus historic data in red, while that of percentile historic data and percentile current data is shown in blue.

The variation of factors with the change in historic radiation counts per second is shown in Figure A3.3. The graph indicates that the scintillation counts from 200 cps to 460 cps be allocated with overall factor below 2.00, while those from 460 and above be allocated with a different factor of above 2.00. Allocation of factors depends on an individual's choice for a project: for this project one overall factor (2.2427) was assigned across the entire area.

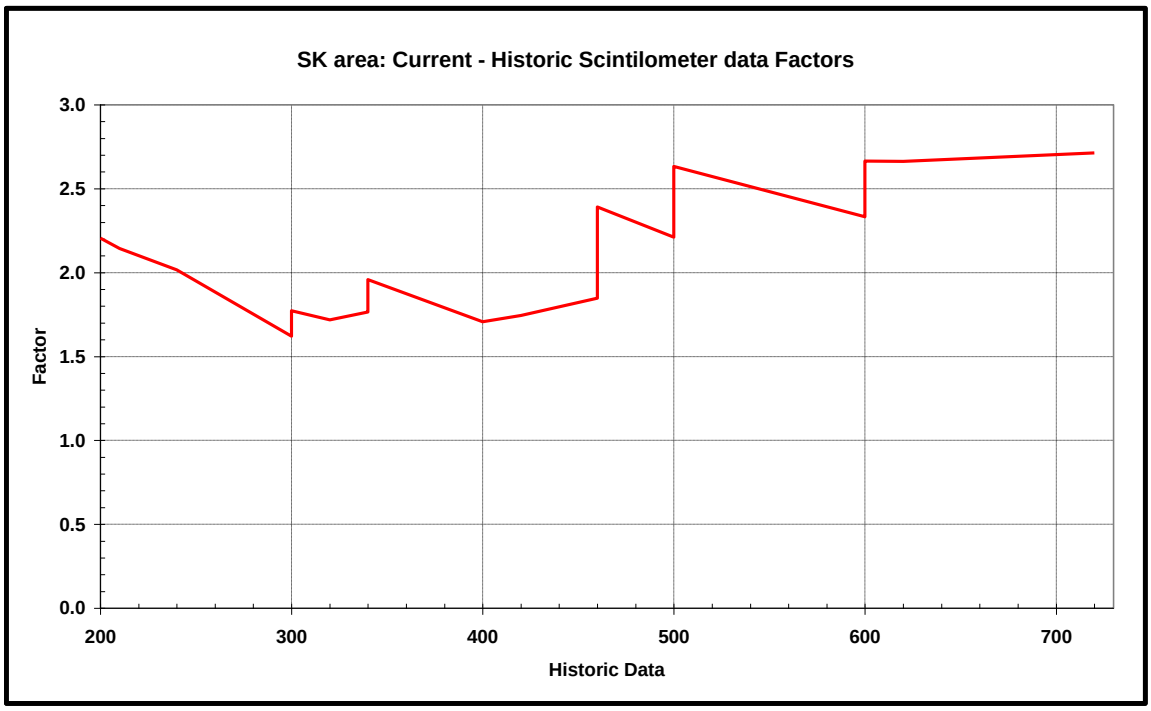

Figure A3.3: Factors applied to each percentile historic data to obtain the percentile current data.

APPENDIX 3

Section B

Radiation count per second (CPS), LO coordinates

Easting	Northing	CPS	Easting	Northing	CPS	Easting	Northing	CPS	Easting	Northing	CPS	Easting	Northing	CPS	Easting	Northing	CPS	Easting	Northing	CPS
-7664.55	53150.72	80	-7698.62	53060.23	120	-7667.74	52918.80	110	-8293.10	53450.15	110	-8276.78	53315.79	600	-8244.76	53167.41	80	-8239.05	53043.65	110
-7708.97	53189.54	110	-7720.88	53081.50	130	-7689.03	52934.27	130	-8313.42	53470.45	80	-8303.88	53338.03	80	-8270.89	53189.65	100	-8262.27	53062.97	100
-7733.03	53208.96	130	-7747.01	53102.77	100	-7712.25	52952.64	130	-8340.52	53490.76	60	-8326.14	53358.34	130	-8293.15	53208.98	60	-8279.69	53082.31	90
-7756.16	53229.30	120	-7769.27	53123.08	90	-7733.54	52970.04	110	-7724.89	52846.07	90	-8352.26	53380.57	80	-8313.63	53228.59	60	-8304.85	53101.65	100
-7781.14	53250.56	100	-7793.46	53140.48	250	-7757.73	52991.31	140	-7749.08	52861.12	120	-8372.59	53397.98	60	-8338.79	53248.89	60	-8326.14	53120.98	290
-7807.98	53269.97	100	-7813.78	53159.82	250	-7781.93	53009.68	150	-7771.34	52879.91	90	-8395.81	53419.25	70	-8362.98	53267.26	90	-8348.40	53140.35	90
-7830.19	53290.31	80	-7839.91	53180.12	600	-7805.15	53031.92	70	-7794.57	52900.21	130	-8420.01	53438.58	60	-8388.14	53289.50	70	-8376.47	53160.62	80
-7846.84	53305.11	80	-7866.04	53199.46	150	-7829.35	53050.29	90	-7817.79	52917.61	160	-7784.85	52775.30	80	-8413.30	53310.77	50	-8395.82	53178.99	70
-7870.90	53328.22	80	-7887.33	53221.70	90	-7851.61	53072.53	150	-7841.99	52938.88	140	-7810.02	52795.60	80	-8437.50	53333.97	40	-8420.98	53200.27	60
-7894.96	53348.56	80	-7905.72	53237.17	80	-7875.80	53092.83	500	-7865.21	52961.11	90	-7830.34	52811.07	100	-8460.72	53351.38	60	-8443.24	53221.54	60
-7921.79	53367.97	80	-7929.91	53260.37	100	-7898.06	53111.20	270	-7890.37	52981.43	70	-7854.53	52830.41	100	-7843.01	52706.70	90	-8470.34	53243.77	90
-7943.08	53389.23	70	-7955.22	53282.96	100	-7923.22	53136.34	280	-7911.66	52998.83	150	-7875.82	52848.78	150	-7867.21	52723.40	100	-8492.60	53265.04	30
-7988.76	53426.75	80	-7979.41	53303.26	90	-7944.51	53152.78	180	-7934.89	53019.13	340	-7903.89	52873.92	110	-7892.37	52741.51	100	-8522.60	53286.32	30
-8007.27	53447.09	90	-8001.67	53323.56	110	-7964.83	53169.21	100	-7961.02	53039.44	1500	-7930.25	52892.82	90	-7910.76	52762.78	110	-8543.88	53305.65	70
-8035.95	53468.35	70	-8024.90	53342.90	80	-7990.20	53191.03	90	-7987.15	53061.67	150	-7946.70	52912.16	60	-7936.89	52783.09	180	-7882.24	52615.98	90
-8054.46	53485.92	70	-8044.25	53357.40	80	-8017.30	53212.30	180	-8006.67	53079.56	200	-7973.80	52932.46	60	-7963.01	52804.36	110	-7903.02	52635.52	90
-8077.59	53503.48	70	-8068.44	53379.64	60	-8037.62	53231.64	200	-8024.09	53100.83	400	-7994.12	52951.80	80	-7983.34	52824.66	130	-7927.47	52656.28	110
-8103.50	53526.59	90	-8092.64	53398.98	180	-8059.88	53252.91	80	-8050.22	53120.17	180	-8015.41	52975.00	100	-8005.59	82844.00	70	-7947.03	52677.05	120
-8126.64	53547.86	90	-8113.93	53416.38	80	-8081.17	53272.25	70	-8075.38	53142.41	150	-8044.44	52992.41	200	-8031.72	52863.33	90	-7969.03	52694.15	150
-8149.77	53563.57	70	-8136.18	53436.69	130	-8104.39	53289.65	50	-8096.67	53159.81	110	-8063.80	53011.75	110	-8050.11	52880.74	110	-7991.04	52712.47	170
-8176.60	53586.68	70	-8159.41	53456.02	70	-8130.52	53308.02	110	-8122.80	53180.12	110	-8082.19	53030.12	110	-8078.17	52904.91	240	-8020.38	52738.12	100
-8200.66	53609.80	70	-8185.54	53476.33	70	-8152.78	53331.23	60	-8145.06	53199.45	100	-8108.31	53053.32	200	-8100.43	52922.31	200	-8042.38	52756.44	100
-8228.42	53629.21	80	-8205.86	53498.56	70	-8171.17	53345.73	60	-8164.41	53217.82	100	-8133.47	53074.59	160	-8121.72	52939.72	70	-8066.83	52778.42	140
-8255.26	53653.25	70	-8232.96	53517.90	50	-8196.33	53367.97	70	-8186.67	53239.10	80	-8154.77	53091.99	90	-8142.04	52961.95	100	-8090.06	52795.52	90
-7630.88	53006.09	120	-8257.15	53538.21	60	-8218.59	53387.30	90	-8211.83	53259.40	80	-8178.96	53113.26	90	-8169.14	52981.29	180	-8110.84	52815.06	90
-7654.11	53024.46	80	-8281.52	53562.88	70	-8243.75	53407.61	80	-8231.30	53277.12	60	-8202.18	53130.67	100	-8188.50	52999.66	100	-8136.51	52837.04	110
-7675.40	53040.90	100	-8304.74	53580.28	80	-8268.91	53427.91	90	-8256.46	53299.36	80	-8223.47	53150.97	100	-8214.86	53022.36	100	-8162.18	52855.37	140

Easting	Northing	CPS	Easting	Northing	CPS	Easting	Northing	CPS	Easting	Northing	CPS	Easting	Northing	CPS	Easting	Northing	CPS	Easting	Northing	CPS
-8182.96	52873.69	90	-8147.19	52721.58	70	-8062.92	52534.49	320	-7967.30	52329.09	110	-8582.07	52862.33	60	-8413.85	52598.94	50	-8317.64	52390.46	130
-8202.52	52890.78	70	-8167.68	52742.06	60	-8088.76	52554.10	200	-7991.58	52348.71	220	-8607.39	52883.49	60	-8434.17	52617.21	50	-8337.96	52410.76	190
-8228.19	52912.77	80	-8194.49	52764.90	80	-8112.52	52573.72	150	-8013.80	52366.77	140	-8629.61	52902.59	60	-8461.93	52638.19	40	-8361.66	52429.36	80
-8250.20	52933.53	100	-8216.56	52786.16	90	-8138.35	52595.40	100	-8034.46	52386.90	160	-8652.86	52922.72	70	-8483.09	52660.72	140	-8381.42	52448.53	160
-8272.20	52955.52	70	-8239.66	52805.59	230	-8162.64	52615.53	70	-8058.23	52404.97	100	-8676.62	52943.89	80	-8505.10	52678.31	50	-8404.14	52470.25	110
-8297.88	52973.84	80	-8257.79	52822.13	270	-8183.30	52635.66	70	-8084.06	52426.65	150	-8701.42	52967.63	80	-8528.46	52699.62	50	-8427.84	52488.52	90
-8319.88	52995.82	80	-8283.01	52842.60	130	-8207.07	52654.24	80	-8105.76	52444.20	280	-8722.09	52986.21	120	-8552.16	52720.94	80	-8452.90	52509.83	30
-8341.88	53011.70	140	-8306.94	52863.27	70	-8227.74	52673.60	60	-8127.46	52465.36	480	-8743.79	53002.22	80	-8573.16	52740.56	50	-8475.25	52527.76	50
-8365.11	53032.46	180	-8329.67	52883.40	60	-8252.53	52696.05	140	-8145.17	52483.81	1200	-8767.04	53023.90	50	-8596.29	52760.06	80	-8494.94	52545.10	30
-8389.56	53053.23	80	-8353.95	52905.59	60	-8275.89	52715.94	120	-8171.51	52503.42	100	-8002.45	52245.85	100	-8618.29	52779.68	80	-8516.92	52565.88	60
-8409.25	53070.86	70	-8375.65	52925.21	70	-8298.65	52736.07	130	-8198.90	52525.58	130	-8024.15	52263.92	240	-8641.66	52799.31	30	-8543.46	52590.81	140
-8434.92	53091.62	90	-8397.35	52942.76	80	-8315.70	52752.07	80	-8226.60	52545.23	150	-8049.47	52284.56	200	-8666.71	52821.30	90	-8565.76	52609.37	110
-8455.71	53112.38	60	-8417.63	52963.64	140	-8341.53	52773.23	260	-8243.85	52563.30	160	-8072.20	52301.60	220	-8687.71	52838.89	600	-8589.65	52629.53	80
-8478.93	53135.59	90	-8441.92	52982.74	110	-8366.85	52795.94	70	-8266.06	52584.46	50	-8093.38	52318.12	140	-8712.43	52858.17	80	-8611.00	52649.88	90
-8503.38	53152.69	100	-8462.58	53001.33	70	-8389.58	52814.01	50	-8286.73	52603.56	60	-8117.15	52341.86	100	-8734.10	52879.14	60	-8631.70	52667.39	110
-8530.28	53171.01	60	-8487.90	53023.52	60	-8413.48	52835.39	50	-8311.53	52626.27	60	-8141.08	52362.08	90	-8759.58	52902.64	90	-8656.66	52688.60	50
-8553.50	53192.99	50	-8508.05	53045.20	70	-8434.67	52856.55	50	-8335.44	52645.19	30	-8165.80	52381.36	150	-8061.08	52172.88	100	-8678.42	52708.76	90
-8575.51	53214.98	80	-8534.99	53066.59	90	-8455.33	52873.59	70	-8358.17	52665.32	50	-8184.43	52398.62	120	-8084.44	52192.16	120	-8699.66	52727.86	90
-7939.07	52545.16	90	-8556.69	53085.69	50	-8478.58	52893.20	70	-8374.70	52682.36	70	-8207.45	52418.24	180	-8110.18	52211.79	170	-8726.74	52746.95	140
-7965.09	52568.00	90	-8580.45	53107.37	60	-8500.80	52915.40	800	-8401.57	52700.94	80	-8231.92	52438.02	110	-8130.50	52231.75	500	-8745.32	52764.98	90
-7987.16	52585.33	110	-8605.25	53128.53	60	-8524.22	52935.25	80	-8426.37	52723.65	60	-8254.60	52457.30	80	-8153.52	52250.01	120	-8769.74	52787.26	90
-8006.08	52605.02	620	-8635.22	53155.37	70	-8549.54	52956.41	60	-8448.07	52745.85	70	-8277.63	52478.28	280	-8177.03	52267.53	360	-8793.10	52809.01	80
-8025.94	52625.49	640	-7952.30	52438.75	100	-8571.24	52972.93	80	-8470.80	52763.91	60	-8301.67	52499.59	130	-8202.77	52290.20	100	-8817.03	52828.74	80
-8053.38	52643.61	160	-7975.55	52457.85	90	-8594.49	52995.64	70	-8494.56	52782.50	80	-8324.02	52518.53	90	-8223.42	52309.14	100	-8098.67	52086.58	140
-8079.39	52664.87	100	-7998.79	52476.44	200	-8616.19	53014.74	120	-8515.75	52802.63	70	-8345.01	52538.16	120	-8244.42	52326.73	110	-8117.77	52106.20	210
-8102.25	52684.56	80	-8023.08	52497.08	200	-8643.05	53035.39	70	-8538.48	52823.79	80	-8370.17	52559.36	30	-8268.46	52346.69	256	-8142.19	52125.30	250
-8125.11	52702.68	80	-8044.78	52516.70	240	-8668.89	53058.62	80	-8561.41	52844.27	90	-8393.53	52578.31	30	-8289.54	52366.44	260	-8164.49	52145.98	180

Easting	Northing	CPS	Easting	Northing	CPS	Easting	Northing	CPS	Easting	Northing	CPS	Easting	Northing	CPS	Easting	Northing	CPS	Easting	Northing	CPS
-8187.85	52163.49	190	-8805.39	52700.33	90	-8660.34	52452.72	80	-8467.33	52158.14	120	-8277.21	51873.16	120	-8894.21	52409.82	80	-8883.48	52284.22	100
-8209.09	52181.52	520	-8828.22	52720.48	110	-8683.17	52472.88	80	-8492.82	52179.89	140	-8298.22	51892.01	130	-8914.15	53429.21	90	-8907.19	52304.68	130
-8234.04	52203.27	180	-8852.11	52740.11	140	-8706.01	52493.03	80	-8518.83	52201.63	270	-8322.47	51914.62	160	-8312.34	51786.95	90	-8928.21	52324.06	120
-8257.93	52222.90	150	-8879.18	52762.39	90	-8727.24	52512.66	80	-8541.66	52221.26	250	-8349.96	51935.62	620	-8833.97	51807.41	120	-8951.92	52343.44	180
-8281.29	52246.23	130	-8136.98	51996.64	140	-8749.13	52531.43	250	-8560.98	52239.64	260	-8368.82	51952.85	150	-8355.99	51825.72	110	-8972.40	52363.90	80
-8299.42	52262.95	260	-8159.81	52015.74	720	-8772.49	52546.94	100	-8581.69	52258.20	290	-8390.37	51924.38	110	-8379.70	51848.87	160	-8993.95	52382.75	80
-8325.96	52281.51	140	-8182.11	52034.83	560	-8796.38	52570.15	50	-8608.23	52279.95	2100	-8430.55	51993.23	190	-8403.95	51869.33	300	-8375.75	51714.73	80
-8348.26	52301.67	130	-8201.75	52052.87	310	-8817.09	52590.84	60	-8632.65	52302.23	140	-8437.35	52012.99	180	-8427.66	51889.79	420	-8396.38	51733.44	80
-8372.68	52320.23	140	-8225.64	52075.15	160	-8841.51	52610.47	120	-8653.36	52321.32	60	-8461.06	52033.99	400	-8448.14	51908.63	270	-8418.55	51751.44	120
-8396.04	52342.51	90	-8250.06	52094.24	100	-8865.93	52631.68	110	-8673.00	52339.36	60	-8482.08	52053.38	110	-8471.40	51929.31	320	-8440.03	51774.97	120
-8419.40	52362.67	110	-8274.57	52113.65	420	-8889.82	52651.31	80	-8696.89	52359.51	50	-8505.79	52070.60	520	-8495.65	51948.15	240	-8464.97	51792.97	150
-8439.83	52380.51	140	-8296.34	52132.75	400	-8910.52	52673.05	100	-8720.25	52380.73	60	-8527.34	52091.60	170	-8518.82	51969.15	180	-8489.91	51814.43	140
-8461.60	52401.19	130	-8318.11	52155.02	110	-8936.01	52694.80	100	-8744.85	52402.29	80	-8551.06	52112.60	310	-8540.38	51986.92	180	-8510.70	51835.19	600
-8486.55	52419.76	130	-8341.99	52175.18	310	-8956.18	52710.71	90	-8768.21	52421.39	90	-8575.85	52133.06	320	-8561.40	52007.92	200	-8532.18	51853.88	580
-8510.44	52442.03	100	-8363.23	52190.56	320	-8172.06	51905.86	70	-8792.09	52441.55	80	-8596.86	52152.44	320	-8581.87	52027.30	170	-8559.20	51876.03	280
-8534.33	52463.25	600	-8383.94	52210.19	120	-8196.48	51923.36	120	-8811.74	52460.11	90	-8621.33	52171.55	380	-8607.36	52046.44	640	-8582.06	51896.80	540
-8551.32	52479.69	60	-8407.83	52230.34	300	-8217.18	51942.46	210	-8835.09	52478.67	110	-8641.27	52191.47	190	-8631.08	52065.82	220	-8599.38	51912.03	200
-8577.87	52500.38	80	-8431.19	52253.68	210	-8240.54	51962.08	150	-8855.80	52498.30	50	-8666.60	52213.01	170	-8655.86	52086.82	280	-8622.94	51932.10	280
-8602.29	52523.72	60	-8456.14	52275.43	220	-8263.37	51981.71	620	-8880.76	52518.99	60	-8689.23	52231.85	320	-8677.96	52106.74	180	-8644.42	51952.87	210
-8624.06	52542.81	70	-8479.62	52295.44	460	-8288.33	52004.52	320	-8901.99	52538.08	80	-8712.40	52252.31	190	-8702.21	52127.20	500	-8666.16	51971.33	260
-8647.58	52562.20	80	-8498.19	52311.89	2000	-8310.09	52021.49	420	-8926.95	52561.95	100	-8731.80	52270.08	90	-8725.38	52143.89	180	-8691.79	51994.18	250
-8670.94	52584.48	100	-8519.97	52333.63	400	-8333.45	52043.24	580	-8949.77	52580.52	130	-8755.52	52290.54	300	-8747.48	52167.04	100	-8770.43	52014.25	120
-8690.59	52600.92	70	-8545.45	52352.73	220	-8355.22	52061.80	130	-8974.37	52601.95	100	-8781.38	52313.15	80	-8769.57	52184.81	90	-8742.36	52035.71	280
-8714.47	52623.73	60	-8567.75	52373.41	100	-8378.14	52079.64	380	-8996.14	52623.70	90	-8801.52	52330.68	110	-8790.59	52202.58	70	-8762.46	52051.63	140
-8736.24	52641.76	50	-8592.70	52393.57	40	-8400.97	52100.85	110	-9020.56	52643.32	120	-8826.85	52350.06	120	-8811.81	52224.46	50	-8786.01	52073.09	100
-8758.54	52661.39	90	-8611.28	52408.42	80	-8422.21	52117.83	110	-9044.98	52665.07	90	-8838.41	52371.60	90	-8836.60	52243.84	100	-8810.96	52093.86	180
-8780.97	52680.17	70	-8637.30	52431.76	80	-8446.09	52137.98	260	-8254.03	51855.40	90	-8869.96	52390.44	70	-8859.23	52264.30	80	-8833.13	52113.24	120

Easting	Northing	CPS	Easting	Northing	CPS	Easting	Northing	CPS	Easting	Northing	CPS	Easting	Northing	CPS	Easting	Northing	CPS	Easting	Northing	CPS
-8851.15	52130.55	160	-10446.20	49906.67	110	-10423.30	50118.97	80	-10114.40	50206.70	230	-10015.40	50367.11	210	-9851.55	50470.04	150	-9567.60	50462.32	340
-8875.40	52150.62	100	-10472.00	29929.34	100	-10118.90	49965.70	60	-10135.30	50223.28	200	-10035.30	50385.87	230	-9870.33	50488.81	180	-9591.90	50485.50	300
-8900.34	52172.78	90	-10495.20	49947.38	110	-10142.70	49987.33	80	-10156.90	50241.31	300	-10060.70	50409.05	380	-9892.43	50505.37	100	-9615.11	50502.05	260
-8221.13	52192.16	90	-10518.00	49968.73	110	-10167.20	50007.52	90	-10182.90	50266.54	260	-10088.30	50430.03	310	-9913.42	50526.34	160	-9637.20	50520.82	260
-8943.99	52211.54	120	-10538.60	49985.21	120	-10191.00	50025.54	200	-10288.00	50236.62	90	-10109.30	50449.90	200	-9939.94	50548.42	110	-9662.62	50544.00	240
-8969.14	52233.39	180	-10562.30	50005.31	90	-10212.70	50045.73	520	-10208.70	50287.63	130	-10129.20	50467.56	180	-9963.14	50569.39	100	-9688.03	50566.08	210
-8992.01	52250.01	120	-10285.60	49872.84	70	-10235.10	50065.92	240	-10228.60	50307.50	110	-10157.40	50489.64	80	-9984.13	50589.26	100	-9711.23	50582.64	250
-9016.26	52273.54	320	-10304.70	49892.42	180	-10256.00	50082.50	250	-10246.30	50326.26	80	-9792.73	50295.36	80	-10008.40	50610.23	80	-9732.22	50604.71	180
-9037.74	52292.93	400	-10327.40	49910.97	180	-10275.50	50103.41	220	-9932.52	50173.93	80	-9818.72	50313.02	90	-9628.36	50392.77	70	-9756.53	50623.48	140
-9058.53	52310.93	210	-10349.10	49933.12	320	-10301.50	50125.04	220	-9961.25	50196.01	150	-9841.92	50337.30	340	-9652.67	50413.75	70	-9773.10	50641.14	110
-9080.69	52333.77	80	-10372.30	49950.13	580	-10326.70	50147.39	50	-9987.76	50223.60	210	-9869.54	50360.48	320	-9674.77	50433.62	200	-9799.62	50661.01	200
-9104.95	52349.69	50	-10395.00	49968.68	240	-10346.90	50166.13	40	-10011.00	50241.27	150	-9890.54	50381.46	400	-9697.97	50453.48	280	-9826.13	50683.09	100
-10419.10	49762.08	80	-10420.80	49991.35	130	-10367.90	50184.16	80	-10033.10	50260.03	130	-9911.53	50399.12	190	-9721.17	50474.46	260	-9847.13	50701.85	110
-10445.10	49779.90	240	-10441.90	50011.45	190	-10081.30	50057.26	90	-10054.10	50281.01	120	-9932.52	50415.68	260	-9747.69	50494.33	230	-9872.54	50719.52	90
-10466.30	49798.68	180	-10463.10	50033.61	90	-10109.50	50079.61	480	-10073.90	50298.67	260	-9955.72	50433.34	260	-9772.00	50514.20	140	-9418.24	50457.09	70
-10488.00	49817.95	260	-10484.80	50051.83	130	-10129.70	50101.96	180	-10094.90	50317.43	130	-9976.72	50455.42	130	-9791.88	50534.07	220	-9438.13	50475.86	70
-10508.80	49838.66	160	-10511.60	50070.38	80	-10151.30	50115.66	170	-10122.60	50339.51	170	-10001.00	50474.18	210	-9812.88	50553.94	290	-9456.91	50493.52	60
-10532.40	49858.23	170	-10197.80	49918.76	90	-10173.00	50137.29	540	-10144.70	50357.17	170	-10027.50	50495.15	250	-9837.18	50571.60	130	-9482.33	50513.39	160
-10556.60	49879.36	140	-10223.60	49938.86	90	-10193.90	50157.48	340	-10170.10	50378.14	180	-10047.40	50516.13	120	-9857.07	50592.57	130	-9508.84	50535.47	220
-10578.80	49897.40	130	-10248.90	49959.98	190	-10216.30	50176.95	220	-10191.10	50395.81	80	-10069.50	50534.89	90	-9885.80	50614.65	130	-9530.94	50553.13	420
-10599.40	49916.98	100	-10270.00	49979.05	180	-10242.30	50199.30	220	-9852.97	50226.92	50	-9685.82	50329.85	210	-9909.00	50634.52	100	-9551.93	50573.00	220
-10624.70	49937.07	100	-10290.70	50000.18	240	-10264.60	50217.32	150	-9876.17	50243.47	90	-9711.23	50358.62	50	-9929.99	50654.39	120	-9576.24	50591.76	280
-10652.10	49958.20	70	-10311.80	50017.70	280	-9996.00	50102.16	80	-9899.38	50264.45	120	-9734.43	50369.59	240	-9952.09	50675.36	70	-9599.44	50614.94	400
-10360.60	49828.35	70	-10332.50	50038.31	50	-10022.00	50124.51	110	-9927.00	50290.94	220	-9753.21	50388.36	340	-9479.21	50391.67	80	-9628.17	50637.02	200
-10381.23	49848.44	130	-10360.30	50058.92	140	-10048.70	50147.58	180	-9950.20	50307.50	230	-9779.73	50409.33	360	-9499.10	50406.11	150	-9649.16	50655.79	440
-10402.90	49869.57	220	-10383.60	50080.32	140	-10069.60	50169.21	180	-9973.40	50330.68	150	-9802.93	50430.30	380	-9520.09	50420.37	100	-9672.36	50675.66	230
-10426.10	49889.15	240	-10405.30	50101.97	140	-10091.30	50187.95	190	-9991.08	50349.44	180	-9828.35	50450.20	280	-9545.50	50441.34	130	-9695.57	50693.32	300

Easting	Northing	CPS	Easting	Northing	CPS	Easting	Northing	CPS	Easting	Northing	CPS	Easting	Northing	CPS	Easting	Northing	CPS	Easting	Northing	CPS
-9719.87	50715.39	130	-9364.98	50652.82	200	-9609.10	50976.90	100	-9301.15	50958.29	170	-9380.58	51143.20	440	-9274.30	51180.72	380	-8974.68	51155.67	110
-9738.66	50733.06	110	-9390.34	50672.20	300	-9630.73	50997.77	130	-9328.08	50980.44	230	-9406.74	51167.24	210	-9217.00	51247.50	240	-8996.17	51177.14	120
-9762.33	50754.75	70	-9414.74	50693.07	340	-9653.11	51014.17	100	-9354.22	51000.22	150	-9427.67	51186.06	200	-9298.18	51199.80	560	-9021.24	51198.61	180
-9786.58	50772.57	110	-9437.35	50712.45	110	-9676.99	51035.79	70	-9374.81	51016.05	120	-9448.60	51201.74	170	-9316.08	51217.69	220	-9041.53	51215.30	260
-9807.27	50791.10	70	-9459.73	50730.34	130	-9700.86	51057.40	70	-9397.78	51035.83	240	-9474.75	51223.69	170	-9344.73	51239.16	320	-9067.79	51232.00	280
-9338.36	50550.93	80	-9482.86	50749.72	400	-9726.97	51076.78	70	-9416.79	51055.61	300	-9499.87	51243.56	120	-9366.22	51257.05	250	-9088.08	51257.05	340
-9354.77	50532.32	80	-9507.48	50770.59	420	-9315.89	50849.44	80	-9441.27	51074.20	940	-9523.97	51263.70	100	-9388.90	51276.13	250	-9114.35	51277.32	380
-9379.03	50550.85	280	-9531.35	50790.72	220	-9340.51	50869.56	170	-9466.38	51096.16	260	-9546.99	51284.60	100	-9411.58	51296.40	220	-9137.03	51295.21	340
-9398.29	50566.53	180	-9554.48	50809.35	190	-9360.65	50888.94	180	-9490.45	51117.07	210	-9563.74	51300.29	80	-9434.26	51317.87	120	-9158.51	51317.87	820
-9422.54	50586.49	240	-9576.98	50829.73	190	-9387.51	50909.07	240	-9513.47	51134.84	130	-9588.85	51320.15	60	-9458.13	51340.53	120	-9181.19	51336.95	230
-9447.51	50606.45	320	-9599.36	50848.37	120	-9411.39	50929.94	160	-9535.44	51152.61	100	-9612.91	51342.10	70	-9479.62	51360.80	160	-9203.87	51360.80	120
-9471.05	50624.98	380	-9619.50	50864.77	60	-9436.01	50950.07	300	-9558.46	51172.47	80	-9035.33	51085.91	70	-9499.91	51379.88	70	-9227.75	51377.50	210
-9493.17	50643.51	480	-9644.12	50887.88	170	-9456.15	50967.96	220	-9584.62	51193.38	80	-9088.81	51017.64	80	-9521.40	51397.77	70	-9249.23	51393.00	340
-9520.27	50662.04	210	-9668.00	50911.73	160	-9479.28	50987.34	160	-9607.64	51211.15	80	-9056.13	51108.17	70	-9544.08	51418.05	70	-9270.72	51415.67	180
-9540.25	50682.71	440	-9691.87	50926.64	100	-9499.42	51003.73	90	-9628.56	51231.01	90	-9115.55	51038.42	70	-9237.30	51264.20	460	-9292.21	51434.74	90
-9567.36	50704.09	420	-9710.52	50947.51	60	-9527.03	51027.59	60	-9649.49	51248.78	70	-9079.90	51128.95	100	-9262.36	51286.86	380	-9314.89	51457.40	70
-9592.33	50724.76	240	-9351.66	50762.65	90	-9548.66	51046.97	70	-9673.56	51267.60	60	-9142.29	51059.20	110	-9287.43	51305.94	500	-9340.71	51478.85	80
-9613.73	50741.15	190	-9373.30	50781.28	130	-9572.54	51065.60	110	-9149.35	50947.71	60	-9160.12	51077.00	110	-9306.53	51317.87	320	-9362.27	51497.16	120
-9637.27	50763.96	130	-9396.43	50801.41	120	-9594.92	51084.98	80	-9174.46	50967.58	100	-9183.58	51097.23	120	-9326.82	51347.68	190	-9382.76	51514.39	120
-9659.45	50781.29	110	-9421.05	50820.79	300	-9618.05	51103.62	70	-9197.48	50987.44	110	-9208.65	51119.89	210	-9349.50	51366.77	110	-9406.47	51534.86	70
-9681.57	50799.11	110	-9446.42	50843.90	270	-9641.18	51124.49	60	-9219.45	51004.16	130	-9097.63	51147.32	130	-9374.57	51389.43	80	-9423.72	51553.17	70
-9706.54	50817.64	110	-9470.29	50864.02	340	-9664.30	51143.12	80	-9243.52	51028.21	200	-9126.28	51167.60	360	-9397.25	51410.89	80	-8892.24	51200.96	80
-9730.79	50838.31	130	-9492.67	50881.17	160	-9688.18	51161.01	80	-9269.67	51049.12	120	-9150.16	51186.68	380	-9419.93	51429.97	110	-8912.72	51221.43	90
-9750.05	50858.98	80	-9515.05	50899.80	220	-9206.11	50876.78	80	-9291.65	51068.98	160	-9231.33	51142.55	170	-9441.42	51446.67	90	-8940.75	51241.89	160
-9302.23	50601.03	120	-9537.44	50919.18	110	-9233.83	50898.15	100	-9313.62	51082.57	250	-9169.26	51208.15	480	-9464.10	51465.75	80	-8962.31	51260.20	890
-9322.68	50660.30	140	-9559.08	50935.58	90	-9256.80	50920.31	220	-9336.64	51106.61	230	-9251.62	51160.44	700	-9485.59	51487.22	70	-8978.48	51280.67	170
-9341.85	50632.70	380	-9587.46	50959.01	50	-9278.98	50937.71	200	-9358.61	51122.29	420	-9193.13	51228.42	800	-8950.81	51135.40	90	-9005.44	51301.10	180

Easting	Northing	CPS	Easting	Northing	CPS	Easting	Northing	CPS	Easting	Northing	CPS	Easting	Northing	CPS	Easting	Northing	CPS	Easting	Northing	CPS	Easting	Northing	CPS
-9029.2	51322.7	240	-9104.9	51515.4	160	-8711.19	51407.88	100	-8744.83	51558.54	240	-8637.93	51590.27	540	-8513.31	51598.10	60	-9126.92	52134.01	100	-9025.98	52167.13	110
-9054.0	51343.1	420	-9129.3	51532.9	80	-8733.70	51428.01	160	-8766.62	51577.50	540	-8661.43	51610.89	360	-8534.96	51615.72	70	-9147.67	52156.44	80	-9043.07	52183.39	100
-9075.5	51363.6	320	-9150.7	51553.3	130	-8758.94	51449.27	300	-8791.92	51596.46	360	-8682.64	51628.64	360	-8559.82	51635.75	300	-8430.78	51645.83	90	-9067.49	52204.54	30
-9098.2	51383.0	420	-9173.1	51571.8	120	-8782.53	51472.49	130	-8815.81	51618.93	320	-8707.29	51647.54	80	-8583.07	51656.57	420	-8454.38	51665.35	460	-9091.90	52224.05	40
-9119.7	51401.3	200	-9194.5	51593.2	110	-8804.80	51488.94	130	-8835.49	51636.48	210	-8732.51	51669.30	440	-8604.72	51675.00	170	-8474.73	51684.86	110	-9116.32	52524.57	30
-9143.4	51423.9	120	-9217.9	51613.6	100	-8825.14	51510.23	220	-8857.98	51656.84	240	-8755.53	51689.13	180	-8626.37	51695.83	420	-8497.51	51705.19	210	-9136.66	52265.52	40
-9167.1	51443.3	100	-9243.2	51635.0	140	-8849.35	51531.51	560	-8881.17	51678.61	140	-8776.16	51708.03	160	-8647.21	51716.65	150	-8522.74	51726.33	220			
-9190.9	51464.9	130	-9260.7	51650.6	90	-8873.56	51550.87	160	-8903.23	51698.76	260	-8797.37	51728.08	180	-8673.67	51235.88	150	-8543.90	51745.85	150			
-9210.3	51486.4	150	-8792.4	51357.7	80	-8891.96	51569.25	300	-8928.53	51718.42	300	-8820.30	51747.55	340	-8693.72	51747.51	230	-8567.51	51763.74	220			
-9235.1	51501.5	90	-8818.7	51537.3	200	-8917.14	51589.57	180	-8952.43	51739.49	140	-8846.67	51767.60	340	-8770.77	51776.73	620	-8591.92	51783.25	380			
-9255.5	51520.9	110	-8842.1	51400.6	180	-8935.54	51608.92	80	-8974.21	51757.75	190	-8869.03	51788.21	200	-8737.01	51794.36	180	-8617.15	51806.83	460			
-9282.5	51545.6	60	-8863.5	51420.0	210	-8964.60	51631.18	110	-8998.81	51778.81	210	-8893.10	51808.26	110	-8761.14	51814.75	340	-8635.87	51827.16	320			
-9303.0	51565.0	90	-8885.9	51442.4	270	-8988.81	51651.50	120	-9019.90	51799.88	150	-8912.59	51826.58	180	-8783.59	51836.38	180	-8661.10	51845.86	270			
-9322.4	57582.3	90	-8911.2	51460.9	680	-9010.12	51672.78	260	-9043.09	51818.13	200	-8935.71	51845.13	340	-8811.64	51855.61	160	-8682.26	51862.94	380			
-9347.2	51603.8	90	-8931.6	51481.3	160	-9029.49	51691.17	120	-9063.47	51839.90	150	-8958.63	51868.61	500	-8833.30	51875.63	420	-8727.02	51904.41	320			
-8829.4	51271.2	100	-8956.0	51499.8	250	-9052.74	51709.55	140	-9085.26	51857.45	160	-8983.28	51886.94	130	-8853.34	51895.66	300	-8753.16	51927.74	240			
-8854.7	51290.7	170	-8978.4	51520.2	420	-9076.94	51731.80	120	-9109.15	51877.82	130	-9005.07	51909.85	110	-8874.99	51913.28	210	-8776.77	51948.06	130			
-8877.1	51314.0	200	-8997.8	51541.6	420	-9095.41	51751.57	120	-9132.35	51898.88	160	-9023.41	51924.16	100	-8901.45	51936.51	190	-8798.74	51965.95	150			
-8900.5	51332.5	320	-9021.2	51563.0	110	-9126.41	51768.99	160	-9159.05	51917.14	100	-9050.35	51947.07	130	-8923.10	51955.74	110	-8817.46	51981.40	440			
-8921.9	51352.0	260	-9047.5	51584.4	70	-9140.93	51787.37	220	-9177.37	51936.38	170	-9072.71	51969.41	210	-8947.15	51978.17	120	-8843.50	52005.80	250			
-8945.3	51373.4	400	-9067.9	51601.0	600	-9169.02	51809.63	140	-9203.38	51956.74	80	-9097.36	57985.44	150	-8965.59	51994.19	640	-8866.29	52026.12	620			
-8969.6	51394.8	320	-9091.3	51622.4	150	-9191.29	51831.88	120	-9220.95	51975.00	110	-9117.57	52008.59	160	-8988.85	52016.62	110	-8888.26	52046.45	100			
-8994.9	51411.3	820	-9113.7	51638.9	160	-9212.60	51850.26	60	-9243.44	51994.66	180	-9141.65	52030.36	168	-9014.58	52037.08	80	-8912.68	52062.71	280			
-9013.4	51432.7	200	-9138.0	51648.6	160	-9234.87	51870.58	60	-9268.04	52017.13	90	-9161.71	52046.39	70	-9037.03	52055.51	100	-8930.59	52078.98	190			
-9034.8	51450.2	210	-9161.4	57683.7	80	-8675.96	51497.45	90	-8569.15	51528.42	80	-9185.22	52065.86	180	-9057.07	52077.14	90	-8956.63	52106.62	60			
-9060.2	51471.6	420	-9183.8	51702.1	70	-8699.85	51517.11	110	-8594.37	51547.32	90	-9206.43	52088.77	70	-9081.93	52097.16	120	-8977.96	52124.85	70			
-9080.6	51491.1	150	-8689.4	51388.8	80	-8723.04	51536.77	140	-8616.72	51567.93	140	-9231.65	52107.10	70	-9103.57	52116.39	150	-8999.94	52144.36	70			

APPENDIX 4
Table 1
Thin section descriptions

U by XRF in ppm	Thin Sections	Quartz	Textures	K-Feldspaar	Textures	Alteration intensity	Plagioclase Feldspar	Textures	Perthites	Perthites	Mica	Textures	Additional Minerals and their attributes	Type of alaskite
147	SK2D	fine crystalline	fractured and at places forms recrystalised pacthes	microcline, common	subhedral (fine to medium)	moderately altered to sericite on the crystal edges	Oligoclase	moderately sericitised in the centers	lamellar	lamellar	(Biotite) fairly common, chloritised biotite, sericite	(Biotite) ragged, (mica) skeletral and vein like, (sericite) grouped and scattered	Topaz, betafite/pyrrhochlore	D
<9	S1	varying grain sizes quartz, common	secondary quartz enclosed in primary quartz (primary-anhedral amoeboid, secondary-well rounded forming composites at places)	microcline, scarse			Oligoclase	anhedral to subhedral	lamellar and patches	lamellar, patches and albite	biotite, chloritised biotite	biotite (ragged), chloritised biotite (very fine grained)	monzonite/zircon, betafite (Fe coated), hematite	E
<9	S1	course to fine grains	large grains, undulose extinction and form composite textures. Smaller grains well rounded, enclosed in feldspars. Some quarts are highly altered.				Oligoclase		pacthes and lamellar	pacthes (overall), lamellar (primary), albite (secondary)	biotite - fairly common, secondary mica	biotite ragged subhedral and skeletal, secondary mica - grouped skeletral	betafite, apatite, zircon, hematite,	E
342	S10	fine to coarse	fine well rounded quartz enclosed in albite, course quartz form composite crysts and undilose extinction	Microcline		sericitised	Oligoclase	anhedral, more altered than quartz	film, lamellar and few pacthy	film (primary), lamellar (secondary), few pacthy	Biotite	ragged	zircon, hematite, pyrrhoclore	C
342	S10	medium to course and some are fine grained	fine quartz -well rounded, course/medium grained show compositing	Microcline		moderately altered to sericite	Oligoclase				secondary mica	found within grains and at boundaries.	hematite	C
158	SK1B	equigranullar, well rounded composite crystals or fine-well rounded, caorse- not rounded.	composite texture	miclocline, common		Low degree of sericitisation	Oligoclase	completely altered	laminallar	laminallar, film	biotite, secondary mica	biotite-ragged euhedral, secondary mica-	betafite (fe caoted), uraninite,hematite (occuring as nodules) and hematite, magnetite, topaz	D

U by XRF in ppm	Thin Sections	Quartz	Textures	K-Feldspaar	Textures	Alteration intensity	Plagioclase Feldspar	Textures	Perthites	Perthites	Mica	Textures	Additional Minerals and their attributes	Type of alaskite
132	SK12E	well rounded fine to medium grained enclosed in feldspars	smaller grains are oval and smooth edged, at places forming composites	microcline, common	with quartz enclosed in it.	moderately altered	Oligoclase	rare	pacthy, film and lamellar	pacthy, film, lamellar	biotite - fairly common, chloritised biotite	biotite - ragged, chloritised biotite - forming multi veins	topaz?, betafite, pyrrhochlore, zircon	D
132	SK12E	fine/medium to coarse	strain exctinction and composite at places.	common, microcline	quartz enclosed in it.	moderately altered	Oligoclase	rare	lamellar	lamellar	secondary mica	concentrated at the crystal boundaries	pyrrhochlore and monzonite	D
132	SK12E	fine grained enclosed in miclocline	oval and smooth edged, at places forming composites	microcline	anhedral	moderate (sericite)	Oligoclase	rare			Quite rare		magnetite and hematite (betafite (few	D
9	SK1A	medium	undilose extinction				Oligoclase	common			Biotite	ragged euhedral	uraninite and hematite zircon	B
9	SK1A	very common, caorse		microcline	ly and found enclosed		Oligoclase	common			sericite	ragged euhedral		B
65	SK1B	equigranullar, well rounded	composite texture	microcline, very common	degree of sericitisa		Oligoclase		lamellar	laminallar, film perthites			hematite, betafite	D
112	SK1E	Fine grained	almost well rounded, altered to sericite				Oligoclase	subhedral			biotite	ragged edges and found between albite and quartz crystals	topaz	D
92	SK2B	fine grained, very common	well rounded, some form composites, others are enclosed in the albites and a few beaded	trace microcline			Oligoclase	subhedral			biotite, sec mica	skeletral	betafite/pyrrhochlore, magnetite and hematite,	E
97	S3	very common,	well rounded, altered to sericite	microcline, common	subhedral	moderately altered to serice	Oligoclase	subhedral	lamellar	lamellar	biotite, secondary mica	biotite ragged euhedral and found between major grains		E
97	S3	well rounded fine grained enclosed in feldspars	composite texture	microcline			Oligoclase		pacthy,	pacthes, albite, microcline	biotite, secondary mica	ragged, veins, skeletral		E

U by XRF in ppm	Thin Sections	Quartz	Textures	K-Feldspaar	Textures	Alteration intensity	Plagioclase Feldspar	Textures	Perthites	Perthites	Mica	Textures	Additional Minerals and their attributes	Type of alaskite
250	SK12A	common,quartz	range between well rounded to amoeboid, some quartz is enclosed in perthites	common, microcline	anhedral		Oligoclase	anhedral	localised lamellar perthites	lamellar perthites	biotite, secondary mica	ragged, euhedral found at the boundary between quartz and albite	magnetite, betafite and hematite	D
250	SK12A	very common, varies from coarse to medium grained	large composite quartz, anhedral	microcline (common)	anhedral		Oligoclase	subhedral	lamellar and predominantly pacthy	lamellar and predominantly pacthy	biotite (rare), secondary mica	biotite (lenticullar, forming veinlike structures), secondary mica (altered from feldspar)	betafite/pyrrhochlore, magnetite zircon and hematite	D
250	SK12A	quartz, common, range from fine to medium grained	well rounded quartz with strin extinction.grain boundary dissolution. Composite texture at places (some quartz are altered to sericite)	microcline (common)	subhedral		Oligoclase	subhedral	patchy perthites	patchy perthites	secondary mica-pale green, biotite (scarse)	secondary mica - forms veins, biotite - euhedral at places forms veins		D
57	SK4	very caorse, common	few enclosed in feldspars, some form composites	common, microcline	moderately altered		albite	very few present	lamellar	lamellar, microcline, albite	biotite, pale green mica	biotite (ragged), pale green mica (ragged)	betafite, hematite	E
57	SK4	fine to medium	rounded quartz in feldspar, large composite quartz, mermektic, anhedral. Crystal boundary dissolution and simple twinning	common, microcline			coarse grained albite	highly altered	albite, film and pacthy	albite, film and pacthy	biotite, secondary mica	biotite (ragged), secondary mica (altered from quartz crysts and feldspar)	hematite, magnetite, betafite (fe caoted), pyrhoclore	E
57	SK4		composite texture	common, microcline					lamellar, pacthy	film, lamellar, pacthes				E
10	SK5B	common, fine/medium grained	well rounded, some quartz enclosed in albite, some quartz is being altered to sericite. Boundary dissolution prsent				albite, very common	subhedral to euhedral differently oriented	lamellar and film	albite, lamellar and film	biotite	ragged		B

U by XRF in ppm	Thin Sections	Quartz	Textures	K-Feldspaar	Textures	Alteration intensity	Plagioclase Feldspar	Textures	Perthites	Perthites	Mica	Textures	Additional Minerals and their attributes	Type of alaskite
48	SK2E	Fine grained	some are elongated, a few beaded (graphic)	microcline	caorse grained, all the quartz seem to be falling into one crystal of the K-feldspar				Lamellar	lamillar	biotite	euhedral ragged		C
48	SK2E	Fine grained	some are elongated (graphic)	microcline	very common, boundaries are undefined, graphic texture	less altered, sericitised			Lamellar	lamillar	secondary mica	skeletral	hematite, magnetite	C
33	K1	medium well rounded grained	equigranullar				albite, very common						topaz, magnetite	E
299	S2	fine to medium/medium to coarse	well rouded	micrcocline, common	anhedral, caorse		Oligoclase	subhedral	minor lamellar and pacthes	lamellar, pacthes	biotite	ragged	pyrite, magnetite, zircon (composites), monzonite, betafite/pyrrhochlore	D
151	SK12D	variable from fine to caorse	medium - rounded, undilose extinction, large - forms composites	microcline	large microcline found at places	completely altered, sericitised	albite	anhedral			biotite, sericte, secondary mica	biotite- ragged euhedra, sericite - veins, secondary mica - found within the feldspar grains and at grain boundaries		C
151	SK12D	very common	enclosed in large feldspars	microcline, common		moderately altered								C
13	SK5A	very common, coarse grains	graphic texture.Simple optically and continous. undilose extinction. Some	moderate, microcline			moderate, oligoclase		film and pacthy perthites	film and pacthy perthites	sericite	clustered/ragged granules texture. Mainly found in the center of the		B

APPENDIX 4
Table 2
Petrographic modal counts

No.	Type	Quartz	Plagioclase	total Alkali	perthites	Biotite	0paque	zircon/other	
SK2D	D	33	8	43	8	3	3	2	100
S1	E	48	37.5	5	6	0.5		3	100
S1	E	48	36	0	12	2		2	100
S1	E	52	36.8	7.5		1.25	0	2.5	100
ave.		**49.3**	**36.8**	**4.2**	**6.0**	**1.3**	**0.0**	**2.5**	**100.0**
S10	C	48	7	42		2	1		100
S10	C	44	4	51		0.5	0.5	0	100
ave.		**46.0**	**5.5**	**46.5**	**0.0**	**1.3**	**0.8**	**0.0**	**100.0**
SK1B	D	27.5	12	45	9.5	1	2	3	100
SK1B	D	39	4	52	3		1	1	100
ave.		**33.3**	**8.0**	**48.5**	**6.3**	**0.5**	**1.5**	**2.0**	**100.0**
SK12E	D	30	10	42	7	5	2	4	100
SK12E	D	26	6	58	5	2		3	100
SK12E	D	31.5	11.5	51	0	0	4	2	100
ave.		**29.2**	**9.2**	**50.3**	**4.0**	**2.3**	**2.0**	**3.0**	**100.0**
SK1A	B	53	34.5	10.5		1		1	100
SK1E	D	53	35	10		1		1	100
SK2B	E	49.5	25.5	20		2		3	100
S3	E	36	5	52	4	3			100
S3	E	35	8.5	52.5	2	2			100
ave.		**35.5**	**6.8**	**52.3**	**3.0**	**2.5**	**0.0**	**0.0**	**100.0**
SK12A	D	39	3	50	2	2	3	1	100
SK12A	D	44	8	43	2.5	0.5	0.5	1.5	100
SK12A	D	33.5	2	60	1.5	3			100
ave.		**38.8**	**4.3**	**51.0**	**2.0**	**1.8**	**1.2**	**0.8**	**100.0**
SK4	E	34.5	5.5	55	2	2	1	1	101
SK4	E	29	2.5	56	6.5	2	2	2	100
SK4	E	33	3	61	3	0			100
ave.		**32.2**	**3.7**	**57.3**	**3.8**	**1.3**	**1.0**	**1.0**	**100.3**
SK5B	B	45	2	38	12	3			100
SK5B	B	39.5	10	50.5					100
ave.		**42.3**	**6.0**	**44.3**	**6.0**	**1.5**	**0.0**	**0.0**	**100.0**
SK2E	C	40	5	50	4	1			100
SK2E	C	35.5	2	46.5	12	1	3		100
ave.		**37.8**	**3.5**	**48.3**	**8.0**	**1.0**	**1.5**	**0.0**	**100.0**
K1	E	39.5	4	51.5	3	0.5	0.5	1	100
S2	D	38.5	6	49.5		3	3		100
SK12D	C	28	18	54					100
SK5A	B	28	4	63.5	4.5				100

APPENDIX 5
Section A

Standards used for calibration of PW1400 XRFS for silicate analysis.
The X-Ray tube used is a Rhodium tube and is run at 50 Am. The method used is from the paper "An accurate X-Ray spectrographic method for the analysis of a wide range of geological samples by K. Norrish and J.T. Hutton." Published in Geochimica et Cosmochimica Acta, 1969, Vol 33, pp. 431 to 453.

Standard	%Fe2O3	%MnO	%TiO2	%CaO	%K2O	%P2O5	%SiO2	%Al2O3	%MgO	%Na2O	%LOI	%Total
NIM-G	2.02	0.02	0	0.79	5.03	0.01	76.31	12.18	0.06	3.39	0.45	100.42
NIM-S	1.41	0.01	0	0.68	15.4	0.12	63.85	17.4	0.46	0.43	0.28	99.7
NIM-N	8.96	0.18	0.2	11.5	0.25	0.03	52.57	16.48	7.49	2.46	-0.4	99.83
NIM-D	16.87	0.22	0.02	0.28	0.01	0.01	38.66	0.3	43.18	0.04	-0.9	99.42
NIM-P	12.77	0.22	0.2	2.67	0.09	0.02	51.39	4.2	25.47	0.37	-0.8	96.03
AN-G	3.39	0.04	0.22	16	0.13	0.01	46.67	30.04	1.81	1.64	0.65	99.84
AC-E	2.54	0.06	0.11	0.34	4.51	0.01	70.63	14.76	0.03	6.57	0.37	99.53
MA-N	0.47	0.04	0.01	0.59	3.19	1.4	66.86	17.69	0.04	5.86	1.82	97.6
AGV-2	6.69	0.1	1.05	5.2	2.88	0.48	59.3	16.91	1.79	4.19	1.59	100.18
FK-N	0.09	0.01	0.02	0.11	12.88	0.02	65.37	18.71	0.01	2.59	0.54	99.82
BHVO-2	12.3	0.17	2.73	11.4	0.52	0.27	49.9	13.5	7.23	2.22	-0.7	99.53
MICA-FE	25.65	0.35	2.5	0.43	8.75	0.45	34.4	19.5	4.55	0.3	2	98.88

Analytical precision for major element analysis.
The analysis is based on duplicate samples representing 5 calibrations.

Element	Standard deviation	Absolute % Error	Relative Error -%	Standard Range %
Fe2O3	0.09	-0.03	-3.7	0.09 - 26.65
MnO	0.01	-0.009	4.8	0.01 - 0.35
TiO2	0.07	-0.04	13.7	0 - 2.69
CaO	0.04	0.003	0.2	0.11 - 16.03
K2O	0.07	0.005	-5.6	0.01 - 15.40
P2O5	0.02	-0.02	14.2	0.01 - 1.40
SiO2	0.36	0.06	-0.09	34.40 - 76.31
Al2O3	0.07	0.07	1.3	0.30 - 30.04
MgO	0.18	-0.05	-6.1	0.03 - 43.18
Na2O	0.13	-0.05	-6.8	0.04 - 6.57
LOI	0.26	-0.21	7.1	
Total	0.58	-0.18	0.2	

APPENDIX 5
Section B
Surface XRF data

Sample #	%SiO2	%TiO2	%Al2O3	%Fe2O3	%MnO	%MgO	%CaO	%Na2O	%K2O	%P2O5	%LOI	%TOTAL	
NIM N (REF)	**52.64**	**0.20**	**16.48**	**8.96**	**0.18**	**7.49**	**11.49**	**2.46**	**0.25**	**0.03**	**-0.40**	**99.78**	
NIM N	50.94	0.25	16.12	9.31	0.18	7.67	11.92	2.59	0.38	0.01	-0.12	99.25	
NIM G (REF)	**76.31**	**0.09**	**12.18**	**2.02**	**0.02**	**0.06**	**0.79**	**3.39**	**5.03**	**0.01**	**0.45**	**100.35**	
NIM G	74.50	0.14	12.35	2.00	0.02	0.00	0.70	3.53	5.03	0.00	0.80	99.07	
NIM D (ref)	**38.96**	**0.02**	**0.30**	**17.00**	**0.22**	**43.51**	**0.28**	**0.04**	**0.01**	**0.00**	**-0.93**	**99.41**	
NIM D	40.48	0.08	0.22	17.47	0.22	43.74	0.20	0.01	0.26	0.00	-0.76	101.92	
AII-G (ref)	**46.30**	**0.22**	**29.80**	**3.36**	**0.04**	**1.80**	**15.90**	**1.63**	**0.13**	**0.01**	**0.65**	**99.84**	
AII-G	46.32	0.27	29.80	3.36	0.05	1.90	16.32	1.52	0.38	0.02	0.80	100.74	
MA-II (ref)	**66.60**	**0.01**	**17.62**	**0.47**	**0.04**	**0.04**	**0.59**	**5.84**	**3.18**	**1.39**	**1.82**	**97.60**	
MA-II	64.92	0.06	18.07	0.44	0.04	0.05	0.55	5.97	3.16	1.40	1.70	96.36	

Sample #	%SiO2	%TiO2	%Al2O3	%Fe2O3	%MnO	%MgO	%CaO	%Na2O	%K2O	%P2O5	%LOI	%TOTAL	
K1	74.16	0.20	14.26	1.38	0.01	0.07	1.56	5.85	1.07	0.05	0.88	99.49	
S1	48.00	0.09	30.32	1.42	0.03	1.72	14.39	4.15	0.21	0.00	0.34	100.67	T4093 again
S2	75.29	0.08	13.99	0.31	0.01	0.00	0.41	4.83	5.45	0.00	0.32	100.69	
S3	72.72	0.11	14.08	0.26	0.01	0.00	0.44	5.19	4.87	0.11	0.47	98.26	
S10	71.44	0.07	13.63	0.28	0.01	0.00	0.57	5.25	5.09	0.23	0.32	96.89	
SK1A	77.08	0.08	12.12	0.50	0.01	0.11	1.21	5.46	1.29	0.01	1.14	99.01	
SK1B	75.72	0.08	13.07	0.59	0.01	0.00	0.26	3.31	6.60	0.11	0.34	100.09	
SK1D	68.25	0.07	17.19	0.24	0.02	0.00	1.53	4.80	6.63	0.78	0.50	100.01	
SK1E	73.67	0.08	14.52	0.37	0.03	0.08	1.67	5.31	2.31	0.00	0.88	98.92	
SK2A	69.44	0.09	15.21	0.35	0.04	0.03	1.83	2.42	8.94	0.03	1.50	99.88	
SK2B	76.03	0.08	14.02	0.50	0.01	0.00	0.80	5.47	2.67	0.00	0.59	100.17	
SK2D	74.85	0.07	13.48	0.33	0.01	0.00	0.63	4.22	5.17	0.12	0.51	99.39	
SK2E	73.05	0.12	13.50	0.52	0.01	0.00	0.11	3.11	7.22	0.00	0.31	97.95	
SK4	74.38	0.08	13.25	0.44	0.01	0.05	0.11	4.13	5.89	0.02	0.43	98.79	
SK5A	73.00	0.06	14.30	0.77	0.01	0.00	0.16	4.73	5.73	0.00	0.34	99.10	
SK5B	73.01	0.07	14.38	0.18	0.01	0.00	0.52	5.22	4.33	0.10	0.38	98.20	
SK8	69.95	0.07	15.72	0.28	0.01	0.01	0.19	3.90	7.71	0.01	0.42	98.27	
SK9	72.06	0.09	14.51	0.28	0.01	0.00	0.34	3.77	6.58	0.04	0.47	98.15	
SK12A	74.55	0.13	13.06	0.85	0.01	0.00	0.20	4.59	5.17	0.02	0.41	98.99	
SK12D	76.47	0.10	12.48	0.45	0.01	0.19	0.52	4.47	4.00	0.00	0.52	99.21	
SK12E	73.93	0.09	13.46	0.34	0.02	0.00	0.35	3.69	6.03	0.01	0.39	98.31	
SV1	59.99	0.87	11.46	5.21	0.05	2.62	6.43	2.28	4.27	0.11	5.27	98.56	

Sample #	Rb	Sr	Y	Zr	Nb	Co	Ni	Cu	Zn	TiO2	V	Cr	Ba
	(ppm)	(ppm)	(ppm)	(ppm)	(ppm)	(ppm)	(ppm)	(ppm)	(ppm)	(%)	(ppm)	(ppm)	(ppm)
LLD	**3**	**3**	**3**	**8**	**3**	**6**	**6**	**6**	**6**	**0.01**	**12**	**12**	**20**
NIM G (ref)	**325**	**10**	**143**	**300**	**53**	**nd**	**8**	**12**	**50**	**0.09**	**2**	**12**	**120**
NIM-G	333	12	153	311	52	6	5	12	49	0.10	2	11	121
K1	82	116	23	177	11	8	188	7	7	0.17	23	55	59
S1	401	42	18	266	112	8	192	<6	7	0.13	24	56	101
S2	434	45	20	106	263	7	10	7	7	0.05	<12	<12	95
S3	648	66	22	29	156	<6	7	<6	7	0.06	<12	<12	121
S10	370	47	33	36	12	8	221	6	7	0.03	<12	51	132
SK1A	98	117	11	33	3	6	535	<6	6	0.05	<12	116	56
SK1B	341	60	76	90	<3	7	6	10	<6	0.04	<12	<12	294
SK1D	293	92	108	85	<3	7	171	<6	8	0.04	<12	50	252
SK1E	119	151	12	35	5	7	189	14	9	0.05	<12	57	174
SK2A	975	216	16	<8	49	7	197	8	6	0.06	<12	47	359
SK2B	168	63	10	25	75	6	7	<6	<6	0.05	<12	13	72
SK2D	435	43	44	211	155	8	7	<6	7	0.04	<12	<12	70
SK2E	441	66	7	43	33	6	205	6	7	0.07	<12	47	120
SK4	439	38	24	25	5	7	<6	<6	4	0.05	<12	<12	116
SK5A	517	29	8	18	10	7	706	<6	<6	0.04	<12	123	55
SK5B	280	40	19	23	12	6	10	<6	6	0.03	<12	<12	57
SK8	564	55	14	19	27	10	246	8	7	0.04	<12	51	110
SK9	500	144	16	<8	290	11	229	16	8	0.06	<12	57	275
SK12A	382	18	55	96	503	8	<6	19	9	0.11	56	13	33
SK12D	330	60	13	<8	133	6	<6	<6	6	0.07	<12	<12	130
SK12E	520	54	19	12	196	8	6	27	9	0.05	<12	12	128
SV1	259	190	24	138	19	23	20	18	18	0.71	77	54	300

Sample	Pb	Ga	La	Ce	Sc	Th	As	U
	(ppm)	(ppm)	(ppm)	(ppm)	ppm)	(ppm)	(ppm)	(ppm)
LLD	**9**	**10**	**20**	**20**	**10**	**12**	**12**	**9**
K1	30	20	86	79	<10	207	<12	33
SI	<9	<10	<20	<20	<10	<12	<12	<9
S2	27	24	21	30	<10	20	<12	299
S3	12	28	20	<20	<10	23	<12	97
S10	14	28	21	<20	<10	<12	<12	18
SK1A	12	16	20	<20	<10	93	<12	9
SK1B	22	12	20	25	<10	40	<12	65
SK1D	19	22	42	96	<10	46	<12	11
SK1E	17	21	23	21	<10	36	<12	36
SK2A	18	28	<20	<20	<10	<12	<12	71
SK2B	13	26	<20	<20	<10	62	<12	92
SK2D	19	23	42	62	<10	76	<12	147
SK2E	13	20	<20	<20	<10	29	<12	48
SK4	36	20	<20	<20	<10	31	<12	57
SK5A	<9	25	<20	<20	<10	<12	<12	13
SK5B	11	28	<20	<20	<10	<12	<12	10
SK8	11	28	20	<20	<10	12	<12	42
SK9	39	25	25	35	<10	70	<12	379
SK12A	42	18	19	15	<10	76	<12	250
SK12D	16	21	22	23	<10	18	<12	151
SK12E	30	23	26	34	<10	25	<12	253
SV1	12	16	42	71	24	34	<12	19

APPENDIX 5
Section B
SK Core XRF data for 2007 drilling program

Sample	%SiO2	%TiO2	%Al2O3	%Fe2O3	%MnO	%MgO	%CaO	%Na2O	%K2O	%P2O5	%LOI	%TOTAL
AC-E (ref)	**70.35**	**0.11**	**14.70**	**2.53**	**0.06**	**0.03**	**0.34**	**6.54**	**4.49**	**0.01**	**0.37**	**99.53**
AC-E	71.27	0.14	14.97	2.58	0.06	0.03	0.36	6.65	4.58	0.02	0.40	101.06
NIM G (REF)	**76.31**	**0.09**	**12.18**	**2.02**	**0.02**	**0.06**	**0.79**	**3.39**	**5.03**	**0.01**	**0.45**	**100.35**
NIM G2	75.73	0.13	12.05	1.84	0.02	0.00	0.71	3.21	4.94	0.02	0.80	99.45
N9944	74.74	0.08	14.51	0.49	0.01	0.15	0.52	4.32	5.26	0.09	0.62	100.79
N9947	74.49	0.10	13.60	0.52	0.01	0.18	0.73	4.88	3.83	0.07	0.44	98.85
N9982	74.21	0.08	12.29	0.38	0.01	0.10	0.38	3.14	5.56	0.05	0.45	96.65
N10062	75.32	0.09	14.01	0.40	0.01	0.08	0.78	4.48	4.47	0.12	0.97	100.73
N10158	73.43	0.09	13.80	0.47	0.01	0.14	0.48	4.36	5.22	0.09	0.43	98.52
N10187	73.04	0.10	14.40	0.55	0.02	0.17	1.15	6.26	2.30	0.28	0.56	98.83
N10290	72.28	0.10	14.20	0.49	0.01	0.21	0.85	3.96	5.38	0.09	1.26	98.83
N10343	76.02	0.13	13.27	0.58	0.01	0.11	0.35	3.92	4.91	0.06	0.76	100.12
N10357	74.13	0.08	12.94	0.42	0.01	0.16	0.44	3.88	5.67	0.09	0.54	98.36
N10456	75.34	0.08	13.01	0.36	0.00	0.05	0.74	4.41	4.27	0.12	0.98	99.36

Sample #	Rb	Sr	Y	Zr	Nb	Co	Ni	Cu	Zn	TiO2	V	Cr	Ba
	(ppm)	(ppm)	(ppm)	(ppm)	(ppm)	(ppm)	(ppm)	(ppm)	(ppm)	(%)	(ppm)	(ppm)	(ppm)
LLD	**3**	**3**	**3**	**8**	**3**	**6**	**6**	**6**	**6**	**0.01**	**12**	**12**	**20**
NIM G (ref)	**325**	**10**	**143**	**300**	**53**	**nd**	**8**	**12**	**50**	**0.09**	**2**	**12**	**120**
NIM-G	323	13	131	269	51	6	3	11	49	0.10	4	17	132
DR-N (ref)	**73**	**400**	**28**	**125**	**8**	**35**	**15**	**50**	**145**	**1.09**	**220**	**42**	**385**
DR-N	74	394	27	126	10	31	21	47	142	1.02	188	35	395
N9944	364	35	68	72	35	5	<6	<6	11	0.05	32	124	74
N9947	435	38	10	14	6	<6	<6	<6	8	0.07	18	114	88
N9982	282	41	34	73	17	<6	10	<6	8	0.06	34	140	76
N10062	307	76	13	35	80	<6	<6	<6	9	0.05	21	120	60
N10158	328	60	16	31	132	<6	<6	<6	9	0.06	14	113	108
N10187	132	54	34	21	123	<6	<6	<6	8	0.07	20	168	76
N10290	388	76	14	67	32	<6	<6	<6	10	0.08	20	103	136
N10343	454	33	18	43	164	<6	<6	<6	9	0.09	37	106	89
N10357	527	33	26	51	44	<6	<6	<6	8	0.04	22	161	83
N10456	401	34	30	54	31	<6	<6	<6	8	0.05	19	135	76

Sample	Pb	Ga	La	Ce	Sc	Th	As	U
	(ppm)	(ppm)	(ppm)	(ppm)	(ppm)	(ppm)	(ppm)	(ppm)
LLD	**9**	**10**	**12**	**12**	**10**	**12**	**12**	**9**
N9944	65	26	<12	28	<10	120	<12	978
N9947	12	21	<12	11	<10	14	<12	69
N9982	36	24	<12	23	<10	61	<12	436
N10062	13	29	<12	19	<10	18	<12	108
N10158	16	25	15	34	<10	16	<12	179
N10187	18	27	21	40	<10	14	<12	175
N10290	11	25	<12	26	<10	49	<12	78
N10343	15	25	<12	24	<10	31	<12	152
N10357	9	26	17	32	<10	27	<12	65
N10456	10	24	14	38	<10	34	<12	48

APPENDIX 5
Section C
SK4 historic core

Sample No.	%SiO2	%TiO2	%Al2O3	%Fe2O3	%MnO	%MgO	%CaO	%Na2O	%K2O	%P2O5	%LOI	%TOTAL
AGV-2 (ref)	**59.30**	**1.05**	**16.91**	**6.69**	**0.10**	**1.79**	**5.20**	**4.19**	**2.88**	**0.48**	**1.59**	**100.18**
AGV-2	57.43	1.00	16.86	6.93	0.10	1.73	5.12	4.19	2.90	0.48	1.35	98.09
NIM G (REF)	**76.31**	**0.09**	**12.18**	**2.02**	**0.02**	**0.06**	**0.79**	**3.39**	**5.03**	**0.01**	**0.45**	**100.35**
NIM G	77.21	0.16	12.38	1.86	0.03	0.00	0.86	3.50	5.10	0.03	0.80	101.93
NIM N (REF)	**52.64**	**0.20**	**16.48**	**8.96**	**0.18**	**7.49**	**11.49**	**2.46**	**0.25**	**0.03**	**-0.40**	**99.78**
NIM N	52.34	0.22	16.06	9.05	0.18	7.55	11.35	2.60	0.33	0.02	-0.12	99.58
NIM S (REF)	**63.63**	**0.00**	**17.34**	**1.40**	**0.01**	**0.46**	**0.68**	**0.43**	**15.35**	**0.12**	**0.28**	**99.70**
NIM S	61.53	0.08	17.40	1.22	0.02	0.37	0.69	0.46	15.17	0.12	0.34	97.40
SK4/43 26I	73.47	0.07	14.01	0.23	0.02	0.11	0.46	3.63	6.10	0.07	0.60	98.77
SK4/43 25I	72.67	0.08	13.92	0.26	0.02	0.15	0.56	4.95	4.60	0.06	0.87	98.14
SK4/43 20I	63.39	0.53	14.61	5.88	0.09	2.70	2.80	0.10	5.22	0.35	2.74	98.41
SK4/43 20-2	70.62	0.06	13.65	0.16	0.01	0.10	2.16	5.24	4.60	0.10	0.94	97.64
SK4/43 22I	71.68	0.10	12.10	2.19	0.31	0.38	3.81	3.58	2.89	0.10	1.17	98.31
SK4/43 8I	59.29	0.79	18.68	3.92	0.07	3.02	2.00	5.31	3.29	0.20	1.52	98.09
SK4/43 27I	72.14	0.08	13.08	0.27	0.03	0.13	1.60	3.81	5.49	0.04	1.47	98.14
SK4/43 13I	76.05	0.08	13.98	0.16	0.02	0.12	0.70	4.97	4.62	0.04	0.71	101.45
SK4/43 18I	74.43	0.10	13.37	0.26	0.02	0.19	0.58	4.65	4.23	0.08	0.56	98.47

Sample #	Rb	Sr	Y	Zr	Nb	Co	Ni	Cu	Zn	TiO2	V	Cr	Ba	Sample #	Pb	Ga	La	Ce	Sc	Th	As	U
	(ppm)	(ppm)	(ppm)	(ppm)	(ppm)	(ppm)	(ppm)	(ppm)	(ppm)	(%)	(ppm)	(ppm)	(ppm)		(ppm)	(ppm)	(ppm)	(ppm)	(ppm)	ppm)	ppm)	ppm)
LLD	**3**	**3**	**3**	**8**	**3**	**6**	**6**	**6**	**6**	**0.01**	**12**	**12**	**20**	**LLD**	**9**	**12**	**12**	**12**	**10**	**12**	**12**	**9**
NIM G (ref	**325**	**10**	**143**	**300**	**53**	**nd**	**8**	**12**	**50**	**0.09**	**2**	**12**	**120**									
NIM-G	324	13	139	269	52	4	3	9	48	0.10	2	6	122									
NIM-S (ref	**530**	**62**	**1**	**20**	**nd**	**3**	**7**	**19**	**10**	**0.05**	**10**	**12**	**2420**									
NIM-S	520	63	2	20	3	10	5	20	16	0.03	13	11	2068									
NIM-P (ref	**4**	**32**	**5**	**15**	**nd**	**110**	**555**	**18**	**100**	**0.20**	**230**	**23950**	**46**									
NIM-P	8	36	6	17	6	107	563	17	107	0.22	228	21681	65									
NIM-D (ref	**nd**	**3**	**nd**	**8**	**nd**	**208**	**2040**	**10**	**90**	**0.02**	**40**	**2870**	**10**									
NIM-D	6	6	4	12	5	232	2030	9	92	0.02	40	2870	10									
SK4/43 26'	458	34	34	15	12	<6	<6	<6	155	0.03	22	132	77	**SK4/43 261**	20	20	<12	35	<10	70	<12	40
SK4/20 25'	314	26	51	23	26	<6	<6	<6	165	0.04	24	148	36	**SK4/20 251**	28	21	<12	19	<10	114	<12	273
SK4/4 201	541	52	147	61	95	9	19	30	152	0.48	235	135	87	**SK4/4 201**	165	31	17	37	15	149	<12	1499
SK4/41 21-	369	20	34	66	112	<6	7	<6	259	0.03	26	144	33	**SK4/41 21-221**	24	25	<12	19	<10	44	<12	189
SK4/4 221	257	90	41	21	47	<6	<6	6	145	0.05	37	118	95	**SK4/4 221**	88	23	<12	30	<10	86	<12	662
SK4/37 81	643	63	86	128	88	10	28	6	1150	0.88	301	153	77	**SK4/37 81**	99	32	36	65	27	88	<12	803
SK4/43 27'	429	35	32	15	13	<6	<6	<6	157	0.04	29	130	72	**SK4/43 271**	28	21	14	35	<10	37	<12	48
SK4/43 13'	351	25	25	64	128	<6	<6	6	417	0.03	21	113	35	**SK4/43 131**	27	24	<12	17	<10	44	<12	192
SK4/43 18'	394	24	36	79	120	6	7	<6	275	0.07	39	146	41	**SK4/43 181**	26	28	<12	20	<10	50	<12	247

APPENDIX 6
SEM element mapping results

Table 1: SEM element mapping results and the suggested mineral name.

Sample No	Pic No	Grain No	U	Nb	Ti	Ta	Si	Th	Ce	Zr	Fe	Mineral Name	Diameter	Add Features
SK1E	7	4			M				T			Aeschynite-Ce	110	
SK1E	7	14			T				T			Aeschynite-Ce	100	
SKZE	1	11			VL				L			Aeschynite-Ce	50	Nodule Si.
SK1E	2				T				T			Aeschynite-Ce	30	
SK1E	2				T				T			Aeschynite-Ce	30	
													320	
SK1E	5	9					H		T		L	Allanite-Ce	50	
													50	
S10	2	9		M	M							betafite	120	surrounded by 12 Si
S10	4	6		H	H						VL	Betafite	150	
S10	4	17	M	H	H							Betafite	10	
S10	6	2	L	M	M							betafite	60	Si, Fe around
SK1B	4	9	T		H							betafite	100	Si, U surround
SK1B	4	14	L		M							betafite	100	22 Si surround it
SK1B	5	18	L		H							betafite	35	
SK1E	6	7			M							betafite	60	
SK1B	6	13	L	M	M							Betafite	100	
SK1E	7	1	H	H	H							betafite	50	
S3	2	6		M	H							betafite	50	
S3	2	7	L	M	M							betafite	100	
S3	2	11		M	H							betafite	120	Si noddule CENTRE
S3	2	13		M	H							betafite	60	Si surround
S3	2	14		M	M							betafite	20	
S3	2	15		M	M							betafite	30	Surrounded by Si
S3	6	5		M	H							betafite	100	
S3	2	16		M	M							betafite	25	
S3	6	7		M	H							betafite	100	
S3	6	8		M	H							betafite	100	5 Si noddules
S3	6	9		M	H							betafite	55	
S3	6	11		M	H							betafite	200	
S3	6	12		M	H							betafite	105	
S3	7	4	L	L	L							betafite	60	Surrounded by Si
S3	7	5		M	H							betafite	50	
S3	7	8		M	H							betafite	60	
S3	7	9		M	H							betafite	15	
S3	7	11		M	H							betafite	80	
S3	7	14		M	H							betafite	85	Surrounded by Si, Fe
S3	7	15		M	H							betafite	110	
S3	1	1		M	H							betafite	90	
S3	1	8		M	H							betafite	90	
S3	3	2	M	M	M							betafite	90	Si around
S3	3	3		M	H							betafite	95	Si on nodule edge
S3	3	4		M	H							betafite	50	
SK8	1	7		L	L							betafite	140	
S3	3	6		M	H							betafite	100	
S3	3	8		M	H							betafite	75	Si on edge noddules
S3	3	9		M	H							betafite	75	
S3	3	11		M	H							betafite	105	
S3	3	12		M	H							betafite	95	

S3	4	1		M	H							betafite	70	
S3	4	2		M	H							betafite	150	Si fracture filled
S3	4	3		M	H							betafite	50	
S3	4	6		M	H							betafite	125	
S3	4	7		M	H							betafite	60	
S3	4	8		M	H							betafite	95	
S3	4	9		M	H							betafite	95	
S3	4	13		M	H							betafite	20	
S3	4	14		M	H							betafite	75	
S3	4	16		L	H							betafite	75	
S3	5	4		M	H							betafite	100	
S3	5	7		M	H							betafite	80	
S3	5	8		M	H							betafite	100	
S3	5	9		M	H							betafite	100	
S3	5	15		M	H							betafite	45	
S3	5	16		M	H							betafite	20	
SK5B	3	7		M	H							betafite	155	
SK5B	3	8		M	H							betafite	180	
SK1B	5	5		M	H							betafite	35	
SKZE	2	10	VL	VL	VL		VL					betafite	50	
SKZE	5	2	H	M	M							betafite	100	
S10	7	10	VL	M	H							betafite	50	
SKZE	5	8	H	M	M							betafite	160	
SK4	1	6	L	M	H							betafite	100	
SK4	1	8	L	M	M							betafite	160	
SK1B	7	9		M	H							Betafite	50	U, Si in 9 centre
SK1B	1?	14		M	H		T					Betafite	15	
S3	3	1		M	H							Betafite	100	
SK4	1	9		M	H							betafite	145	
SK4	1	10	L	L	H							betafite	120	
SK4	1	13		L	M							betafite	20	
SK1B	7	12	T	M	H						L	betafite	40	
S10	4	3		M	H						L	betafite	100	
SK1B	5	13		M	H						H	betafite	35	
S3	2	12		L	T						H	betafite	10	
SK12E	4	1		M	M							Betafite	100	
S1	2	3	VL		L						H	betafite	70	
SK1E	7	5	M	L	M						H	betafite	100	
SK12E	3	5		T	L						H	betafite	70	
													6540	80
SK1A	3	6							L			Cebaite-Ce	50	
K1	7	3							L			Cebaite-Ce	80	contain Si around
SK2A	7								M			Cebaite-Ce	40	
													170	3
SK4	6	12		M	H		M				L	Davidite	160	
SV1	4	7			L		L				M	Davidite	40	Ti cracks
SKZE	3	16			VL		H				H	Davidite	30	
SKZE	3	17			VL		L				L	Davidite	50	Stacked with 16
SK4	3	7	M		H		H				L	Davidite	150	contain stripes of 15
SKZE	2	1			VL		T				H	Davidite	150	Ti cracks
SKZE	2	2			VL		T				H	Davidite	130	Ti cracks
SKZE	2	3			VL		T				H	Davidite	160	Ti cracks
SKZE	2	4			VL		T				H	Davidite	200	Ti cracks
SKZE	2	5			VL		T				H	Davidite	110	Ti cracks
SKZE	2	9			VL		VL				H	Davidite	100	Ti cracks
S10	4	19	L	L	L		H				L	Davidite	20	
SK1E	4	14			M		H				L	Davidite	30	

SK1E	4	15			M		M				L	Davidite	85	
SK1E	5	1			H		H				L	Davidite	40	
SK1E	5	2			L		H				L	Davidite	40	
SK1E	5	7			M		M				M	Davidite	30	
SK9	7	6	VL	L			VL				H	Davidite	180	
SK12E	2	17		T	VL		H				H	Davidite	70	
SK12E	2	18		T	VL		H				H	Davidite	30	17 and 18 are layered
SK12E	3	4		VL	T		L		T		H	Davidite	100	
SK12E	7	8	L		L		M				H	Davidite	100	
SK9	4	11	VL	M	L		L				H	Davidite	150	
SK2D	5	6	L	L	VL		L				H	Davidite	100	
													2255	23
SK1A	1	2					M		L			Dollaseite-Ce	55	Ti surrounded
SK1E	6	12					M		L			Dollaseite-Ce	45	
SK1E	1	7					M		M			Dollaseite-Ce	60	
S1	1	1		VL			L		M			Dollaseite-Ce	110	Si stains
S1	1	3		VL			L		M			Dollaseite-Ce	90	Si surround
SK1E	5	11	L				M		VL			Dollaseite-Ce	150	
SK1E	6	6					M		L			Dollaseite-Ce	60	
SK12D	4	10					L		VL			Dollaseite-Ce	150	
SK12D	4	13					H		T			Dollaseite-Ce	50	
SK12D	6	5					H		VL		T	Dollaseite-Ce	130	Fe staining
SK12D	2	22					H		VL			Dollaseite-Ce	50	
SK1A	3	14					H		L			Dollaseite-Ce	60	
													1010	11
SK2D	5	11									H	Fe oxide/hydroxide	40	Ti, Si, Nb, U surrounds
SV1	1	7									H	Fe oxide/hydroxide	100	Si surround
SV1	1	10									H	Fe oxide/hydroxide	110	Ti cracks
SV1	1	11									H	Fe oxide/hydroxide	150	Ti cracks
SV1	1	12									H	Fe oxide/hydroxide	5	
SK9	3	3									H	Fe oxide/hydroxide	40	Fe oxide on around
SK9	3	18									H	Fe oxide/hydroxide	40	Fe oxide on around
SK9	6	7									H	Fe oxide/hydroxide	200	
SK9	6	9									H	Fe oxide/hydroxide	130	
SK9	6	16									H	Fe oxide/hydroxide	100	
S10	3	14									H	Fe-hydro/oxide	5	
SK1B	4	2									H	Fe-oxide/hydroxide	60	
SK1B	4	3									H	Fe-oxide/hydroxide	50	
SK1B	4	4									H	Fe-oxide/hydroxide	50	
SK1B	4	5									H	Fe-oxide/hydroxide	50	
SK1B	4	13									H	Fe-oxide/hydroxide	75	
SK1B	4	15									M	Fe-oxide/hydroxide	30	
SK1B	4	17									H	Fe-oxide/hydroxide	110	
SK1B	4	18									H	Fe-oxide/hydroxide	100	
SK1B	4	19									H	Fe-oxide/hydroxide	50	

SK1B	4	21									H	Fe-oxide/hydroxide	15	
SK1B	5	1									H	Fe-oxide/hydroxide	60	
SK1B	5	2									H	Fe-oxide/hydroxide	120	
SK1B	5	3									H	Fe-oxide/hydroxide	140	
SK1B	5	4									H	Fe-oxide/hydroxide	90	
SK1B	5	6									H	Fe-oxide/hydroxide	55	
SK1B	5	7									H	Fe-oxide/hydroxide	80	Si alterations
SK1B	5	9									H	Fe-oxide/hydroxide	90	Has Si attached to it
SK1B	5	10									H	Fe-oxide/hydroxide	55	
SK1B	5	14									H	Fe-oxide/hydroxide	100	
SK1B	5	15									H	Fe-oxide/hydroxide	125	
SK1B	5	16									H	Fe-oxide/hydroxide	90	
SK1B	5	17									H	Fe-oxide/hydroxide	35	
SK1B	5	20									H	Fe-oxide/hydroxide	15	
SK1B	6	3									H	Fe-oxide/hydroxide	125	
SK1B	6	5									H	Fe-oxide/hydroxide	10	
SK1B	6	8									H	Fe-oxide/hydroxide	35	
SK1B	6	10									H	Fe-oxide/hydroxide	90	
SK1B	6	11									H	Fe-oxide/hydroxide	10	
SK1B	6	12									H	Fe-oxide/hydroxide	40	
SK1B	6	17									H	Fe-oxide/hydroxide	90	
SK1B	6	19									H	Fe-oxide/hydroxide	30	
SK1B	7	1									H	Fe-oxide/hydroxide	60	
SK1B	7	2									H	Fe-oxide/hydroxide	100	
SK1B	7	6									H	Fe-oxide/hydroxide	90	
SK1B	7	8									H	Fe-oxide/hydroxide	50	
SK1B	3	1									H	Fe-oxide/hydroxide	55	
SK1B	3	2									H	Fe-oxide/hydroxide	50	
SK1B	3	3									H	Fe-oxide/hydroxide	35	
SK1B	3	4									H	Fe-oxide/hydroxide	60	
SK1B	3	6									H	Fe-oxide/hydroxide	20	
SK1B	3	8									H	Fe-oxide/hydroxide	15	
SK1B	3	10									H	Fe-oxide/hydroxide	100	
SK1B	3	11									H	Fe-oxide/hydroxide	40	
SK1B	3	12									H	Fe-oxide/hydroxide	60	
SK1B	3	14									H	Fe-oxide/hydroxide	30	
SK1E	4										M	fe-	15	

												oxide/hydroxide		
SK1E	5	17									T	Fe-oxide/hydroxide	50	
SK1E	5										M	Fe-oxide/hydroxide	10	
S1	2	6									H	Fe-oxide/hydroxide	45	
S1	4	2									H	Fe-oxide/hydroxide	100	Ti cracks
S1	4	3									H	Fe-oxide/hydroxide	80	Ti cracks
S1	4	4									H	Fe-oxide/hydroxide	150	Ti cracks
S1	4	5									H	Fe-oxide/hydroxide	25	Ti cracks
S1	4	6									H	Fe-oxide/hydroxide	50	Ti cracks
S1	4	7									H	Fe-oxide/hydroxide	95	Ti cracks
S1	4	8									H	Fe-oxide/hydroxide	60	Ti cracks
S1	4	9									H	Fe-oxide/hydroxide	75	Ti cracks
S1	4	10									H	Fe-oxide/hydroxide	95	Ti cracks
S1	4	11									H	Fe-oxide/hydroxide	75	Ti cracks
S3	3	22									H	Fe-oxide/hydroxide	30	
S3	3	23									H	Fe-oxide/hydroxide	30	
S1	5	9									H	Fe-oxide/hydroxide	25	
S1	5	10									H	Fe-oxide/hydroxide	50	
S1	5	15									H	Fe-oxide/hydroxide	10	
S3	5	6									H	Fe-oxide/hydroxide	50	
SK5B	4	11									H	Fe-oxide/hydroxide	50	
SV1	6	2									H	Fe-oxide/hydroxide	160	
SV1	6	3									H	Fe-oxide/hydroxide	155	Ti cracks
SV1	6	4									H	Fe-oxide/hydroxide	100	Ti cracks
SV1	6	5									H	Fe-oxide/hydroxide	50	Ti cracks
SV1	6	6									H	Fe-oxide/hydroxide	60	Ti cracks
SV1	6	7									H	Fe-oxide/hydroxide	100	
SV1	4	1									H	Fe-oxide/hydroxide	180	
SV1	4	2									H	Fe-oxide/hydroxide	160	Ti cracks
SV1	4	3									H	Fe-oxide/hydroxide	100	
SV1	4	4									H	Fe-oxide/hydroxide	90	Ti cracks
SV1	4	8									H	Fe-oxide/hydroxide	60	
SV1	4	9									H	Fe-oxide/hydroxide	55	
SV1	2	17									H	Fe-oxide/hydroxide	110	
SK2A	3	18									H	Fe-oxide/hydroxide	50	
K1	2										L	Fe-oxide/hydroxide	5	
K1	2										L	Fe-oxide/hydroxide	5	

K1	2										L	Fe-oxide/hydroxide	5	
K1	6	10									H	Fe-oxide/hydroxide	40	
K1	6	11									H	Fe-oxide/hydroxide	40	
K1	6	12									H	Fe-oxide/hydroxide	35	
K1	6	13									H	Fe-oxide/hydroxide	30	
S2	1										H	Fe-oxide/hydroxide	60	
S2	1										H	Fe-oxide/hydroxide	50	
S2	1										H	Fe-oxide/hydroxide	30	
S2	1										H	Fe-oxide/hydroxide	30	
S2	1										H	Fe-oxide/hydroxide	30	
S2	1										H	Fe-oxide/hydroxide	30	
S2	1										H	Fe-oxide/hydroxide	30	
S2	1										H	Fe-oxide/hydroxide	30	
SK8	7	11									H	Fe-oxide/hydroxide	10	
SV1	5	10									H	Fe-oxide/hydroxide	100	Ti cracks
SV1	5	11									H	Fe-oxide/hydroxide	100	
SV1	5	12									H	Fe-oxide/hydroxide	150	Ti cracks
SV1	3	1									H	Fe-oxide/hydroxide	50	
SV1	3	4									H	Fe-oxide/hydroxide	170	Ta cracks
SV1	3	5									H	Fe-oxide/hydroxide	100	Ta cracks
SV1	3	6									H	Fe-oxide/hydroxide	110	
SV1	3	8									M	Fe-oxide/hydroxide	100	
SKZE	3	12									H	Fe-oxide/hydroxide	30	
													7730	115
SK5B	3	4					H				M	Fe-silicate	100	
SK5B	3	5					H				M	Fe-silicate	150	
SK1B	7	14					H				H	Fe-silicate	75	
SK1E	4	8					H				L	Fe-silicate	40	
SK1E	4	22					M				L	Fe-silicate	20	
SK1E	6	13					H				M	Fe-silicate	85	
SK2A	3	2					H				L	Fe-silicate	55	
S3	7						H				H	Fe-silicate	10	
SK5B	6	11					H				M	Fe-silicate	20	Nodule 3
SV1	4	6					H				L	fe-silicate	50	
SV1	3	9					L				H	fe-silicate	100	
SKZE	4	2					H				L	Fe-silicate	20	around 7
SKZE	4	10					M				H	Fe-silicate	100	
SK12E	4	8					L				H	Fe-silicate	100	
SK4	7	6					M				H	Fe-silicate	180	
S10	3	16					M				H	Fe-silicate	10	
S10	3	17					M				H	Fe-silicate	10	
S10	3	18					M				H	Fe-silicate	10	
S1	2	9					M				M	Fe-silicate	50	
SK2D	6	12					H				M	Fe-silicate	30	around 11

SK4	3	14					M				H	Fe-silicate	50	
SK4	7	8					H				M	Fe-silicate	100	
SK1B	4	10					M				M	Fe-silicate	90	
SK1E	5	16					H				T	Fe-silicate	50	
SK1A	3	9					VL				H	Fe-silicates	50	
K1	5	5					L				H	Fe-silicates	50	Contain Si around
K1	5	6					L				H	Fe-silicates	50	Contain Si around
K1	5	7					L				H	Fe-silicates	50	Contain Si around
K1	5	8					L				H	Fe-silicates	50	Contain Si around
K1	5	9					L				H	Fe-silicates	50	Contain Si around
K1	5	10					L				H	Fe-silicates	50	Contain Si around
K1	5						L				H	Fe-silicates	50	Contain Si around
K1	5						L				H	Fe-silicates	50	Contain Si around
K1	5						L				H	Fe-silicates	50	Contain Si around
K1	7	11					L				H	Fe-silicates	150	
S2	3	17					H				M	Fe-silicates	5	arround 13
SK8	3	8					M				M	Fe-silicates	15	surrounded by 9
													2175	36
SK1B	7	11			H						L	Ilmenite	50	
SK1B	4	22			H						H	Ilmenite	30	
SK1B	7	15			H						L	Ilmenite	15	
SK1E	4	2			L						L	ilmenite	30	
SK1E	4	19			L						L	ilmenite	60	Si staining
S1	3	7			T						H	Ilmenite	90	Contain Ti cracks
S1	3	8			T						H	Ilmenite	95	Contain Ti cracks
S1	3	9			T						H	Ilmenite	60	Contain Ti cracks
S1	3	10			T						H	Ilmenite	100	Contain Ti cracks
S1	3	11			T						H	Ilmenite	110	Contain Ti cracks
S1	3	12			T						H	Ilmenite	50	Contain Ti cracks
S1	3	13			T						H	Ilmenite	30	Contain Ti cracks
S1	3	14			T						H	Ilmenite	150	
S1	3	15			T						H	Ilmenite	50	
S1	3	16			T						H	Ilmenite	10	
S1	3	17			T						H	Ilmenite	30	
S1	2	7			L						H	Ilmenite	20	
SV1	1	8			VL						H	Ilmenite	80	Ti cracks
SV1	1	9			VL						H	Ilmenite	50	Ti cracks, Si surround
S1	6	5			T						H	Ilmenite	105	Ti cracks
S1	6	6			T						H	Ilmenite	50	Ti cracks
S1	6	7			T						H	Ilmenite	90	Ti cracks
S1	6	8			T						H	Ilmenite	80	Ti cracks
S1	6	9			T						H	Ilmenite	70	Ti cracks
S1	6	10			T						H	Ilmenite	65	Ti cracks
S1	5	1			L						H	Ilmenite	140	
S1	5	2			L						H	Ilmenite	60	Ti cracks
S1	5	3			L						H	Ilmenite	100	Ti cracks
S1	5	5			L						H	Ilmenite	100	Ti cracks
S1	5	3			L						H	Ilmenite	150	
S1	5	4			L						H	Ilmenite	75	Ti cracks
S1	5	5			L						H	Ilmenite	140	Ti cracks
S1	5	7			L						H	Ilmenite	100	Ti cracks
SV1	6	1			M						H	ilmenite	100	Ti cracks
SV1	5	7			L						H	ilmenite	150	
SV1	5	8			L						H	ilmenite	100	
SV1	5	9			L						H	ilmenite	150	
SV1	4	5			L						H	ilmenite	100	Ti cracks
SV1	3	2			L						H	Ilmenite	60	
SV1	3	3			M						H	Ilmenite	150	Ta cracks

SV1	3	7			L						H	Ilmenite	50	
SV1	3	10			L						H	Ilmenite	150	Ta cracks
SV1	2	12			L						H	Ilmenite	150	Ta cracks
SV1	2	13			VL						H	Ilmenite	120	
SV1	2	16			L						H	Ilmenite	100	
SV1	2	18			L						H	Ilmenite	50	
SV1	2	19			L						H	Ilmenite	40	
SKZE	7	3			L						H	ilmenite	100	Ti cracks
SKZE	7	4			L						H	ilmenite	150	Ti cracks
SKZE	7	5			L						H	ilmenite	150	Ti cracks/ Si around
SKZE	7	6			L						H	ilmenite	150	Ti cracks
SKZE	7	7			L						H	ilmenite	70	Ti cracks
SKZE	7	8			L						H	ilmenite	100	Ti cracks
SKZE	7	9			L						H	ilmenite	110	Ti cracks/ Si around
SKZE	7	10			L						H	ilmenite	80	Ti cracks
SKZE	7	14			L						H	ilmenite	60	Si around
SKZE	3	1			VL						H	Ilmenite	100	
SKZE	3	2			VL						H	Ilmenite	140	
SKZE	3	3			VL						H	Ilmenite	120	
SKZE	3	4			VL						H	Ilmenite	100	
SKZE	3	5			VL						H	Ilmenite	100	
SKZE	3	6			VL						H	Ilmenite	150	
SKZE	3	7			VL						H	Ilmenite	100	
SKZE	3	8			VL						H	Ilmenite	110	
SKZE	3	9			VL						H	Ilmenite	50	
SKZE	3	10			VL						H	Ilmenite	150	
SKZE	3	11			VL						H	Ilmenite	90	
SKZE	3	13			H						L	Ilmenite	40	at bottom of 9
SKZE	2	6			VL						H	Ilmenite	50	Ti cracks
SKZE	2	7			VL						H	Ilmenite	50	Ti cracks
SKZE	2	8			VL						H	Ilmenite	40	Ti cracks
SK12E	7	15			L						H	ilmenite	200	contain rutile cracks
SK12E	7	18			L		T				H	ilmenite	150	contain rutile cracks
SK9	4	14			L						H	Ilmenite	90	contain rutile cracks
SK9	5	19			L						H	Ilmenite	100	
SK9	5	20			M						H	Ilmenite	150	
K1	2	3			L						H	ilmenite	50	
K1	2	4			L						H	ilmenite	50	
K1	3	4			VL						H	ilmenite	50	
K1	3	5			VL						H	ilmenite	50	
K1	3	6			VL						H	ilmenite	35	
K1	3	7			VL						H	ilmenite	30	
K1	3	8			VL						H	ilmenite	15	
K1	3	9			VL						H	ilmenite	15	
K1	4	4			M						H	ilmenite	50	Si arround the grains
K1	4	5			M						H	ilmenite	50	Si arround the grains
K1	4	6			M						H	ilmenite	50	Si arround the grains
K1	4	7			M						H	ilmenite	50	Si arround the grains
K1	4	8			M						H	ilmenite	50	Si arround the grains
K1	4	9			M						H	ilmenite	10	Si arround the grains
K1	7	7			L						H	ilmenite	50	
K1	7	8			L						H	ilmenite	100	
K1	7	9			L						H	ilmenite	70	
SK12A	1				M						H	ilmenite	30	
SK12A	1				M						H	ilmenite	30	
SK12A	1				M						H	ilmenite	30	
SK12A	1				M						H	ilmenite	30	
SK12A	1				M						H	ilmenite	30	
SK12A	1				M						H	ilmenite	30	

SK12A	3				M						H	ilmenite	30	
SK12A	3				M						H	ilmenite	30	
SK12A	3				M						H	ilmenite	30	
SK12A	3				M						H	ilmenite	30	
SK12A	3				M						H	ilmenite	30	
SK12A	3				M						H	ilmenite	30	
SK12A	3				M						H	ilmenite	30	
SK12A	4	5			L						H	ilmenite	30	
SK12A	4	6			L						H	ilmenite	30	
SK12A	4	7			L						H	ilmenite	30	
SK12A	4	8			L						H	ilmenite	30	
SK12A	4	9			L						H	ilmenite	30	
SK12A	4	10			L						H	ilmenite	30	
SK12A	4	11			L						H	ilmenite	30	
SK12A	4	12			L						H	ilmenite	30	
SK12A	5				VL						H	ilmenite	80	
SK12A	5				VL						H	ilmenite	50	
SK12A	5				VL						H	ilmenite	35	
SK12A	5				VL						H	ilmenite	35	
SK12A	5				VL						H	ilmenite	35	
SK12A	5				VL						H	ilmenite	30	
SK12A	5				VL						H	ilmenite	30	
SK12A	5				VL						H	ilmenite	35	
SK12A	5				VL						H	ilmenite	35	
SK12A	5				VL						H	ilmenite	35	
SK12A	6				L						H	ilmenite	70	
SK12A	6				L						H	ilmenite	45	
SK12A	6				L						H	ilmenite	45	
SK12A	6				L						H	ilmenite	45	
SK12A	6				L						H	ilmenite	45	
SK12A	6				L						H	ilmenite	30	
SK12A	7				VL						H	ilmenite	60	
SK12A	7				VL						H	ilmenite	50	
SK12A	7				VL						H	ilmenite	45	
SK12A	7				VL						H	ilmenite	45	
SK12A	7				VL						H	ilmenite	45	
SK12A	7				VL						H	ilmenite	45	
SK12A	7				VL						H	ilmenite	45	
SK12A	7				VL						H	ilmenite	25	
SK12A	7				VL						H	ilmenite	25	
SK8	3	9			M						H	ilmenite	90	
													9515	140
SK1E	5	4	L		L		M		T		T	Khristovite-Ce	100	
SKZE	6	8			L		L		VL			Khristovite-Ce	150	
SKZE	5	6			H		L		VL			Khristovite-Ce	140	
SK12D	3	14		T	L		L		VL			Khristovite-Ce	100	Contain U-silicates
SK12D	4	11			H		H		L			Khristovite-Ce	100	
SK12E	6	8			L		L		VL			Khristovite-Ce	160	
													750	7
SK1E	5	7	L				M	L	VL			monazite	150	
SK1A	4	1	VL	T			M	VL	T			monazite	150	
													300	2
SK2D	5	9		M	L		L		M			Nacareniobsite-Ce	100	
SK2D	7	11		M	L		L		M			Nacareniobsite-Ce	100	
SK4	3	8		L	VL		L		M		L	Nacareniobsite-	100	

												Ce		
SK4	6	4		M			L		L			Nacareniobsite-Ce	160	
K1	3	3		T			M		T			Nacareniobsite-Ce	30	
K1	5	3		VL			L		T			Nacareniobsite-Ce	50	
K1	5	4		VL			L		L			Nacareniobsite-Ce	50	
K1	6	3		VL			M	T	T			Nacareniobsite-Ce	50	
K1	6	4		VL			M	T	L			Nacareniobsite-Ce	45	
SK2D	2			L			T	T	L			Nacareniobsite-Ce	50	
SK2D	2			L			T	T	L			Nacareniobsite-Ce	50	
SK8	4	7		L			L		L			Nacareniobsite-Ce	20	
SK2A	1	2		T			T		VL			Nacareniobsite-Ce	30	
K1	2	5		VL			L		L			Nacareniobsite-Ce	30	
													865	14
S10	4	18		M	M				M			Niobo-Aeschynite-Ce	6	
SK2D	5	6		M	L				H			Niobo-Aeschynite-Ce	90	
SK1D	4	16		M	L				M			Niobo-Aeschynite-Ce	60	
SK1D	5	10		M	L				H			Niobo-Aeschynite-Ce	50	Si surround
SK4	2	1		M	L				M			Niobo-Aeschynite-Ce	100	
K1	4	1		VL	T			T	T			Niobo-Aeschynite-Ce	100	
													406	6
S10	2	34		M			M			L		Niobokuleskite	10	
S10	3	1		H	T		H			T		Niobokuleskite	120	
S10	4	11		H			H			T		Niobokuleskite	150	3 noddules of U in 19
SK1B	6	15		H			H			L		Niobokuleskite	160	
SK1B	6	18		H			H			L		Niobokuleskite	50	
SK1B	7	4		H			H			T		Niobokuleskite	90	
SK1E	4	11	H	H			H			L		Niobokuleskite	105	
SK1E	4	21	H	H			H			L		Niobokuleskite	20	
SK5B	2	1		H			H			L		Niobokuleskite	50	
SKZE	2	12		H			H			VL		Niobokuleskite	140	
SKZE	5	1	VL	H			H			L		Niobokuleskite	160	
SK12D	2	18		H			H			L		Niobokuleskite	90	
SK12D	5	1		H			H			VL		Niobokuleskite	225	
SK12D	6	4		H			H			VL		Niobokuleskite	150	
SK12D	6	12		H			H			T		Niobokuleskite	150	
SK12E	5	1	T	H			H			VL		Niobokuleskite	150	
SK12E	2	7		H	T		H			VL		Niobokuleskite	170	
SK2D	7	4		H			H			L		Niobokuleskite	200	
SK2D	7	5		H			H			L		Niobokuleskite	200	
SK1A	3	1	T	H			H			T		Niobokuleskite	65	
SK1A	5	1		H			H			VL		Niobokuleskite	65	
SK1A	6	2		H			H			L		Niobokuleskite	65	
K1	2	2		H			H			L		Niobokuleskite	50	
K1	4	3		H						L		Niobokuleskite	65	
K1	5	1		H			H			VL		Niobokuleskite	65	
K1	6	1		H			H			VL		Niobokuleskite	35	
K1	6	2		H			H			L		Niobokuleskite	25	

K1	7	1		H			H			L		Niobokuleskite	60	
S2	3	1		H			H			VL		Niobokuleskite	100	
S2	3	2		H			H			VL		Niobokuleskite	60	
S2	3	3		H			H			VL		Niobokuleskite	45	
S2	3	4		H			H			VL		Niobokuleskite	45	
S2	3	5		H			H			VL		Niobokuleskite	45	
S2	4			H			H			VL		Niobokuleskite	80	
S2	4			H			H			VL		Niobokuleskite	40	
S2	4			H			H			VL		Niobokuleskite	35	
S2	4			H			H			VL		Niobokuleskite	35	
S2	4			H			H			VL		Niobokuleskite	35	
S2	4			H			H			VL		Niobokuleskite	35	
S2	4			H			H			VL		Niobokuleskite	35	
S2	5			H			H			VL		Niobokuleskite	60	
S2	5			H			H			VL		Niobokuleskite	30	
S2	5			H			H			VL		Niobokuleskite	30	
S2	5			H			H			VL		Niobokuleskite	30	
S2	6			H			H			VL		Niobokuleskite	70	
S2	6			H			H			VL		Niobokuleskite	50	
S2	6			H			H			VL		Niobokuleskite	50	
S2	6			H			H			VL		Niobokuleskite	50	
S2	6			H			H			VL		Niobokuleskite	50	
S2	6			H			H			VL		Niobokuleskite	20	
S2	7			H			H			VL		Niobokuleskite	70	
S2	7			H			H			VL		Niobokuleskite	50	
S2	7			H			H			VL		Niobokuleskite	40	
S2	7			H			H			VL		Niobokuleskite	30	
S2	1			H			H			T		Niobokuleskite	110	
S2	1			H			H			T		Niobokuleskite	35	
S2	1			H			H			T		Niobokuleskite	30	
SK1E	2			H			H			VL		Niobokuleskite	75	
SK1E	3			H			H			T		Niobokuleskite	50	
SK1E	3			H			H			T		Niobokuleskite	50	
SK2D	2			H			H			L		Niobokuleskite	30	
SK12A	1			H			H			L		Niobokuleskite	50	
SK12A	1			H			H			L		Niobokuleskite	50	
SK12A	3			H			H			VL		Niobokuleskite	10	
SK12A	4	1		H			H			L		Niobokuleskite	55	
SK12A	5		L	H			L			L		Niobokuleskite	50	
SK12A	5		VL	H			VL			VL		Niobokuleskite	50	
SK12A	5		VL	H			VL			VL		Niobokuleskite	50	
SK12A	6			H			H			VL		Niobokuleskite	10	
SK12A	6			H			H			VL		Niobokuleskite	5	
SK8	3	1		H			H			VL		Niobokuleskite	20	
SK1A	6			H			H			L		Niobokuleskite	70	
SK2A	7			H			H			VL		Niobokuleskite	70	
SK2A	7			H			H			VL		Niobokuleskite	60	
													5035	72
SKZE	1	3		H	VL							Pyrochlore	150	Alteration
SK1B	5	11		M								Pyrochlore	100	
SK1B	5	12		M								Pyrochlore	75	
SK1B	3	9		M								Pyrochlore	70	
SK1E	4	4	H	M								Pyrochlore	105	
S10	1	1		L								Pyrochlore	100	
S10	1	2		L								Pyrochlore	50	
S10	1	3		L								Pyrochlore	75	
S10	1	4		L								Pyrochlore	40	
S10	1	5		L								Pyrochlore	140	

S10	1	6		L								Pyrochlore	110	
S10	1	7		L								Pyrochlore	40	
S10	1	8		L								Pyrochlore	100	
S10	1	9		L								Pyrochlore	100	
S10	1	10		L								Pyrochlore	110	
S10	1	11		L								Pyrochlore	110	
S10	1	12		L								Pyrochlore	20	
S10	2	1		H								Pyrochlore	175	
S10	2	2		H								Pyrochlore	100	
S10	2	5		VL								Pyrochlore	15	
S10	2	8		M								pyrochlore	110	
S10	2	10		H								pyrochlore	100	
S10	2	11		H								pyrochlore	95	Zr, Si, Nb noddule on edge
S10	3	2		M								Pyrochlore	100	3 Si, Fe noddules on edge
S10	3	3		M								Pyrochlore	90	
S10	3	4		M								Pyrochlore	100	
S10	3	5		M								Pyrochlore	60	
S10	3	6		M								Pyrochlore	60	1 Si noddule enclosed
S10	3	7		M								Pyrochlore	110	
S10	3	8		M								Pyrochlore	70	
S10	3	10		M								Pyrochlore	60	1 Si noddule enclosed
S10	3	11		M								Pyrochlore	50	
S10	3	12		M								Pyrochlore	150	
S10	3	13		M								Pyrochlore	50	
S10	3	15		M								Pyrochlore	80	
S10	4	2		M								Pyrochlore	100	
S10	4	4		M								Pyrochlore	110	
S10	4	7		M								Pyrochlore	100	
S10	4	8		M								Pyrochlore	90	
S10	4	9		M								Pyrochlore	40	
S10	4	10		M								Pyrochlore	110	
S10	4	12		M								Pyrochlore	150	
S10	4	14		M								Pyrochlore	100	
S10	6	1		M								Pyrochlore	10	
S10	6	3		M								Pyrochlore	35	Si noddule on edge
S10	6	4		M								Pyrochlore	100	
S10	6	5		M								Pyrochlore	120	
S10	6	7		M								Pyrochlore	35	Alternating with 11
S10	6	8		M								Pyrochlore	75	
S10	6	9		M								Pyrochlore	90	Si noddule on edge
S10	6	10		M								Pyrochlore	75	Si noddule in centre
S10	7	2		M								Pyrochlore	35	
S10	7	3		M								Pyrochlore	105	
S10	7	4		M								Pyrochlore	90	
S10	7	5		M								Pyrochlore	100	
S10	7	7		M								Pyrochlore	100	
S10	7	8		M								Pyrochlore	45	
S10	7	9		M								Pyrochlore	100	Si noddules centre
S10	7	11		M								Pyrochlore	40	
S10	7	12										Pyrochlore	10	
S10	7	15		M								Pyrochlore	100	
S10	7	16		M								Pyrochlore	90	
SK1B	1	2	L	H	M		VL					pyrochlore	60	
SK1B	1	6	L	H	M		VL					pyrochlore	60	
SK1B	1	9	M	H	M		VL					pyrochlore	80	
SK1B	4	11		M								Pyrochlore	60	
SK1B	4	16		M								Pyrochlore	65	
SK1B	4	20		M								Pyrochlore	20	

SK1B	4			H								Pyrochlore	10	
SK1B	5	19		M								Pyrochlore	40	
SK1B	6	14		M								Pyrochlore	10	
SK1B	6	16		H								Pyrochlore	10	
SK1B	6	20		M								Pyrochlore	5	
SK1B	7	5		M								Pyrochlore	90	
SK1B	7	7		M								Pyrochlore	80	
SK1B	7	10		M								Pyrochlore	30	
SK1B	7	16		M								Pyrochlore	50	
SK1B	7	17		M								Pyrochlore	95	
SK1B	3	5		M								Pyrochlore	20	
SK1B	3	13		M								Pyrochlore	20	
SK1E	4	17	H	M								Pyrochlore	150	6 Si noddules on edge
SK1E	4	18	H	M								Pyrochlore	100	Si staining
SK1E	5	3		M								Pyrochlore	80	
SK1E	5	8		M								Pyrochlore	50	
SK1E	5	18		M								Pyrochlore	50	
SK1E	6	4		M								Pyrochlore	70	
SK1E	6	7			M							Pyrochlore	60	
SK1E	7	7		H								Pyrochlore	35	
SK2A	3	5		M								Pyrochlore	90	
SK2A	3	6		M								Pyrochlore	50	
SK2A	3	10		M								Pyrochlore	60	
SK2A	3	14		M								Pyrochlore	30	
SK2D	5	1		M								Pyrochlore	45	
SK2D	5	2		M								Pyrochlore	90	
SK2D	5	4		M								Pyrochlore	100	
SK2D	5	7		M								Pyrochlore	60	
SK2D	5	8		M								Pyrochlore	90	
SK2D	5	9		M								Pyrochlore	100	
SK2D	5	10		M								Pyrochlore	90	
SK2D	5	12		M								Pyrochlore	50	
SK2D	5	13		M								Pyrochlore	20	
SK1D	6	1		M								Pyrochlore	75	
SK1D	6	2		M								Pyrochlore	75	High Si stains
SK1D	6	3		M								Pyrochlore	70	Si noddule on the edge
SK1D	6	4		M								Pyrochlore	130	
SK1D	6	5		M								Pyrochlore	10	
S3	3	14		M	L							Pyrochlore	55	
SK1D	6	8		M								Pyrochlore	100	
SK1D	6	9		M								Pyrochlore	90	
SK1D	6	11		M								Pyrochlore	45	
SK1D	6	12		M								Pyrochlore	90	
SK1D	7	2		M								Pyrochlore	60	
SK1D	7	3		M								Pyrochlore	80	
SK1D	7	4		M								Pyrochlore	10	
SK1D	7	5		M								Pyrochlore	15	
SK1D	7	6		M								Pyrochlore	110	
SK1D	7	7		M								Pyrochlore	110	
SK1D	7	8		M								Pyrochlore	90	
SK1D	7	9		M								Pyrochlore	30	
SK1D	7	10		M								Pyrochlore	40	
SK1D	7	11		M								Pyrochlore	50	
SK1D	7	12		M								Pyrochlore	40	
SK1D	7	14		M								Pyrochlore	110	
SK1B	1?	1		M			T					Pyrochlore	40	
SK1B	1?	7		L	M		T					Pyrochlore	100	
SK1B	1?	9		M			T					Pyrochlore	55	
SK1B	1?	10		M			T					Pyrochlore	50	

SK1B	1?	13		M			T					Pyrochlore	140	High Si, Nb nodule centre
SK1D	2	1		M								Pyrochlore	50	
SK1D	2	2		M								Pyrochlore	130	
SK1D	2	3		M								Pyrochlore	100	Si noddule on edge
SK1D	2	4		M								Pyrochlore	110	
SK1D	2	5		M								Pyrochlore	40	
SK1D	2	6		M								Pyrochlore	90	3 Si noddules on the edge
SK1D	2	7		M								Pyrochlore	100	
SK1D	2	8		M								Pyrochlore	110	Si noddule on edge
SK1D	2	9		M								Pyrochlore	75	
SK1D	2	10		M								Pyrochlore	100	
S3	7	1		M	L		T					Pyrochlore	30	
SK1D	2	11		M								Pyrochlore	90	
SK1D	2	12		M								Pyrochlore	30	
SK1D	2	13		M								Pyrochlore	80	
SK1D	2	14		M								Pyrochlore	100	
SK1D	4	1		M								Pyrochlore	70	
SK1D	4	2		M								Pyrochlore	105	
SK1D	4	3		M								Pyrochlore	40	
SK1D	4	4		M								Pyrochlore	55	4 Si noddule on edge
SK1D	4	5		M								Pyrochlore	105	
SK1D	4	6		M								Pyrochlore	100	Si noddule on edge
SK1D	4	7		M								Pyrochlore	75	
SK1D	4	8		M								Pyrochlore	100	Si noddule on edge
SK1D	4	9		M								Pyrochlore	100	Si surround
SK1D	4	10		M								Pyrochlore	50	
SK1D	4	11		M								Pyrochlore	130	Si surround
SK1D	4	12		M								Pyrochlore	100	Si surround
SK1D	4	13		M								Pyrochlore	125	
SK1D	4	14		M								Pyrochlore	80	
SK1D	4	15		M								Pyrochlore	20	
SK1D	5	1		M								Pyrochlore	45	
SK1D	5	2		M								Pyrochlore	30	
SK1D	5	3		M								Pyrochlore	45	
SK1D	5	4		M								Pyrochlore	105	
SK1D	5	5		M								Pyrochlore	90	
SK1D	5	6		M								Pyrochlore	60	
SK1D	5	7		M								Pyrochlore	55	
SK1D	5	8		M								Pyrochlore	90	Si noddule on edge
SK1D	5	9		M								Pyrochlore	60	Si surround
SK1D	5	11		M								Pyrochlore	100	
SK1D	5	12		M								Pyrochlore	60	
SK1D	5	13		M								Pyrochlore	100	
SK1D	5	14		M								Pyrochlore	15	
S3	2	1		L								Pyrochlore	20	
S3	2	2		L								Pyrochlore	55	
S3	2	3		L								Pyrochlore	50	
S3	2	4		L								Pyrochlore	50	
S3	2	5		L								Pyrochlore	20	
S3	2	8		L								Pyrochlore	100	
S3	2	9		L								Pyrochlore	75	
S3	2	10		L								Pyrochlore	130	Si, Nb noddule centre
S1	3	3		M			T					Pyrochlore	75	
S1	3	6		M			T					Pyrochlore	60	Attached to 5
S1	2	8		L								Pyrochlore	55	
K1	1	3		L								Pyrochlore	75	
K1	1	4		L								Pyrochlore	60	
K1	1	5		L								Pyrochlore	60	
K1	1	6		L								Pyrochlore	30	

K1	1	7		L								Pyrochlore	120	
K1	1	8		L								Pyrochlore	100	
K1	1	9		L								Pyrochlore	105	
K1	1	10		L								Pyrochlore	15	
K1	1	11		L								Pyrochlore	100	
K1	1	12		L								Pyrochlore	80	
K1	1	13		L								Pyrochlore	110	
S3	6	10		L								Pyrochlore	65	
S3	6	13		L								Pyrochlore	80	
S3	6	16		L								Pyrochlore	20	
S3	6	17		L								Pyrochlore	50	
S3	6	18		L								Pyrochlore	15	
S3	7	2	L	M	L		VL					pyrochlore	90	
S3	7	3		L								pyrochlore	140	
S3	7	6	L	M	L							pyrochlore	110	
S3	7	7	L	M	L		VL					pyrochlore	100	Surrounded by Si
S3	7	10		L								pyrochlore	50	
S3	7	12		M								pyrochlore	30	Surrounded by Si
S3	7	13		L								pyrochlore	105	
S3	7	16		M	L		VL					pyrochlore	50	
S3	1	2		L								Pyrochlore	110	
S3	1	3		L								Pyrochlore	55	
S3	1	4		H	L							Pyrochlore	60	
S3	1	7		L								Pyrochlore	55	
S3	1	9		L								Pyrochlore	50	
S3	1	10		L								Pyrochlore	100	
S1	6	1	T		T		VL					pyrochlore	150	
S1	6	2		L								Pyrochlore	70	
S1	6	4		L								Pyrochlore	20	
S1	5	7		M								Pyrochlore	60	
S1	5	8		M								Pyrochlore	60	
S1	5	9		M								Pyrochlore	100	
S1	4	16		L								pyrochlore	55	
S1	1	5	VL	M	L							pyrochlore	50	
S1	5	6		M	L							pyrochlore	50	
S1	5	8		M								pyrochlore	10	
S1	5	11		L								pyrochlore	90	
S1	5	12		L								pyrochlore	65	
S1	5	13		L								pyrochlore	105	
S3	4	4		L								Pyrochlore	55	
S3	4	5		L								Pyrochlore	95	
S3	4	11		L								Pyrochlore	50	
S3	4	15		L								Pyrochlore	50	
S3	5	11		M								Pyrochlore	40	
S3	5	12		M								Pyrochlore	20	
S2	1	3		M								Pyrochlore	30	
S2	1	4		M								Pyrochlore	30	
S2	1	7		M								Pyrochlore	55	
S2	1	8		M								Pyrochlore	50	
S2	1	9		M								Pyrochlore	30	
S2	1	12	M	M								Pyrochlore	50	
S2	1	13	M	M								Pyrochlore	120	
S2	1	14	M	M								Pyrochlore	80	
S2	1	15		M								Pyrochlore	10	
S2	1	16	M	M								Pyrochlore	20	
S2	1	17	M	M								Pyrochlore	100	
SK5B	2	2		L								Pyrochlore	150	
SK5B	2	3		L								Pyrochlore	170	
SK5B	2	4		L								Pyrochlore	90	

SK5B	2	5		L								Pyrochlore	150	
SK5B	2	6		L								Pyrochlore	130	
SK5B	2	7		L								Pyrochlore	160	
SK5B	2	8		L								Pyrochlore	150	
SK5B	2	9		L								Pyrochlore	80	
SK5B	2	10		L								Pyrochlore	160	
SK5B	2	11		L								Pyrochlore	100	
SK5B	2	12		L								Pyrochlore	110	
SK5B	2	13		L								Pyrochlore	100	
SK5B	3	1		L								Pyrochlore	60	
SK5B	3	2		L								Pyrochlore	160	
SK5B	3	3		L								Pyrochlore	90	
SK5B	3	6		L								Pyrochlore	150	
SK5B	3	11		L								Pyrochlore	110	
SK5B	3	12		L								Pyrochlore	90	
SK4	5	10	H	M	L						VL	Pyrochlore	150	
SK5B	3	14		L								Pyrochlore	150	
SK5B	3	15		L								Pyrochlore	60	
SK5B	3	17		L								Pyrochlore	70	
SK5B	4	1		L								Pyrochlore	151	
SK5B	4	2		L								Pyrochlore	25	
SK5B	4	3		L								Pyrochlore	50	
SK5B	4	4		L								Pyrochlore	190	
SK5B	4	6		L								Pyrochlore	100	
SK5B	4	7		L								Pyrochlore	40	Attached VL nodule on Fe
SK5B	4	8		L								Pyrochlore	80	
SK5B	4	9		L								Pyrochlore	20	
SK5B	4	10		L								Pyrochlore	130	
SK5B	4	12		L								Pyrochlore	160	
SK5B	4	14		L								Pyrochlore	100	
SK5B	4	15		L								Pyrochlore	140	
SK5B	4	16		L								Pyrochlore	180	
SK5B	4	18		L								Pyrochlore	50	
SK5B	5	3		L								pyrochlore	200	
SK5B	5	5		L								pyrochlore	100	
SK5B	5	6		L								pyrochlore	70	
SK5B	5	8		L								pyrochlore	30	
SK5B	5	9		L								pyrochlore	155	
SK5B	5	10		L								pyrochlore	150	
SK5B	6	1		M								pyrochlore	160	
SK5B	6	2		M								pyrochlore	100	
SK5B	6	3		M								pyrochlore	150	
SK5B	6	4		M								pyrochlore	150	
SK5B	6	6		M								pyrochlore	50	
SK5B	6	7		M								pyrochlore	200	
SK5B	6	8		M								pyrochlore	150	
SK5B	6	9		M								pyrochlore	150	
SK5B	6	12		M								pyrochlore	150	
SK5B	6	13		M								pyrochlore	20	
SK1E	5	6		L								pyrochlore	100	
SK1E	5	16		L								pyrochlore	90	
SK1E	5	17		L								pyrochlore	150	
SK1E	7	17		L								pyrochlore	90	
SV1	7	17		L								Pyrochlore	150	
SV1	5	13		L								pyrochlore	100	
SV1	2	14		L								Pyrochlore	150	
SV1	2	15		L								Pyrochlore	100	
SKZE	1	1		H			VL					Pyrochlore	100	

SKZE	5	15	H	M	L							pyrochlore	110	
SKZE	4	22		L								pyrochlore	40	
SK12D	2	21		L								pyrochlore	90	
SK12D	3	9		L			VL					Pyrochlore	200	
SK12D	3	16	L	M	L							Pyrochlore	200	
SK12E	4	15	L	M	L							Pyrochlore	100	
SK12A	2	1		M								Pyrochlore	150	
SK12A	2	2		M								Pyrochlore	160	
SK12A	2	3		M								Pyrochlore	180	
SK12A	2	5		M								Pyrochlore	100	
SK12A	2	6		M								Pyrochlore	110	
SK12A	2	7		M								Pyrochlore	130	
SK12A	2	8		M								Pyrochlore	160	
SK12A	2	9		M								Pyrochlore	120	
SK12A	2	10		M								Pyrochlore	150	
SK12A	2	14		M								Pyrochlore	50	
SK12A	2	15		M								Pyrochlore	60	
SK9	1	3			T							pyrochlore	40	
SK9	1	6		L								pyrochlore	200	
SK9	1	12		L								pyrochlore	80	
SK9	2	8		L			VL					Pyrochlore	190	
SK9	2	15		L			VL					Pyrochlore	100	
SK9	2	16		L			VL					Pyrochlore	50	
SK9	2	17		L								Pyrochlore	50	
SK9	3	5		L			VL					Pyrochlore	160	
SK9	3	6		L	L		VL					Pyrochlore	50	
SK9	3	20		L								Pyrochlore	140	
SK9	4	7		L			VL					Pyrochlore	190	
SK9	4	8		L			VL					Pyrochlore	100	
SK9	4	9	L	M	L		VL					Pyrochlore	150	
SK9	5	9		L								Pyrochlore	90	
SK9	5	10		L								Pyrochlore	50	
SK9	5	11		L								Pyrochlore	140	
SK9	5	12		L								Pyrochlore	100	
SK9	5	13		L								Pyrochlore	90	
SK9	5	17		L								Pyrochlore	170	
SK9	6	3		L								Pyrochlore	150	
SK9	6	4	L	M								Pyrochlore	100	
SK9	6	5		L								Pyrochlore	150	
SK9	6	6	VL	M								Pyrochlore	160	
SK9	6	8		M								Pyrochlore	50	
SK9	6	11		L								Pyrochlore	50	
SK9	6	12		L								Pyrochlore	30	
SK9	6	13	VL	M								Pyrochlore	90	
SK9	6	14	VL	M								Pyrochlore	50	
SK9	6	17		L								Pyrochlore	90	
SK9	7	12		M			VL					Pyrochlore	100	
SK8	1	2		L								pyrochlore	210	
SK8	1	3		L								pyrochlore	190	
SK8	1	4		L								pyrochlore	150	
SK8	1	5		L								pyrochlore	149	
SK8	1	6		L								pyrochlore	150	
SK12E	2	11		H								pyrochlore	50	
SK2A	3	1		M								Pyrochlore	120	
SK2A	3	2		M								Pyrochlore	60	
SK2A	3	9		L			VL					Pyrochlore	110	
SK2A	3	19		M								Pyrochlore	100	
SK2D	6	3		M								pyrochlore	130	
SK2D	6	4		M								pyrochlore	150	

SK2D	6	5	L	H	M		VL					pyrochlore	50	
SK2D	6	7		M			VL					pyrochlore	50	
SK2D	6	15		M								pyrochlore	50	
SK2D	6	16		M								pyrochlore	30	
SK2D	7	1		M								Pyrochlore	200	
SK2D	7	3		M								Pyrochlore	150	
SK2D	7	7		M								Pyrochlore	150	
SK2D	7	8		M								Pyrochlore	140	
SK2D	7	10		M								Pyrochlore	100	
SK2D	7	16		L								Pyrochlore	50	
SK2D	1	2		M								pyrochlore	50	
SK2D	1	5		M								pyrochlore	60	
SK2D	1	6		M								pyrochlore	100	
SK2D	1	7		M								pyrochlore	130	
SK2D	1	8		M								pyrochlore	150	
SK2D	1	9		M								pyrochlore	100	
SK2D	1	11		M								pyrochlore	100	
SK2D	1	12		M								pyrochlore	150	
SK2D	1	13		M								pyrochlore	50	
SK2D	1	14		M								pyrochlore	150	
SK2D	1	15		M								pyrochlore	150	
SK2D	1	16		M								pyrochlore	140	
SK2D	1	17		M								pyrochlore	150	
SK2D	1	18		M								pyrochlore	160	
SK2D	1	22		M								pyrochlore	30	
SK4	2	2		M								pyrochlore	140	
SK4	2	3		M								pyrochlore	100	
SK4	2	6		M								pyrochlore	130	
SK4	2	7		M								pyrochlore	110	
SK4	2	8		M								pyrochlore	100	
SK4	3	6		M								pyrochlore	160	
SK4	3	9		M								pyrochlore	150	
SK4	3	11		M								pyrochlore	200	
SK4	3	12		M								pyrochlore	150	
SK4	4	1		M								pyrochlore	150	
SK4	4	5	M	L								pyrochlore	80	
SK4	4	6	M	L								pyrochlore	100	
SK4	4	8		L								pyrochlore	150	
SK4	4	11		M								pyrochlore	200	
SK4	4	12		M								pyrochlore	100	
SK4	4	14		M								pyrochlore	110	
SK4	5	5		M								pyrochlore	200	
SK4	5	8		M								pyrochlore	150	
SK4	5	9		M								pyrochlore	200	
SK4	5	11		M								pyrochlore	100	
SK4	6	3	M	L								pyrochlore	100	
SK4	6	5		M								pyrochlore	100	
SK4	7	14		M								pyrochlore	50	
SK4	7	15		M								pyrochlore	30	
SK4	1	3	L	M	L							Pyrochlore	140	
SK4	1	5		M								Pyrochlore	150	
SK4	1	11		M								Pyrochlore	150	
SK1A	2			L								pyrochlore	150	
SK1A	2			L								pyrochlore	150	
SK1A	5	7		T	H							pyrochlore	150	
SK1A	5	8		M			T					pyrochlore	150	
SK1A	7	5		M								pyrochlore	150	
K1	2	6		L								pyrochlore	15	Contain Si around
K1	2	7		L								pyrochlore	15	Contain Si around

K1	3	10		L								pyrochlore	25	
K1	4	2		VL				T				pyrochlore	70	
S2	3	15		M								pyrochlore	25	
S2	3	16		M								pyrochlore	50	
S2	7			L								pyrochlore	50	
S2	1		L		M							pyrochlore	60	
S2	1			M								pyrochlore	35	
S2	1			M								pyrochlore	35	
S2	1			M								pyrochlore	35	
SK1E	3			M								pyrochlore	50	
SK1E	3			M								pyrochlore	50	
SK1E	3			M								pyrochlore	50	
SK1E	3			M								pyrochlore	50	
SK2D	2			M								pyrochlore	20	
SK2D	2			M								pyrochlore	10	
SK2D	2			M								pyrochlore	10	
SK2D	2			M								pyrochlore	10	
SK2D	2			M								pyrochlore	10	
SK2D	2			M								pyrochlore	10	
SK12A	1			M								pyrochlore	55	
SK12A	1			M								pyrochlore	20	
SK12A	3			H								pyrochlore	60	
SK12A	7		L	H	VL						T	pyrochlore	120	
SK12A	7		L	H	VL							pyrochlore	100	
SK12A	7		L	H	VL							pyrochlore	30	
SK8	3	12		M								pyrochlore	50	
SK8	3	13		M								pyrochlore	30	
SK8	3	14		M								pyrochlore	30	
SK8	3	15		M								pyrochlore	30	
SK8	4	11		M								pyrochlore	50	
SK8	4	12		M								pyrochlore	50	
SK8	4	13		M								pyrochlore	50	
SK8	4	14		M								pyrochlore	50	
SK8	4	15		M								pyrochlore	50	
SK8	4	16		M								pyrochlore	50	
SK8	5	8	L	H			VL					pyrochlore	40	
SK8	6	10		H								pyrochlore	50	
SK8	6	11		H								pyrochlore	50	
SK8	6	12		H								pyrochlore	10	
SK8	6	13		H								pyrochlore	20	
SK8	6	14		H								pyrochlore	40	
SK8	7	10		M								pyrochlore	200	
SK2A	4			M								pyrochlore	40	
SK2A	4			M								pyrochlore	40	
SK2A	4			M								pyrochlore	20	
SK2A	4			M								pyrochlore	10	
SK1B	6	6		M								pyrochlore	50	
SK1A	7			H								pyrochlore	70	
													40315	468
S10	2	12			H							rutile	50	
SK1A	1				H							rutile	5	
SK1B	7	13			H							Rutile	55	
SK1B	7	18			H							Rutile	20	
SK1B	3	7			H							Rutile	100	
SK1B	3	15			H							Rutile	150	Si nuddlues on the edge
SK1E	6	5			H							rutile	50	Partly contain Si
SK1E	7	2			M							rutile	90	
SK1E	7	4			M							rutile	80	

SK1E	7	5			M							rutile	95	
SK1E	7	6			M							rutile	90	
SK1E	7	10			M							rutile	50	
SK1E	7	11			M							rutile	75	
SK1B	1?	6			H		T					Rutile	55	
SK1E	1	2			M							rutile	105	
SK1E	1	3			M							rutile	40	
SK1E	1	5			M							rutile	100	
SK1E	1	6			M							rutile	25	
SK1E	1	12			M							rutile	100	
SK1E	1	15			M							rutile	60	
S1	1	2			L							Rutile	60	
S1	1	4			L							Rutile	105	
S1	1	6			L							Rutile	55	Ti cracks, Si nodule
S1	1	7			L							Rutile	55	
S1	1	8			L							Rutile	165	Ti cracks
S1	1	9			L							Rutile	75	2 attached to 9
S1	1	10			L							Rutile	45	Ti cracks
S1	1	11			L							Rutile	75	Ti cracks
S1	1	12			L							Rutile	80	Ti cracks
S1	1	13			L							Rutile	145	Ti cracks
S3	3	16			H							Rutile	100	
S3	3	18			T							Rutile	20	Si around
S1	5	14			L							Rutile	25	
S3	5	18			H							Rutile	30	
S2	1	4			L							Rutile	110	Ti cracks
S2	1	5			L							Rutile	150	Ti cracks
S2	1	6			L							Rutile	100	Ti cracks
S2	1	7			L							Rutile	60	Ti cracks
S2	1	8			L							Rutile	90	Ti cracks
S2	1	9			L							Rutile	150	
S2	1	10			L							Rutile	70	
SK1E	7	6			M							rutile	150	
SK1E	7	7			M							rutile	140	
SK1E	7	15			M							rutile	100	
SK1E	7	16			M							rutile	110	
SV1	7	9			L							Rutile	110	Ta cracks
SV1	7	10			L							Rutile	120	Ta cracks
SV1	7	11			L							Rutile	100	
SV1	7	12			VL							Rutile	150	
SV1	7	13			L							Rutile	100	Ta cracks
SV1	7	14			L							Rutile	110	Ta cracks
SV1	5	14			L							Rutile	50	Ti cracks
SV1	4	15			H							Rutile	30	nodule on 3
SKZE	1	7			VL							Rutile	200	
SKZE	1	8			VL							Rutile	150	
SKZE	1	9			VL							Rutile	100	
SKZE	1	10			VL							Rutile	90	
SKZE	1	12			VL							Rutile	150	
SK9	7	15			L							Rutile	50	
SK2A	3	17			H							rutile	30	
SK1A	3	10			H							rutile	50	
SK1E	2				T							rutile	40	
SK1E	2				T							rutile	40	
SK2A	1	4			M							rutile	100	
SK2A	1	5			M							rutile	100	
SK2A	1	6			M							rutile	60	
SK2A	1	7			M							rutile	100	
SK2A	1	8			M							rutile	50	

SK2A	1	9			M							rutile	50	
SK2A	1				M							rutile	15	
SK2A	1				M							rutile	10	
SK2A	1				M							rutile	10	
SK2A	1				M							rutile	50	
													5875	73
SK1E	6	15					M	L				Thorite	60	
SK1E	7	13					M	L				Thorite	100	
S1	3	1					M	L				Thorite	75	
S1	2	5					T	L				Thorite	100	surrounded by 5
S3	4	17					L	T				Thorite	70	
SK1E	6	9					M	L				thorite	100	
SK1E	6	11					M	T				thorite	90	
SV1	7	6					L	L				Thorite	160	
K1	3	2					M	VL				thorite	20	
													775	10
SK1E	7	11	VL		VL			VL				Thorutite	160	
													160	1
SK2A	3	13			H		H					titanite	50	
SK1E	5	11			H		H					titanite	60	Fe zone around
SK1A	1	7			M		L					titanite	10	
SK1B	1	1			H		H					Titanite	90	
SK1B	1	4			M		H					Titanite	40	
SK1B	1	5			M		H					Titanite	25	
SK1B	1	7			M		H					Titanite	60	
SK1B	1	8			M		H					Titanite	50	
SK1E	4	9			M		H					Titanite	145	Fe staining
SK2A	3	7			M		M					titanite	100	
SK1B	1?	16			H		T					Titanite	75	
S1	5	4			L		L					Titanite	50	
SK1E	5	9			L		M					Titanite	160	
SK1E	5	12			L		M					Titanite	70	
SK1E	5	18			L		M					Titanite	50	
SK1E	6	14			H		M					titanite	100	
SK1E	7	2			M							titanite	150	
SK1E	7	9			VL		L					titanite	80	
SK1E	7	10			VL		L					titanite	100	
SK1E	7	13			T		H					titanite	30	
SK1E	7	18			VL		H					titanite	30	nodule on Si-Ti
SV1	3	12			L		H					titanite	150	
SKZE	1	6			VL		L					titanite	50	
SKZE	7	16			L		H					titanite	110	Ti cracks
SKZE	6	9			L		L					titanite	120	
SKZE	6	11			L		L					titanite	170	
SKZE	5	3			H		L					Titanite	70	
SK12D	1	4			H		H					titanite	120	
SK12D	1	5			H		H					titanite	150	
SK12D	1	11			L		H					titanite	100	
SK12D	1	14			H		H					titanite	100	
SK12D	1	15			H		M					titanite	50	
SK12D	2	9			L		H				T	titanite	150	
SK12D	2	17			M		H					titanite	110	
SK12D	2	19			M		H					titanite	100	
SK12D	3	8			L		H					titanite	140	
SK12D	3	12			H		L					titanite	100	
SK12D	4	4			H		H					titanite	120	

SK12D	4	5			H		H					titanite	150	
SK12D	4	14			H		L					titanite	150	
SK12D	5	7			L		H					Titanite	50	
SK12D	5	8			L		H					Titanite	150	
SK12D	6	3			L		H					Titanite	160	Fe staining
SK12D	6	6			M		H					Titanite	150	Fe staining
SK12D	6	10			M		H					Titanite	100	
SK12D	7	2			M		H					titanite	190	
SK12D	7	3			M		H					titanite	110	
SK12E	5	2			H		L					Titanite	100	
SK12E	5	12			H		L					Titanite	150	
SK12E	6	9			L		M					titanite	140	
SK12E	6	12			L		M					titanite	40	
SK12E	6	13			L		M					titanite	150	
SK9	1	8			M		M					titanite	110	
SK9	1	13			M		M					titanite	130	
SK12E	3	13			H		M					titanite	100	
SK2A	3	13			H		H					Titanite	60	
SK2D	6	2			T		H					titanite	110	
SK4	3	13			H		H					titanite	140	
SK4	5	1			H		H					titanite	100	
SK4	6	1			M		H					titanite	120	
SK4	6	7			H		H					titanite	110	
SK1A	5	5			M		H					titanite	60	
SK1A	5	6			M		H					titanite	60	
SK1A	7	3			H		H					titanite	60	
SK1A	7	4			H		H					titanite	60	
K1	7	10			M		H					titanite	40	
SK1E	3				M		H					Titanite	50	
SK2A	4				M		H					Titanite	20	
SK2A	4				M		H					Titanite	70	
SK1A	7				H		H					Titanite	15	
SK1A	7				H		H					Titanite	30	
													6670	71
S10	4		H									uraninite	10	
S10	4		H									uraninite	10	
S10	4		H									uraninite	10	
SK1A	1		H									Uraninite	5	
SK1A	1		H									Uraninite	5	
SK1A	1		H									Uraninite	5	
SK1B	1	13	M									Uraninite	20	
SKZE	5	5	H									uraninite	130	Slightly altered Si
SK12D	6	16	H									uraninite	40	
SK4	3	15	H									Uraninite	5	
SK1A	3	2	M									uraninite	5	Noddules in 1
SK1A	3	3	M									uraninite	5	Noddules in 1
SK1A	3	4	M									uraninite	5	Noddules in 1
SK1A	3	5	M									uraninite	5	Noddules in 1
SK1A	5	2	M									uraninite	5	center of 1
SK1A	5	3	M									uraninite	5	
K1	5	2	L									uraninite	5	
S2	2	1	T									uraninite	5	
S2	2	2	T									uraninite	120	
S2	2	3	T									uraninite	50	
													450	20
SK1B	6	9	VL					L				uranothorite	50	
SK1E	6	1	L				M	L				Uranothorite	130	

SK1E	7	12	H				M				VL	Uranothorite	40	
SK5B	3	16	L				L	L				Uranothorite	50	
SK1E	6	2	L				M	L				Uranothorite	180	
SKZE	5	7	VL				L	L				uranothorite	150	
SK1E	6	8	L				M	VL				uranothorite	150	
SK12E	5	13	T				M	L				uranothorite	150	
SK4	3	10	L				M	VL				uranothorite	100	
SK1A	6	1	VL				H	L	T			uranothorite	100	
SK1A	7	1	VL				H	L	T			uranothorite	100	
SK1A	7	2	V				H	L	T			uranothorite	100	
K1	2	1	L				M	L				uranothorite	10	
SK2A	1	1	VL				M	T				uranothorite	50	
SK1A	7		T				M	T				uranothorite	70	
SK1A	7		T				M	T				uranothorite	70	
SK1A	6		L				M	L				uranothorite	120	
SK1A	4		L				H	L				uranothorite	110	
													1730	17
SK9	3	16					H					u-silicates	40	Fe oxide on around
S10	1	13					H					u-silicates	90	
S10	1	14					H					u-silicates	10	8 Si noddules around
S10	1	15					H					u-silicates	5	
S10	1	16					H					u-silicates	5	
S10	1	17					H					u-silicates	5	
S10	1	18					H					u-silicates	5	
S10	1	19					H					u-silicates	5	
S10	1	20					H					u-silicates	5	
S10	1	21					H					u-silicates	5	
S10	1	22					H					u-silicates	5	
S10	1	23					H					u-silicates	5	
S10	1	24					H					u-silicates	5	
S10	1	25					H					u-silicates	5	
S10	1	26					H					u-silicates	5	
S10	1	27					H					u-silicates	5	
S10	2	3					H					u-silicates	40	
S10	2	13					H					u-silicates	10	
S10	2	14					H					u-silicates	5	
S10	2	15					H					u-silicates	5	
S10	2	16					H					u-silicates	5	
S10	2	17					H					u-silicates	5	
S10	2	18					H					u-silicates	5	
S10	2	19					H					u-silicates	5	
S10	2	20					H					u-silicates	5	
S10	2	21					H					u-silicates	5	
S10	2	22					H					u-silicates	5	
S10	2	23					H					u-silicates	5	
S10	2	24					H					u-silicates	5	
S10	2	25					H					u-silicates	5	
S10	2	26					H					u-silicates	5	
S10	2	27					H					u-silicates	5	
S10	2	28					H					u-silicates	5	
S10	2	29					H					u-silicates	5	
S10	2	30					H					u-silicates	5	
S10	2	31					H					u-silicates	5	
S10	2	32					H					u-silicates	5	
S10	2	33					H					u-silicates	5	
S10	3	19					M					u-silicates	5	
S10	3	20					M					u-silicates	5	
S10	4	1					H					u-silicates	30	

S10	4	5					H					u-silicates	100	
S10	4	15					H					u-silicates	50	
S10	6	6					L					u-silicates	140	
S10	6	13					H					u-silicates	50	
S10	6						H					u-silicates	10	
S10	6						H					u-silicates	10	
S10	6						H					u-silicates	10	
S10	7	6					H					u-silicates	15	9 Noddules
S10	7	13					H					u-silicates	50	
S10	7	14					H					u-silicates	60	
S10	7	17					H					u-silicates	60	
S10	7						H					u-silicates	5	
S10	7						H					u-silicates	5	
S10	7						H					u-silicates	5	
S10	7						H					u-silicates	5	
S10	7						H					u-silicates	5	
S10	7						H					u-silicates	5	
S10	7						H					u-silicates	5	
S10	7						H					u-silicates	5	
S10	7						H					u-silicates	5	
S10	7						H					u-silicates	5	
S10	7						H					u-silicates	5	
S10	7						H					u-silicates	5	
SK1A	1	3					L					u-silicates	75	
SK1A	1	5					H					u-silicates	90	
SK1A	1	6					H					u-silicates	15	
SK1B	1	3					H					u-silicates	50	
SK1B	1	10					H					u-silicates	50	
SK1B	4	7					H					u-silicates	75	Nb noddules in centre
SK1B	4	8					H					u-silicates	100	Attached to 21
SK1B	4	12					H					u-silicates	140	
SK1B	4						H					u-silicates	10	
SK1B	4						H					u-silicates	10	
SK1B	4						H					u-silicates	10	
SK1B	4						H					u-silicates	10	
SK1B	4						H					u-silicates	10	
SK1B	4						H					u-silicates	10	
SK1B	4						H					u-silicates	10	
SK1B	4						H					u-silicates	10	
SK1B	4						H					u-silicates	10	
SK1B	4						H					u-silicates	10	
SK1B	4						H					u-silicates	10	
SK1B	4						H					u-silicates	10	
SK1B	4						H					u-silicates	10	
SK1B	4						H					u-silicates	10	
SK1B	4						H					u-silicates	10	
SK1B	4						H					u-silicates	10	
SK1B	4						H					u-silicates	10	
SK1B	4						H					u-silicates	10	
SK1B	4						H					u-silicates	10	
SK1B	4						H					u-silicates	10	
SK1B	4						H					u-silicates	10	
SK1B	5	8										u-silicates	25	
SK1B	5						H					u-silicates	30	
SK1B	5						H					u-silicates	25	
SK1B	6	4					H					u-silicates	95	
SK1B	6	7										u-silicates	20	
SK1B	6	21										u-silicates	45	

SK1B	3						H					u-silicates	10	
SK1E	4	1					M					u-silicates	75	
SK1E	4	3					M					u-silicates	100	
SK1E	4	5					H					u-silicates	60	
SK1E	4	6					H					u-silicates	10	10 Si noddules
SK1E	4	7					H					u-silicates	15	
SK1E	4	10					H					u-silicates	50	
SK1E	4	12					M					u-silicates	90	
SK1E	4	13					H					u-silicates	40	
SK1E	4	16					H					u-silicates	30	
SK1E	4	20					H					u-silicates	130	
SK1E	4						H					u-silicates	10	
SK1E	4						H					u-silicates	10	
SK1E	4						H					u-silicates	10	
SK1E	4						H					u-silicates	10	
SK1E	4						H					u-silicates	10	
SK1E	4						H					u-silicates	10	
SK1E	4						H					u-silicates	10	
SK1E	4						H					u-silicates	10	
SK1E	4						H					u-silicates	10	
SK1E	4						H					u-silicates	5	
SK1E	4						H					u-silicates	5	
SK1E	4						H					u-silicates	5	
SK1E	4						H					u-silicates	5	
SK1E	4						H					u-silicates	5	
SK1E	4						H					u-silicates	5	
SK1E	4						H					u-silicates	5	
SK1E	4						H					u-silicates	5	
SK1E	5	5					H					u-silicates	55	
SK1E	5	6					H					u-silicates	85	
SK1E	5	13					H					u-silicates	100	
SK1E	5	14					H					u-silicates	50	
SK1E	5						M					u-silicates	10	
SK1E	6	2					H					u-silicates	100	
SK1E	6	3					M					u-silicates	60	Contain high Si fractures
SK1E	6	6					M					u-silicates	40	
SK1E	6						H					u-silicates	30	
SK1E	6						H					u-silicates	15	
SK1E	7	3					H					u-silicates	100	
SK1E	7	8					H					u-silicates	90	
SK1E	7	9					H					u-silicates	50	
SK1E	7	14					M				L	u-silicates	55	
SK1E	7	15					L					u-silicates	50	14 attached to 15
SK2A	3	4					H					u-silicates	35	
SK2A	3	8					H					u-silicates	110	
SK2A	3	9					H					u-silicates	100	
SK2D	5						H					u-silicates	10	
SK2D	5						H					u-silicates	10	
SK2D	5						H					u-silicates	10	
SK2D	5						H					u-silicates	10	
SK2D	5						H					u-silicates	10	
SK2D	5						H					u-silicates	10	
SK2D	5						H					u-silicates	10	
SK2D	5						H					u-silicates	10	
SK2D	5						H					u-silicates	10	
SK1D	6						H					u-silicates	15	
SK1D	6						H					u-silicates	10	
SK1D	7	1					H					u-silicates	55	
SK1D	7						H					u-silicates	10	

SK1B	1?	11					T					u-silicates	35	
SK1B	1?	12					T					u-silicates	110	
SK1D	2						H					u-silicates	10	
SK1D	2						H					u-silicates	10	
SK1D	2						H					u-silicates	10	
SK1D	2						H					u-silicates	10	
SK1D	4						H					u-silicates	5	
SK1D	4						H					u-silicates	5	
SK1D	4						H					u-silicates	5	
SK1D	4						H					u-silicates	5	
SK1D	4						H					u-silicates	5	
SK1D	4						H					u-silicates	5	
SK1D	4						H					u-silicates	5	
SK1D	4						H					u-silicates	5	
SK1D	4						H					u-silicates	5	
SK1D	4						H					u-silicates	5	
SK1D	4						H					u-silicates	5	
SK1D	4						H					u-silicates	5	
SK1D	4						H					u-silicates	5	
SK1D	4						H					u-silicates	5	
SK1D	4						H					u-silicates	5	
SK1D	4						H					u-silicates	5	
SK1D	4						H					u-silicates	5	
SK1D	4						H					u-silicates	5	
SK1D	4						H					u-silicates	5	
SK1D	4						H					u-silicates	5	
SK1D	4						H					u-silicates	5	
SK1D	4						H					u-silicates	5	
SK1D	4						H					u-silicates	5	
SK1D	4						H					u-silicates	5	
SK1D	4						H					u-silicates	5	
SK1D	4						H					u-silicates	5	
SK1D	4						H					u-silicates	5	
SK1D	5						H					u-silicates	10	
SK1D	5						H					u-silicates	10	
SK1D	5						H					u-silicates	10	
SK1E	1	1					M					u-silicates	20	
SK1E	1	13					M					u-silicates	50	Ti, Si stripes
S3	2	17					H					u-silicates	30	
S3	2	18					H					u-silicates	50	attached to 14
S3	2	19					H					u-silicates	10	2 Si noddule
S3	2						H					u-silicates	10	
S3	2						H					u-silicates	10	
S3	2						H					u-silicates	10	
S3	2						H					u-silicates	10	
S3	2						H					u-silicates	10	
S1	3	5					H					u-silicates	30	
S1	3	18					H					u-silicates	5	20 Si noddules
S1	3						H					u-silicates	5	
S1	3						H					u-silicates	5	
S1	3						H					u-silicates	5	
S1	3						H					u-silicates	5	
S1	3						H					u-silicates	5	
S1	3						H					u-silicates	5	
S1	3						H					u-silicates	5	
S1	3						H					u-silicates	5	
S1	3						H					u-silicates	5	

S1	3						H					u-silicates	5	
S1	3						H					u-silicates	5	
S1	3						H					u-silicates	5	
S1	3						H					u-silicates	5	
S1	3						H					u-silicates	5	
S1	3						H					u-silicates	5	
S1	3						H					u-silicates	5	
S1	3						H					u-silicates	5	
S1	3						H					u-silicates	5	
S1	3						H					u-silicates	5	
S1	3						H					u-silicates	5	
S1	2	2					M					u-silicates	90	
S1	2	4					L					u-silicates	90	
K1	1	1					H					u-silicates	90	
K1	1	2					H					u-silicates	10	4 Si noddules
K1	1						H					u-silicates	10	
K1	1						H					u-silicates	10	
K1	1						H					u-silicates	10	
K1	1						H					u-silicates	10	
SV1	1	1					H					u-silicates	80	
SV1	1	2					H					u-silicates	110	
SV1	1	3					H					u-silicates	140	
SV1	1	4					H					u-silicates	20	
SV1	1	5					H					u-silicates	65	
SV1	1	6					H					u-silicates	75	
SV1	1						H					u-silicates	10	
SV1	1						H					u-silicates	10	
S3	6	1					H					u-silicates	45	
S3	6	2					H					u-silicates	80	
S3	6						H					u-silicates	5	
S3	6						H					u-silicates	5	
S3	6						H					u-silicates	5	
S3	6						H					u-silicates	5	
S3	6						H					u-silicates	5	
S3	6						H					u-silicates	5	
S3	6						H					u-silicates	5	
S3	6						H					u-silicates	5	
S3	6						H					u-silicates	5	
S3	6						H					u-silicates	5	
S3	7						H					u-silicates	10	
S3	7						H					u-silicates	10	
S3	7						H					u-silicates	10	
S3	1	11					H					u-silicates	15	attached to 8
S3	1	12					H					u-silicates	40	Attached to 12
S1	6	3					L					u-silicates	120	
S1	5	6					L					u-silicates	75	
S1	5	10					L					u-silicates	10	
S1	4	13					M					u-silicates	55	
S1	1	14					H					u-silicates	20	
S1	1	15					H					u-silicates	10	
S1	1	16					H					u-silicates	10	
S3	4	19					H					u-silicates	10	U-silicate
S2	1	5					H					u-silicates	80	
S2	1	18					H					u-silicates	15	
S2	1	1					L					u-silicates	30	
S2	1	2					M					u-silicates	75	
SK5B	2	14					H					u-silicates	5	8 Nodules on Si
SK5B	3	9					H					u-silicates	70	a nodule Si on 8
SK5B	3	18					H					u-silicates	30	

SK5B	4	5					L					u-silicates	20	at lower edge of 4
SK5B	4	13					M					u-silicates	150	
SK5B	5	1					H					u-silicates	10	3 Noddules Si
SK5B	5	2					H					u-silicates	100	
SK5B	6	5					M					u-silicates	50	
SK5B	6	10					H					u-silicates	20	
SK1E	5	1					M					u-silicates	50	
SK1E	5	4					H					u-silicates	70	
SK1E	5	8					M					u-silicates	40	Onbottom edge of 7
SK1E	5	10					H					u-silicates	100	
SK1E	5	13					H					u-silicates	101	
SK1E	5	14					H					u-silicates	150	
SK1E	5	15					H					u-silicates	50	
SK1E	5	19					M					u-silicates	50	
SK1E	6	1					M					u-silicates	100	
SK1E	6	7					H					u-silicates	140	
SK1E	6	10					L					u-silicates	120	
SK1E	6	12					H					u-silicates	150	
SK1E	6	17					L					u-silicates	40	
SK1E	7	1					H					u-silicates	145	
SK1E	7	8					H					u-silicates	160	
SV1	7	1					H					u-silicates	100	
SV1	7	2					H					u-silicates	150	
SV1	7	3					H					u-silicates	150	
SV1	7	4					H					u-silicates	60	
SV1	7	5					H					u-silicates	20	
SV1	7	7					H					u-silicates	140	
SV1	7	8					M					u-silicates	155	
SV1	7	15					H					u-silicates	50	
SV1	7	16					H					u-silicates	120	
SV1	7	19					VL					u-silicates	20	on edge of 18
SV1	7	20					H					u-silicates	50	
SV1	6	8					H					u-silicates	50	
SV1	6	9					H					u-silicates	100	
SV1	6	10					H					u-silicates	150	
SV1	6	11					H					u-silicates	50	
SV1	6	12					H					u-silicates	100	
SV1	6	13					H					u-silicates	50	
SV1	6	14					M					u-silicates	100	
SV1	5	1					H					u-silicates	120	
SV1	5	2					H					u-silicates	160	
SV1	5	3					H					u-silicates	120	
SV1	5	4					H					u-silicates	200	
SV1	5	5					H					u-silicates	150	
SV1	5	6					H					u-silicates	100	
SV1	5	15					H					u-silicates	50	nodule
SV1	5	16					H					u-silicates	100	nodule
SV1	4	10					H					u-silicates	150	
SV1	4	11					H					u-silicates	100	
SV1	4	12					H					u-silicates	100	
SV1	4	13					H					u-silicates	100	
SV1	4	14					H					u-silicates	40	
SV1	3	13					H					u-silicates	90	
SV1	3	14					H					u-silicates	120	
SV1	3	15					H					u-silicates	50	
SV1	3	16					H					u-silicates	150	
SV1	3	17					H					u-silicates	90	
SV1	2	1					H					u-silicates	50	
SV1	2	2					H					u-silicates	150	

SV1	2	3					H					u-silicates	160	
SV1	2	4					H					u-silicates	100	
SV1	2	5					H					u-silicates	140	
SV1	2	6					H					u-silicates	149	
SV1	2	7					H					u-silicates	150	
SV1	2	8					H					u-silicates	150	
SV1	2	9					H					u-silicates	100	
SV1	2	10					H					u-silicates	40	
SV1	2	11					H					u-silicates	50	
SV1	2	20					H					u-silicates	150	
SKZE	1	16					H					u-silicates	15	attached to 5
SKZE	1	17					L					u-silicates	10	
SKZE	7	15					H					u-silicates	50	
SKZE	3	19					H					u-silicates	50	at bottom of 15
SKZE	2	13					H					u-silicates	100	
SKZE	2	14					L					u-silicates	50	
SKZE	2	15					H					u-silicates	50	
SKZE	6	1					H					u-silicates	200	
SKZE	6	2					H					u-silicates	200	
SKZE	6	3					H					u-silicates	150	
SKZE	6	17					H					u-silicates	40	0n top of 14
SKZE	5	18					H					u-silicates	20	attached to 15
SKZE	4	1					M					u-silicates	190	
SKZE	4	5					H					u-silicates	150	
SKZE	4	14					H					u-silicates	40	nodule attached on 6
SKZE	4	15					H					u-silicates	60	
SKZE	4	17					H					u-silicates	180	
SK12D	1	7					H					u-silicates	40	
SK12D	1	10					H					u-silicates	150	
SK12D	1	12					H					u-silicates	140	
SK12D	1	13					H					u-silicates	50	
SK12D	2	1					H					u-silicates	150	
SK12D	2	4					H					u-silicates	140	
SK12D	2	7					L					u-silicates	40	
SK12D	2	20					H					u-silicates	50	
SK12D	3	3					H					u-silicates	50	nuddule on 2
SK12D	3	17					H					u-silicates	5	
SK12D	4	7					H					u-silicates	40	
SK12D	4	12					H					u-silicates	140	
SK12D	5	10					H					u-silicates	50	attached to 9
SK12D	5	14					H					u-silicates	50	
SK12D	6	1					H					u-silicates	150	
SK12D	6	9					H					u-silicates	50	
SK12D	7	1					H					u-silicates	200	
SK12D	7	4					H					u-silicates	160	
SK12D	7	5(B)					H					u-silicates	50	attached to 5
SK12E	4	2					H					u-silicates	50	attahed to 1
SK12E	4	3					H					u-silicates	140	
SK12E	4	4					L					u-silicates	190	contain Fe alterations
SK12E	4	7					H					u-silicates	40	
SK12E	4	9					H					u-silicates	50	attached to 8
SK12E	4	10					H					u-silicates	60	
SK12E	4	12					H					u-silicates	200	
SK12E	4	18					H					u-silicates	40	
SK12E	4	20					H					u-silicates	50	Attached to 19
SK12E	4	21					H					u-silicates	5	Attached to 4
SK12E	6	2					H					u-silicates	150	
SK12E	6	3					H					u-silicates	200	
SK12E	6	7					M					u-silicates	20	

SK12E	6	17					M					u-silicates	20	
SK12E	7	2					H					u-silicates	100	
SK12E	7	4					H					u-silicates	50	
SK12E	7	7					H					u-silicates	50	
SK12E	7	11					H					u-silicates	140	
SK12E	7	16					H					u-silicates	40	
SK12A	2	4					H					u-silicates	140	
SK12A	2	11					M					u-silicates	60	
SK12A	2	12					H					u-silicates	40	
SK12A	2	13					H					u-silicates	20	
SK9	1	1					H					u-silicates	150	
SK9	1	4					H					u-silicates	50	
SK9	1	5					H					u-silicates	90	
SK9	1	7					H					u-silicates	90	
SK9	1	9					H					u-silicates	100	
SK9	1	11					H					u-silicates	100	
SK9	1	16					H					u-silicates	40	nodules on Si
SK9	2	3					H					u-silicates	40	
SK9	2	9					H					u-silicates	20	
SK9	3	4					H					u-silicates	50	
SK9	3	9					H					u-silicates	100	
SK9	3	11					H					u-silicates	60	
SK9	4	2					H				T	u-silicates	200	
SK9	5	3					H					u-silicates	40	on the edge of 2
SK9	5	5					H					u-silicates	100	
SK9	5	8					H					u-silicates	100	
SK9	5	16					H					u-silicates	40	
SK9	6	1					H					u-silicates	150	
SK9	6	2					H					u-silicates	100	
SK9	6	10					H					u-silicates	60	
SK9	7	4					H					u-silicates	100	
SK9	7	7					H					u-silicates	90	
SK8	1	1					H					u-silicates	90	
SK8	1	8					H					u-silicates	5	
SK8	1	9					H					u-silicates	5	
SK8	1	10					H					u-silicates	5	
SK8	1	11					H					u-silicates	5	Attached to pyrochlore
SK8	1	12					H					u-silicates	5	Attached to pyrochlore
SK8	1	13					H					u-silicates	5	Attached to pyrochlore
SK12E	2	10					H					u-silicates	80	
SK12E	2	14					H					u-silicates	30	
SK12E	2	21					H					u-silicates	30	on edges of 20
SK12E	3	7					H					u-silicates	50	
SK12E	3	10					H					u-silicates	120	
SK12E	3	12					H					u-silicates	80	
SK12E	3	15					H					u-silicates	30	
SK12E	1	2					H					u-silicates	50	
SK12E	1	5					H					u-silicates	70	
SK12E	1	15					H					u-silicates	100	
SK2A	3	3					H					u-silicates	170	
SK2A	3	7					H					u-silicates	150	
SK2A	3	10					H					u-silicates	50	
SK2A	3	12					H					u-silicates	70	
SK2A	3	14					VL					u-silicates	40	
SK2A	3	16					H					u-silicates	20	NOdules on Ti
SK2D	5	13					H					u-silicates	40	
SK2D	6	14					H					u-silicates	40	
SK2D	7	2					H					u-silicates	20	nodule in 1
SK2D	7	6					H					u-silicates	100	

SK2D	7	13					M					u-silicates	40	
SK2D	7	14					H					u-silicates	20	
SK2D	1	3					H					u-silicates	20	
SK2D	1	10					H					u-silicates	40	
SK2D	1	19					H					u-silicates	30	Around 18
SK2D	1	20					H					u-silicates	100	
SK2D	1	21					H					u-silicates	40	Nodule in center of 6
SK2D	1	23					H					u-silicates	40	Nodule on 24
SK2D	1						H					u-silicates	40	Nodule on 24 centre
SK2D	1						H					u-silicates	40	Nodule on 24
SK4	2	4					H					u-silicates	50	
SK4	2	5					H					u-silicates	150	
SK4	2	9					H					u-silicates	20	Nodule on Si
SK4	2	10					H					u-silicates	50	
SK4	3	5					H					u-silicates	40	
SK4	4	15					H					u-silicates	20	
SK4	5	2					M					u-silicates	20	
SK4	5	12					H					u-silicates	50	
SK4	6	2					H					u-silicates	60	
SK4	6	6					L					u-silicates	200	
SK4	6	9					H					u-silicates	40	
SK4	6	10					H					u-silicates	30	
SK4	7	1					H					u-silicates	100	
SK4	7	11					H					u-silicates	60	
SK4	1	1					H					u-silicates	100	
SK4	1	2					H					u-silicates	150	
SK1A	2						H					u-silicates	70	
SK1A	3	7					H					u-silicates	70	
SK1A	3	8					H					u-silicates	70	
SK1A	3	11					H					u-silicates	70	mingled with 10
SK1A	3	12					H					u-silicates	70	
SK1A	3	13					H					u-silicates	70	
SK1A	5	4					VL					u-silicates	70	
SK1A	6	3					H					u-silicates	70	
SK1A	6	4					H					u-silicates	70	
SK1A	6	5					H					u-silicates	70	
SK1A	6	6					H					u-silicates	70	
SK1A	6	7					H					u-silicates	70	
SK1A	7	6					H					u-silicates	70	
SK1A	7	7					M					u-silicates	70	
SK1A	7	8					H					u-silicates	70	
K1	2						H					u-silicates	40	Contain Fe around
K1	2						H					u-silicates	40	Contain Fe around
K1	2						H					u-silicates	40	Contain Fe around
K1	2						H					u-silicates	40	Contain Fe around
K1	2						H					u-silicates	40	Contain Fe around
K1	4						M					u-silicates	30	
K1	4						M					u-silicates	30	
K1	4						M					u-silicates	30	
K1	4						M					u-silicates	30	
K1	4						M					u-silicates	30	
K1	4						M					u-silicates	30	
K1	6	5					H					u-silicates	30	
K1	6	6					H					u-silicates	40	
K1	6	7					H					u-silicates	20	
K1	6	8					M					u-silicates	10	
K1	6	9					M					u-silicates	10	
K1	7	5					M					u-silicates	60	
K1	7	6					T					u-silicates	60	

SK1E	2						H					u-silicates	50	
SK1E	2						H					u-silicates	50	
SK1E	2						H					u-silicates	15	
SK1E	2						H					u-silicates	15	
SK1E	2						H					u-silicates	15	
SK1E	2						H					u-silicates	15	
SK1E	3						H					u-silicates	50	
SK1E	3						H					u-silicates	50	
SK1E	3						H					u-silicates	50	
SK8	3	10					H					u-silicates	15	
SK8	3	11					H					u-silicates	30	
SK8	4	8					H					u-silicates	50	
SK8	4	9					H					u-silicates	30	
SK8	4	10					H					u-silicates	10	surrounds 5
SK8	7	6					H					u-silicates	5	
SK8	7	7					H					u-silicates	150	
SK8	7	8					H					u-silicates	5	
SK8	7	9					H					u-silicates	10	
SK2A	4						H					u-silicates	20	
SK2A	4						H					u-silicates	20	
SK2A	4						H					u-silicates	30	
SK2A	4						H					u-silicates	100	
SK2A	4						H					u-silicates	100	
SK2A	7						M					u-silicates	70	
SK2A	7						M					u-silicates	70	
SK2A	7						M					u-silicates	60	
SK2A	7						M					u-silicates	60	
SK2A	7						M					u-silicates	40	
SK2A	7						M					u-silicates	40	
SK2A	7						M					u-silicates	20	
SK1B	1?	5					T					u-silicates	60	
SK1E	7	3					H					u-silicates	20	Si nodule on 2
SK12D	5	2					H					u-silicates	120	
S1	2	10					M					u-silicates	5	20 Si noddules
S1	2						M					u-silicates	5	
S1	2						M					u-silicates	5	
S1	2						M					u-silicates	5	
S1	2						M					u-silicates	5	
S1	2						M					u-silicates	5	
S1	2						M					u-silicates	5	
S1	2						M					u-silicates	5	
S1	2						M					u-silicates	5	
S1	2						M					u-silicates	5	
S1	2						M					u-silicates	5	
S1	2						M					u-silicates	5	
S1	2						M					u-silicates	5	
S1	2						M					u-silicates	5	
S1	2						M					u-silicates	5	
S1	2						M					u-silicates	5	
S1	2						M					u-silicates	5	
S1	2						M					u-silicates	5	
S1	2						M					u-silicates	5	
R2800E2Z	3	15					H					u-silicates	40	
R2800E2Z	3	16					H					u-silicates	40	
R2800E2Z	3	17					H					u-silicates	40	
R2800E2Z	3	18					H					u-silicates	40	
R2800E2Z	3	19					H					u-silicates	40	
R2800E2Z	3	20					H					u-silicates	40	

R2800E2Z	3	21					H					u-silicates	40	
R2800E2Z	3	22					H					u-silicates	40	
R2800E2Z	3	23					H					u-silicates	40	
R2800E2Z	3	24					H					u-silicates	40	
R2800E2Z	3						H					u-silicates	10	
S3	3	24					H					u-silicates	5	
S3	3	25					H					u-silicates	5	
S3	3	26					H					u-silicates	5	
S3	3	27					H					u-silicates	5	
S3	3	28					H					u-silicates	5	
S3	3	29					H					u-silicates	5	
S3	3	30					H					u-silicates	5	
S3	3	31					H					u-silicates	5	
S3	3	32					H					u-silicates	5	
S3	3	33					H					u-silicates	5	
S3	3	34					H					u-silicates	5	
S3	3	35					H					u-silicates	5	
S3	3	36					H					u-silicates	5	
S1	5	1					H					u-silicates	25	
S1	5	2					M					u-silicates	75	
S1	5	16					L					u-silicates	5	Si noddule
S2	5						H					u-silicates	40	
S2	5						H					u-silicates	45	
SK12A	1						H					u-silicates	15	
SK12A	1						H					u-silicates	15	
SK12A	1						H					u-silicates	15	
SK12A	1						H					u-silicates	15	
SK12A	4	13					H					u-silicates	10	
SK12A	4	14					H					u-silicates	100	surrounds 2
SK12A	4	15					H					u-silicates	90	
SK1A	7						H					u-silicates	15	
SK1A	7						H					u-silicates	10	
SK1A	7						H					u-silicates	50	
													27540	
SK8	6	15	T				H					u-silicate	10	Around 2
SKZE	4	9	T				H					U-silicate	50	around 8
SKZE	4	20	T				H					U-silicate	20	around 19
SK12D	3	4	T				H					u-silicate	60	around to 5
SK12D	3	15	T				H					u-silicate	50	Around to 16
SKZE	5	9	T				H					u-silicate	50	around 8
SKZE	5	17	T				H					u-silicate	50	around 16
SKZE	4	4	T				H					U-silicate	50	around 3
SKZE	4	11	T				H					U-silicate	60	around 10
SKZE	4	13	T				H					U-silicate	50	arround 12
SK2D	6	9	T				H					U-silicate	20	around 8
SK4	4	2	T				H					u-silicate	20	Around 1
SK4	4	4	T				H					u-silicate	40	around 3
SK4	4	7	T				H					u-silicate	50	around 6
SK4	1	4	T				H					U-silicate	40	around 3
SK4	1	7	T				M					U-silicate	50	Around 13
SK8	6	16	T				H					u-silicate	10	around 6
SK2A	1	3	T				M					u-silicate	10	Around 6
SK12A	6		L				L					U-silicate	50	
K1	7	2	T				M					u-silicate	60	
SK1E	2		L				L					u-silicate	50	
SK4	4	10	M				M					u-silicate	50	
SK4	5	4	M				M					u-silicate	150	
SK4	5	7	L				M				T	u-silicate	110	
SK4	7	4	M				M					U-silicate	120	

SK4	7	9	VL				M					U-silicate	60	
SK4	7	12	T				M					U-silicate	50	
SK1E	2		L				L					u-silicate	50	
SK1E	2		L				L					u-silicate	50	
SK1E	3		H				L					u-silicate	50	
SK1E	3		L				L					u-silicate	50	
SK12A	6		L				L					U-silicate	50	
SK4	3	1	H				M					u-silicate	150	
SK12E	5	10	H				H					u-silicate	40	
SK1E	6	15	H				M					u-silicate	70	
SK1E	6	3	H				M					u-silicate	100	
SK1E	1	4	H				M					U-silicate	80	
SK1E	6	8	H				M					U-silicate	45	
SK1E	6	9	H				M					U-silicate	50	
SK1E	6	10	M				H					U-silicate	70	Attached o 9
SK1B	4	6	L				L					U-silicate	100	
SK1B	4		H				H					U-silicate	10	
SK1B	7		H				H					U-silicate	10	
SK1E	6	14	L				M					u-silicate	95	
SK1E	1	9	M				M					U-silicate	50	
SK1E	1	10	M				M					U-silicate	100	
SK1E	1	11	M				M					U-silicate	60	
SK1E	1	14	M				M					U-silicate	105	
S3	4	18	L				L					U-silicate	10	U-silicate
SK1E	5	2	H				M					U-silicate	100	
SK1E	5	3	M				M					U-silicate	150	
SK1E	6	4	H				H					u-silicate	110	
SK1E	6	16	H				M					u-silicate	50	
SK1E	7	12	M		VL		M					u-silicate	50	
SK12E	4	16	L				H					u-silicate	30	Attached to 15
SK12E	5	11	M				VL					u-silicate	100	
SK12E	5	17	VL				H					u-silicate	60	
SK12E	6	4	L				H					u-silicate	200	
SK9	3	13	L				H					u-silicate	100	
SK12E	1	8	T	T			H					u-silicate	50	8 is on top of 7
SK12E	1	9		T			H					u-silicate	100	1 Nodule on U-Nb
SK2A	3	5	VL				H					u-silicate	200	
SK4	3	2	H				M					u-silicate	140	
SK4	3	4	M				H					u-silicate	150	
													4375	670
SK1B	7	3	M		H		H					u-titanite	75	
SK12D	2	2	L		L		L					u-titanite	50	
													125	2
SK1E	1	8		H			H					Vuoriyarvite-K	100	
S1	2	1		H			H					Vuoriyarvite-K	55	
SK9	2	1		H			H					Vuoriyarvite-K	200	
SK1B				H			H					Vuoriyarvite-K	10	
S10	7	1	H	M	M		M					Vuoriyarvite-K	50	Si noddules, 1 centre, 1 edge
SK1E	6	11	M	M	M		M					Vuoriyarvite-K	60	
SK2A	3	1	M	M	M		L					Vuoriyarvite-K	100	
SK2A	3	3	L	M	M		L					Vuoriyarvite-K	135	
SK2A	3	11	T	M	M		M					Vuoriyarvite-K	20	
SK2A	3	12	L	H	M		M					Vuoriyarvite-K	50	
SK2D	5		L	M	M		M					Vuoriyarvite-K	15	
S3	4	10	L	M	M		L					Vuoriyarvite-K	60	
S3	4	12		M	M		L					Vuoriyarvite-K	7	U around

S3	5	17		M	L		M					Vuoriyarvite-K	100	
SK5B	5	4	VL	M	H		L					Vuoriyarvite-K	60	
SKZE	6	13	T	L	L		L					Vuoriyarvite-K	40	
SKZE	5	12	H	M	M		M					Vuoriyarvite-K	90	
SK12D	5	16		M	L		L					Vuoriyarvite-K	50	
SK2A	3	4		L	H		H					Vuoriyarvite-K	150	
SK2A	3	6	L	M	L		M					Vuoriyarvite-K	100	
SK4	3	3		M	H		M					Vuoriyarvite-K	200	
SK4	5	6	L	L	M		M					Vuoriyarvite-K	50	
SK4	1	12	M	L	H		L					Vuoriyarvite-K	30	
S10	2	4	L	H	M		M					Vuoriyarvite-K	100	surrounded by 3 Si
S10	2	7	L	H	M		H					Vuoriyarvite-K	90	surrounded by 5 Si
SK1A	1	1	VL	VL			L	L				Vuoriyarvite-K	90	
SK1E	5	10	H		T		M					Vuoriyarvite-K	60	
SK1E	5	12	L		T		M	L				Vuoriyarvite-K	70	Si zone
SK1E	5	15	M		T		H					Vuoriyarvite-K	75	
S3	7	17		M			H					Vuoriyarvite-K	40	attached to 9
SK9	6	15	VL	M	L		M					Vuoriyarvite-K	40	
SK2D	5	1					H					Vuoriyarvite-K	100	
SK2D	5	10			L		H	VL				Vuoriyarvite-K	40	
SKZE	3	18	L	M	VL		M					Vuoriyarvite-K	100	
SKZE	3	20		H			H			L		Vuoriyarvite-K	50	
SK12D	6	11	VL	M	L		L					Vuoriyarvite-K	80	
SK9	3	2	L	M	L		L					Vuoriyarvite-K	160	
SK2A	3	8	M	M	L		M					Vuoriyarvite-K	100	
SK2A	3	11		M	L		L					Vuoriyarvite-K	50	
SK2A	3	15	L	H	M		M					Vuoriyarvite-K	30	Nodules on Si
SK2A	3	20	M	H	M		L					Vuoriyarvite-K		
SK2D	5	14	M	H	M		M					Vuoriyarvite-K	50	
SK2D	7	9	L	M	L		L					Vuoriyarvite-K	200	
SK4	6	8	H	L	VL		M				L	Vuoriyarvite-K	190	
S10	3	9		M			H					Vuoriyarvite-K	60	
S10	4	13		H			H					Vuoriyarvite-K	120	
S10	4	16	VL	M			H					Vuoriyarvite-K	40	
S10	6	11		H			H					Vuoriyarvite-K	15	
S10	6	12		M			H					Vuoriyarvite-K	80	
S10	6	14		M			H					Vuoriyarvite-K	8	9 noddules
S10	6			M			H					Vuoriyarvite-K	8	
S10	6			M			H					Vuoriyarvite-K	8	
S10	6			M			H					Vuoriyarvite-K	8	
S10	6			M			H					Vuoriyarvite-K	8	
S10	6			M			H					Vuoriyarvite-K	8	
S10	6			M			H					Vuoriyarvite-K	8	
S10	6			M			H					Vuoriyarvite-K	8	
S10	6			M			H					Vuoriyarvite-K	8	
S10	6			M			H					Vuoriyarvite-K	5	
SK1A	1	4		H			H					Vuoriyarvite-K	75	3 noddules of U in centre
SK1B	1	11		H			H					Vuoriyarvite-K	60	
SK1B	1	12		H			H					Vuoriyarvite-K	75	
SK1B	4	1		H			H					Vuoriyarvite-K	120	
SK1B	6	1		H			H					Vuoriyarvite-K	30	
SK1B	6	2		H			H					Vuoriyarvite-K	100	
SK2D	5	3		H			H					Vuoriyarvite-K	40	
SK2D	5	5		M			H					Vuoriyarvite-K	45	
SK2D	5	14		M			H					Vuoriyarvite-K	10	10 Si noddules
SK1D	6	6		H			H					Vuoriyarvite-K	90	
SK1D	6	10		M			H					Vuoriyarvite-K	50	
SK1D	7	13		M	M		M		T		T	Vuoriyarvite-K	120	Si noddules
SK1B	1?	2		H			H					Vuoriyarvite-K	75	

SK1B	1?	3		H			H					Vuoriyarvite-K	60	
SK1B	1?	4		H			H					Vuoriyarvite-K	100	
SK1B	1?	8		H			H					Vuoriyarvite-K	80	
SK1B	1?	15		H			H					Vuoriyarvite-K	100	
S1	3	2		H			H					Vuoriyarvite-K	50	
S1	3	4		H			H					Vuoriyarvite-K	75	
S3	6	3	L	M	L		L					Vuoriyarvite-K	95	Si stains
S3	6	4	L	M	L		L					Vuoriyarvite-K	150	
S3	6	6	L	M	L		L					Vuoriyarvite-K	50	
S3	6	14		M			H					Vuoriyarvite-K	5	4 Si noddules
S3	6	15		M			H					Vuoriyarvite-K	55	
S3	1	5	L	M	L		L					Vuoriyarvite-K	150	
S3	1	6	L	M	L		L					Vuoriyarvite-K	50	
S1	4	12		H			H					Vuoriyarvite-K	100	
S1	4	14	T	M			L					Vuoriyarvite-K	75	
S1	4	15	T	M			L					Vuoriyarvite-K	65	
S3	5	1		M			M					Vuoriyarvite-K	90	
S3	5	2		M			M					Vuoriyarvite-K	40	
S3	5	3		M			M					Vuoriyarvite-K	50	
S3	5	5		M			M					Vuoriyarvite-K	100	
S3	5	10		M			M					Vuoriyarvite-K	60	
S2	1	1		H			H					Vuoriyarvite-K	50	
S2	1	2		H			H					Vuoriyarvite-K	100	
S2	1	10		H			H					Vuoriyarvite-K	40	
S2	1	11		H			H					Vuoriyarvite-K	20	
SK5B	4	17		L			M					Vuoriyarvite-K	30	Attached to 8
SK5B	5	7		L			H					Vuoriyarvite-K	50	
SK1E	6	5	M	M	L		M					Vuoriyarvite-K	120	
SK1E	6	13		M			L					Vuoriyarvite-K	100	
SKZE	1	2		H	VL		H					Vuoriyarvite-K	60	
SKZE	1	4	L	M	VL		L					Vuoriyarvite-K	200	
SKZE	1	5		H			L					Vuoriyarvite-K	150	attached to 6 and 16
SKZE	7	1	L	M	L		L					Vuoriyarvite-K	110	
SKZE	7	2	L	M	L		L					Vuoriyarvite-K	150	
SKZE	7	11	L	M	L		L					Vuoriyarvite-K	180	
SKZE	7	12		H			H					Vuoriyarvite-K	30	nodule
SKZE	7	13		H			H					Vuoriyarvite-K	150	
SKZE	3	14	L	M	L		M					Vuoriyarvite-K	100	
SKZE	3	15	L	M	L		M					Vuoriyarvite-K	130	
SKZE	2	11	L	M	VL		M					Vuoriyarvite-K	150	
SKZE	6	4	L	M	L		L					Vuoriyarvite-K	100	
SKZE	6	5	L	M	L		L					Vuoriyarvite-K	110	
SKZE	6	6	L	M	L		L					Vuoriyarvite-K	200	
SKZE	6	7	L	M	L		H					Vuoriyarvite-K	100	
SKZE	6	10	VL	M	L		L					Vuoriyarvite-K	150	
SKZE	6	12	T	M	L		L					Vuoriyarvite-K	150	
SKZE	6	14	VL	M	L		L					Vuoriyarvite-K	50	
SKZE	6	15	L	M	L		L					Vuoriyarvite-K	20	
SKZE	6	16	VL	M	L		L					Vuoriyarvite-K	50	
SKZE	5	4	H	M	M		L					Vuoriyarvite-K	100	
SKZE	5	10	H	M	VL		L					Vuoriyarvite-K	40	
SKZE	5	11	H	M			L					Vuoriyarvite-K	150	
SKZE	5	13	H	M	M		L					Vuoriyarvite-K	120	
SKZE	5	14	H	M	M		L					Vuoriyarvite-K	100	
SKZE	5	16	H	M	M		M					Vuoriyarvite-K	150	
SKZE	4	3	L	M	L		M					Vuoriyarvite-K	100	
SKZE	4	6	L	M	M		M					Vuoriyarvite-K	140	
SKZE	4	7		M	L		L					Vuoriyarvite-K	50	
SKZE	4	8	L	M	L		M					Vuoriyarvite-K	100	

SKZE	4	12	L	M	M		M					Vuoriyarvite-K	100	
SKZE	4	16	L	M	M		M					Vuoriyarvite-K	160	
SKZE	4	18	L	M	M		L					Vuoriyarvite-K	100	
SKZE	4	19	L	M	M		L					Vuoriyarvite-K	100	
SKZE	4	21	L	M	M		M					Vuoriyarvite-K	170	
SK12D	1	1	M	M	L		M					Vuoriyarvite-K	100	
SK12D	1	2	M	M	L		M					Vuoriyarvite-K	150	
SK12D	1	3	VL	M	L		M					Vuoriyarvite-K	60	
SK12D	1	6	L	M			M					Vuoriyarvite-K	140	
SK12D	1	8	M	M	L		M					Vuoriyarvite-K	150	
SK12D	1	9	M	M	L		M					Vuoriyarvite-K	30	
SK12D	2	3	L	M	L		L				T	Vuoriyarvite-K	200	
SK12D	2	5	VL	M	L		L					Vuoriyarvite-K	150	
SK12D	2	6	L	M	L		L					Vuoriyarvite-K	200	
SK12D	2	8	L	M	L		L				T	Vuoriyarvite-K	160	
SK12D	2	10	VL	M	L		L					Vuoriyarvite-K	100	
SK12D	2	11	L	M	L		L					Vuoriyarvite-K	130	
SK12D	2	12	L	M	L		L					Vuoriyarvite-K	100	
SK12D	2	13	L	M	L		L					Vuoriyarvite-K	140	
SK12D	2	14	L	M	L		L					Vuoriyarvite-K	90	
SK12D	2	15	L	M	L		L					Vuoriyarvite-K	100	
SK12D	2	16	L	M	L		L					Vuoriyarvite-K	180	
SK12D	3	1	L	M	L		L					Vuoriyarvite-K	160	
SK12D	3	2	L	M	L		L					Vuoriyarvite-K	150	
SK12D	3	5	L	M	L		L					Vuoriyarvite-K	50	
SK12D	3	6	L	M	L		L					Vuoriyarvite-K	180	
SK12D	3	7	L	M	L		L					Vuoriyarvite-K	160	
SK12D	3	10	L	M	L		L					Vuoriyarvite-K	100	
SK12D	3	11	VL	M	L		L					Vuoriyarvite-K	160	
SK12D	3	13	VL	M	L		L					Vuoriyarvite-K	110	
SK12D	4	1	L	M	M		L					Vuoriyarvite-K	140	
SK12D	4	2	L	M	L		L					Vuoriyarvite-K	150	
SK12D	4	3	VL	M	L		L					Vuoriyarvite-K	100	
SK12D	4	6	VL	H	M		L					Vuoriyarvite-K	140	
SK12D	4	8	L	M	L		L					Vuoriyarvite-K	150	
SK12D	4	9	VL	M	L		L					Vuoriyarvite-K	40	
SK12D	5	3	L	M	L		L					Vuoriyarvite-K	100	
SK12D	5	4	L	M	L		L					Vuoriyarvite-K	130	
SK12D	5	5	L	M	L		L					Vuoriyarvite-K	110	
SK12D	5	6	VL	M	L		L					Vuoriyarvite-K	160	
SK12D	5	9	L	M	L		L					Vuoriyarvite-K	100	
SK12D	5	11	L	M	L		L					Vuoriyarvite-K	110	
SK12D	5	12		M			VL					Vuoriyarvite-K	200	
SK12D	5	13	L	M			L					Vuoriyarvite-K	40	
SK12D	5	15	L	M	L		L					Vuoriyarvite-K	100	
SK12D	6	2	VL	M	L		M					Vuoriyarvite-K	150	
SK12D	6	7	L	M	L		M					Vuoriyarvite-K	160	
SK12D	6	8	L	M	L		M					Vuoriyarvite-K	150	
SK12D	6	13		M	L		M					Vuoriyarvite-K	140	
SK12D	6	14	L	M	L		M					Vuoriyarvite-K	100	
SK12D	6	15	L	M	L		M					Vuoriyarvite-K	30	
SK12D	7	5		M			M					Vuoriyarvite-K	200	
SK12D	7	6	L	H	M		H					Vuoriyarvite-K	150	
SK12D	7	7		H	M		L					Vuoriyarvite-K	100	
SK12D	7	8		H	M		VL					Vuoriyarvite-K	60	
SK12D	7	9	VL	H	M		M					Vuoriyarvite-K	120	
SK12D	7	10	L	H	M		M					Vuoriyarvite-K	100	
SK12D	7	11	L	H	M		M					Vuoriyarvite-K	160	
SK12D	7	12	L	H	M		M					Vuoriyarvite-K	145	

SK12D	7	13	L	H	M		M					Vuoriyarvite-K	100	
SK12D	7	14	L	H	M		M					Vuoriyarvite-K	140	
SK12D	7	15	VL	H	M		M					Vuoriyarvite-K	100	
SK12D	7	16	L	H	M		M					Vuoriyarvite-K	160	
SK12E	4	5		M	L		L					Vuoriyarvite-K	50	
SK12E	4	6	T	M	L		L					Vuoriyarvite-K	150	
SK12E	4	11	VL	M	M		L					Vuoriyarvite-K	180	
SK12E	4	13	L	M	M		L					Vuoriyarvite-K	170	
SK12E	4	14	L	M	M		L					Vuoriyarvite-K	110	
SK12E	4	17		M	M		L					Vuoriyarvite-K	150	
SK12E	4	19	VL	M	M		L					Vuoriyarvite-K	120	
SK12E	5	3	M	M			L					Vuoriyarvite-K	105	
SK12E	5	4		M	L		L					Vuoriyarvite-K	100	
SK12E	5	5	VL	M	L		L					Vuoriyarvite-K	130	
SK12E	5	6	T	M	L		L					Vuoriyarvite-K	100	
SK12E	5	7		M	L		L					Vuoriyarvite-K	150	
SK12E	5	8	L	M	L		L					Vuoriyarvite-K	50	
SK12E	5	9	M	M	L		L					Vuoriyarvite-K	150	
SK12E	5	14	VL	M			L					Vuoriyarvite-K	120	
SK12E	5	15	L	M	L		VL					Vuoriyarvite-K	155	
SK12E	5	16	L	M	L		M					Vuoriyarvite-K	150	
SK12E	6	1	L	M	L		M					Vuoriyarvite-K	50	
SK12E	6	5	L	M	L		M					Vuoriyarvite-K	150	
SK12E	6	6	L	H	L		M					Vuoriyarvite-K	130	
SK12E	6	10	VL	M	L		M					Vuoriyarvite-K	150	
SK12E	6	11	L	H	L		M					Vuoriyarvite-K	200	
SK12E	6	14	VL	M	L		M					Vuoriyarvite-K	130	
SK12E	6	15	L	M	L		M					Vuoriyarvite-K	30	
SK12E	6	16	VL	M	L		M					Vuoriyarvite-K	50	
SK12E	6	18	L	H	L		M					Vuoriyarvite-K	100	
SK12E	7	1	L	M	L		M				T	Vuoriyarvite-K	100	
SK12E	7	3	VL	VL	T		M	VL				Vuoriyarvite-K	120	
SK12E	7	5	VL	M	L		M					Vuoriyarvite-K	100	
SK12E	7	6	L	M	L		L					Vuoriyarvite-K	190	
SK12E	7	9	L	M	L		L					Vuoriyarvite-K	100	
SK12E	7	10		M			H				VL	Vuoriyarvite-K	105	
SK12E	7	12	VL	M	L		M					Vuoriyarvite-K	90	
SK12E	7	13	VL	M	L		L					Vuoriyarvite-K	130	
SK12E	7	14	VL	M	L		L					Vuoriyarvite-K	100	
SK12E	7	17		H	L		H					Vuoriyarvite-K	110	
SK12E	7	19	L	M	L		L					Vuoriyarvite-K	60	
SK9	1	2	T	M	L		L					Vuoriyarvite-K	100	
SK9	1	10	T	M	L		L					Vuoriyarvite-K	180	
SK9	1	14		M	L		L					Vuoriyarvite-K	40	
SK9	1	15		M	L		L					Vuoriyarvite-K	100	
SK9	2	2	T	M	L		L					Vuoriyarvite-K	100	
SK9	2	4	T	M	L		L					Vuoriyarvite-K	100	
SK9	2	5	VL	M	L		L					Vuoriyarvite-K	150	
SK9	2	6		L	VL		VL					Vuoriyarvite-K	120	
SK9	2	7	VL	M	L		L					Vuoriyarvite-K	150	
SK9	2	10	L	M	L		L					Vuoriyarvite-K	90	
SK9	2	11	L	M	L		L					Vuoriyarvite-K	110	
SK9	2	12	VL	M	L		L					Vuoriyarvite-K	110	
SK9	2	13	VL	M	L		L					Vuoriyarvite-K	180	
SK9	2	14	VL	M	L		L					Vuoriyarvite-K	130	
SK9	3	1		H			H					Vuoriyarvite-K	150	
SK9	3	7	VL	M	L		L					Vuoriyarvite-K	110	
SK9	3	8	L	M	L		L					Vuoriyarvite-K	170	
SK9	3	10	VL	M	L		L					Vuoriyarvite-K	190	

SK9	3	12	L	M	L		L					Vuoriyarvite-K	150	
SK9	3	14	L	M	L		L					Vuoriyarvite-K	90	
SK9	3	15		M	L		L					Vuoriyarvite-K	170	
SK9	3	17	L	M	L		M					Vuoriyarvite-K	90	
SK9	3	19		M	L		VL					Vuoriyarvite-K	100	
SK9	3	21		L			VL					Vuoriyarvite-K	120	
SK9	4	1		H			H					Vuoriyarvite-K	190	
SK9	4	3		H			H					Vuoriyarvite-K	110	
SK9	4	4		H			H					Vuoriyarvite-K	30	
SK9	4	5	VL	M	L		M				T	Vuoriyarvite-K	160	
SK9	4	6		M	L		L					Vuoriyarvite-K	100	
SK9	4	10	L	M	L		L					Vuoriyarvite-K	120	
SK9	4	12	VL	M	L		L					Vuoriyarvite-K	80	
SK9	4	13	T	M	L		L					Vuoriyarvite-K	100	
SK9	5	1		H			H					Vuoriyarvite-K	40	
SK9	5	2	L	M	L		L					Vuoriyarvite-K	150	
SK9	5	4	VL	M	L		L					Vuoriyarvite-K	200	
SK9	5	6	H	M	T		L					Vuoriyarvite-K	50	
SK9	5	7	L	M			L					Vuoriyarvite-K	200	
SK9	5	14		M	L		H					Vuoriyarvite-K	40	
SK9	5	15	VL	M	L		M					Vuoriyarvite-K	180	
SK9	7	1	L	M	L		L					Vuoriyarvite-K	150	
SK9	7	2		M	L		L					Vuoriyarvite-K	50	
SK9	7	3	VL	M	L		L					Vuoriyarvite-K	100	
SK9	7	5	VL	M	L		M					Vuoriyarvite-K	150	
SK9	7	8	VL	M	L		L					Vuoriyarvite-K	120	
SK9	7	9		H			H					Vuoriyarvite-K	130	
SK9	7	10	VL	M	L		L					Vuoriyarvite-K	140	
SK9	7	11	L	M			L					Vuoriyarvite-K	150	
SK9	7	13		L			M					Vuoriyarvite-K	50	
SK9	7	14		M	L		L					Vuoriyarvite-K	60	
SK12E	2	1	L	M	M		M					Vuoriyarvite-K	150	
SK12E	2	2	T	M	L		L					Vuoriyarvite-K	100	2 noddle of U-silicate
SK12E	2	3		M	L		H					Vuoriyarvite-K	100	1 noddle of U-silicate
SK12E	2	4	VL	M	L		L					Vuoriyarvite-K	150	
SK12E	2	5	VL	M	M		M					Vuoriyarvite-K	100	
SK12E	2	6		T	VL		H					Vuoriyarvite-K	50	
SK12E	2	8			VL		H					Vuoriyarvite-K	50	
SK12E	2	9	VL	M	M		L					Vuoriyarvite-K	50	
SK12E	2	12	L	M	M		M					Vuoriyarvite-K	150	
SK12E	2	13	L	M	M		M					Vuoriyarvite-K	100	
SK12E	2	15		H	T		H					Vuoriyarvite-K	150	
SK12E	2	16	L	H	M		L					Vuoriyarvite-K	100	
SK12E	2	19	L	M	M		L					Vuoriyarvite-K	160	
SK12E	2	20	L	M	M		M					Vuoriyarvite-K	150	
SK12E	3	1	VL	L	VL		M	T			VL	Vuoriyarvite-K	150	
SK12E	3	2	M	M	M		M					Vuoriyarvite-K	100	
SK12E	3	3		H			H					Vuoriyarvite-K	60	
SK12E	3	6		T	T		T					Vuoriyarvite-K	100	
SK12E	3	8	M	M	M		M					Vuoriyarvite-K	105	
SK12E	3	9	L	M	T		M					Vuoriyarvite-K	170	
SK12E	3	11	L	M	M		M					Vuoriyarvite-K	150	
SK12E	3	14	T	M	M		M					Vuoriyarvite-K	140	
SK12E	3	16	VL	M	M		M					Vuoriyarvite-K	120	
SK12E	3	17	VL	M	M		M					Vuoriyarvite-K	170	
SK12E	3	18	L	H	M		L					Vuoriyarvite-K	50	
SK12E	1	1	L	M	M		M					Vuoriyarvite-K	100	
SK12E	1	3		H			H					Vuoriyarvite-K	70	
SK12E	1	4	M	M	M		M					Vuoriyarvite-K	150	

SK12E	1	6		H	M		L					Vuoriyarvite-K	40	
SK12E	1	7	T	VL	M		L					Vuoriyarvite-K	70	
SK12E	1	10	M	H	M		M					Vuoriyarvite-K	80	
SK12E	1	11		VL	M		VL					Vuoriyarvite-K	130	
SK12E	1	12	L	H	L		M					Vuoriyarvite-K	50	
SK12E	1	13	M	M	L		M					Vuoriyarvite-K	90	
SK12E	1	14	L	H	M		M					Vuoriyarvite-K	100	
SK2D	5	2		M			L					Vuoriyarvite-K	150	
SK2D	5	3		H			H					Vuoriyarvite-K	60	
SK2D	5	4		M			L					Vuoriyarvite-K	150	
SK2D	5	5		M			L					Vuoriyarvite-K	160	
SK2D	5	7		M			L					Vuoriyarvite-K	140	
SK2D	5	8		M			L					Vuoriyarvite-K	110	
SK2D	5	11		M			L					Vuoriyarvite-K	140	
SK2D	5	12		M			L					Vuoriyarvite-K	60	
SK2D	6	1		H			H					Vuoriyarvite-K	100	
SK2D	6	6	M	H	M		M					Vuoriyarvite-K	70	
SK2D	6	8		M	L		M		T			Vuoriyarvite-K	160	
SK2D	6	10	L	H	M		M					Vuoriyarvite-K	155	
SK2D	6	11		M			M					Vuoriyarvite-K	150	
SK2D	6	13		M			M					Vuoriyarvite-K	100	
SK2D	7	12		M	L		M					Vuoriyarvite-K	50	
SK2D	7	15		M			L					Vuoriyarvite-K	50	
SK2D	1	1		M	L		M		VL			Vuoriyarvite-K	150	
SK4	4	3	M	L			M					Vuoriyarvite-K	110	
SK4	4	9	H	VL	VL		L					Vuoriyarvite-K	130	
SK4	4	13		M			M					Vuoriyarvite-K	100	
SK4	4	16	H	VL	VL		M					Vuoriyarvite-K	110	
SK4	4	17		M			L					Vuoriyarvite-K	120	
SK4	5	3		M			L					Vuoriyarvite-K	100	
SK4	5	13	H	L			L					Vuoriyarvite-K	160	
SK4	6	11		M			H					Vuoriyarvite-K	20	
SK4	7	2		M			L					Vuoriyarvite-K	110	
SK4	7	3		M			L					Vuoriyarvite-K	100	
SK4	7	5		M			L					Vuoriyarvite-K	150	
SK4	7	7		M			L					Vuoriyarvite-K	40	
SK4	7	10		M			L					Vuoriyarvite-K	50	
SK4	7	13		M			L					Vuoriyarvite-K	180	
SK1A	2		M	H	M		L					Vuoriyarvite-K	80	
SK1A	2		M	H	M		L					Vuoriyarvite-K	80	
SK1A	2		M	H	M		L					Vuoriyarvite-K	80	
SK1A	2		M	H	M		L					Vuoriyarvite-K	80	
SK1A	2		M	H	M		L					Vuoriyarvite-K	80	
SK1A	2		M	H	M		L					Vuoriyarvite-K	80	
SK1A	2		M	H	M		L					Vuoriyarvite-K	80	
K1	3	1		H			H					Vuoriyarvite-K	80	
S2	2	4	L	H	L		L					Vuoriyarvite-K	50	
S2	2	5	L	H	L		L					Vuoriyarvite-K	50	
S2	2	6	VL	H	L		L					Vuoriyarvite-K	50	
S2	2	7	VL	H	L		L					Vuoriyarvite-K	50	
S2	2	8	VL	H	L		L					Vuoriyarvite-K	30	
S2	2	9	VL	H	L		L					Vuoriyarvite-K	25	
S2	2	10	VL	H	L		L					Vuoriyarvite-K	60	
S2	3	6	M	H	M		M					Vuoriyarvite-K	50	
S2	3	7	M	H	M		M					Vuoriyarvite-K	50	
S2	3	8	M	H	M		M					Vuoriyarvite-K	50	
S2	3	9	M	H	M		M					Vuoriyarvite-K	50	
S2	3	10	M	H	M		M					Vuoriyarvite-K	50	
S2	3	11	M	H	M		M					Vuoriyarvite-K	50	

S2	3	12	M	H	M		M					Vuoriyarvite-K	50	
S2	3	13	M	H	M		M					Vuoriyarvite-K	50	
S2	3	14	M	H	M		M					Vuoriyarvite-K	30	
S2	4		M	H	M		M					Vuoriyarvite-K	50	
S2	4		M	H	M		M					Vuoriyarvite-K	50	
S2	4		M	H	M		M					Vuoriyarvite-K	50	
S2	4		M	H	M		M					Vuoriyarvite-K	50	
S2	4		M	H	M		M					Vuoriyarvite-K	50	
S2	4		M	H	M		M					Vuoriyarvite-K	50	
S2	5		L	M	M		M					Vuoriyarvite-K	60	
S2	5		L	M	M		M					Vuoriyarvite-K	60	
S2	5		L	M	M		M					Vuoriyarvite-K	40	
S2	5		L	M	M		M					Vuoriyarvite-K	30	
S2	5		L	M	M		M					Vuoriyarvite-K	40	
S2	5		L	M	M		M					Vuoriyarvite-K	30	
S2	5		L	M	M		M					Vuoriyarvite-K	30	
S2	5		L	M	M		M					Vuoriyarvite-K	30	
S2	5		L	M	M		M					Vuoriyarvite-K	30	
S2	5		L	M	M		M					Vuoriyarvite-K	30	
S2	5		L	M	M		M					Vuoriyarvite-K	30	
S2	6		L	H	M		M					Vuoriyarvite-K	150	
S2	6		L	H	M		M					Vuoriyarvite-K	50	
S2	6		L	H	M		M					Vuoriyarvite-K	40	
S2	6		L	H	M		M					Vuoriyarvite-K	15	
S2	6		L	H	M		M					Vuoriyarvite-K	15	
S2	6		L	H	M		M					Vuoriyarvite-K	15	
S2	7		L	H	L		L					Vuoriyarvite-K	50	
S2	7		L	H	L		L					Vuoriyarvite-K	50	
S2	7		L	H	L		L					Vuoriyarvite-K	50	
S2	7		L	H	L		L					Vuoriyarvite-K	50	
S2	7		L	H	L		L					Vuoriyarvite-K	30	
S2	7		L	H	L		L					Vuoriyarvite-K	30	
S2	7		L	H	L		L					Vuoriyarvite-K	25	
S2	7		L	H	L		L					Vuoriyarvite-K	25	
S2	7		L	H	L		L					Vuoriyarvite-K	25	
S2	7		L	H	L		L					Vuoriyarvite-K	25	
S2	7		L	H	L		L					Vuoriyarvite-K	25	
S2	7		L	H	L		L					Vuoriyarvite-K	25	
S2	7		L	H	L		L					Vuoriyarvite-K	25	
SK1E	2		L	M			L					Vuoriyarvite-K	50	
SK2D	2		L	H	L		L					Vuoriyarvite-K	50	
SK2D	2		L	H	L		L					Vuoriyarvite-K	50	
SK12A	3		VL	H			M					Vuoriyarvite-K	50	
SK12A	3		VL	H			M					Vuoriyarvite-K	50	
SK12A	3		VL	H			M					Vuoriyarvite-K	50	
SK12A	3		VL	H			M					Vuoriyarvite-K	50	
SK12A	3		VL	H			M					Vuoriyarvite-K	50	
SK12A	4	2	M	H	L		L					Vuoriyarvite-K	30	
SK12A	4	3	M	H	L		L					Vuoriyarvite-K	30	
SK12A	4	4	M	H	L		L					Vuoriyarvite-K	30	
SK12A	6		L	H	L		L					Vuoriyarvite-K	70	
SK8	3	2	M	M	M		L					Vuoriyarvite-K	100	
SK8	3	3	M	M	M		L					Vuoriyarvite-K	100	
SK8	3	4	M	M	M		L					Vuoriyarvite-K	50	
SK8	3	5	M	M	M		L					Vuoriyarvite-K	50	
SK8	3	6	M	M	M		L					Vuoriyarvite-K	50	
SK8	3	7	M	M	M		L					Vuoriyarvite-K	30	
SK8	4	1	L	M	M		M					Vuoriyarvite-K	10	
SK8	4	2	L	M	M		M					Vuoriyarvite-K	20	

SK8	4	3	L	M	M		M					Vuoriyarvite-K	40	
SK8	4	4	L	M	M		M					Vuoriyarvite-K	50	
SK8	4	5	L	M	M		M					Vuoriyarvite-K	50	
SK8	4	6	L	M	M		M					Vuoriyarvite-K	50	
SK8	5	1	L	H	M		VL					Vuoriyarvite-K	100	
SK8	5	2	L	H	M		VL					Vuoriyarvite-K	50	
SK8	5	3	L	H	M		VL					Vuoriyarvite-K	30	
SK8	5	4	L	H	M		VL					Vuoriyarvite-K	40	
SK8	5	5	L	H	M		VL					Vuoriyarvite-K	40	
SK8	5	6	L	H	M		VL					Vuoriyarvite-K	40	
SK8	5	7	L	H	M		VL					Vuoriyarvite-K	40	
SK8	5	9		H			H					Vuoriyarvite-K	40	
SK8	6	1	VL	H	M		L					Vuoriyarvite-K	100	
SK8	6	2	VL	H	M		L					Vuoriyarvite-K	100	
SK8	6	3	VL	H	M		L					Vuoriyarvite-K	100	
SK8	6	4	VL	H	M		L					Vuoriyarvite-K	10	
SK8	6	5	VL	H	M		L					Vuoriyarvite-K	20	
SK8	6	6	VL	H	M		L					Vuoriyarvite-K	50	
SK8	6	7	VL	H	M		L					Vuoriyarvite-K	50	
SK8	6	8	VL	H	M		L					Vuoriyarvite-K	50	
SK8	6	9	VL	H	M		L					Vuoriyarvite-K	60	
SK8	7	1	VL	M	M		L					Vuoriyarvite-K	100	
SK8	7	2	VL	M	M		L					Vuoriyarvite-K	100	
SK8	7	3	VL	M	M		L					Vuoriyarvite-K	50	
SK8	7	4	VL	M	M		L					Vuoriyarvite-K	30	
SK8	7	5	VL	M	M		L					Vuoriyarvite-K	30	
SK2A	4		L	H	M		M					Vuoriyarvite-K	100	
SK2A	4		L	H	M		M					Vuoriyarvite-K	100	
SK2A	4		L	H	M		M					Vuoriyarvite-K	10	
SK2A	4		L	H	M		M					Vuoriyarvite-K	15	
SK2A	7		VL	H	M		L					Vuoriyarvite-K	100	
SK2A	7		VL	H	M		L					Vuoriyarvite-K	10	458
													41059	
R2800E2Z	3	1	H									uraninite	100	
R2800E2Z	3	2	H									uraninite	90	
R2800E2Z	3	3	H									uraninite	50	
R2800E2Z	3	4	H									uraninite	35	
R2800E2Z	3	5	H									uraninite	100	
R2800E2Z	3	6	H									uraninite	95	Si on the edge
R2800E2Z	3	7	H									uraninite	95	
R2800E2Z	3	8	H									uraninite	80	
R2800E2Z	3	9	H									uraninite	140	
R2800E2Z	3	10	H									uraninite	75	
R2800E2Z	3	11	H									uraninite	45	
R2800E2Z	3	12	H									uraninite	100	
R2800E2Z	3	13	H									uraninite	180	
R2800E2Z	3	14	H									uraninite	120	

APPENDIX 7
QEMSCAN Analysis

Table 1. Mineralogical calculated assay (Mass %), mineral abundance/composition (Mass %) and average grain/particle sizes (µm) of six samples, two size fractions each, from the Rössing SK-area.

Sample No	SK4/4 20I			SK4/4 22I			SK4/43 27I			N10062			N9947			N10456		
Fraction	Combined	-90µm	-150/+90µm	Combined	-90µm	-150/+90µm	Combined	-90µm	-150/+90µm	Combined	-90µm	-150/+90µm	Combined	-90µm	-150/+90µm	Combined	-90µm	-150/+90µm
Particle Size	18.04	15.4	21.3	22.15	18.0	22.7	19.87	17.0	20.6	23.03	18.7	26.1	20.75	19.2	22.9	18.76	17.9	22.1
Particle Size Distribution (Mass %)	100.00	46.96	53.04	100.00	9.97	90.03	100.00	16.89	83.11	100.00	33.84	66.16	100.00	53.61	46.39	100.00	76.05	23.95
Mineralogical Calculated Assays (Mass %)																		
Element	Combined	-90µm	-150/+90µm	Combined	-90µm	-150/+90µm	Combined	-90µm	-150/+90µm	Combined	-90µm	-150/+90µm	Combined	-90µm	-150/+90µm	Combined	-90µm	-150/+90µm
Na	1.98	2.07	1.91	2.57	2.68	2.56	2.16	2.25	2.14	3.22	3.39	3.13	3.16	3.28	3.02	2.76	2.73	2.85
Na (chemical)	*0.07*			*2.66*			*2.83*			*3.32*			*3.62*			*3.27*		
Mg	2.39	1.95	2.78	1.11	1.02	1.11	0.61	0.68	0.60	0.65	0.67	0.63	0.62	0.63	0.62	0.54	0.58	0.43
Mg (chemical)	*1.63*			*0.23*			*0.08*			*0.05*			*0.11*			*0.03*		
Al	7.37	7.32	7.42	6.23	6.58	6.19	7.11	7.37	7.05	7.17	7.64	6.92	7.20	7.48	6.87	7.96	8.10	7.52
Al (chemical)	7.73			6.40			6.92			7.41			7.20			6.89		
Si	28.92	29.78	28.16	35.27	###	35.33	34.44	33.68	###	34.96	34.12	35.38	34.98	34.54	35.48	33.80	33.54	34.62
Si (chemical)	*29.63*			*33.51*			*33.72*			*35.21*			*34.82*			*35.22*		
K	4.48	4.26	4.68	2.40	2.61	2.37	4.62	4.59	4.62	3.17	3.34	3.08	3.30	3.38	3.21	4.73	4.87	4.28
K (chemical)	*4.33*			*2.40*			*4.56*			*3.71*			*3.18*			*3.54*		
Ca	1.13	1.08	1.17	0.65	0.74	0.64	0.81	1.10	0.76	0.49	0.58	0.44	0.39	0.41	0.36	0.36	0.36	0.36
Ca (chemical)	*2.00*			*2.72*			*1.14*			*0.56*			*0.52*			*0.53*		
Fe	5.35	4.89	5.75	1.73	1.78	1.73	0.65	0.75	0.63	0.65	0.73	0.61	0.67	0.68	0.65	0.71	0.74	0.61
Fe (chemical)	*4.11*			*1.53*			*0.19*			*0.28*			*0.36*			*0.25*		
Nb	0.00	0.00	0.00	0.00	0.00	0.00	0.00	0.00	0.00	0.00	0.00	0.00	0.00	0.00	0.00	0.00	0.00	0.00
Nb (chemical)	*0.01*			*0.00*			*0.00*			*0.01*			*0.00*			*0.00*		
U	0.11	0.13	0.10	0.04	0.07	0.04	0.01	0.02	0.01	0.01	0.02	0.01	0.08	0.11	0.04	0.01	0.01	0.01
U (chemical)	*0.15*			*0.07*			*0.00*			*0.01*			*0.01*			*0.00*		
Mineral Abundance/Composition (Mass %)																		
Sample No	SK4/4 20I			SK4/4 22I			SK4/43 27I			N10062			N9947			N10456		
Mineral	Combined	-90µm	-150/+90µm	Combined	-90µm	-150/+90µm	Combined	-90µm	-150/+90µm	Combined	-90µm	-150/+90µm	Combined	-90µm	-150/+90µm	Combined	-90µm	-150/+90µm
Uraninite	0.09	0.11	0.07	0.02	0.03	0.02	0.01	0.02	0.01	0.01	0.02	0.00	0.08	0.11	0.04	0.01	0.01	0.01
U-silicate	0.05	0.05	0.05	0.03	0.05	0.03	0.00	0.00	0.00	0.00	0.00	0.00	0.02	0.02	0.01	0.00	0.00	0.00
Betafite/Pyrochlore	0.01	0.01	0.01	0.02	0.02	0.02	0.00	0.00	0.00	0.02	0.03	0.02	0.00	0.00	0.00	0.02	0.02	0.01
Quartz	20.93	23.35	18.78	40.41	37.31	40.75	33.07	30.60	33.58	32.43	28.34	34.52	32.36	29.73	35.39	26.46	25.42	29.75
K-feldspar	23.18	21.66	24.52	14.70	15.52	14.60	28.15	27.27	28.33	19.82	20.39	19.52	20.13	20.18	20.08	28.77	29.41	26.73
Feldspar (Albite)	24.55	25.39	23.80	32.30	33.69	32.14	26.22	27.36	25.99	38.85	40.96	37.77	38.20	39.66	36.52	33.31	32.96	34.40

Chlorite	8.84	7.27	10.24	6.66	5.95	6.74	3.10	3.41	3.04	3.65	3.74	3.60	3.06	2.94	3.21	2.84	3.03	2.23
Biotite	7.35	5.93	8.60	0.61	0.79	0.59	0.99	1.09	0.97	0.64	0.72	0.59	1.09	1.28	0.87	0.75	0.79	0.62
Muscovite	5.75	6.96	4.68	2.82	3.64	2.72	5.87	6.79	5.68	3.36	4.21	2.92	3.84	4.43	3.16	6.29	6.76	4.80
Calcite/Dolomite	1.48	1.45	1.51	0.39	0.51	0.37	1.40	2.07	1.26	0.26	0.40	0.18	0.10	0.14	0.05	0.11	0.11	0.10
Fe-oxides/hydroxides	4.41	4.08	4.71	1.22	1.38	1.20	0.29	0.37	0.28	0.22	0.30	0.18	0.30	0.32	0.28	0.43	0.44	0.40
Ilmenite/Rutile	0.22	0.23	0.21	0.04	0.05	0.03	0.01	0.04	0.01	0.05	0.07	0.04	0.04	0.03	0.04	0.08	0.07	0.10
Apatite	0.57	0.51	0.62	0.14	0.20	0.13	0.05	0.05	0.05	0.17	0.19	0.15	0.13	0.12	0.13	0.12	0.12	0.10
Monazite	0.00	0.00	0.00	0.00	0.00	0.00	0.00	0.00	0.00	0.00	0.00	0.00	0.00	0.00	0.00	0.01	0.01	0.00
Zircon	0.06	0.06	0.06	0.02	0.02	0.02	0.01	0.01	0.01	0.02	0.03	0.02	0.03	0.02	0.03	0.03	0.03	0.03
Fe-sulphides	1.36	1.48	1.25	0.07	0.06	0.07	0.00	0.01	0.00	0.02	0.03	0.02	0.02	0.02	0.01	0.01	0.01	0.00
Galena	0.01	0.00	0.01	0.00	0.00	0.00	0.00	0.00	0.00	0.00	0.00	0.00	0.00	0.00	0.00	0.00	0.00	0.00
Molybdenite	0.00	0.00	0.00	0.00	0.00	0.00	0.00	0.00	0.00	0.00	0.00	0.00	0.00	0.00	0.00	0.00	0.00	0.00
Scheelite	0.00	0.00	0.00	0.00	0.01	0.00	0.03	0.03	0.02	0.00	0.00	0.00	0.00	0.00	0.00	0.00	0.00	0.00
Other	1.14	1.45	0.87	0.58	0.76	0.56	0.79	0.90	0.77	0.49	0.57	0.45	0.59	0.98	0.14	0.77	0.79	0.72
Average Particle/Grain Size (µm)																		
Sample No	SK4/4 20I			SK4/4 22I			SK4/43 27I			N10062			N9947			N10456		
Mineral	Combined	- 90µm	- 150/+90µm	Combined	- 90µm	- 150/+90µm	Combined	- 90µm	- 150/+90µm	Combined	- 90µm	- 150/+90µm	Combined	- 90µm	- 150/+90µm	Combined	- 90µm	- 150/+90µm
Average Particle Size	18	15	21	22	18	23	20	17	21	23	19	26	21	19	23	19	18	22
Uraninite	16	17	15	9	9	9	7	7	7	8	8	8	18	20	15	8	8	8
U-silicate	11	11	11	15	16	15	11	10	11	12	6	12	11	11	10	13	14	8
Betafite/Pyrochlore	11	12	11	13	14	13	13	11	14	26	24	29	20	0	20	29	26	64
Quartz	14	13	15	21	16	21	19	15	19	21	16	24	19	17	21	16	15	21
K-feldspar	19	17	21	20	18	21	21	17	22	20	18	21	18	19	18	18	18	22
Feldspar (Albite)	14	13	15	17	15	17	16	14	17	20	16	22	19	18	20	16	15	18
Chlorite	9	9	10	14	11	14	7	7	7	8	8	8	7	7	7	7	7	7
Biotite	10	9	11	6	6	6	7	7	7	6	6	6	8	8	8	6	6	6
Muscovite	6	6	6	6	6	6	6	6	6	6	6	6	6	6	6	6	6	6
Calcite/Dolomite	11	12	11	10	10	10	17	17	17	14	13	15	11	11	13	12	12	13
Fe-oxides/hydroxides	6	6	6	8	8	8	7	8	7	7	7	7	7	7	7	7	7	7
Ilmenite/Rutile	11	12	11	16	13	16	15	21	12	20	17	25	22	17	29	19	18	23
Apatite	21	16	27	23	20	24	24	15	27	27	22	33	26	20	40	18	17	26
Monazite	20	15	26	6	0	6	67	0	67	6	6	6	13	12	17	24	24	17
Zircon	7	8	7	7	8	7	9	8	9	7	7	7	11	11	11	12	11	17
Fe-sulphides	20	18	22	20	17	21	8	9	7	15	13	16	18	15	30	9	10	7
Galena	7	7	7	6	6	6	0	0	0	6	6	0	8	9	6	11	0	11
Molybdenite	0	0	0	11	11	0	0	0	0	0	0	0	0	0	0	0	0	0
Scheelite	0	0	0	16	22	11	24	24	24	0	0	0	0	0	0	0	0	0
Other	6	6	6	6	6	6	6	6	6	6	6	6	6	6	6	6	6	6

APPENDIX 8
QEMSCAN particle maps

The legend below applies to all particle maps in appendix 8.

- Uraninite
- U-silicate
- Betafite/Pyrochlore
- Quartz
- K-Feldspar
- Feldspar-Ab
- Chlorite
- Biotite
- Muscovite
- Calcite
- Fe-oxides/hydroxides
- Ilmenite/Rutile
- Apatite
- Zircon
- Gypsum
- Other

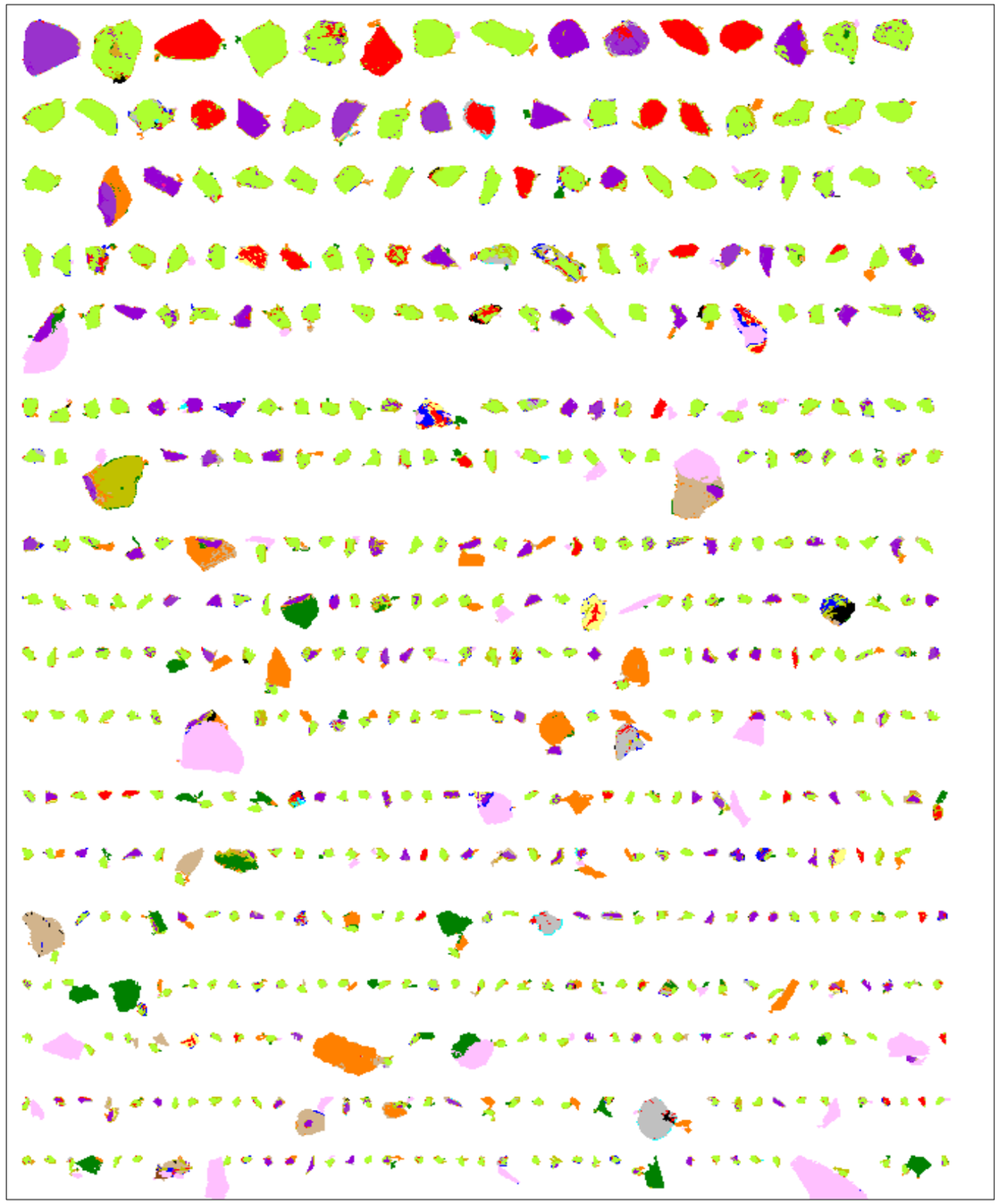

Figure 1 Uranium mineral QEMSCAN particle maps for the -90 µm fraction of SK 4-4 22I. Particles are sorted using the area of uranium phases. This sorting would emphasise coarse grains.

Figure 2 Uranium mineral QEMSCAN particle maps for the +90 µm fraction of SK 4-4 22I. Particles are sorted using the area of uranium phases. This sorting would emphasise coarse grains.

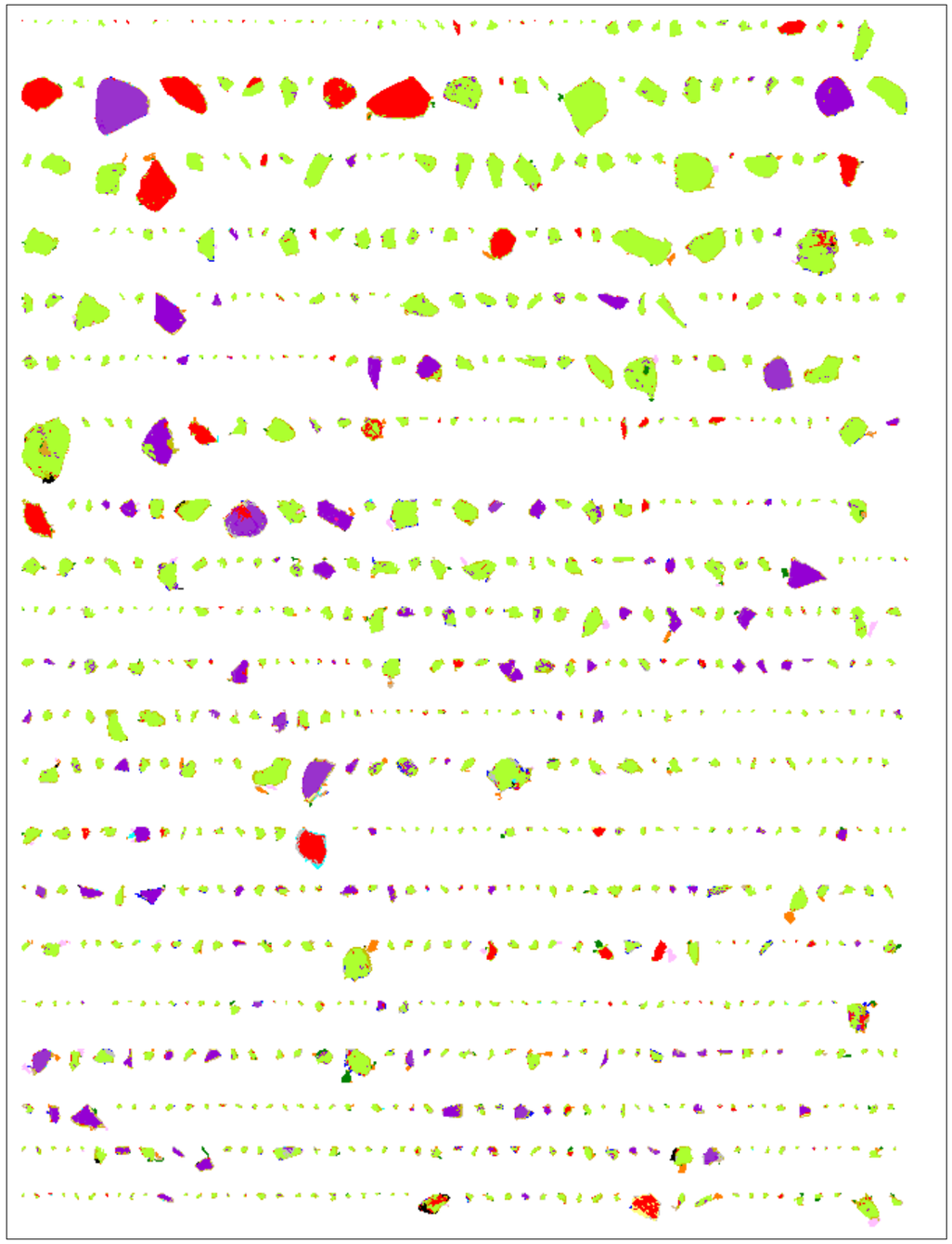

Figure 3 Uranium mineral QEMSCAN particle maps for the -90 µm fraction of SK 4-4 22I. Particles are sorted using the area percentage of uranium phases. This sorting would emphasise liberated grains.

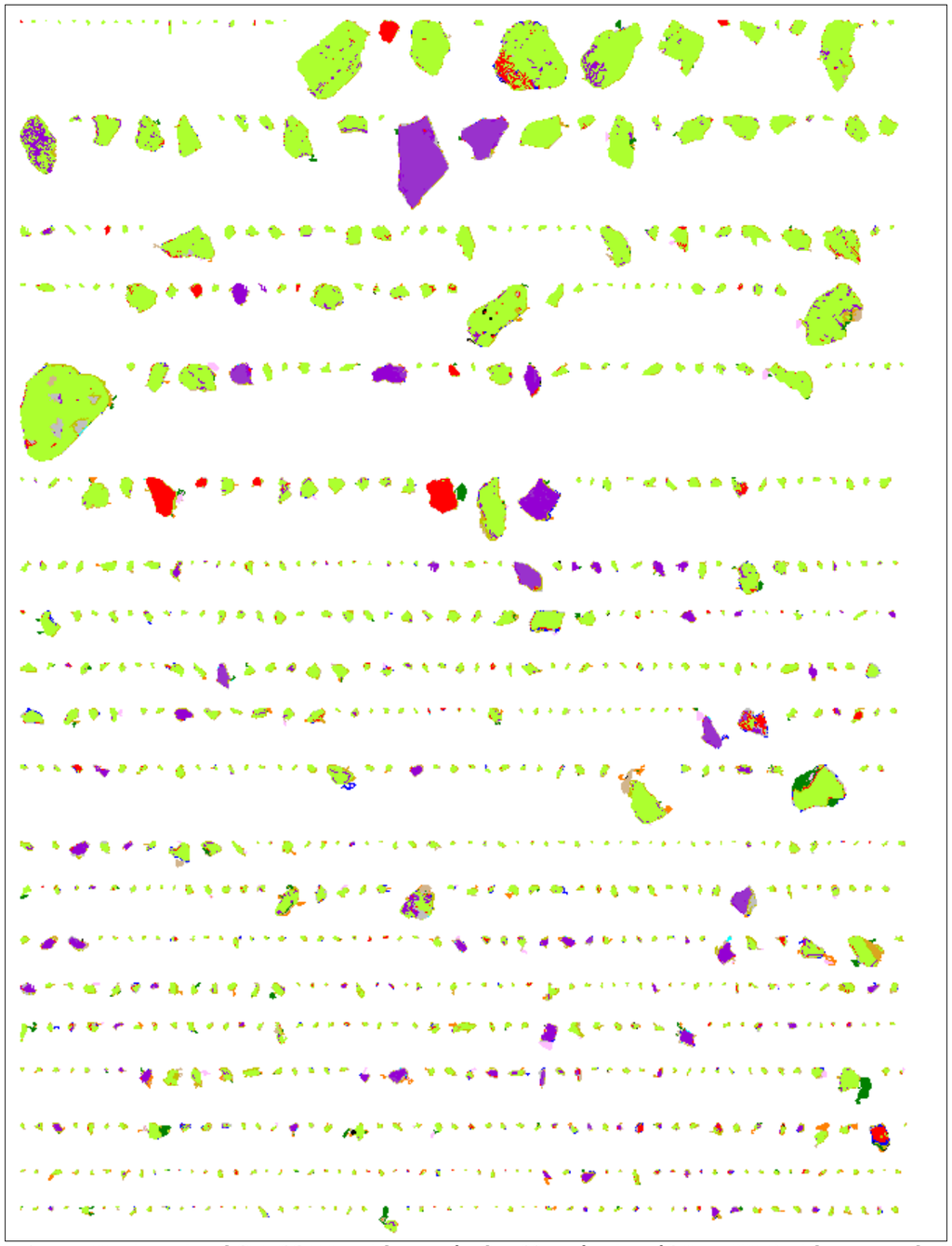

Figure 4 Uranium mineral QEMSCAN particle maps for the +90 µm fraction of SK 4-4 22I. Particles are sorted using the area percentage of uranium phases. This sorting would emphasise liberated grains.

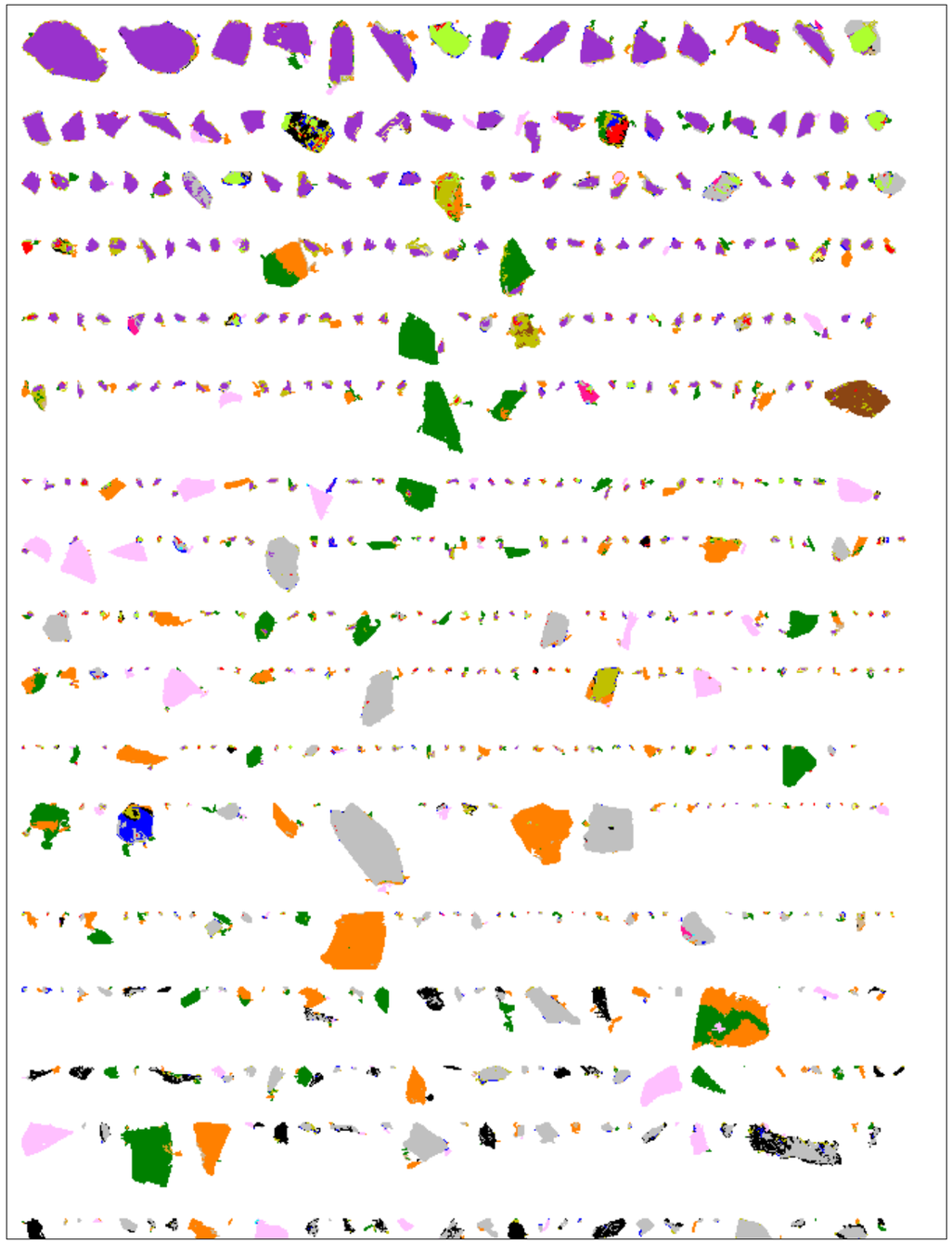

Figure 5 Uranium mineral QEMSCAN particle maps for the -90 µm fraction of N10456. Particles are sorted using the area of uranium phases. This sorting would emphasise coarse grains.

Figure 6 Uranium mineral QEMSCAN particle maps for the +90 µm fraction of N10456. Particles are sorted using the area of uranium phases. This sorting would emphasise coarse grains.

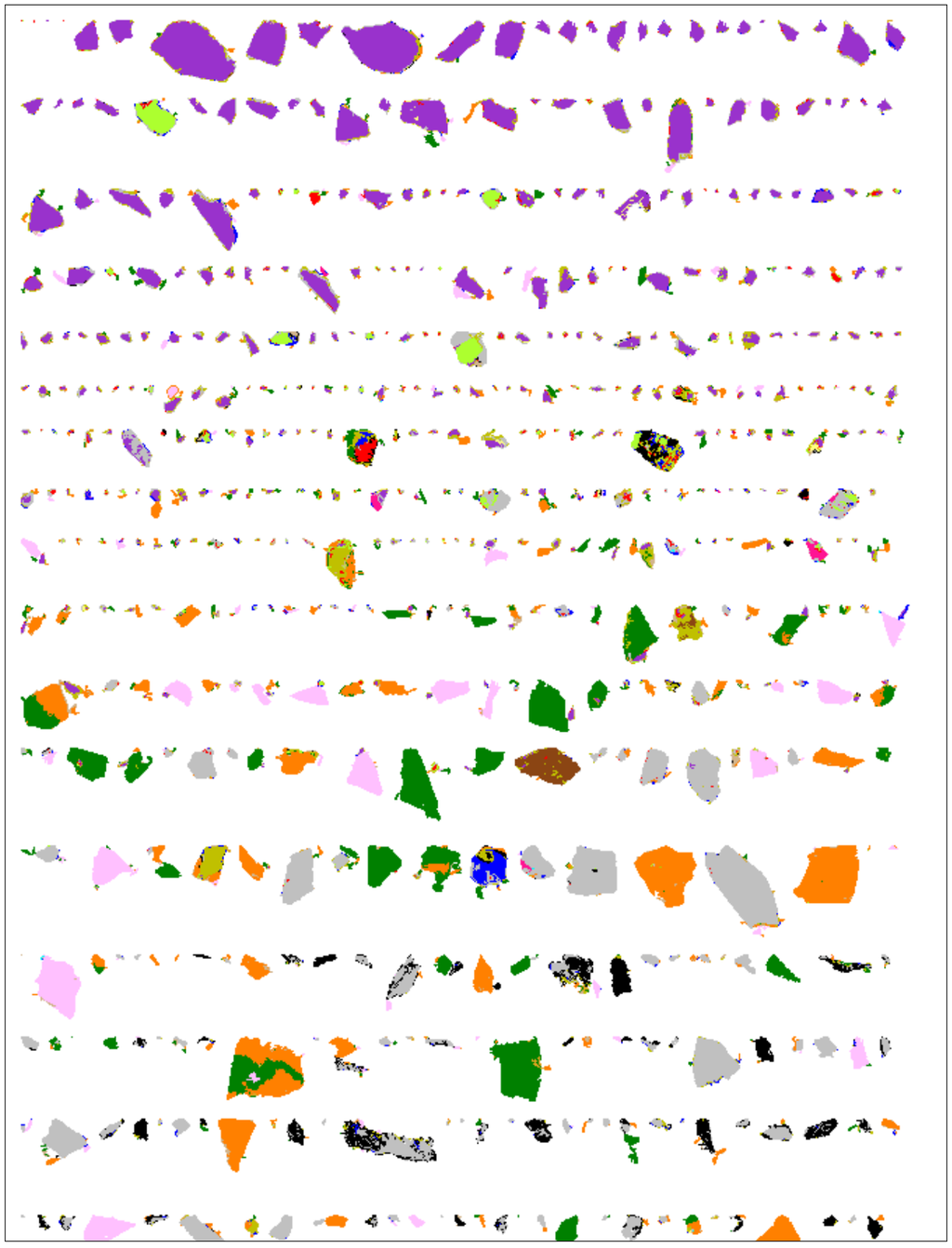

Figure 7 Uranium mineral QEMSCAN particle maps for the -90 µm fraction of N10456. Particles are sorted using the area percentage of uranium phases. This sorting would emphasise liberated grains.

Figure 8 Uranium mineral QEMSCAN particle maps for the +90 µm fraction of N10456. Particles are sorted using the area percentage of uranium phases. This sorting would emphasise liberated grains.